

N 70 20589
NASA GR 102505

A STUDY OF THE COUPLING OF ACOUSTIC ENERGY FROM
THE TROPOSPHERE TO THE IONOSPHERE

Final Technical Report
Contract NAS8-21079

15 February 1969

**CASE FILE
COPY**



Prepared for

GEORGE C. MARSHALL SPACE FLIGHT CENTER
NATIONAL AERONAUTICS AND SPACE ADMINISTRATION
Huntsville, Alabama 35812

Prepared by

David G. Detert

AVCO CORPORATION
APPLIED TECHNOLOGY DIVISION
"Formerly Space Systems Division"
Environmental Sciences and Technology Directorate
Lowell, Massachusetts 01851

A STUDY OF THE COUPLING OF ACOUSTIC ENERGY FROM
THE TROPOSPHERE TO THE IONOSPHERE

Final Technical Report
Contract NAS8-21079

15 February 1969

Prepared for

GEORGE C. MARSHALL SPACE FLIGHT CENTER
NATIONAL AERONAUTICS AND SPACE ADMINISTRATION
Huntsville, Alabama 35812

Prepared by

David G. Detert

AVCO CORPORATION
APPLIED TECHNOLOGY DIVISION
"Formerly Space Systems Division"
Environmental Sciences and Technology Directorate
Lowell, Massachusetts 01851

ABSTRACT

This report describes the efforts of the second twelve months of a continuing program (the first year's efforts being under Air Force sponsorship) of experimental measurements to investigate the possibility of coupling between ground level and ionospheric effects through the propagation of low frequency acoustic waves. The two tropospheric sources considered in this study are the static firing of large rocket engines at NASA/MSFC and the occurrence of local thunder storms. The observing system consists of a network of three, short-baseline, near vertical incidence hf Doppler sounding paths near Huntsville, Alabama, each operating with three simultaneous transmission frequencies.

The report discusses the general operation of the experiment and the experimental findings relative to ionospheric dynamics phenomena caused by static test events and local meteorological disturbances.

A three-dimensional acoustic ray-tracing computer program is briefly described, and a Fortran listing is given.

ACKNOWLEDGMENT

The original inspiration for this program was generated in large measure by Samuel Coroniti, until recently of Avco/SSD. The arrangements for field site selection and usage were made by William T. Roberts of NASA/MSFC, who also served as technical monitor for the contract.

Michael Thomas of Avco/Huntsville was responsible for the installation of the two field sites established under this program, including the development of their equipments, and he directed all aspects of the subsequent operation of the four sites utilized for the measurement series. This program would not have been possible without the personal attention and effort he gave to the experiment.

Spectral processing of the recorded doppler data was carried out with facilities at the Rome Air Development Center, made available through the generosity of Major Donald Wippermann there. The personal interest of Kenneth Ford of the RADC Data Reduction Center lead to the development of substantial improvements in processing procedures; he was also responsible for the careful processing of the bulk of the records.

Charles Moo of Avco/SSD served as a willing and continuous source of advice and encouragement in this program. Barbara Willey provided all the graphics for this report, and Ethel Ouellette who patiently typed the final and numerous earlier drafts of the text.

TABLE OF CONTENTS

	<u>Page</u>
I. Introduction	1
II. Experimental Operations	5
III. Static Test Results	11
IV. Thunderstorm Observations	22
V. Other Phenomena	31
VI. Conclusions	35
VII. References	36
Appendices	
A. Modifications to Heathkit DX60-A Transmitters (prepared by Michael Thomas, Avco/Huntsville)	39
B. Data Collection Log	41
C. Doppler Data Recorded During Static Tests	45
D. The Propagation of Acoustic-Gravity Waves Through the Middel Atmosphere (prepared by Charles Moo, Avco/SSD)	102
E. Acoustic Ray-Tracing Program (prepared by Sheldon Weinstein, Avco/SSD)	104
Fortran IV Listing of Acoustic Ray-Tracing Computer Program	124
Flow Charts of Acoustic Ray-Tracing Computer Program	139

LIST OF ILLUSTRATIONS

<u>Figure No.</u>		<u>Page No.</u>
1 (a).	Experimental configuration for monitoring static firings	2
1 (b).	Experimental configuration for monitoring ionospheric perturbations	3
2.	Typical Doppler data record, 15-16 February 1968; Huntsville, Alabama	7
3.	Tracings of Doppler data records, showing effects due to MSFC static rocket tests	13
4.	Tracings of Doppler data records, showing effects due to MSFC static rocket tests	14
5.	Tracings of Doppler data records, showing effects due to MSFC static rocket tests	15
6.	Tracings of Doppler data records, showing effects due to MSFC static rocket tests	16
7.	Schematic representation of onset times for other measurements of static test and explosion effects	19
8.	Phase-locked loop data showing thunderstorm effects, 18 August 1967: Huntsville, Alabama	23
9 (a).	Doppler data showing thunderstorm effects, 15-16 May 1968: Huntsville, Alabama	25
9 (b).	Doppler data showing thunderstorm effects, 15-16 May 1968: Huntsville, Alabama	26
9 (c).	Doppler data showing thunderstorm effects, 15-16 May 1968: Huntsville, Alabama	27
9 (d).	Doppler data showing thunderstorm effects, 15-16 May 1968: Huntsville, Alabama	28
10.	Doppler data showing thunderstorm effects, 11 March 1968: Huntsville, Alabama	29

LIST OF ILLUSTRATIONS (Cont'd)

<u>Figure No.</u>		<u>Page No.</u>
11.	Doppler data showing sunrise effects, 21 April 1968: Huntsville, Alabama	32
12.	Doppler data showing frequency spreading, 23-24 March: Huntsville, Alabama	33
13.	Doppler data showing unusual oscillatory behavior . . 20-21 April 1968: Huntsville, Alabama	34
14.	Doppler data record, 20 April 1967: Huntsville, Alabama	49
15.	Doppler data record, 9 May 1967: Huntsville, Alabama	50
16 (a).	Doppler data record, 19 May 1967: Huntsville, Alabama	51
16 (b).	Doppler data record, 19 May 1967: Huntsville, Alabama	52
17.	Doppler data record, 22 May 1967: Huntsville, Alabama	53
18.	Doppler data record, 9 June 1967: Huntsville, Alabama	54
19.	Doppler data record, 14 June 1967: Huntsville, Alabama	55
20.	Doppler data record, 1 August 1967: Huntsville, Alabama	56
21 (a).	Doppler data record, 3 August 1967: Huntsville, Alabama	57
21 (b).	Doppler data record, 3 August 1967: Huntsville, Alabama	58
22.	Doppler data record, 16 August 1967: Huntsville, Alabama	59

LIST OF ILLUSTRATIONS (Cont'd)

<u>Figure No.</u>		<u>Page No.</u>
23.	Doppler data record, 1 September 1967: Huntsville, Alabama	60
24 (a).	Doppler data record, 28 September 1967: Huntsville, Alabama	61
24 (b).	Doppler data record, 28 September 1967: Huntsville, Alabama	62
25.	Doppler data record, 19 October 1967: Huntsville, Alabama	63
26 (a).	Doppler data record, 26 October 1967: Huntsville, Alabama	64
26 (b).	Doppler data record, 26 October 1967: Huntsville, Alabama	65
27 (a).	Doppler data record, 16 November 1967: Huntsville, Alabama	66
27 (b).	Doppler data record, 16 November 1967: Huntsville, Alabama	67
28 (a).	Doppler data record, 30 November 1967: Huntsville, Alabama	68
28 (b).	Doppler data record, 30 November 1967: Huntsville, Alabama	69
29.	Doppler data record, 19 December 1967: Huntsville, Alabama	70
30.	Doppler data record, 25 January 1968: Huntsville, Alabama	71
31 (a).	Doppler data record, 6 February 1968: Huntsville, Alabama	72
31 (b).	Doppler data record, 6 February 1968: Huntsville, Alabama	73

LIST OF ILLUSTRATIONS (Cont'd)

<u>Figure No.</u>		<u>Page No.</u>
32 (a).	Doppler data record, 14 February 1968: Huntsville, Alabama	74
32 (b).	Doppler data record, 14 February 1968: Huntsville, Alabama	75
33 (a).	Doppler data record, 20 February 1968: Huntsville, Alabama	76
33 (b).	Doppler data record, 20 February 1968: Huntsville, Alabama	77
33 (c).	Doppler data record, 20 February 1968: Huntsville, Alabama	78
34 (a).	Doppler data record, 21 February 1968: Huntsville, Alabama	79
34 (b).	Doppler data record, 21 February 1968: Huntsville, Alabama	80
35.	Doppler data record, 12 March 1968: Huntsville, Alabama	81
36.	Doppler data record, 19 March 1968: Huntsville, Alabama	82
37.	Doppler data record, 27 March 1968: Huntsville, Alabama	83
38 (a).	Doppler data record, 9 April 1968: Huntsville, Alabama	84
38 (b).	Doppler data record, 9 April 1968: Huntsville, Alabama	85
39 (a).	Doppler data record, 23 April 1968: Huntsville, Alabama	86
39 (b).	Doppler data record, 23 April 1968: Huntsville, Alabama	87

LIST OF ILLUSTRATIONS (Cont'd)

<u>Figure No.</u>		<u>Page No.</u>
40 (a).	Doppler data record, 10 May 1968: Huntsville, Alabama	88
40 (b).	Doppler data record, 10 May 1968: Huntsville, Alabama; processed with low analyzer gain	89
40 (c).	Doppler data record, 10 May 1968: Huntsville, Alabama; processed with intermediate analyzer gain	90
40 (d).	Doppler data record, 10 May 1968: Huntsville, Alabama; processed with high analyzer gain	91
41 (a).	Doppler data record, 15 May 1968: Huntsville, Alabama	92
41 (b).	Doppler data record, 15 May 1968: Huntsville, Alabama	93
41 (c).	Doppler data record, 15 May 1968: Huntsville, Alabama	94
42.	Doppler data record, 20 April 1967: Huntsville, Alabama	95
43.	Doppler data record, 19 May 1967: Huntsville, Alabama	96
44.	Doppler data record, 14 June 1967: Huntsville, Alabama	97
45.	Doppler data record, 3 August 1967: Huntsville, Alabama	98
46.	Phase-locked loop data record, 3 August 1967: Huntsville, Alabama	99
47.	Phase path perturbation extracted from Figure 46	100

LIST OF ILLUSTRATIONS (Cont'd)

<u>Figure No.</u>		<u>Page No.</u>
48.	Doppler data record, 16 August 1967: Huntsville, Alabama	101
49.	Ray-tracing program geometry	107
50.	Acoustic ray-tracing input data: height vs. temperature	111
51.	Acoustic ray-tracing input data: height vs. sound speed	112
52.	Acoustic ray-tracing input data: height vs. total wind velocity	113
53.	Acoustic ray-tracing input data: height vs. wind direction	114
54.	Acoustic ray-tracing input data: height vs. x-component of wind velocity	115
55.	Acoustic ray-tracing input data: height vs. y-component of wind velocity	116
56.	Acoustic ray-tracing output data: height vs. x-distance	117
57.	Acoustic ray-tracing output data: height vs. y-distance	118
58.	Acoustic ray-tracing output data: y-distance vs. x-distance	119
59.	Acoustic ray-tracing output data: x-distance vs. time	120
60.	Acoustic ray-tracing output data: y-distance vs. time	121
61.	Acoustic ray-tracing output data: height vs. time	122

LIST OF TABLES

<u>Table No.</u>		<u>Page No.</u>
1.	Spectral Analysis Parameters, RADC Data Reduction Center	9
2.	NASA/MSFC Static Test Firings Monitored by the Doppler Sounding Experiment	47

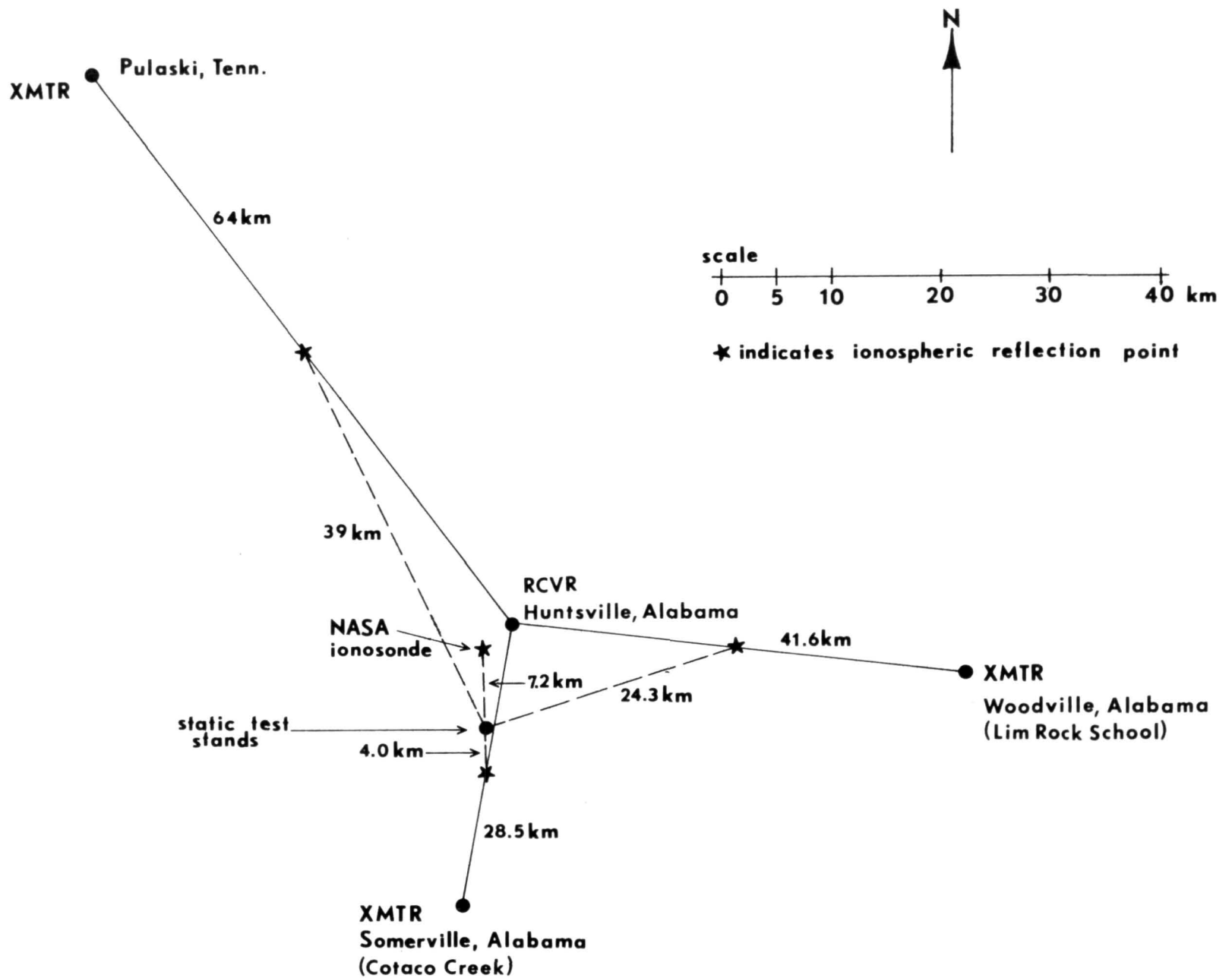
I. INTRODUCTION

In April of 1967 an experimental program was begun in the vicinity of Huntsville, Alabama to study coupling between ground level phenomena and ionospheric effects, concentrating specifically on perturbations produced in the ionosphere by the static firings of large rocket engines at NASA/MSFC and by local meteorological disturbances. Due to the nature of these "sources," it was assumed that any coupling which would be detected was achieved by the mechanism of vertically propagating low-frequency acoustic waves.

The basic observing technique employed in this experimental program has been remote radio sensing of the ionosphere by hf vertical incidence Doppler soundings, in which the apparent variations in the received frequency of various vertically propagated ultra-stable hf/cw radio signals are monitored at a single receiving site on the ground. The resultant Doppler shifts are related to the dynamics of the ionospheric region in which the waves are reflected. Details of this measurement approach have been given by a number of workers 1, 2, 3. The first year of this research program was sponsored by the Rome Air Development Center, under contract F30602-67-C-0016, which called for the establishment of one near vertical incidence Doppler sounding path, over which three fixed frequencies in the range 2 to 6 MHz were continuously transmitted. Data were collected for some five months.

This report describes the results of a second year of effort in the Huntsville experimental program. The objectives of this second phase were similar to those of the first year, but the observing system was substantially expanded to include three different near vertical incidence Doppler sounding paths of differing lengths, each transmitting three simultaneous frequencies. The experiment was operated over a period of eight months, and included approximately 1000 hours of operation in which all nine signals were simultaneously present, in addition to many more hours in which a smaller number of signals were recorded. Figure 1 (a) shows the configuration of the four sites established near Huntsville, Alabama, for this phase of the program, with the relevant distances between the ionospheric reflection points and the NASA/MSFC static test stands. Figure 1 (b) shows the same map, with the distances marked between ionospheric reflection points.

The results of the first year's experimental operation have been reported elsewhere 4, 5 but can be summarized briefly as showing encouraging evidence of ionospheric perturbations being produced by several of the static rocket tests which were monitored. It appeared that the acoustic output spectra of the various tests were sufficiently similar to rule out variations in test characteristics as being the cause of the limited number of successfully detected events, and it seems likely that either the characteristics of the intervening media or the electron density configuration at the particular ionospheric reflection heights were



-2-

Figure 1 (a): Experimental configuration for monitoring static firings

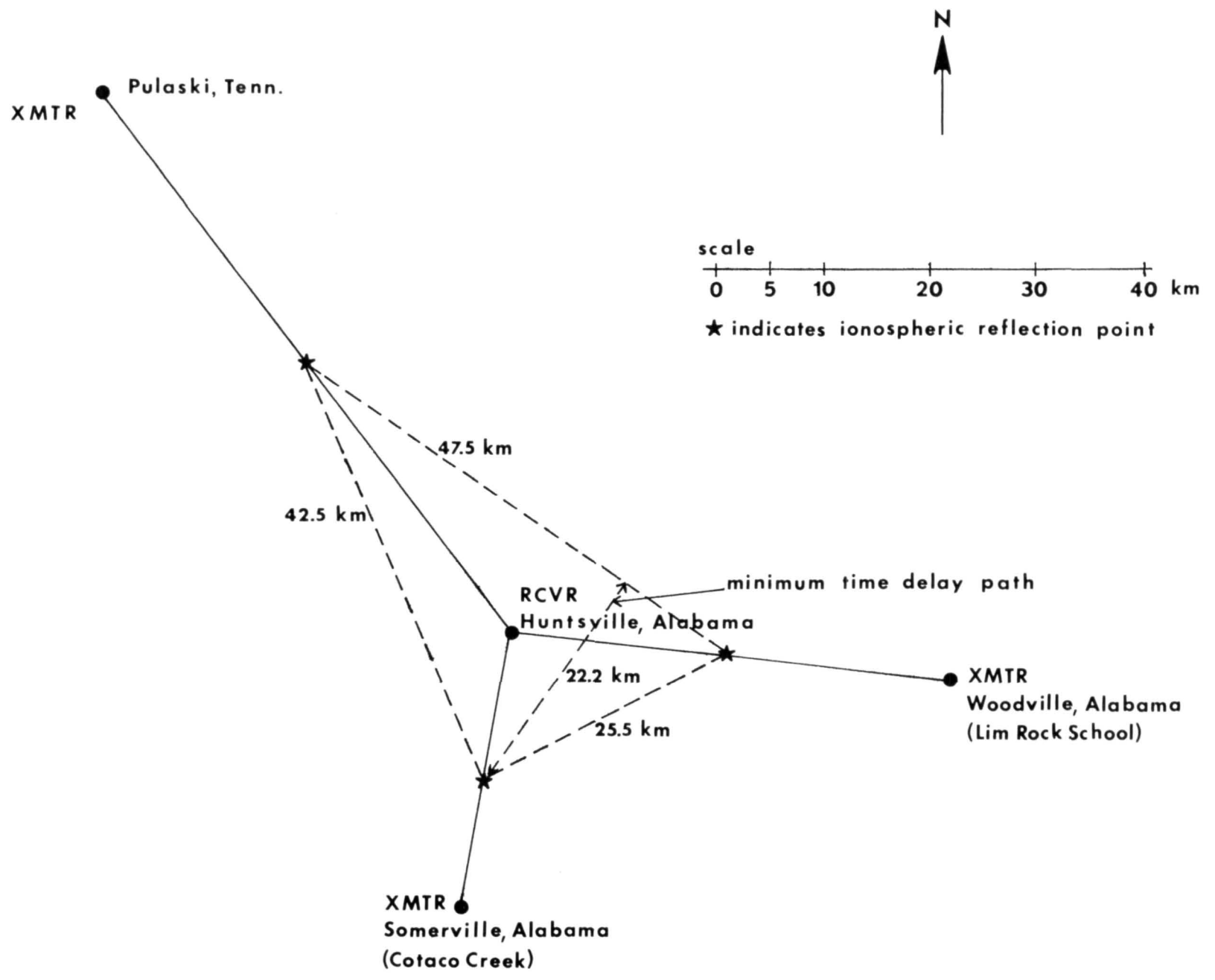


Figure 1 (b): Experimental configuration for monitoring ionospheric perturbations

therefore responsible for this aspect of the observations. The results for the case of thunderstorm induced interactions were few and inconclusive. The expected perturbations due to traveling ionospheric disturbances (TID's) and solar flares (SFD's) were observed in substantial numbers.

The intent of the second year's program was to substantially expand the observing capabilities, so that a three-dimensional, short-baseline picture could be obtained of the ionospheric perturbations which the Doppler sounding technique could observe, and to extend the Doppler data processing procedures to improve frequency resolution and optimize data presentations for different effects. The use of three frequencies over each of the three transmission paths shown in Figure 1 provided continuous monitoring of nine different points in the ionosphere at three different heights.

The results of the second year's program are the subject of this report. In addition to a summary of the experimental operations, detailed discussions of data taken during static firings, and data showing effects related to local meteorological disturbances, appendices containing a log of the data collection periods, and the Fortran listing and description of an acoustic ray-tracing program adapted for use in this study, are included.

II. EXPERIMENTAL OPERATIONS

A. EQUIPMENT

The principal equipment development effort in this program consisted of the installation of transmitter sites at the Pulaski County Airport near Pulaski, Tennessee, and at the Limrock Elementary School, located near Woodville, Alabama. At each of these sites, two 70-foot towers were erected and three inverted vee antennas were installed: two at right angles to each other on one tower, and one on the second tower. Coaxial cables were laid and buried in the ground between the antennas and the three transmitters housed in existing buildings at both sites. Oscillator units, consisting of power supplies and individual crystal oscillators in shielded cans, were fabricated for each location.

Heathkit DX-60A transmitters were employed, but they proved to be difficult to maintain in continuous operation for long periods of time. Utilizing certain suggestions made by John E. Jones of ITSA/Boulder in this regard, and after some additional troubleshooting by Michael Thomas of Avco/Huntsville, they were modified as described in Appendix A. These changes proved to be adequate for continuous operation for periods of the order of weeks. Several Viking Valiant transmitters were also placed into service during the program as replacements for the Heathkits, and these proved to be more easily adapted to the required mode of operation as well as considerably more reliable.

Frequency allocations available for this experiment were 6.185, 5.735, 4.760, 4.081, 2.732, and 1.9985 MHz. At the Cotaco Creek site, the transmitters and oscillators were set to operate at any three of these frequencies, designated here as f_1 , f_2 , and f_3 . At the Limrock site, the transmitters were operated at $f_1 + \Delta$, $f_2 + \Delta$, and $f_3 + \Delta$, while at the Pulaski site they were operated at $f_1 - \Delta$, $f_2 - \Delta$, and $f_3 - \Delta$. Values of Δ ranged from 10 Hz to 2 Hz, the latter value being adopted in the later portion of the program when it became apparent that this provided adequate separation between signals for all except the most drastic Doppler variations. In this format, a single receiver at the Avco/Huntsville receiving site, tuned to frequency f_1 , actually received three signals, all of which were recorded together on a single track of the magnetic tape recorder. The three transmissions clustered about each frequency were not resolved into separate signals until the spectral analysis process, where frequency resolutions of the order of tenths of a Hertz were sufficient to display the independent variations of each transmission. Also in the latter portion of the program a 30 second break in all the recorded data was placed at the beginning of each hour, and this proved to be the simplest and least

confusing method of depositing a permanent time reference on each of the three data channels.

Figure 2 shows a typical 24-hour sequence of Doppler records taken with the Cotaco transmissions only, for three different frequencies during February 15-16, 1968. A log of all the data collection periods in the operation of this experiment is given in Appendix B.

Two microbarographs of the type developed by Claerbout⁶ were built and placed at the Limrock and Pulaski sites, to be operated together with a similar unit built under the earlier RADC program. Several months of data were taken successfully with the RADC microbarograph, which was operated at the Cotaco site and later at the Avco/Huntsville plant. Approximately a month of data was collected with the microbarograph at the Limrock site. Considerable difficulties were encountered with the ink-type strip chart recorders during unattended field operation, and this proved to be the limiting factor in the amount of data collected at the Limrock site as well as the total cause of the fact that no data of any significance was recorded at the Pulaski site.

A narrowband electronic filter was built with an effective bandwidth of 2 Hz, to be used for separation of the three clustered signals at each experiment frequency when conducting spectral analysis of the recorded data at a playback speedup factor of 64 times. This is required for amplitude variation analysis of the individual transmissions, and is easily positioned in frequency over the signal of interest during the processing sequence.

B. DOPPLER DATA RECORDING AND PROCESSING

It developed that the Ampex FR-1107 tape recorder being used to record Doppler data on magnetic tape at the Avco/Huntsville receiving site was capable of operation at two slower speeds than the previously employed 15/16 ips. Either 15/32 or 15/64 ips could be achieved by replacing the existing capstan drive shaft with one having 1/4 the circumference, a standard item available from Ampex. This was done, producing the following three significant improvements in recording and processing procedures:

- (a) One 10-inch reel of magnetic tape covered approximately 49 hours of data, instead of the previous 12 1/4 hours, and the receiving equipment required proportionately less attention for continuous operation.
- (b) Spectral processing at the same playback speed utilized before-- 60 ips--increased the effective frequency resolution by a factor of

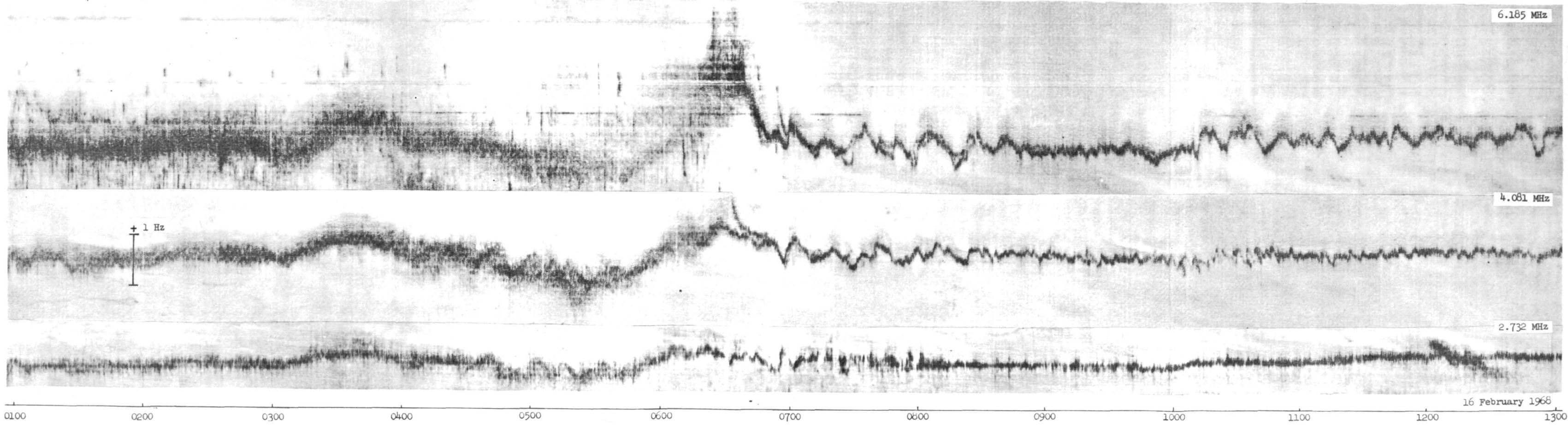
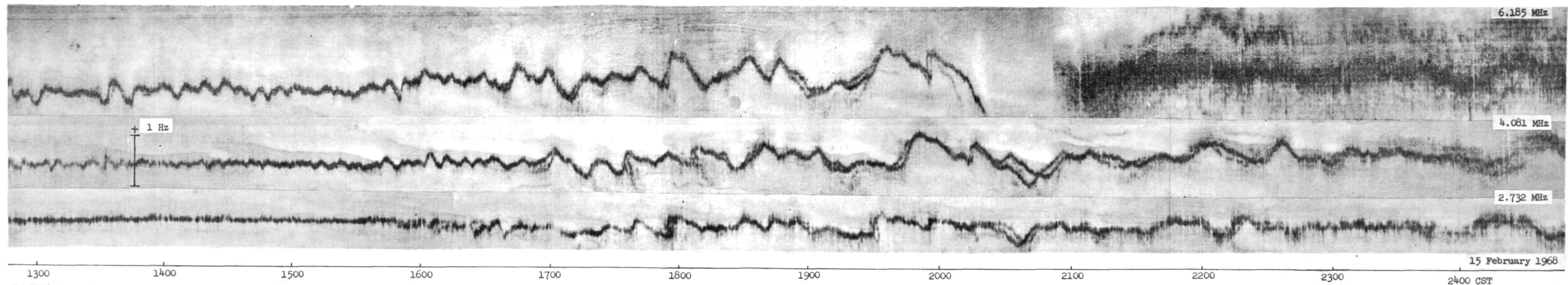


Figure 2: Typical Doppler data record,
15-16 February 1968; Huntsville, Alabama

four, and expanded the frequency scale of the analyzer output (in terms of the Hertz/inch of the resultant spectral record) by the same amount, regardless of the processor involved. This change aided substantially in identifying small Doppler deviations in the recorded data.

(c) Spectral processing time for routine analysis was reduced by a factor of four over that previously required for the same period of data recording.

The only apparent disadvantage of this approach was that the output of the spectrum analyzers is then compressed in time by a factor of four. This has proven to be beneficial in identifying longer-period Doppler variations, however, and could of course be eliminated by slowing the tape playback speed anytime fine time resolution is required.

It became apparent that achieving the same increase in resolution and expansion of the output display for the older data recorded at 15/16 ips would aid tremendously in its analysis also, so it was arranged to re-record selected earlier tapes in a fashion which would allow further effective speed-up in the analysis process. It was then possible to process any of the data tapes at several different speedup factors, with the resolutions and processing times shown in Table 1 for the two most commonly used RADC DRC analyzers.

C. RADAR OBSERVATIONS OF STATIC TEST SHOCKS

One of the features of static tests which seems to be important in consideration of possible resultant ionospheric effects is the propagation of the shock wave generated by the explosive onset of the engine burn. It was suggested by Dr. Gideon Kantor at Avco/SSD that the work of Allen and Weiner⁷ with the EMAC probe concept might be applicable in this context. They examined in detail the possibility of utilizing radar returns from acoustic shock fronts to measure wind velocity, turbulence, and air temperature--the so-called electromagnetic acoustic probing technique.

Previous tests of this concept performed by the Midwest Research Institute were severely limited in observable range by the high acoustic frequency used in the experiment (about 20 KHz). Instead of radar reflections from an acoustic multiple wave train, Allen and Weiner proposed reflections from a single acoustic shock front by coherent integration of the pulsed Doppler radar signal. They suggested propagating an acoustic shock wave generated by a single sinusoidal half-wave pulse whose wavelength corresponds to approximately 100 Hz or lower. At the time of their study, no

TABLE 1. SPECTRAL ANALYSIS PARAMETERS

RADC Data Reduction Center

Wideband Rayspan

Narrowband Rayspan

Processing Time
per data channel

Playback Speedup Factor	Wideband Rayspan				Narrowband Rayspan				Processing Time per data channel	
	Frequency Resolution	Frequency Width of Display	Displayed Hertz per Record Inch	Displayed inches/hour	Frequency Resolution	Frequency Width of Display	Displayed Hertz per Record Inch	Displayed Inches/hour	15/16 ips Recording	15/64 ips Recording
64	3/8 Hz	60 Hz	7.8	8	1/6 Hz	20 Hz	2.6	10 3/4	12 minutes	48 minutes
128	3/16	30	3.9	4	1/12	10	1.3	5 3/8	6	24
256	3/32	15	1.95	2	1/24	5	.65	2 3/4	3	12

such source at significant power levels was available, but the large static tests at MSFC provide both a shock wave at ignition and tremendous energies at the frequency range of interest.

The 15 second firing of an S1B engine on January 25 was monitored using the 3 cm wavelength CPS-9 weather radar available at the MSFC meteorological station, but without any positive results. A second attempt to observe the static test shock, using the MSFC weather radar and the ESSA 10 cm installation at the Madison County Airport, was also unsuccessful.

In their report discussing the problem of obtaining observable radar echoes from shock fronts, Allen and Weiner indicate that the two most crucial factors are the range at which observation is attempted and the electromagnetic wavelength of the radar. In an example which they compute for an FPS-20 radar (23 cm wavelength and 5000 kw peak power output), it is estimated that the maximum range for observation, assuming conditions of low atmospheric attenuation and with no turbulence or steady transverse winds, is approximately five miles. The presence of turbulence decreases the range limit significantly, and transverse winds reduce it drastically. On the matter of wavelength, they demonstrate theoretically that the radar wavelength should be longer than the transverse thickness of the shock front being probed. It is not clear at present what thicknesses are typical for static tests shocks, but for sonic booms the thickness appears to be on the order of 1-20 cm^{8,9}.

Applying these facts to the static test situation, it seems possible that the MSFC weather radar may operate at too high a frequency (3.2 cm), and it seems likely that the ESSA radar is too far distant (approximately 10 miles with 60 kw) even though its frequency is more appropriate (10 cm). Allen and Weiner had also suggested that coherent detection techniques be employed to enhance observation of any moving fronts, and neither radar employed here had that capability.

III. STATIC TEST RESULTS

One of the prime initial motivations of the Huntsville experimental Doppler sounding program, and the aspect of the study which has been the subject of the principal effort to date, is the idea that the release of energy during the static firing of a large rocket engine on the ground might be sufficiently great to produce a measurable perturbation in the ionosphere, at least directly overhead the location of the test. The results of several other earlier experiments encouraged this. In 1966 Marcos¹⁰ reported that it was possible to generate an ionospheric perturbation, detectable with vertical incidence Doppler sounding techniques, by flying a supersonic aircraft in a trajectory which focused the resultant shock front at a point in the upper atmosphere. In the same year, Barry, Griffiths, and Taenzer¹¹ reported that substantial, predictable ionospheric perturbations were observed by vertical incidence phase sounders following the explosion of 500 tons of TNT at ground level. So the possibility of low frequency waves propagating upwards into the ionosphere from a source with sufficient energy at the requisite frequencies was clearly established.

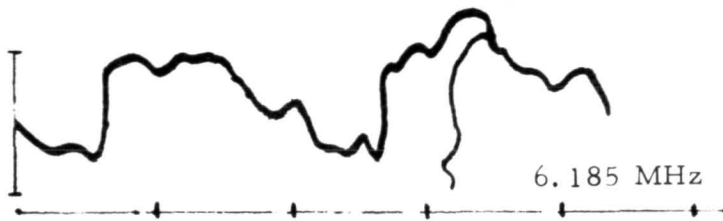
During the course of the first phase of this program, the fact that several static tests firings had previously been monitored elsewhere for the purpose of detecting possible ionospheric effects came to light. The details of these tests and their effects were described in an earlier report⁵, but the essence of these results is repeated here for the sake of completeness. In the winter of 1964-65 Stanford Research Institute personnel monitored three static firings of solid fuel, one million pound thrust engines, near San Francisco, California, using a vertical incidence swept-frequency ionosonde located 48.5 km from the test stand¹². In each case clear evidence of Sporadic-E-like traces appeared following tests, at frequencies considerably higher than any background Sporadic-E otherwise observed. The onset times of this phenomenon varied considerably, and will be discussed in more detail below. For two of these tests, fixed frequency vertical incidence phase path sounders were also operated on several frequencies at varying distances from the test stand, and positive indications of ionospheric perturbations were obtained in the resultant phase records, although the details of these variations have not been reported. In February 1966 a vertical incidence ITT phase sounder was operated at four frequencies during the static firing of a 3.6 million pound thrust, solid fuel engine near Miami, Florida. Notable perturbations appeared in the phase data on all four frequencies, and unusual and significant Sporadic-E-like echoes were also observed in the records, which were taken some 60 km from the test stand.

With these results in mind, the Doppler records taken during 30 static rocket engine tests at NASA/MSFC have been processed and analyzed in detail in an

attempt to identify ionospheric perturbations associated with the ground level firings. The particular booster engines involved are the F1, the S1B, and the S1C, with 1.5 million, 1.6 million, and 7.5 million pounds of thrust, respectively. It was decided, on the basis of considerable experimenting with various frequency and time scales for presenting the Doppler records, that the output of the narrowband Rayspan analyzer at a speedup factor of 128 times was the most useful for analysis of static test period data, representing an expanded frequency scale without excessive time compression of the data, and this processing format was utilized to produce the uniform set of static test Doppler records presented in Appendix C.

Thirteen of the test records show secondary traces which can be considered as being possibly due to vertically propagating wave motions generated by the static tests. For ease of analysis the candidate signal traces have been extracted from these thirteen cases and reproduced in Figures 3 through 6, with approximately 50 minutes of record being given in each case from the time of onset of the test. A great deal of consideration and visual analysis of the data records has gone into the selection of these candidate effects. Most of the data sequences were spectrally analyzed a number of times with differing processing gains in an attempt to positively identify the existence of any small amplitude secondary traces which may have been present. An illustration of this process is found in Figures 40 (b) - (d) in Appendix C, in which the same segment of data is reprocessed with three different gain settings. The candidate traces selected from these figures are shown in the 10 May 1968 case in Figure 6. Since, as is evident after even a cursory review of the data presented in Appendix C, any effects which may be associated with the static tests are of the same or smaller Doppler deviation magnitude than the perturbations which occur naturally on the Doppler records, and since they may also be of smaller signal intensity, the selection process leading to the data presented in Figures 3-6 is necessarily subjective and based on the analyst's experience with vertical incidence Doppler data and his educated judgment of what the various signal traces and their variations represent.

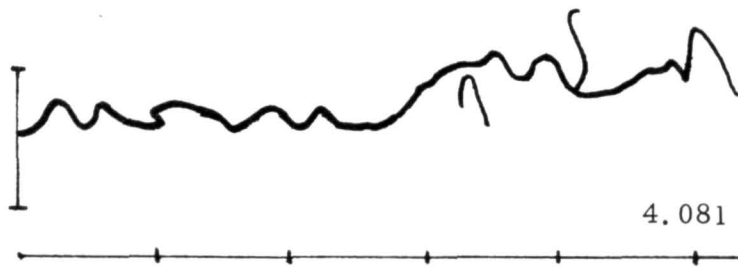
With these qualifying statements in mind, it is useful to consider the common characteristics present in the secondary traces shown in Figures 3-6, in an attempt to consider what they may indicate collectively concerning their relationship (if any) to the static firings which they follow. First, the frequency shifts of the candidate traces show a negative Doppler deviation, which is what should occur for perturbations moving away from the observer. Second, the secondary traces can be conveniently grouped into three classes: (a) those which begin with a large negative deviation with respect to the main signal trace, and then show a decreasing amount of negative Doppler with time until they merge with the main trace; (b) those which begin at the main signal trace and show with time an increasing amount of negative Doppler deviation with respect to the main signal; and (c) those which are never connected with the



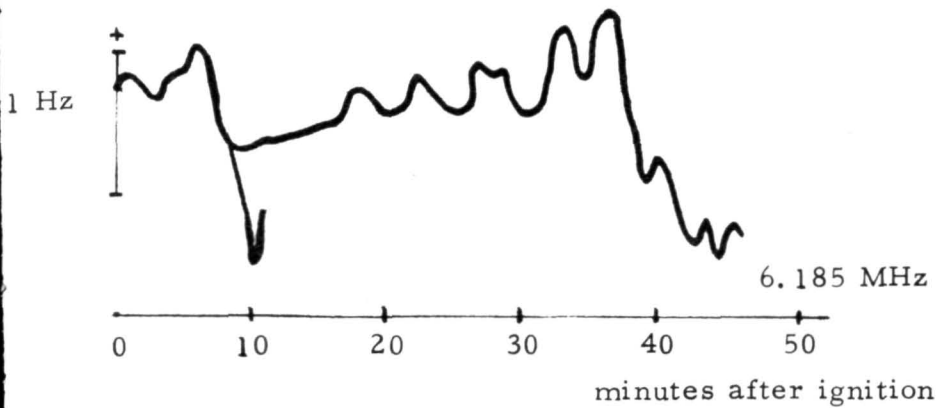
20 April 1967 F1-61
1301 CST 40 sec



19 May 1967 F1-62
1328:06 CDT 25.0 sec

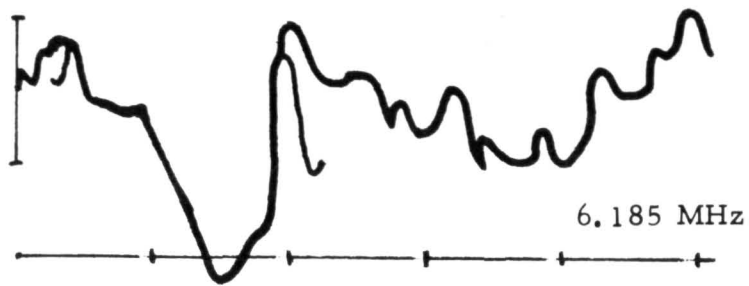


14 June 1967 F1-65
1400 CDT 41 sec



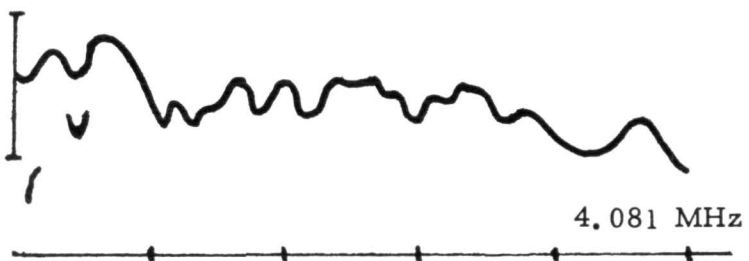
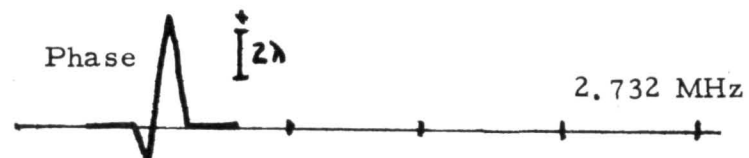
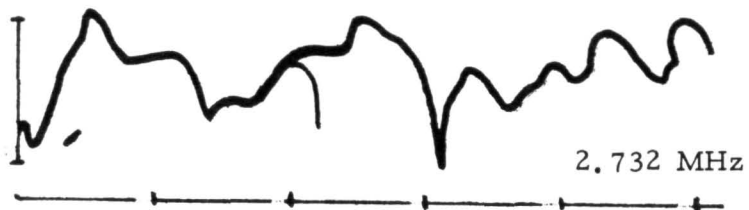
1 August 1967 SIC
1500 CDT 3 sec

Figure 3: Tracings of Doppler data records, showing effects due to MSFC static rocket tests



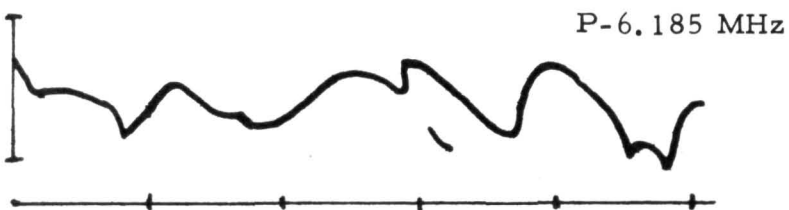
3 August 1967
1920:00 CDT

S1C
40 sec



16 August 1967
1352 CDT

F1-68
41 sec



26 October 1967
1311:57 CDT

F1-72
43.7 sec

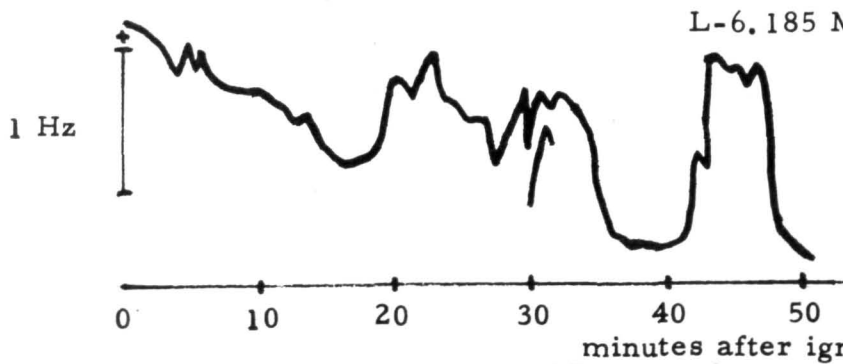
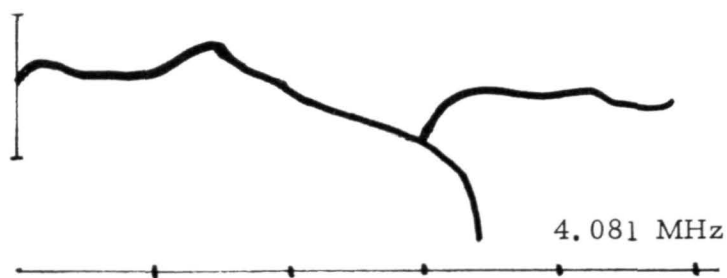
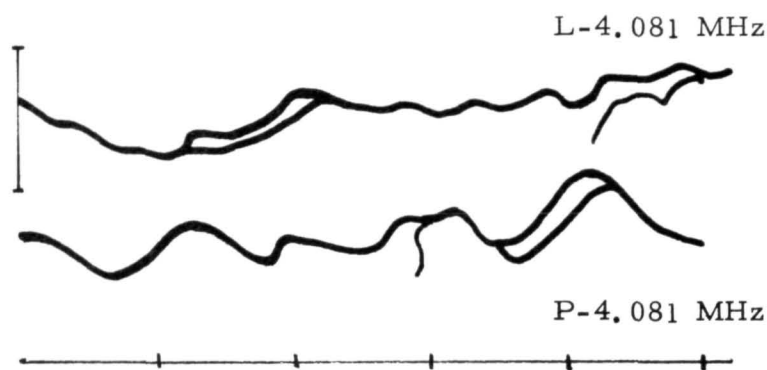


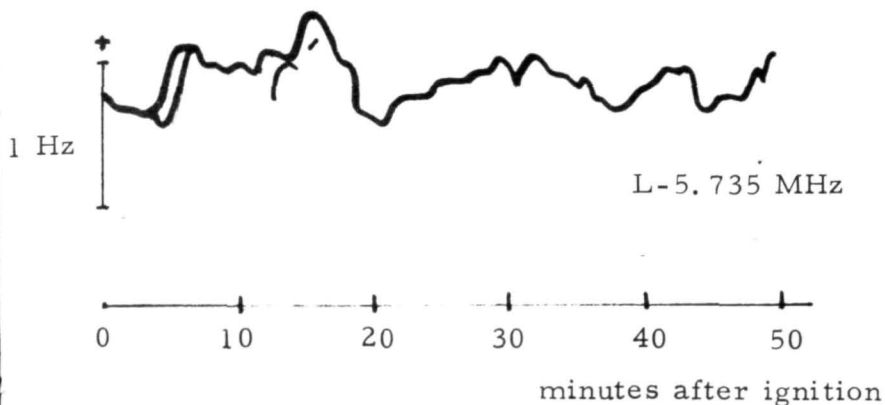
Figure 4: Tracings of Doppler data records, showing effects due to MSFC static rocket tests



19 December 1967 SIB-48
 1640:24 CST 35.50 sec



6 February 1968 SIB-50
 1640 CST 15.46 sec



20 February 1968 F1-76
 1440 CST 25.56 sec

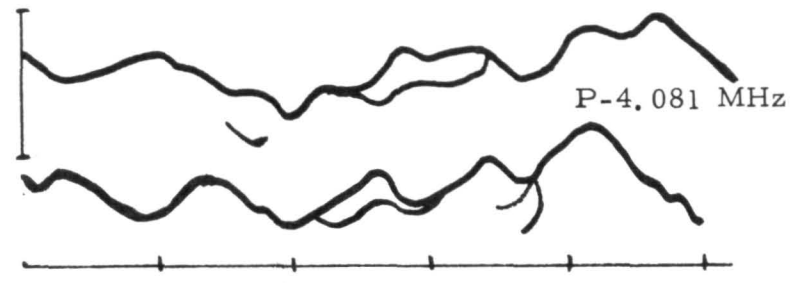
Figure 5: Tracings of Doppler data records, showing effects due to MSFC static rocket tests



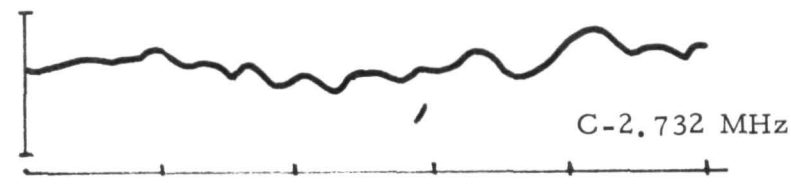
21 February 1968 SIB-52
1640 CST 3.00 sec

C-5.735 MHz

L-4.081 MHz

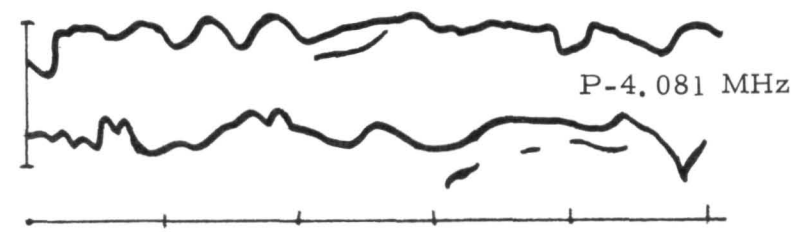


P-4.081 MHz



C-2.732 MHz

C-4.081 MHz



P-4.081 MHz

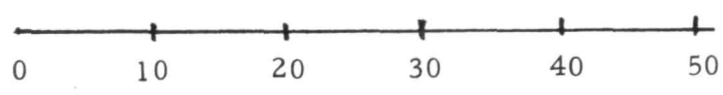
9 April 1968 SIB-53
1639:59 CST 35.30 sec



L-5.735 MHz

C-5.735 MHz

10 May 1968 F1-80
1458 CDT 90.74 sec



minutes after ignition

Figure 6: Tracings of Doppler data records, showing effects due to MSFC static rocket tests

main trace, but which occur for only a brief period and/or have an essentially constant negative amount of Doppler deviation with respect to the main trace.

The 20 April 1967 data is an example of the first type; the effects in the 3 August 1967 data which begin approximately 20 minutes after the onset of the test are an example of the second group; and the Limrock data for the 21 February 1968 test exhibits behavior of the third category.

The first two types of effects are suggestive of the presence of an overdense rising reflecting surface. In the first case a second reflecting raypath is established (not necessarily at vertical incidence) from the rising surface before it reaches the height of reflection of the main (and undeviated) signal. Due to refractive effects, as the height of reflection of this secondary surface nears that of the undisturbed raypath, the effective Doppler shift is decreased, until the two signal traces merge when the rising surface passes through the undisturbed reflecting region. In the second case, the secondary reflection is not established until after the rising front passes through the undisturbed reflection region, and it then continues to maintain a second raypath (probably at oblique angles) as the refractive effects of the reflecting region are diminished and the Doppler deviation reaches larger values more representative of the velocity of the frontal surface. This latter situation is similar to the effect observed when the principal vertical incidence reflection signal is lost at night due to the decrease of foF2 below the operating frequency, a good example of which is seen in the 6.185 MHz data shown in Figure 2 around 2000 CST.

The third class of traces, unlike those of the first two groups, show signal strength amplitudes similar to those of the main undisturbed traces, and exhibit a negative Doppler shift which does not meet at any point with the main trace. These suggest the formation of dense Sporadic-E-like clouds which move away from the test stands and the Doppler sounding path. It should be noted in this regard that the Sporadic-E-like echoes which were observed by SRI following the static tests which they monitored increased in apparent range with time, indicating either vertical propagation or (more likely, given that the sounder, located 48.5 km from the test stand, was probably receiving the echoes at oblique incidence) horizontal motions away from the observing region.

One fact to be noted about the data in Figures 3-6 is that none of these secondary traces is, unfortunately, unique to the static test period data (although their occurrence in general is rare), and one may draw one of two conclusions from this fact: either (a) these traces are not related to the static test occurrences, or (b) there are other sources of vertically propagating waves in addition to static tests. In any case, these traces are definitely not similar to those associated typically with horizontally traveling atmospheric waves, sometimes called traveling ionospheric disturbances (TID's).

One other parameter to note is the length of time elapsing between the static firing and the onset of the ionospheric effects. The travel time for a vertically

propagating sound wave to reach an ionospheric height of 200 km from the ground should be on the order of 10 minutes, assuming an average sound speed of 300 m/sec. But no consistency is found in the candidate effects in this regard. Several of the apparent perturbations begin within a few minutes after the start of the test firing. Some occur within 10 to 20 minutes after the firing, which would be reasonable for simple acoustic propagation, and a number appear to onset after a 30 minute delay. Here again it is useful to consider the results of other experiments, and the data presented schematically in Figure 7 is intended to show the various delay times of the ionospheric effects which followed the aforementioned static rocket firings monitored by SRI and ITT, as well as the data obtained by Barry, Griffiths, and Taenzler of Stanford Research Laboratories (SEL) following the ground level explosion of TNT. It can be seen that time delays of the three basic orders observed in the Huntsville data also occurred in these cases. (The dotted lines extending from the E_s occurrences in the ITT data are intended to indicate that data records before and after the intervals covered by the solid lines were not available for analysis.)

More recently, Kaschak has reported on the times of arrival of low frequency acoustic waves at long distances from the trajectories of large launched rocket engines ¹³, showing the propagation of acoustic waves with supersonic velocities (500-1000 m/sec) and subsonic velocities (190-240 m/sec), in addition to the more usual waves with group speeds of the order of 300 m/sec. Further, any combination of one, two, or all of the three types of propagated waves may be observed following a particular launch. (Unfortunately, it has not been possible to date to detect acoustic waves associated with static rocket firings at long distances ¹⁴.) Thus, although the physical understanding of either the supersonic or subsonic wave propagation is at present lacking, it is clear that the firing of large rocket engines can produce waves of all three speed classes, and that the existence of these types of propagation can be used to explain the differing time delays found in the Huntsville observations.

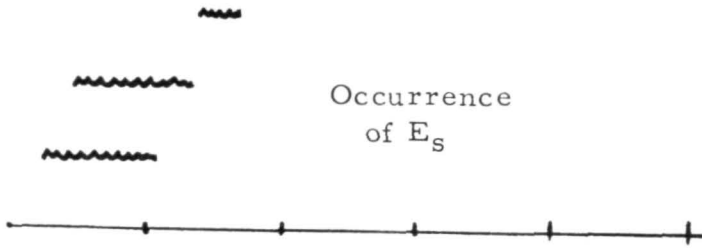
It should be noted here that the Huntsville static firings did not produce any notable effects in microbarograph records taken during the six tests for which such data was available. This seems reasonable in view of what is known of the acoustic spectra of static tests, given the 30 second period upper frequency cut-off of the microbarograph sensors.)

From the preceding discussion, then, it is possible to suggest a model for the occurrence of atmospheric effects following ground level static tests of large rocket engines. Since the acoustic spectra of the burn period of static tests does not show adequate energy at frequencies sufficiently low enough to support propagation to high altitudes ⁵, it can be concluded that any upper atmospheric effect must be due to the shock waves generated at engine ignition and/or cutoff. These waves presumably degenerate into linear acoustic waves

SRI Tests: C-4 ionosonde
(48.5 km distant)

17 December 1964 1345 PST
12 February 1965 1055 PST
21 April 1965 1159 PST

Occurrence
of E_s

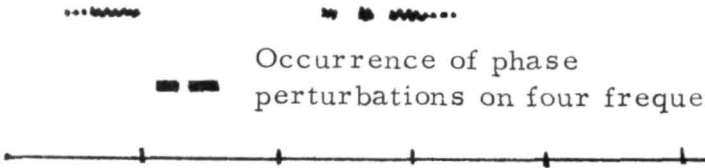


ITT Tests: Vertical-incidence
phase sounder with
four fixed frequencies
(~ 60 km distant)

24 February 1966 1901 EST

Occurrence of E_s at 2.6 MHz

Occurrence of phase
perturbations on four frequencies



SEL Test: Two vertical-
incidence phase
sounders with two
fixed frequencies each.
(85 km distant, in
opposite directions)

17 July 1964 1058 MST

Occurrence of phase perturbations
5.5 MHz

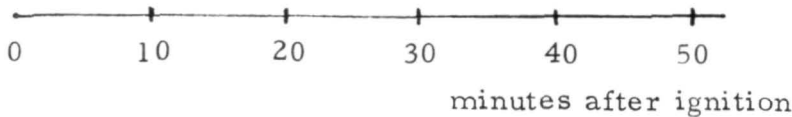


Figure 7: Schematic representation of onset times for other measurements of static test and explosion effects

(with a range of velocities) at some distance from the test location, and continue to propagate essentially vertically up through the ionosphere ¹¹. On some occasions the vertical temperature profile and the sequence of horizontal wind shears existing between the ground and the lower ionosphere are of such a nature that acoustic energy is not permitted to reach E or F region heights in detectable amounts. (See a discussion of this point in Appendix D.) On other occasions, conditions are favorable for the formation of Sporadic-E-like clouds, which move away from a position directly over the test stand with the wind speed prevalent at their height of formation. On yet other occasions a detectable wave continues to propagate to F region heights and produces a vertically propagating reflecting surface as it passes through the reflection region of the main signal. The velocities of propagation of the detected perturbations present a physical puzzle, but the SRI, ITT and Kaschak results present convincing evidence of both subsonic and supersonic acoustic wave propagation in addition to the expected sound speed motions.

One more interesting point should be considered here. In all the Doppler records showing perturbations following NASA/MSFC static tests, the candidate traces are of a secondary nature, existing in addition to the main and undisturbed signal return. In the case of the Barry, Griffiths, and Taenzer phase data, and in the two available cases of phase path records taken during static rocket tests (the ITT record of the 24 February 1966 test and the Avco phase-locked loop data of 3 August 1967 given in Figures 46-47 of Appendix C), the apparent phase perturbations appear in the principal reflected signal, and no secondary echoes or signals of any type are observed. Also, in these latter two cases the maximum Doppler shift calculable from the phase data is less than 0.1 Hz, and in the case of the ground level TNT explosion the maximum Doppler shift would approach 1.5 Hz (since the explosion contained rather large energies at much lower frequencies than is the case of static tests⁵).

It seems therefore that if a simple acoustic wave were propagating upward with normal sound speed from any of the Huntsville static tests, it might not be observed in the Doppler records due to the small frequency shift which it would likely produce. Thus perhaps the only effects which might be observed in addition to Sporadic-E would be the motions of secondary reflecting fronts whenever they might exist and if they possessed sufficient density perturbations. This is because the Doppler measurement technique is particularly sensitive to signals being returned with substantial frequency shift, even though the signal strength amplitudes of the returns may be small. It seems clear that, with the difficulties apparent in relating small Doppler perturbations to specific static tests, a vertical incidence phase sounding measurement approach would be strongly recommended for any further investigations of this nature.

The evidence amassed in this section for the existence of ionospheric perturbations generated by the static firing on the ground of large rocket engines

leads convincingly to the conclusion that such coupling can occur. Taken individually, the Doppler data records collected in the Huntsville experimental program are not adequate to demonstrate this coupling, but taken together as a group they do permit the conclusion that low frequency acoustic waves can propagate from the static test event to ionospheric heights and create observable Doppler perturbations there. It may also be stated that strong evidence exists for modes of acoustic wave propagation at both supersonic and subsonic speeds.

IV. THUNDERSTORM OBSERVATIONS

As a result of an initial suggestion made by Pierce and Coroniti¹⁵, one of the purposes of this experiment has been to look for ionospheric Doppler variations which might be related to meteorological phenomena. Various indirect evidence, largely statistical, for relating meteorological and ionospheric effects has been presented over the years (a summary is given in Reference 5), but until recently no evidence linking specific disturbed weather conditions with specific ionospheric events had ever been presented.

The concept of Pierce and Coroniti grew out of the fact that certain frequencies of atmospheric pressure oscillations are preferred for vertically propagating pressure waves³, and these are present in significant magnitudes in the thunderstorm cloud-top oscillation data reported by Anderson¹⁶. There is now some doubt as to whether the vertical motions of individual cumulus towers possess sufficient energy (although Pierce and Coroniti estimate 10^{17} ergs for a single oscillating cumulus tower) to produce detectable effects at ionospheric heights. Nor do the thunderclaps occurring in meteorological storms possess sufficient energy at low enough frequencies to generate ionospheric disturbances¹⁷. But as a result of Pierce and Coroniti's suggestion, Georges of ITSA/ESSA began looking in his steep incidence Doppler sounding records (taken on a network of paths surrounding Little Rock, Arkansas) for variations related to meteorological phenomena, and reported twelve instances in which he observed extended sequences of otherwise rare oscillations with three to four minute periods^{3, 18}. And in each case he found strong echoes in weather radar data taken in the vicinity of his observing stations. According to Georges, these oscillations can persist intermittently for several days, have no apparent connection with geomagnetic or solar activity, exhibit an apparent upward phase velocity when seen on multi-frequency soundings, and are sufficiently localized geographically as to appear only on those paths of his network which are themselves located over the radar-indicated disturbance region. In every case of the appearance of these oscillations on the Doppler records which he examined, a weather disturbance was also present; the converse was not true, however.

The Huntsville Doppler records have since been examined for evidences of similar three-to-four minute period oscillations, with a number of occurrences being found. Figure 8 shows a 2.735 MHz vertical incidence cw phase record taken with the Avco phase-locked loop device which was tested for a short period at Huntsville⁵. Thunderclouds were visible shortly after 1400 CDT, as indicated by site personnel on the record, and the hourly weather radar summary plots for this day show signs of disturbed weather conditions developing over Huntsville between 1345 and 1445 CDT. The phase oscillations exhibit periods between two to three minutes,

Phase Path Variations

2.732 MHz

Huntsville, Alabama

18 August 1967

-23-

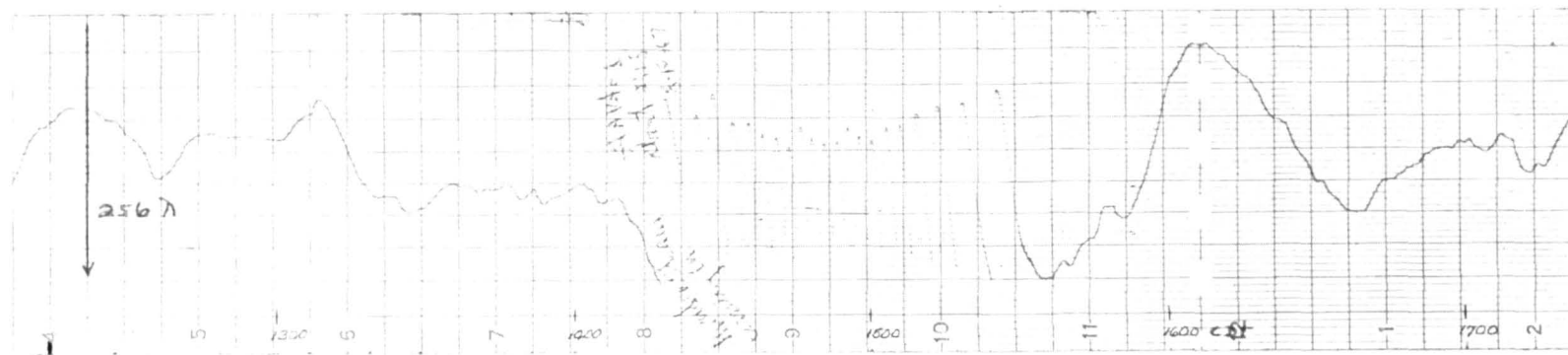


Figure 8: Phase-locked loop data showing thunderstorm effects, 18 August 1967: Huntsville, Alabama

and cease at about 1530; the weather radar records show a removal of the disturbance from the Huntsville area between 1545 and 1645 CDT. The vertical incidence Doppler records taken during this period did not give any positive indication of similar oscillatory behavior, however.

Figures 9(a)-9(d) contain twenty hours of Doppler records which exhibit the most marked occurrence of 3-5 minute period oscillations observed in the data collected at Huntsville. The oscillatory behavior begins at about 2200 CDT on 15 May 1968 and lasts to 0630 CDT on 16 May. The weather radar summary charts first show disturbed regions over the Huntsville area on the 2245 CDT hourly map for 15 May, and these continue until the 1145 CDT map the following day. There is an abrupt cessation of the Doppler oscillations at sunrise, even though the storm activity continues into the morning.

The most remarkable feature of this record is the fact that for each frequency on which these oscillations are visible, they are in phase (within the 30 seconds resolution of these particular records) on the two or three transmissions present. This means that the ionospheric reflection regions under surveillance at each frequency are moving up and down together under the influence of a vertically propagating wave. That this effect could not be produced by any horizontal wave motion can be seen by considering the horizontal separation distances of the three ionospheric reflection points shown in Figure 1 (b). Even at the sound speed of 300 m/sec, it would take on the order of $2 \frac{1}{2}$ minutes for a horizontally propagating wave to travel between the Pulaski and Limrock path reflection points. Or in the worst case, if a wave were moving horizontally in a direction perpendicular to the line between the Limrock and Pulaski sites, at 300 m/sec it would take 74 seconds for it to pass from the reflection points of those two paths to that of the Cotaco path (along the line marked "minimum time delay path"). Thus the oscillations must be due to vertically propagating wave motions with periods of 3-5 minutes. In contrast, the oscillations present in the Doppler records before 2000 CST, at which time the Fredricksburg magnetograms show mildly disturbed behavior, are out of phase by the order of minutes on any given frequency. The magnetic disturbance condition subsides after 2000 CST, and no indication of magnetic activity is present during the 3-5 minute period oscillations sequence.

Figure 10 contains $5 \frac{1}{2}$ hours of Doppler records taken on 11 March 1968, showing the beginning of a sequence of 3-4 minute period oscillations beginning at about 1950 CST in the higher frequency records. A tornado was sighted near Huntsville at about 2000 CST, and the weather radar summary charts show the first signs of severe weather disturbances in the hourly map issued at 1945 CST; these continue to at least 2345 CST. (No Doppler data was recorded after 2302 CST.) No indication of disturbed magnetic conditions is present in the Fredricksburg magnetograms for this period, and again the oscillations are in phase for each frequency on which transmission were recorded.

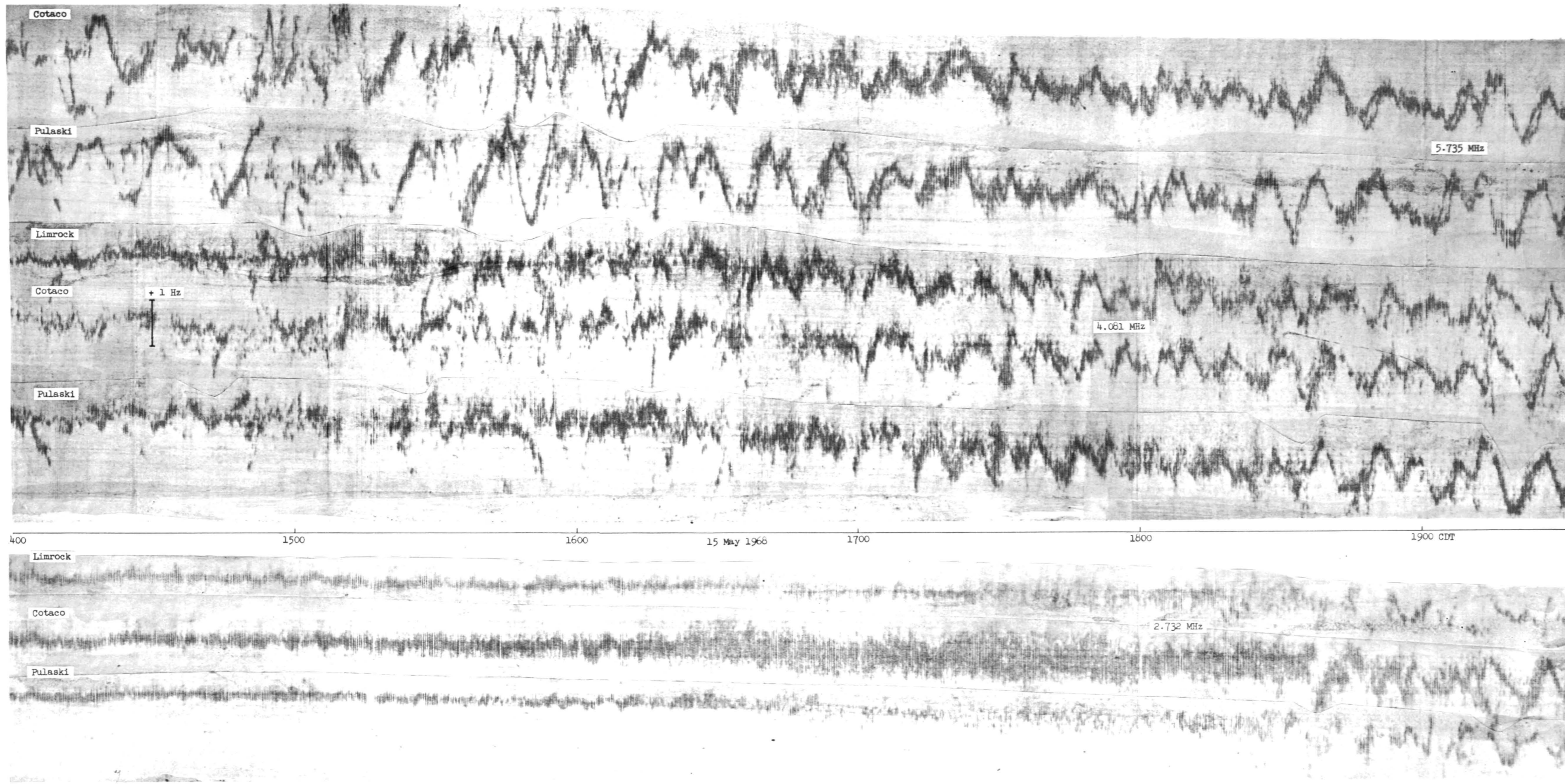


Figure 9 (a): Doppler data showing thunderstorm effects,
15-16 May 1968: Huntsville, Alabama

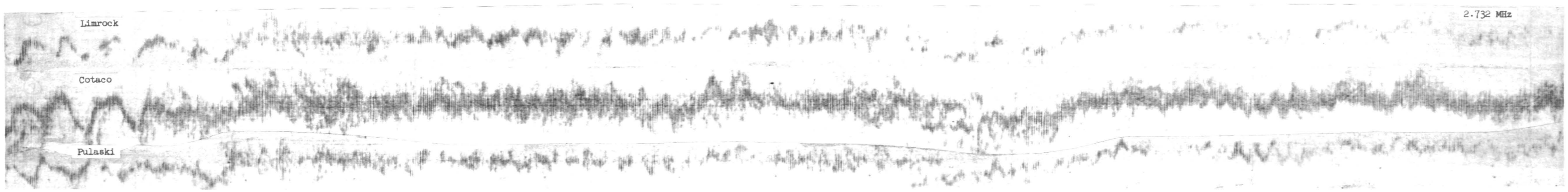
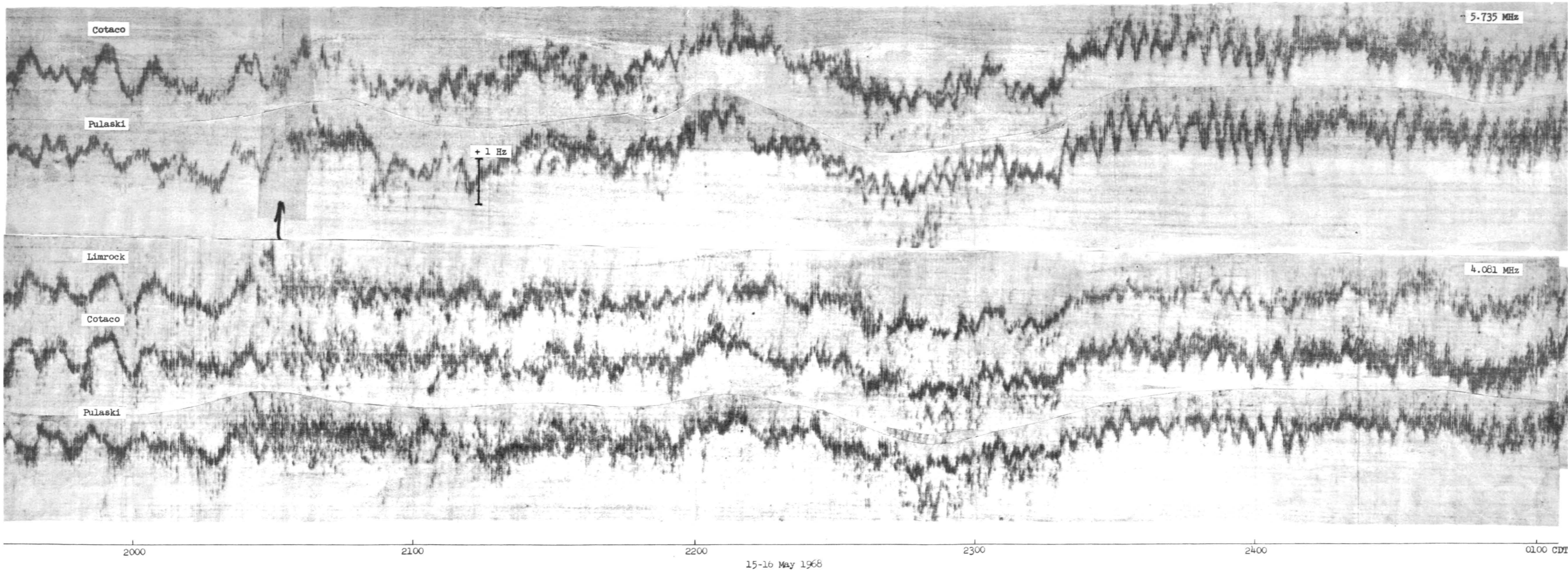


Figure 9 (b): Doppler data showing thunderstorm effects,
15-16 May 1968: Huntsville, Alabama

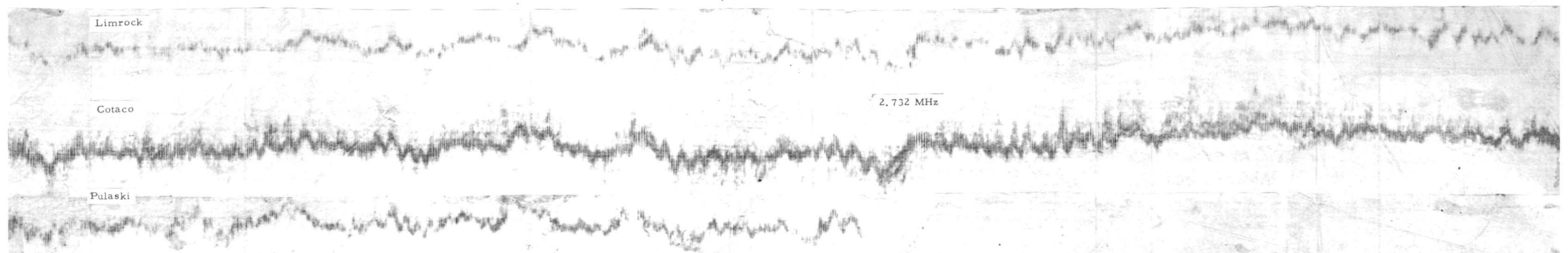
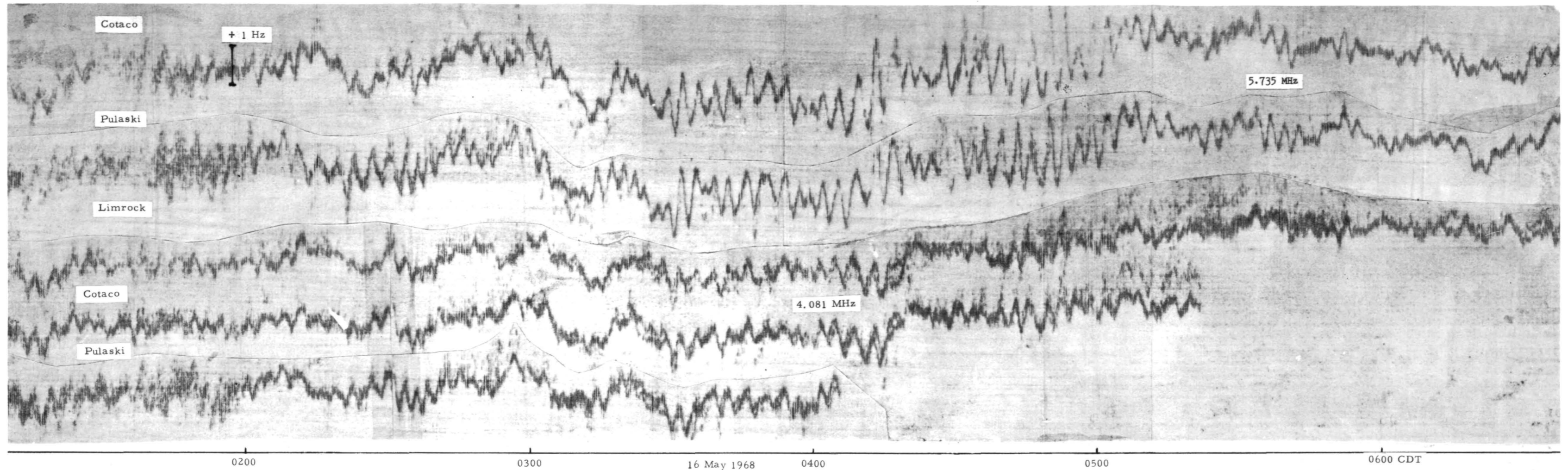


Figure 9 (c): Doppler data showing thunderstorm effects,
15-16 May 1968: Huntsville, Alabama

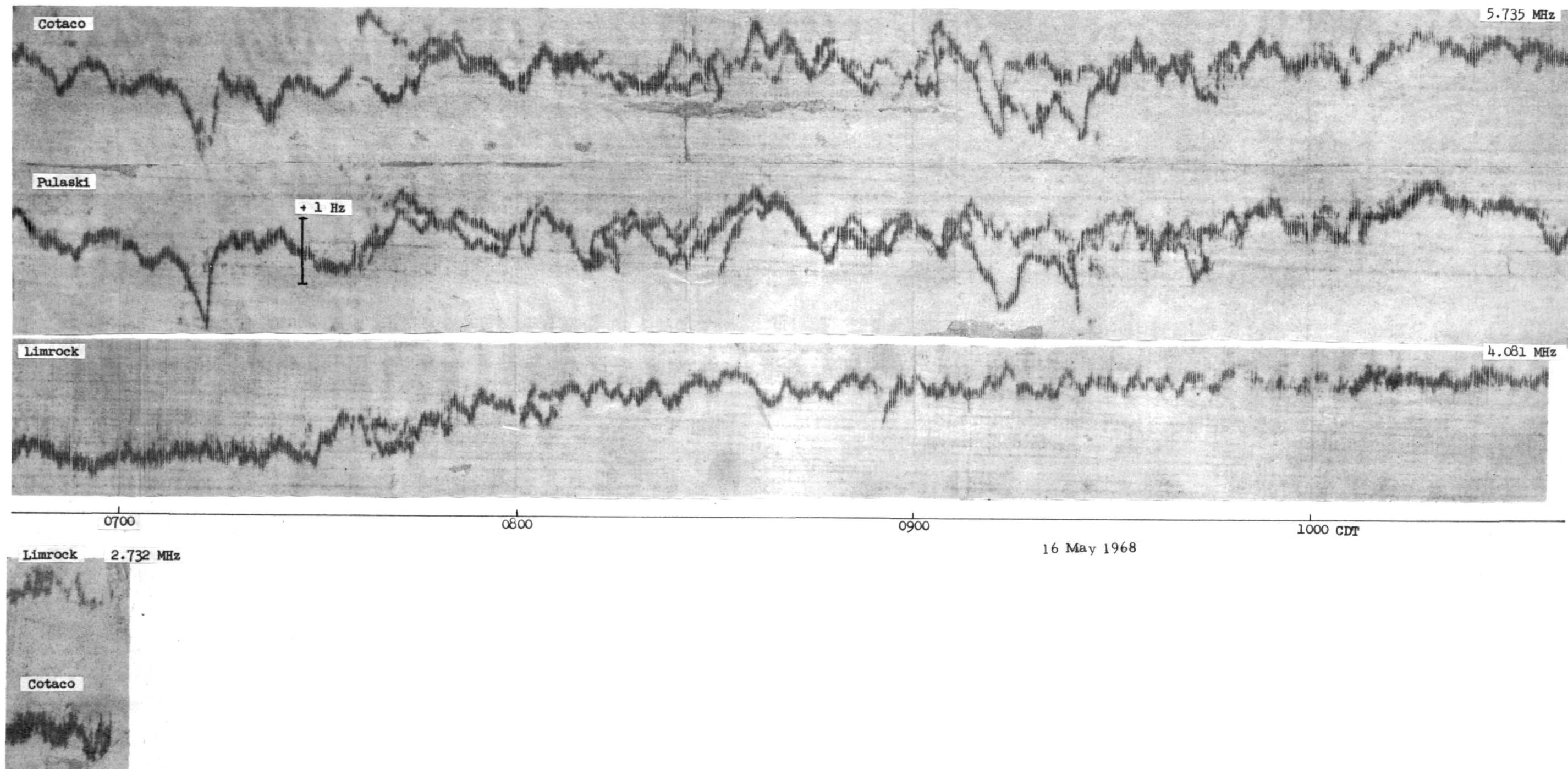


Figure 9 (d): Doppler data showing thunderstorm effects, 15-16 May 1968: Huntsville, Alabama

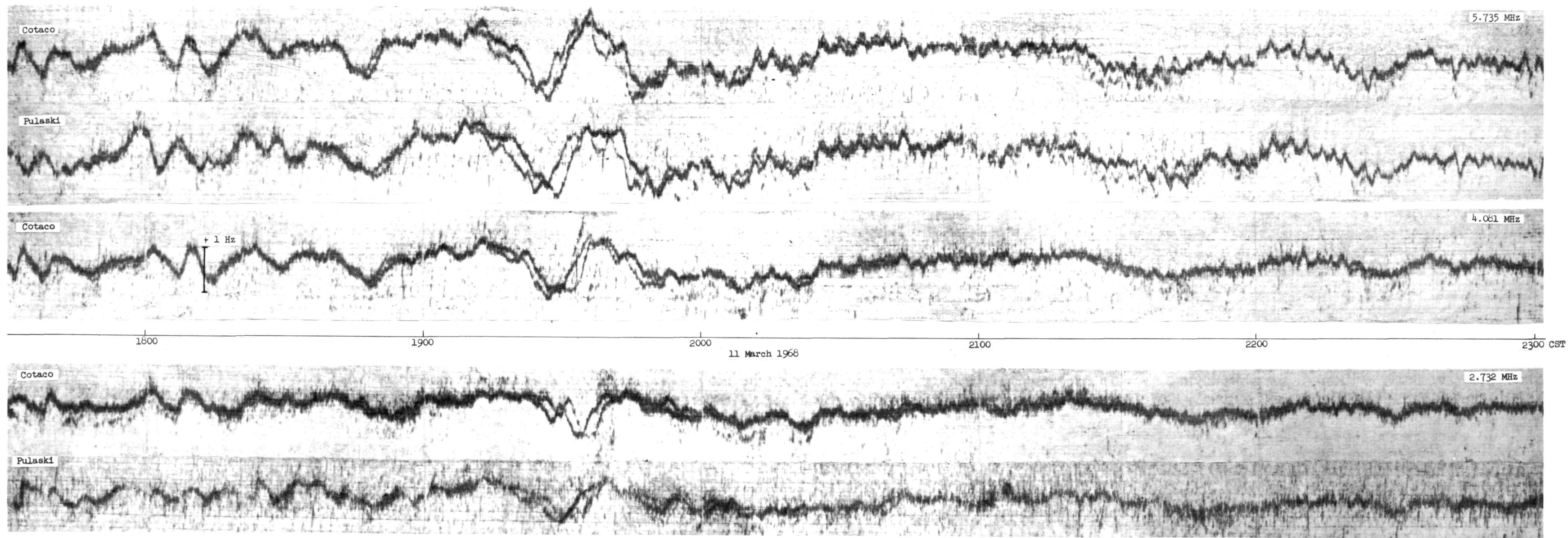


Figure 10: Doppler data showing thunderstorm effects,
11 March 1968: Huntsville, Alabama

It is important to note that without the presence of three simultaneous and spatially separated transmissions on a single frequency, it would not be possible to positively identify the existence of vertically propagating waves. For example, with two paths it could always be conjectured that a horizontally propagating wavefront was in operation with a fortuitous directional orientation that caused it to onset at both reflection points at essentially the same instant of time. But this cannot be the case when the oscillations show phase concurrence over three different paths with reflection regions separated by distances between 26 and 48 km. Thus, these data provide the first positive identification of the vertically propagating nature of the waves associated with the characteristic 3-5 minute oscillatory periods.

Not all the Doppler data recorded during the entire Huntsville experimental program has been reprocessed with the expanded frequency scale spectral analysis which is necessary to detect these small oscillations, so no statistics of occurrence of this phenomenon are available at this reading. The next step in any further analysis of the meteorological coupling phenomenon using this data would be to survey all the Doppler records (after they have been appropriately processed) for occurrences of these oscillations. Then the hourly weather radar summary charts should be scanned during all the hours that the Huntsville Doppler sounding experiment was operated, and a list compiled of all the times during which severe weather disturbances were present in the Huntsville area. The size of the logical intersection of these two sets of data, compared particularly with those cases in which Doppler oscillations were observed when no weather disturbances were extant, would then provide a measure of the confidence that should be placed in the interpretation that these oscillations are indeed caused by thunderstorms below. Those periods in which thunderstorm activity occurred without producing detectable ionospheric oscillations -- and these should be numerous -- would likely indicate the presence of conditions in the temperature and wind profiles of the intervening atmosphere which inhibit the upward propagation of acoustic waves at these frequencies.

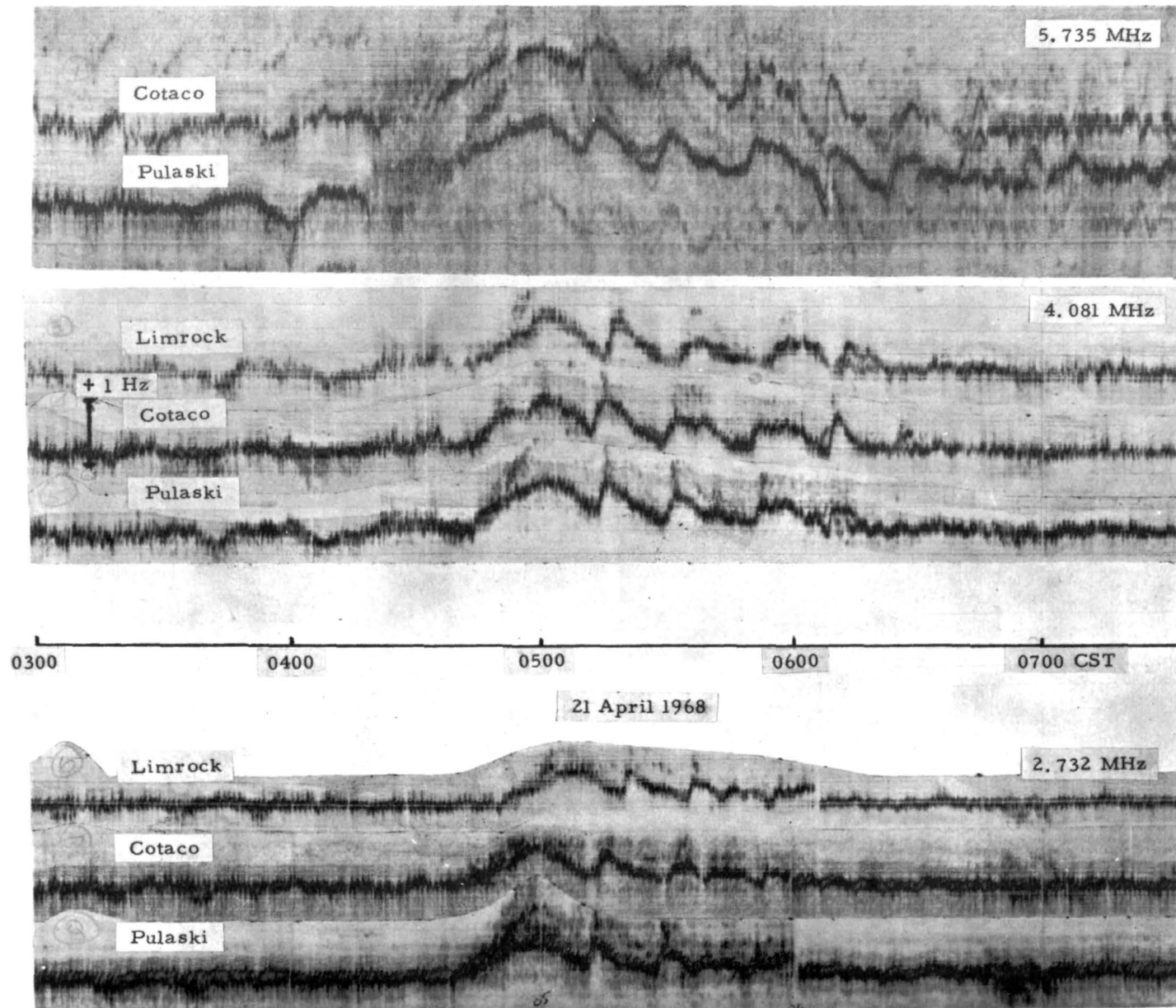
The evidence of Georges and the results detailed above, lend considerable weight to the identification of the 3-5 minute period oscillations in the Doppler records as indications of tropospheric-ionospheric coupling through the mechanism of long period acoustic waves. Further analysis along the lines discussed above, and additional measurements during months when storms are characteristically frequent, should aid in evaluating this tentative conclusion.

V. OTHER PHENOMENA

Three other types of Doppler perturbations are worth noting, because their unique appearance clearly signals their presence when they occur. On some mornings following ionospheric sunrise, a sequence of long period oscillations is present for an hour or so, as illustrated in Figure 11. Here the variations have a period of approximately 20 minutes, and persist for perhaps 70 minutes. On the day previous to this record, no oscillatory behavior of note is observed during or following sunrise. Both of these days are among the five magnetically most quiet days in April, and no indications are present on the Fredricksburg magnetograms to distinguish the two sunrise periods. The relationship of these apparent motions to the occurrence of sunrise seems fairly clear, but no explanation is presently available for their generation or, for that matter, their lack of generation, on any particular day.

Figure 12 shows some 12 hours of Doppler records, the feature of interest being the spreading in the Doppler signals occurring on all frequencies between 0000 and 0300 CST. The magnitude of the spread increases with signal frequency, and all the traces show the presence of several very long period oscillations, the amplitude of which also increases with frequency. One possible explanation of this effect, which has been observed on a number of different occasions, is the occurrence of Spread-F conditions in the ionosphere over Huntsville. Without ionogram data it is not possible to confirm or disprove this, and the correct explanation is still an open question. March 24 was one of the five magnetically disturbed days of March 1968, and this correlation appears to prevail in the several other cases of this phenomenon which have been observed in the Huntsville Doppler records.

Figure 13 shows the simultaneous occurrence of a series of several oscillations on all frequencies and paths, with a period of approximately three minutes, beginning at 0010 CST on 21 April 1968. The Fredricksburg magnetograms show similar oscillations in all components at this same time. Norman Chang of ITSA/Boulder indicates that this effect is occasionally observed in all Doppler records, always accompanied by magnetogram oscillations, but that its nature is not presently understood.¹⁹ He reports that similar oscillations appear in the ITSA/Boulder Doppler records at the same time on 21 April.



- 32 -

Figure 11: Doppler data showing sunrise effects, 21 April 1968: Huntsville, Alabama

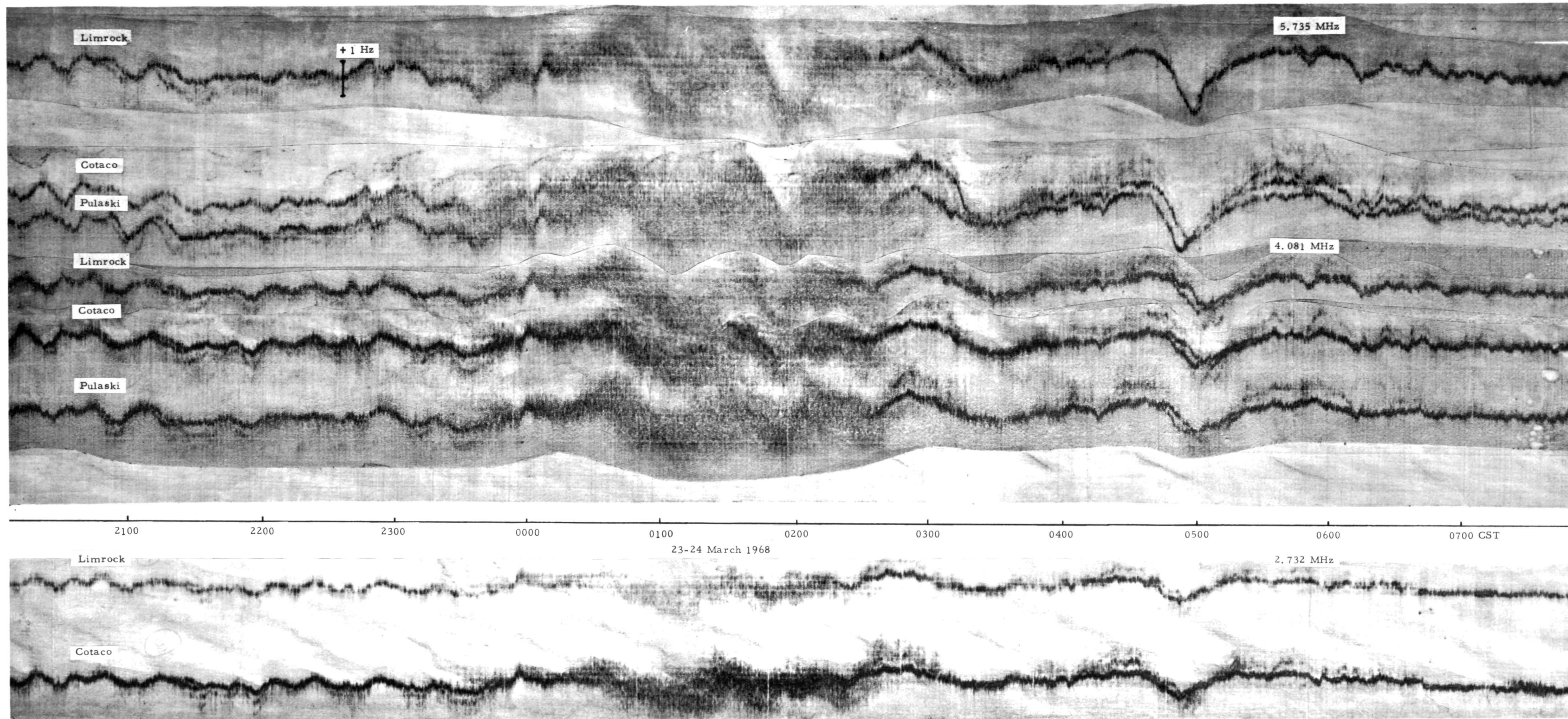
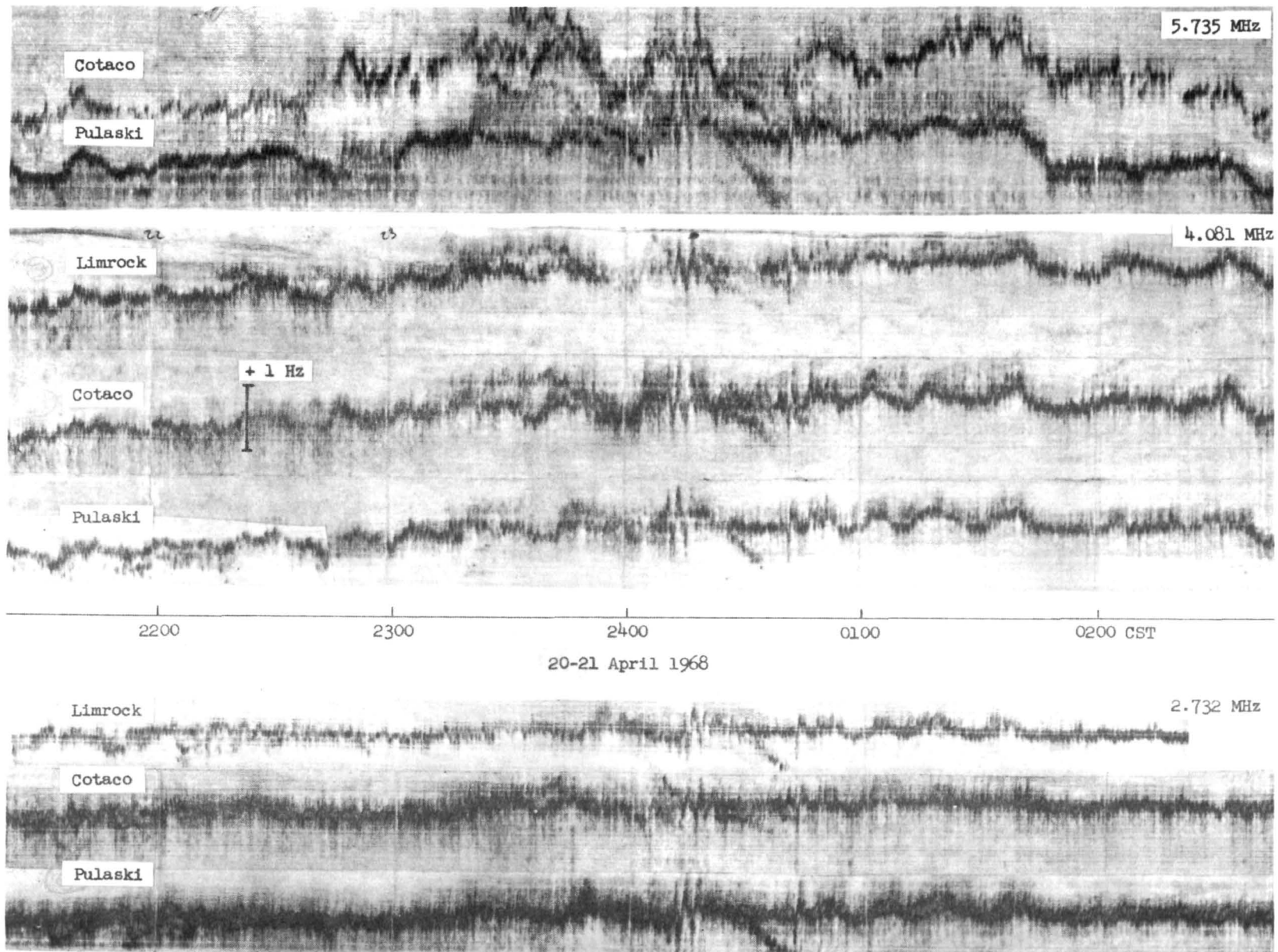


Figure 12: Doppler data showing frequency spreading
23-24 March: Huntsville, Alabama



-34-

Figure 13: Doppler data showing unusual oscillatory behavior
20-21 April 1968: Huntsville, Alabama

VI. CONCLUSIONS

It is clear that the results of this study, taken with similar measurements reported elsewhere, demonstrate that it is possible for ground level sources to generate acoustic waves of adequate energy and sufficiently low frequency to propagate upward to ionospheric heights. Some of the resultant electron density perturbations in the ionosphere are subsequently detectable by hf vertical incidence Doppler sounding techniques.

In the case of static firing tests of large rocket engines, it has been shown that, in addition to the expected vertically propagating simple acoustic waves traveling with the speed of sound in the medium, it is possible on occasion for the test to generate waves with both higher and lower velocities. In many instances, however, no Doppler observable ionospheric perturbations are produced whatsoever.

In the case of local thunderstorms, evidence has been added to a growing body of data which demonstrates that long sequences of ionospheric oscillations with periods in the 3-5 minute range may be produced by low frequency acoustic waves propagating upward from meteorologically disturbed regions. In particular, data has been shown which proves that these waves are indeed propagating vertically, as distinguished from the common horizontal wave motions which are constantly present in the ionosphere.

It can be inferred from the discussions of the difficulties of detecting small amplitude, slowly varying motions in the ionosphere with the Doppler sensing technique (primarily because it is a velocity sensitive measurement) that, in the cases of both static rocket tests and local thunderstorms, it would be of considerable assistance to employ a radio sensing technique with more sensitivity to the small scale perturbations in electron density occurring in the radio raypath reflection region. The hf vertical incidence phase sounding technique has been shown, in other experiments discussed in this report, to possess a substantial capability in this regard, and it is therefore recommended that implementation of such instrumentation be seriously considered in any further experimental programs of this type.

VII. REFERENCES

1. Watts, J. M. and K. Davies, Rapid frequency analysis of fading radio signals, JGR 65, 2295 (1960).
2. Davies, K., and D. M. Baker, On frequency variations of ionospherically propagated hf radio signals, Radio Science 1, 545 (1966).
3. Georges, T. M., HF Doppler studies of traveling ionospheric disturbances, JATP 30, 735 (1968).
4. Detert, D. G. and C. A. Moo, Doppler effects of atmospheric disturbances on hf radio propagation, AGARD-EPC Symposium, Ankara, Turkey, October 1967.
5. Detert, D. G., Acoustic-gravity wave study, Final Report, RADC-TR-68-53, April 1968.
6. Claerbout, J. F., Electromagnetic effects of atmospheric gravity waves, Interim Tech. Report, MIT Geophysics Laboratory, May 1967.
7. Allen, C. H. and S. D. Weiner, Study directed toward optimization of operating parameters of the EMAC probe for the remote measurement of atmospheric parameters, Final Report, AFCRL-63-596, September 1963.
8. Maglieri, D. J., Some effects of airplane operations and the atmosphere on sonic boom signatures, JASA 39, S36 (1966).
9. Pierce, A. D., Private communication, MIT, April 1968.
10. Marcos, F. A., Aircraft induced ionospheric disturbances, AFCRL-66-229, April 1966.
11. Barry, G. H., L. J. Griffiths, and J. C. Taenzer, HF radio measurements of high-altitude acoustic waves from a ground-level explosion, JGR 71, 4173 (1966).
12. Leonard, R. S., P. B. Bentley, and R. A. Barnes, Jr., Multiple-frequency forward-propagation study - Project VELA SIERRA, Semi-Annual Tech. Rept. 2, SRI Project 5224, January 1966 (SECRET).

VII. REFERENCES (Cont'd)

13. Kaschak, G. R., Long-range supersonic propagation of infrasonic noise generated by missiles, JGR 74, 914 (1969).
14. Donn, W. L., E. Posmentier, U. Fehr, and N. K. Balachandran, Infrasound at long range from Saturn V, 1967, Science 162, 1116 (1968).
15. Pierce, A. D. and S. C. Coroniti, A mechanism for the generation of acoustic-gravity waves during thunderstorm formation, Nature 210, 1209 (1966).
16. Anderson, C. E., A study of the pulsating growth of cumulus clouds, AFCRL-TR-60-417, December 1960.
17. Few, A. A., A. J. Dessler, D. J. Latham, and M. Brook, A dominant 200-Hertz peak in the acoustic spectrum of thunder, JGR 72, 6149 (1967).
18. Georges, T. M., Ionospheric effects of atmospheric waves, ESSA Tech. Report IER57-ITSA54, October 1967.
19. Chang, N. J. F., Private communication, ITSA/Boulder, July 1968.
20. Pierce, A. D., Geometric acoustics theory of waves from a point source in a temperature and wind-stratified atmosphere, AVSSD-0135-66-CR, August 1966.
21. Hines, C. O., The upper atmosphere in motion, Q.J.R. Met. Soc. 89, 1 (1963).
22. Gossard, E. E., Vertical flux of energy into the lower ionosphere from internal gravity waves generated in the troposphere, J.G.R. 67, 745 (1962).
23. Pitteway, M. L. V., and C. O. Hines, The viscous damping of atmospheric gravity waves, Can. J. Phys. 41, 1935 (1963).
24. Hines, C. O., Internal gravity waves at ionospheric heights, Can. J. Phys. 38, 1441 (1960).
25. Friedman, J. P., Propagation of internal gravity waves in a thermally stratified atmosphere, J G R 71, 1033 (1966).

VII. REFERENCES (Cont'd)

26. Bretherton, F. P., The propagation of groups of internal gravity waves in a shear flow, *Q.J.R. Met. Soc.* 92, 466 (1966).
27. Booker, J. R., and F. P. Bretherton, The critical layer for internal gravity waves in a shear flow, *J. Fluid Mech.* 27, 513 (1967).
28. Hines, C. O., and C. A. Reddy, On the propagation of atmospheric gravity waves through regions of wind shear, *J G R* 72, 1015 (1967).
29. Eliassen, A., and E. Palm, On the transfer of energy in stationary mountain waves, *Geofys. Publ.* 22, 1 (1961).
30. Roberts, W. T., Private communication, NASA/MSFC, 1967.
31. Salmela, H. A., Meteorological Rocket Network Wind Statistics, Interim Notes on Atmospheric Properties No. 68, AFCRL, February 1967.
32. Rosenberg, N. W., Ionospheric Winds - A Statistical Analysis, *Space Research VIII*, 673 (1968).
33. Smith, R. E. and D. K. Weidner, Space Environment Criteria Guidelines for Use in Space Vehicle Development (1968 Revision), NASA TMX-53798, October 1968.
34. U. S. Standard Atmosphere Supplements, 1966, U. S. Government Printing Office, Washington, D. C.

APPENDIX A

MODIFICATIONS TO HEATHKIT DX60-A TRANSMITTERS

(Prepared by Michael Thomas, Avco/Huntsville)

The Heathkit DX-60A amateur transmitters selected for use in this experiment proved to be unreliable when operated continuously for long periods of time in the cw mode. Several minor circuit changes were required to alleviate this condition. It was also necessary to adjust inductors L2 and L3 to allow the transmitters to operate at frequencies other than those in the normal amateur bands (refer to the transmitter schematic drawing in the manufacturer's manual for the circuit elements described here).





Modifications

1. Resistors R10 and R30 were changed from 4700 ohms and 22K ohms, respectively, to 12 K ohms and 15K ohms. The purpose of this change is to shift the bias point of the power amplifier tube from about -40 volts to about -60 volts and thus to prevent the tube from destroying itself should the drive signal be lost.
2. Resistor R28 was changed from 10K ohms at 2W to 10K ohms at 5W, since under normal operating conditions this resistor dissipates about 1.5W.
3. Cathode bias was added to both of the 6CL6 tubes. This was done with a 330 ohm 1/2W cathode resistor and a 0.1 mf 50V bypass capacitor. Without this modification the plate current becomes excessive if the drive signal is removed.
4. Tank coil L2 was removed and replaced with several molded rf chokes (National type R-1550). These chokes are soldered directly to the switch wafer, relieving the necessity of tapping a continuously wound coil. The exact value of the coils depends upon the desired frequencies.
5. The power amplifier tank coil L3 was replaced by a section of Air Dux #1410T coil stock and then tapped at the appropriate points.

APPENDIX B

DATA COLLECTION LOG

Tape No.	Date	Start Time	Stop Time	Frequencies
96	9/27/67	1526 CDT	0405 (9/28)	Cotaco 2.732 MHz 4.081 6.185
97	9/28	0741	1525	Pulaski 4.081 6.185
98	9/28	1529	0406 (9/29)	
99	9/29	0747	1538	
100	9/29	1545	0400 (9/30)	
101	10/2	0745	1610	
102	10/2	1615	0430 (10/3)	
103	10/3	0750	1600	
104	10/3	1610	0425 (10/4)	
105	10/4	0845	2100	
106	10/5	0800	1530	
107	10/5	1535	0350 (10/6)	
108	10/9	0810	1530	
109	10/9	1535	0350 (10/10)	
110	10/10	0800	1520	
111	10/10	1530	0345 (10/11)	
112	10/11	0745	1520	
113	10/11	1530	0345 (10/12)	
114	10/12	0745	1525	
115	10/12	1535	0350 (10/13)	
116	10/13	0815	2030	
117	10/16	0813	1545	
118	10/16	1547	0402 (10/17)	
119	10/17	0751	1526	
120	10/17	1531	0346 (10/18)	
121	10/18	0753	1531	
122	10/18	1535	0350 (10/19)	
123	10/19	0750	1535	
124	10/19	1537	0352 (10/20)	
125	10/20	0753	1535	
126	10/20	1545	0400 (10/21)	
127	10/23	0800	1615	
128	10/24	0755	1610	
129	10/25	0745	1542	
130	10/25	1545	0400 (10/26)	
131	10/26	0807	1622	
132	10/27	0857	1530	
133	10/27	1532	0347 (10/28)	
134	10/30	0745 CST	1530	

Tape No.	Date	Start Time	Stop Time	Frequencies	
135	10/30/67	1535 CST	0350 (10/31)		
136	10/31	0745	1552		
137	10/31	1555	0410 (11/1)		
138	11/1	0809	2024 (11/2)		
139	11/2	0800	2015 (11/3)		
140	11/7	0854	2109 (11/8)		
141	11/16	1115	2330		
142	11/30	0759	1534		Cotaco 2.732 MHz 4.081 5.735
143	11/30	1536	0351 (12/1)		Pulaski 2.732 4.081 5.735
144	12/1	0750	1545		Limrock 2.732 4.081 5.735
145	12/1	1543	0358 (12/2)		 intermittent operation of Pulaski and Limrock transmitters
146	12/2	1145	2400		
147	12/7	0920	2135		
148	12/9	1510	0325 (12/10)		
149	12/11	0843	2058		
150	12/18	0810	2025		
151	12/19	0737	1952		
152	12/20	0810	2025		
153	12/21	0756	2011		
154	12/27	1538	0353 (12/28)		
155	1/3/68	1540	0355 (1/4)	 Cotaco } 2.723 MHz Pulaski } 4.081 Limrock } 5.735	
156	1/25	1145	2355		
157	2/6	1430	1555 (2/8)		
158	2/12	0900	1000 (2/14)		
159	2/14	1330	1520 (2/16)		
160	2/16	1530	1630 (2/18)		
161	2/19	0800	1010 (2/21)		
162	2/21	1025	1225 (2/23)		
163	2/23	1245	1300 (2/25)		
164	2/28	0855	1000 (3/1)		
165	3/4	1530	1630 (3/6)		
166	3/7	0755	0855 (3/9)		
167	3/11	0750	0800 (3/13)		
168	3/13	0805	1400 (3/15)		

Tape No.	Date	Start Time	Stop Time	Frequencies
169	3/15/68	1500 CST	1600 (3/17)	↓
170	3/18	0750	0805 (3/20)	
171	3/20	0810	0745 (3/22)	
172	3/22	0750	0850 (3/24)	
173	3/27	0800	0800 (3/29)	
174	3/29	0810	0910 (3/31)	
175	4/1	0740	0740 (4/3)	
176	4/3	0750	0740 (4/5)	
177	4/5	0745	0845 (4/7)	
178	4/8	0755	0855 (4/10)	
179	4/11	0750	0850 (4/13)	
180	4/15	0800	1520 (4/17)	
181	4/17	1530	1535 (4/19)	
182	4/19	1540	1640 (4/21)	
183	4/22	0825	1530 (4/24)	
184	4/24	1535	1540 (4/26)	
185	4/26	1540	1640 (4/28)	
186	4/29	0755 CDT	0810 (5/1)	
187	5/1	0815	0915 (5/3)	
188	5/3	1500	1600 (5/5)	
189	5/6	1510	1610 (5/8)	
190	5/9	0740	1530 (5/10)	
191	5/10	1535	2205	
192	5/15	0730	0115 (5/17)	
192	5/27	0814	0816 (5/29)	
193	5/29	0820	0820 (5/31)	

APPENDIX C

DOPPLER DATA RECORDED DURING STATIC
TESTS AT NASA/MSFC

Table 2 lists all the NASA/MSFC static rocket engine tests which have been monitored by the Doppler sounding experiment at Huntsville, including data taken under both the preceding RADC program and the present study reported here.

As discussed in Section III of this report, all the static test Doppler records were reprocessed with uniform time and frequency scales on the narrowband Rayspan analyzer at an effective speedup factor of 128 times. This results in a frequency display with approximately 1.3 Hertz per record inch, with a processing resolution of 1/12 Hertz. Figures 14 through 41 in this Appendix reproduce those records.

Figures 40(b) - (d) are reproductions of the same data interval, processed with increasing gain in the spectrum analyzer, to illustrate the problems encountered in identifying small amplitude signal traces in the presence of other strong signals. It should be clear from these three records that intensity modulating the displayed signal trace to indicate amplitude levels is an inadequate, though efficient, processing technique when more than a few decibels of amplitude resolution are encountered.

Figures 42 through 48 are reproduced from a report written earlier during the course of this experimental program ⁵. They contain Doppler data processed with different time and frequency scales and resolutions, and are given here to aid in the interpretation of certain small amplitude traces which are related to the static firing events (see Section III). Figures 46 and 47 show phase path variations and perturbations recorded with the Avco phase-locked loop monitoring device ⁵ operating during the 3 August 1967 test.

Table 2

NASA/MSFC Static Test Firings Monitored
by the Doppler Sounding Experiment

Tape No.	Date	Start Time	Duration	Booster
1	4/20/67	1301 CST	40 seconds	F1-61
13	5/9	1705:31 CDT	35.3	S1B-46
18	5/19	1328:06	25.004	F1-62
20	5/22	1733	145.7	S1B-47
20	5/22	1800:59	46.004	F1-63
32	6/9	1300	41	F1-64
38	6/14	1400	41	F1-65
53	8/1	1500:00	3	S1C
54	8/3	1920:00	40	S1C
71	8/16	1352	41	F1-68
88	9/1	1103	46	F1-69
97	9/28	1303	44.39	F1-70
123	10/19	1300	45.18	F1-71
131	10/26	1311:57	43.70	F1-72
141	11/16	1316 CST	45.31	F1-73
142	11/30	1313	44.85	F1-74
151	12/19	1640:24	35.50	S1B-48
156	1/25/68	1708	15.50	S1B-49
157	2/6	1640	15.46	S1B-50

Table 2 (Cont'd)

NASA/MSFC Static Test Firings Monitored
by the Doppler Sounding Experiment

Tape No.	Date	Start Time	Duration	Booster
159	2/14	1630:01 CST	15.20	S1B-51
161	2/20	1306	0.00*	F1-75
161	2/20	1440	25.56	F1-76
162	2/21	1640	3.00	S1B-52
167	3/12	1337	25.75	F1-77
170	3/19	1257	25.44	F1-78
173	3/27	1258	26.54	F1-79
178	4/9	1639:59	35.39	S1B-53
183	4/23	1640	145.30	S1B-54
190	5/10	1458 CDT	90.74	F1-80
191	5/15	1535	121.30	F1-81

* Test aborted during ignition

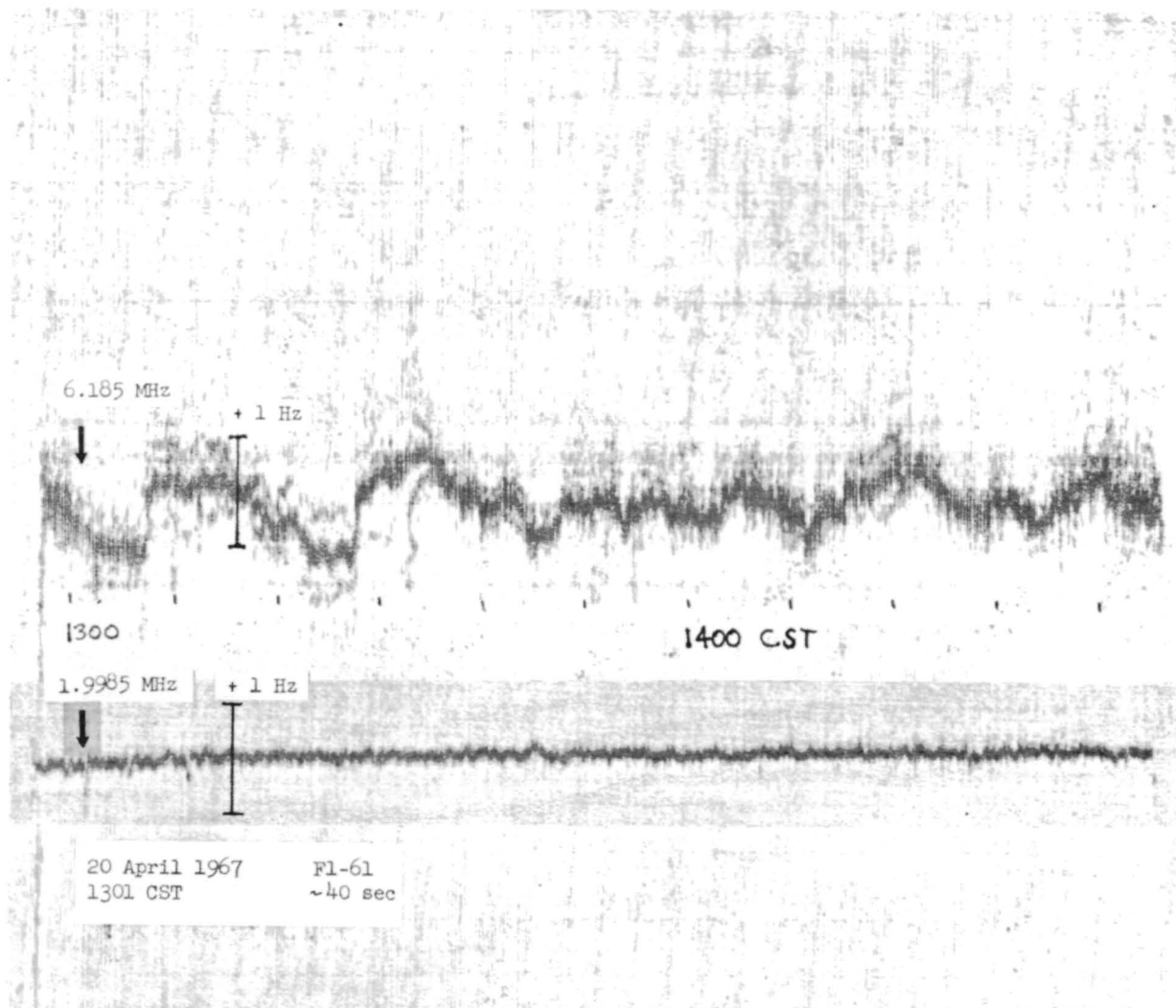


Figure 14: Doppler data record, 20 April 1967: Huntsville, Alabama

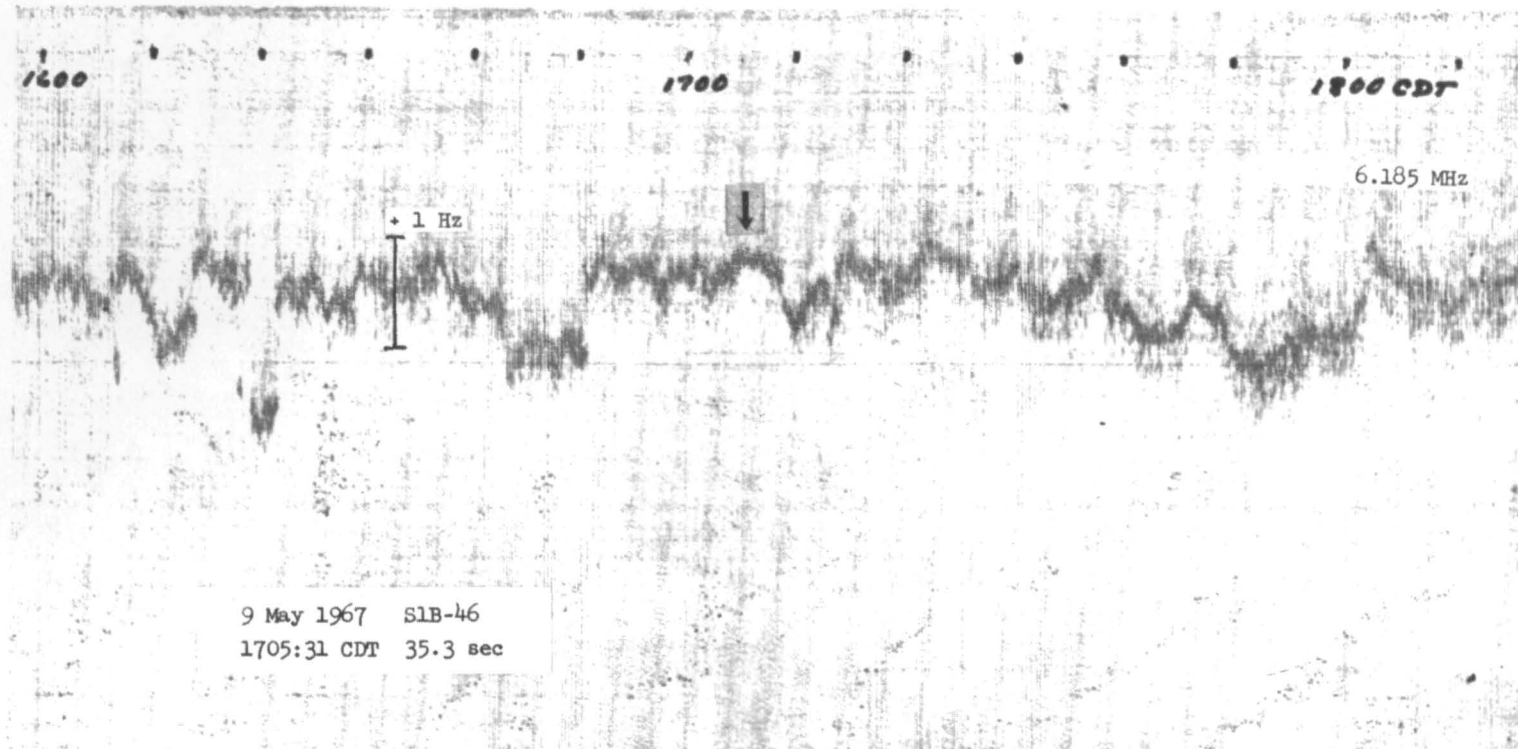


Figure 15: Doppler data record, 9 May 1967: Huntsville, Alabama

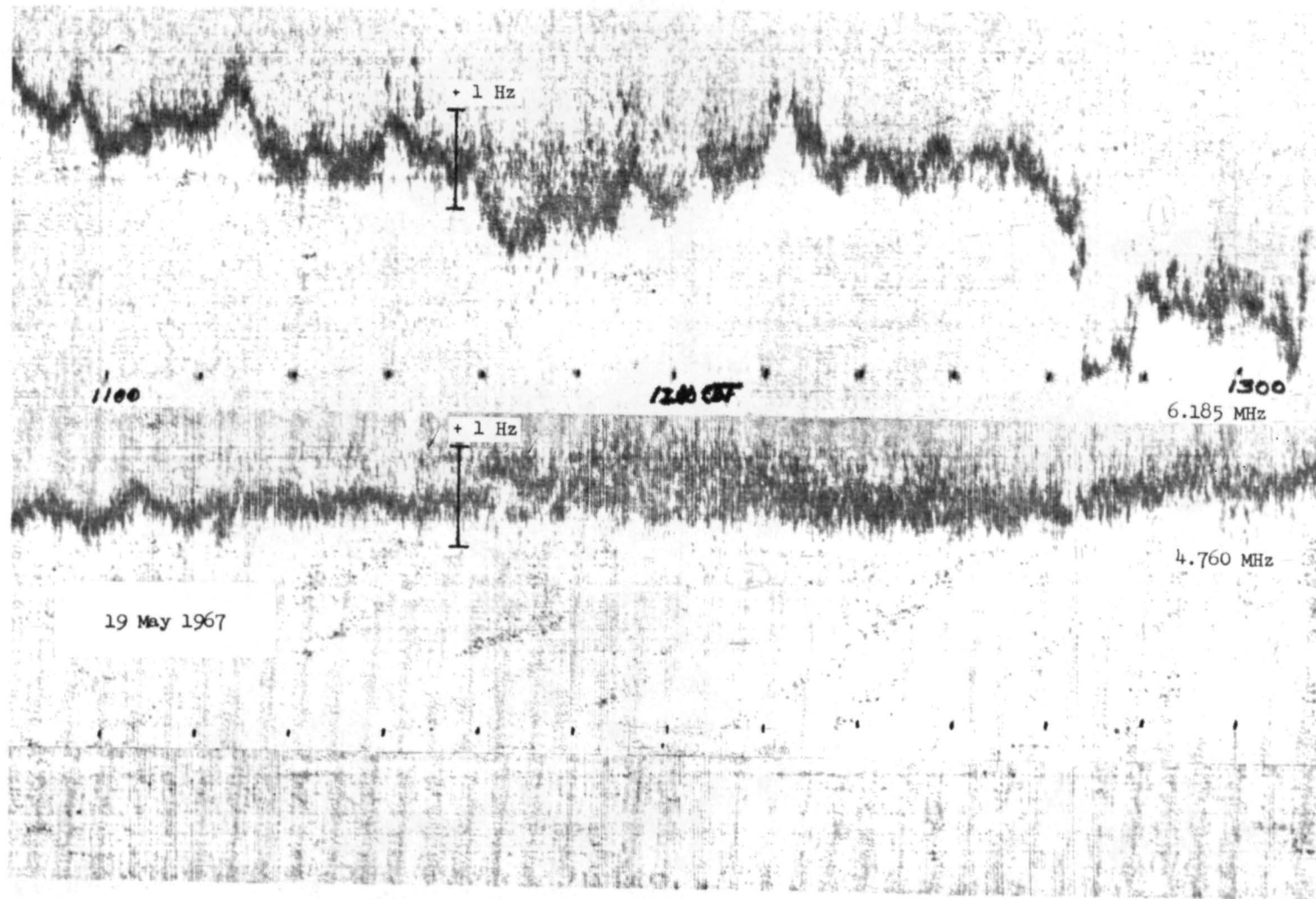


Figure 16 (a): Doppler data record, 19 May 1967: Huntsville, Alabama

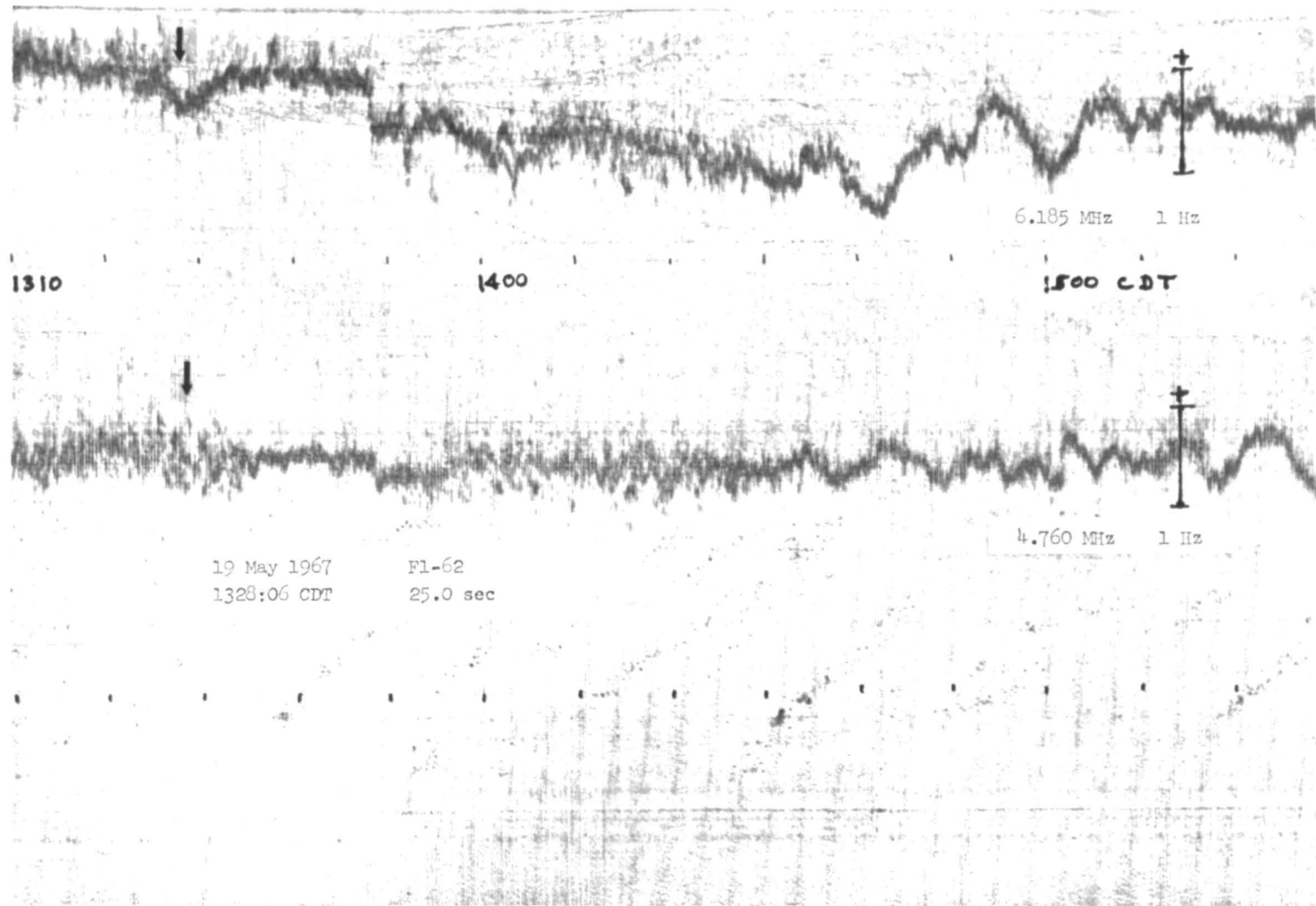
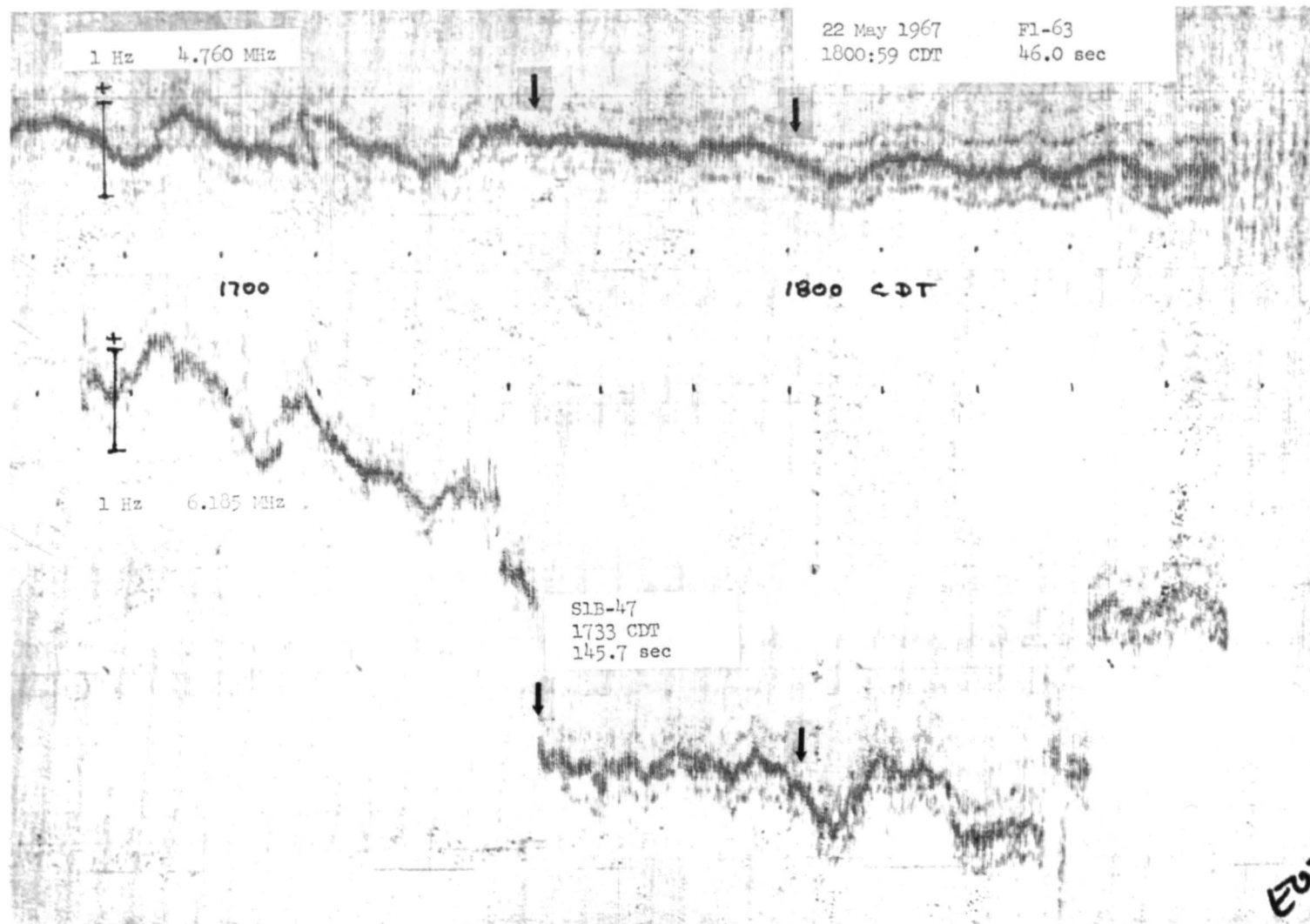


Figure 16 (b): Doppler data record, 19 May 1967: Huntsville, Alabama



-53-

Figure 17: Doppler data record, 22 May 1967: Huntsville, Alabama

-54-

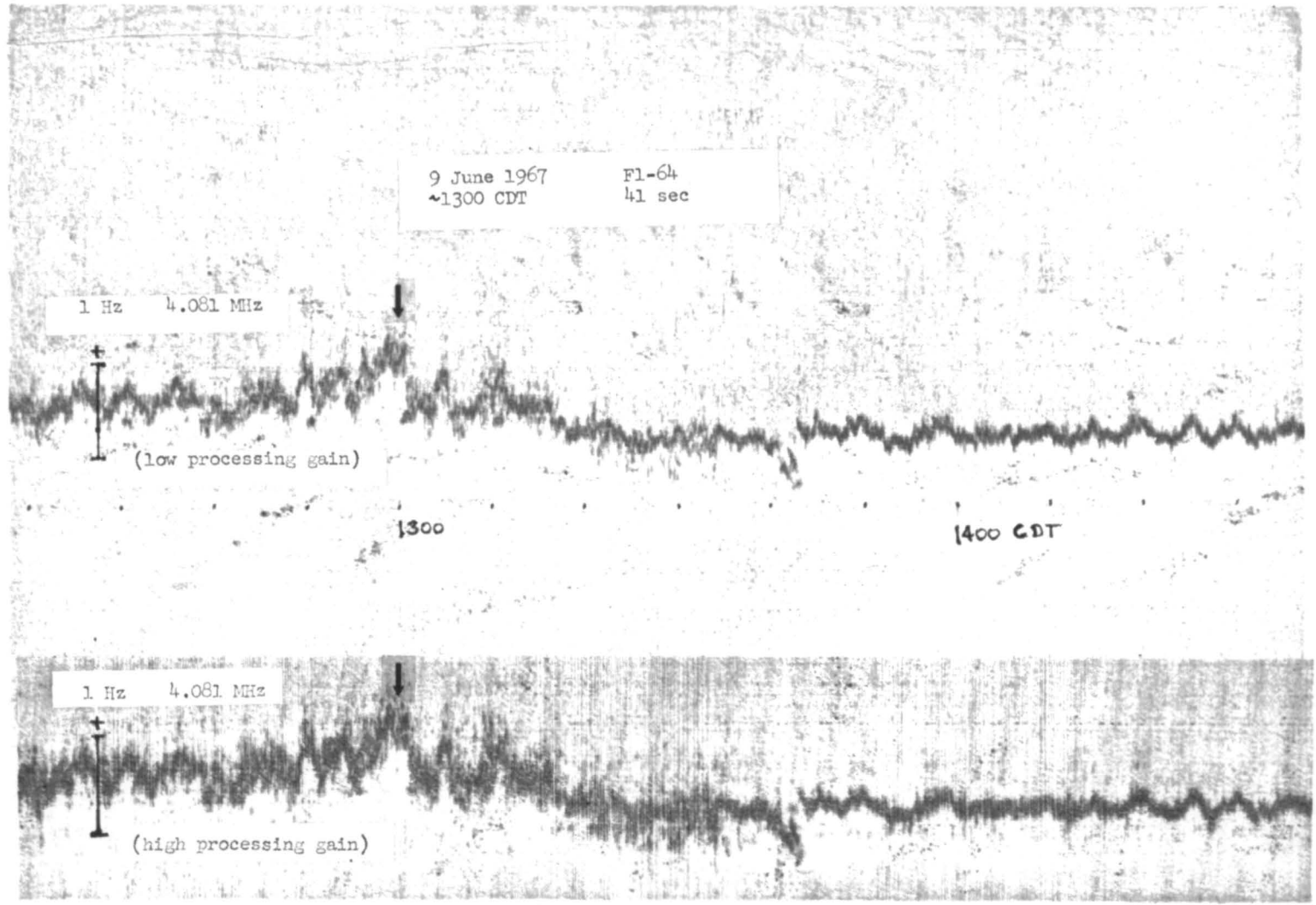


Figure 18: Doppler data record, 9 June 1967: Huntsville, Alabama

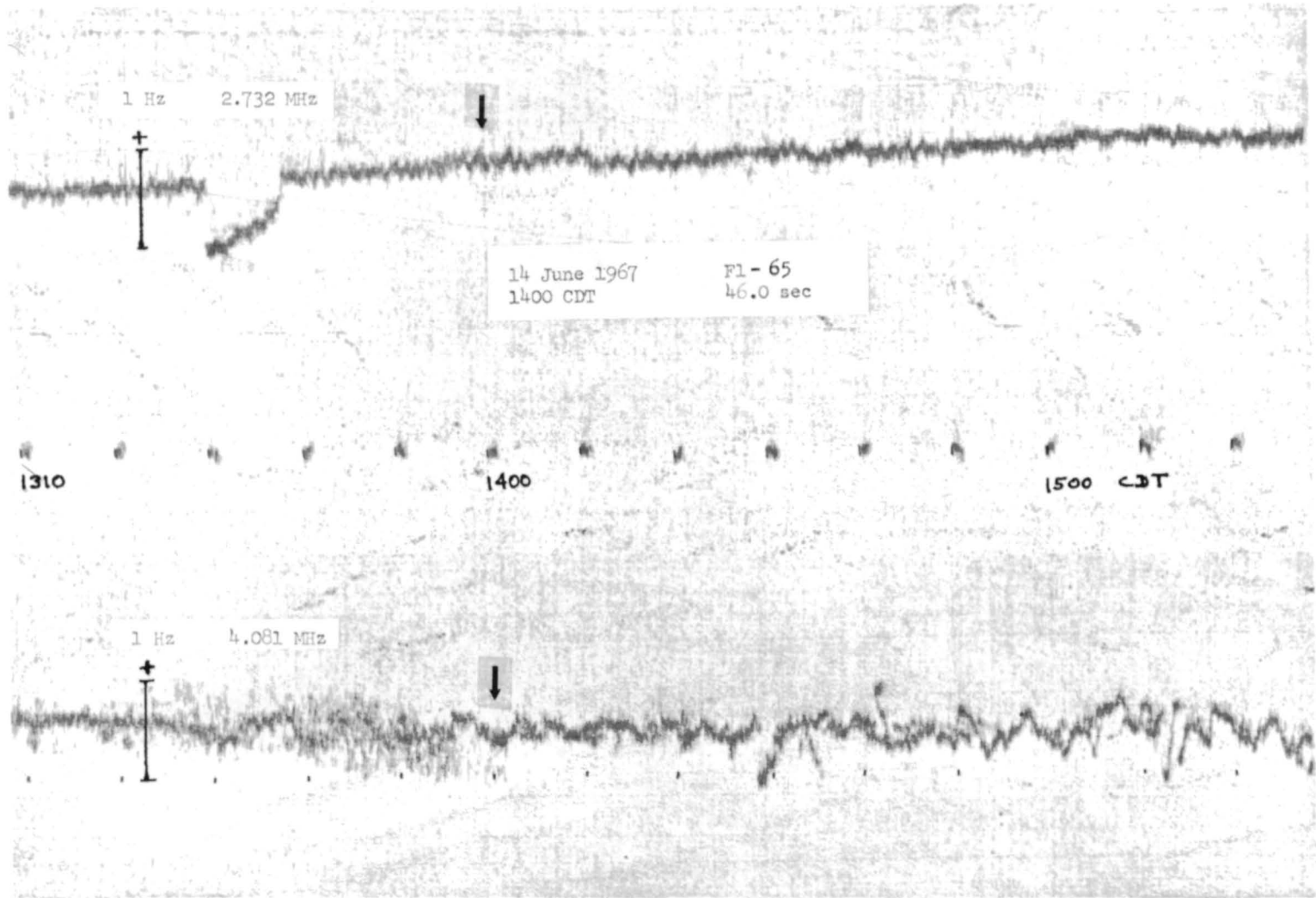


Figure 19: Doppler data record, 14 June 1967: Huntsville, Alabama

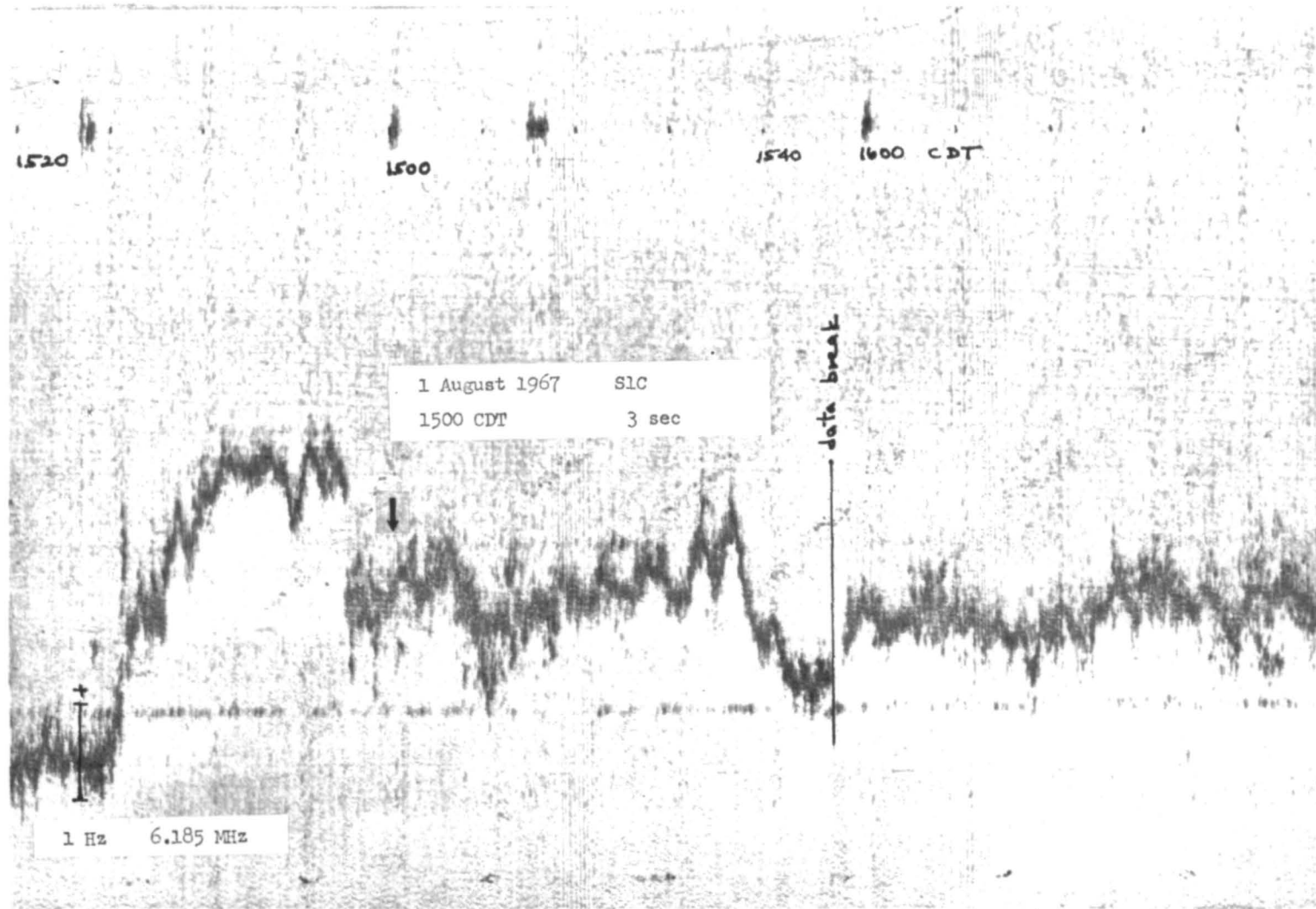


Figure 20: Doppler data record, 1 August 1967: Huntsville, Alabama

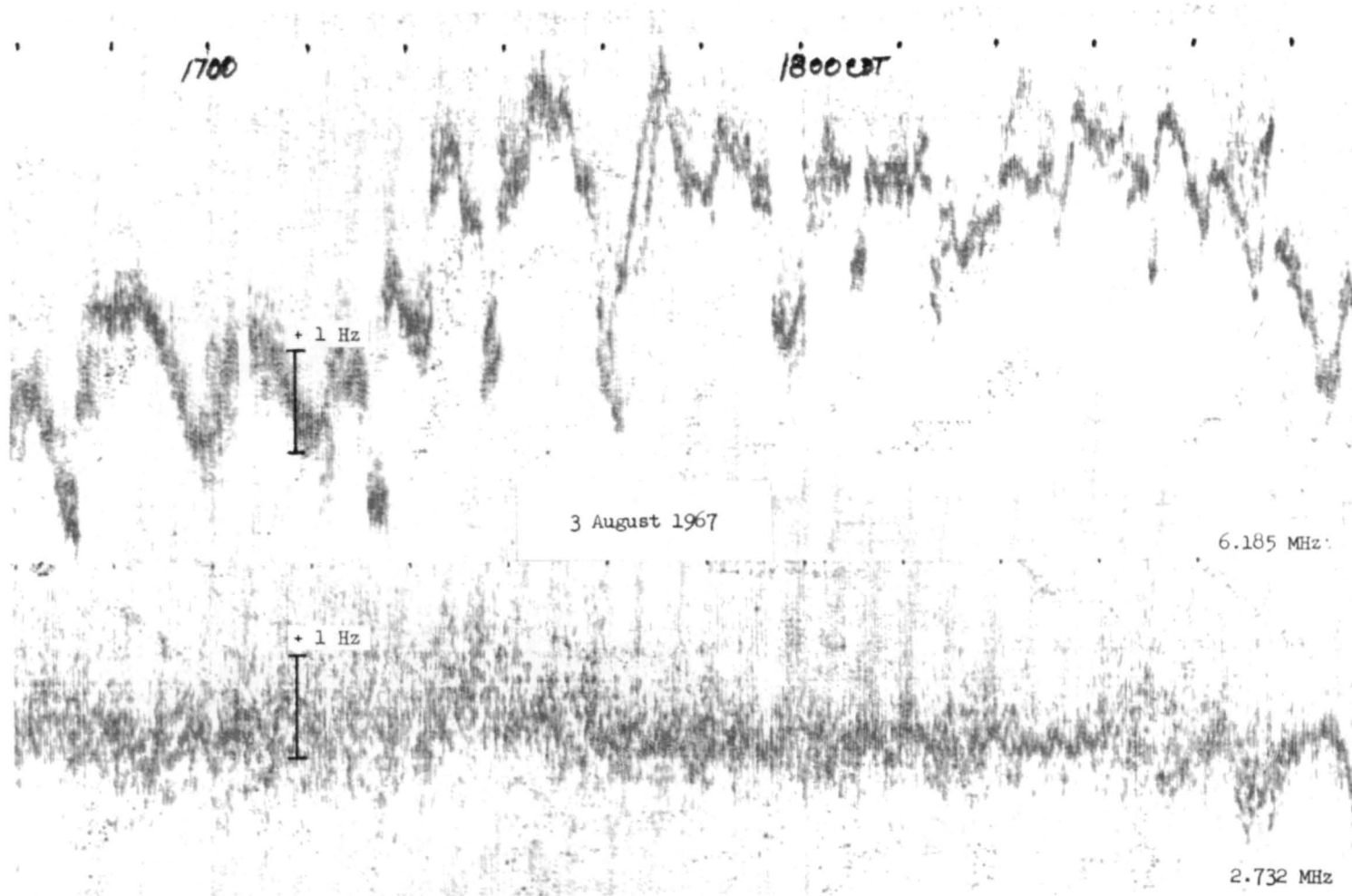


Figure 21 (a): Doppler data record, 3 August 1967: Huntsville, Alabama

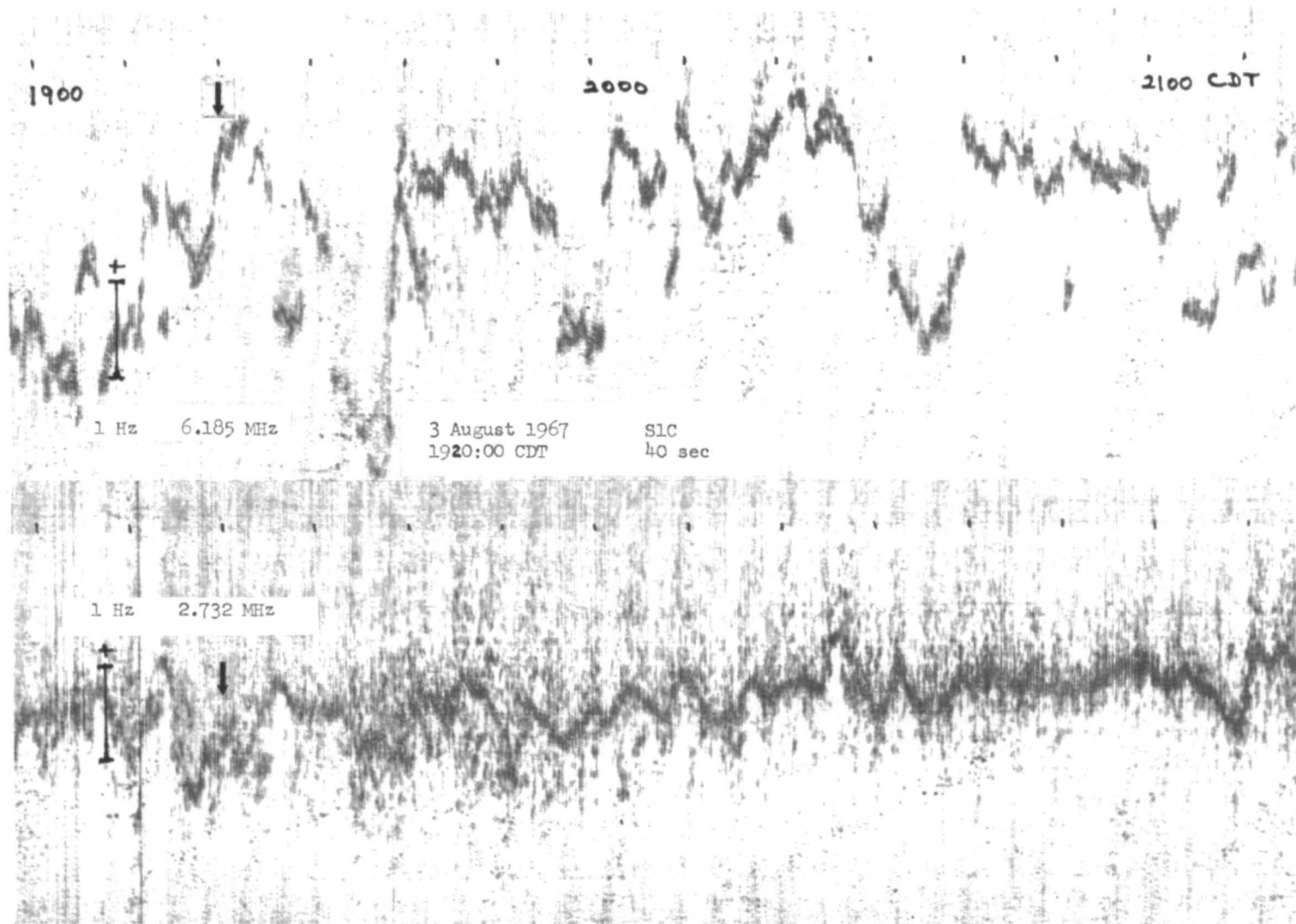


Figure 21 (b): Doppler data record, 3 August 1967: Huntsville, Alabama

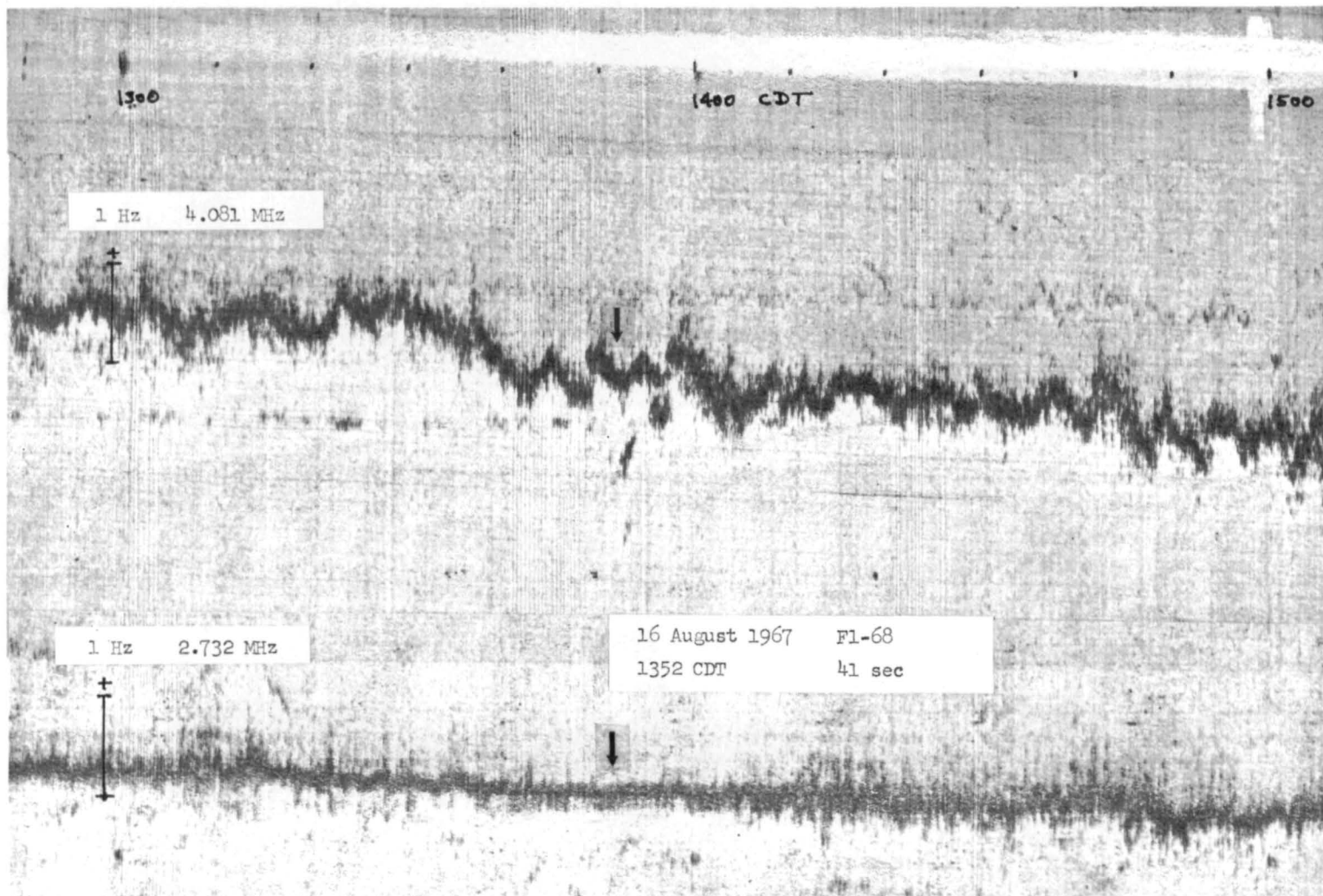


Figure 22: Doppler data record, 16 August 1967: Huntsville, Alabama

-60-

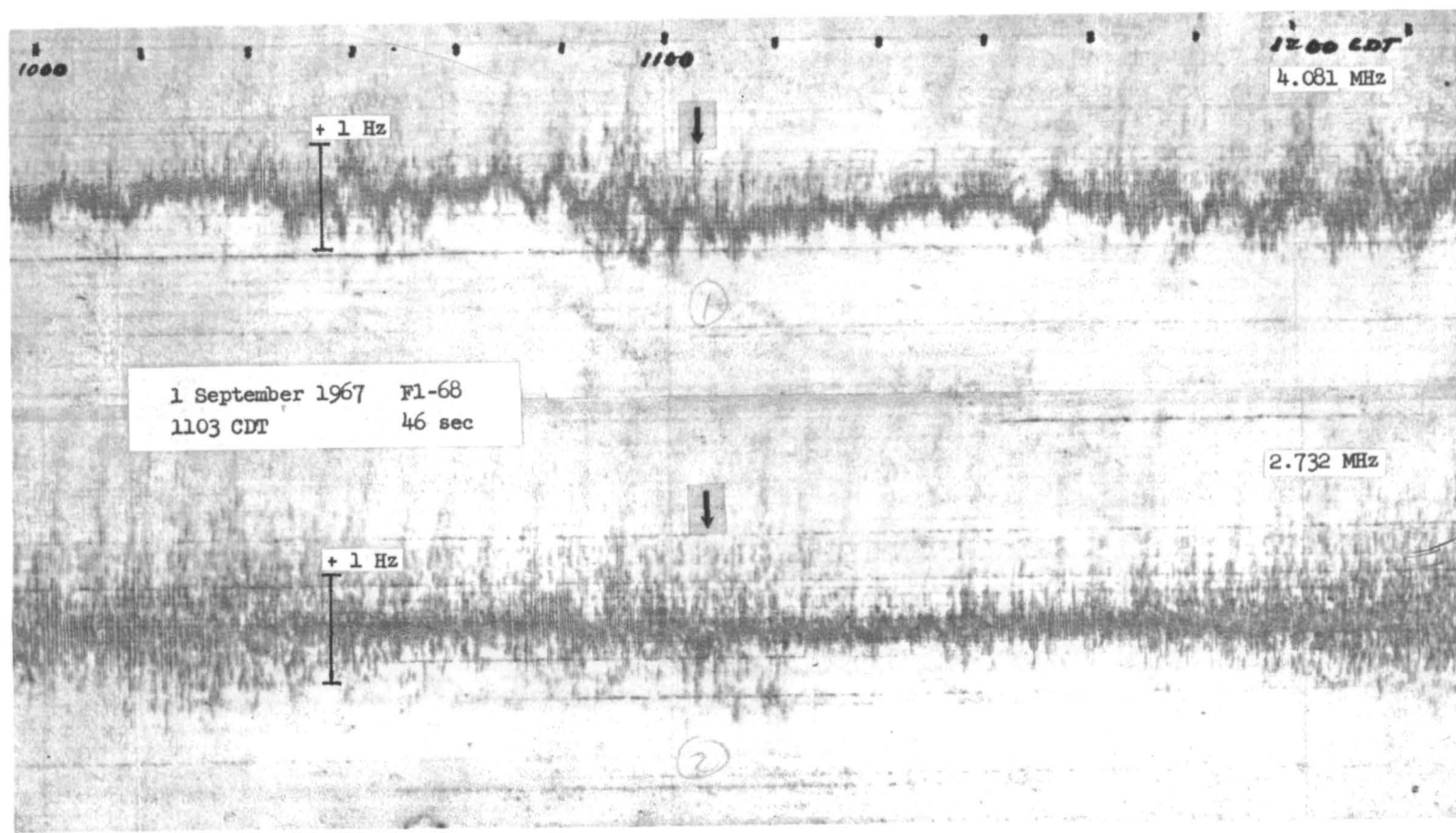


Figure 23: Doppler data record, 1 September 1967: Huntsville, Alabama

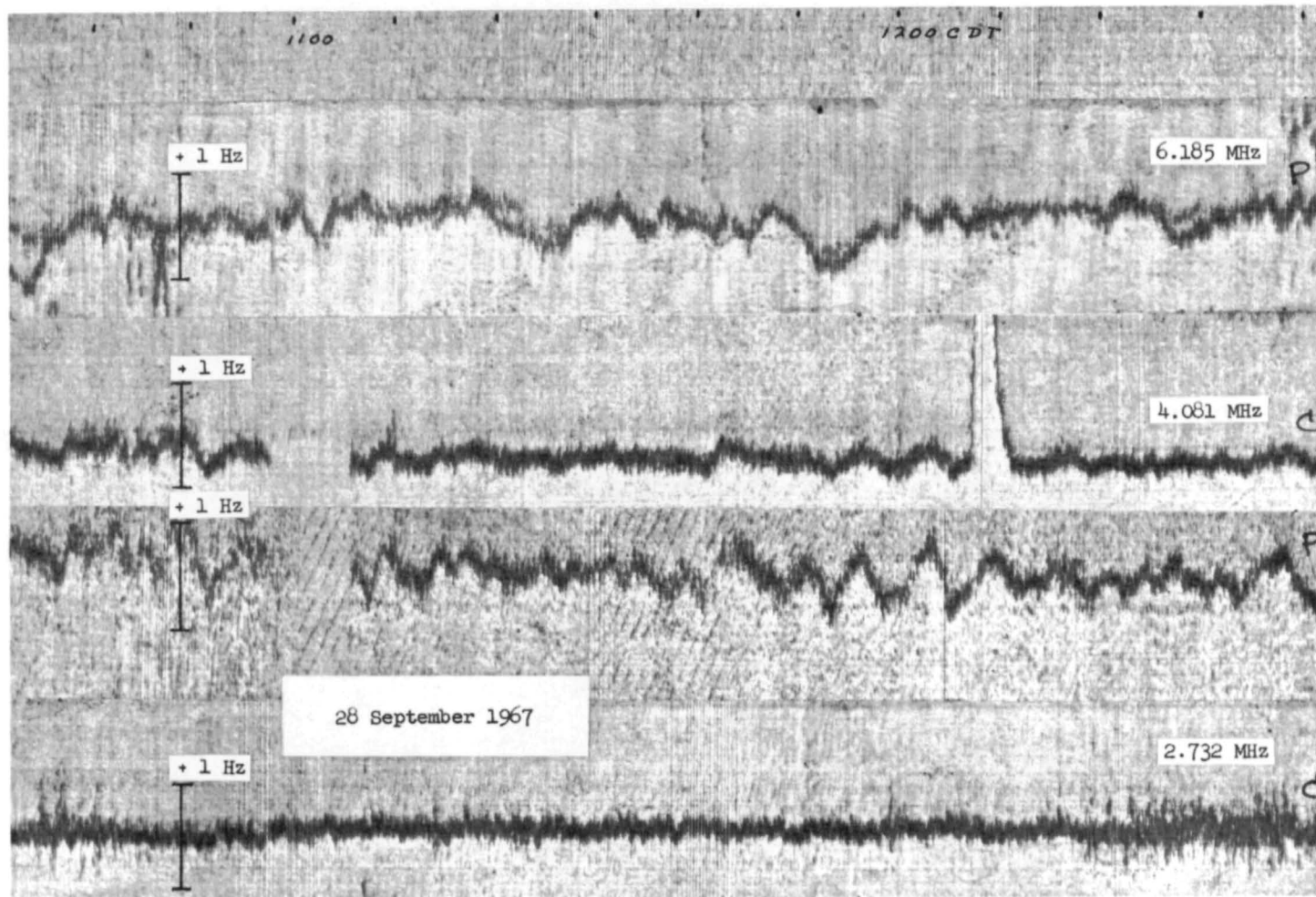
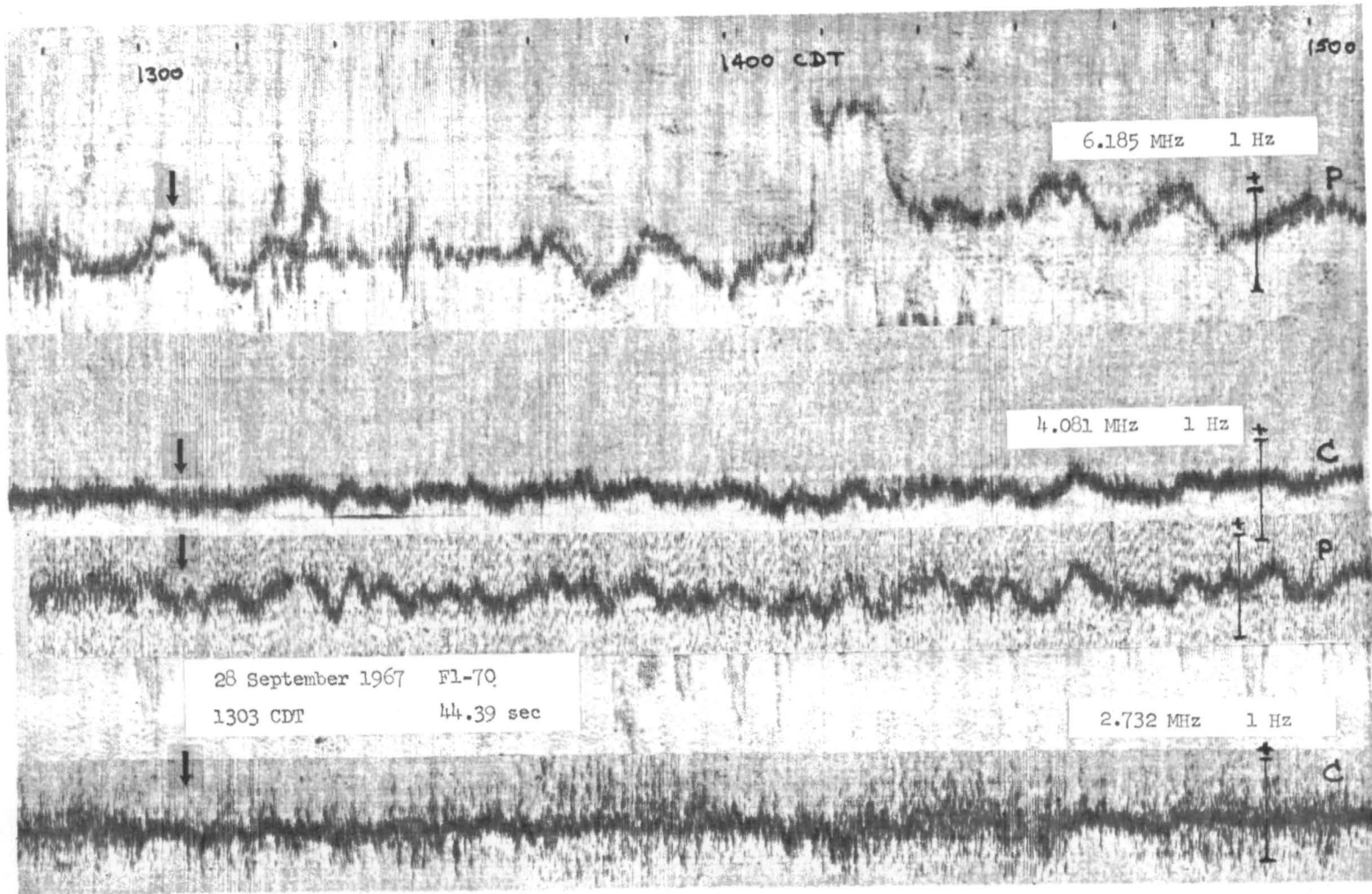


Figure 24 (a): Doppler data record, 28 September 1967: Huntsville, Alabama



-62-

Figure 24 (b): Doppler data record, 28 September 1967: Huntsville, Alabama

-63-

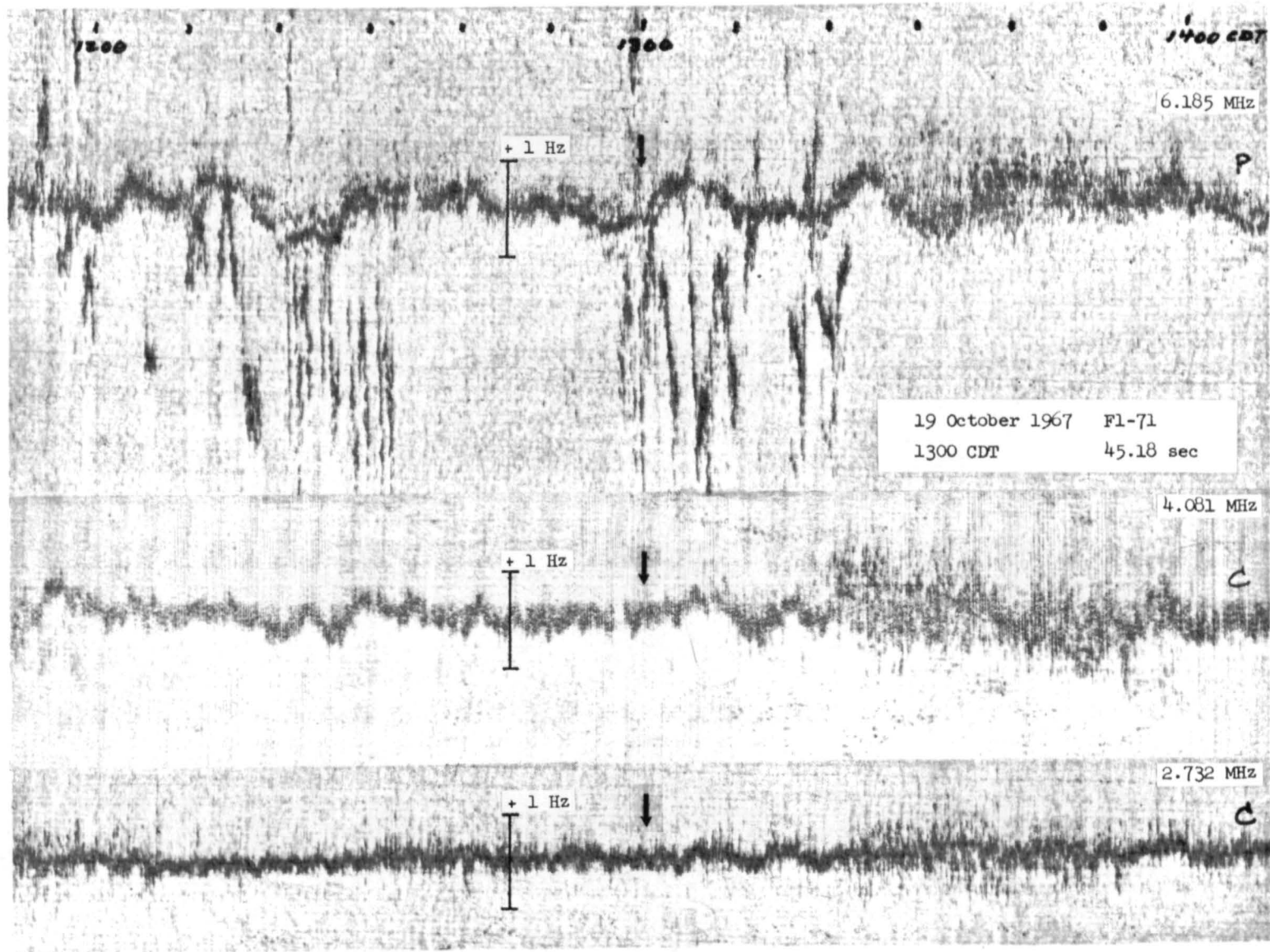
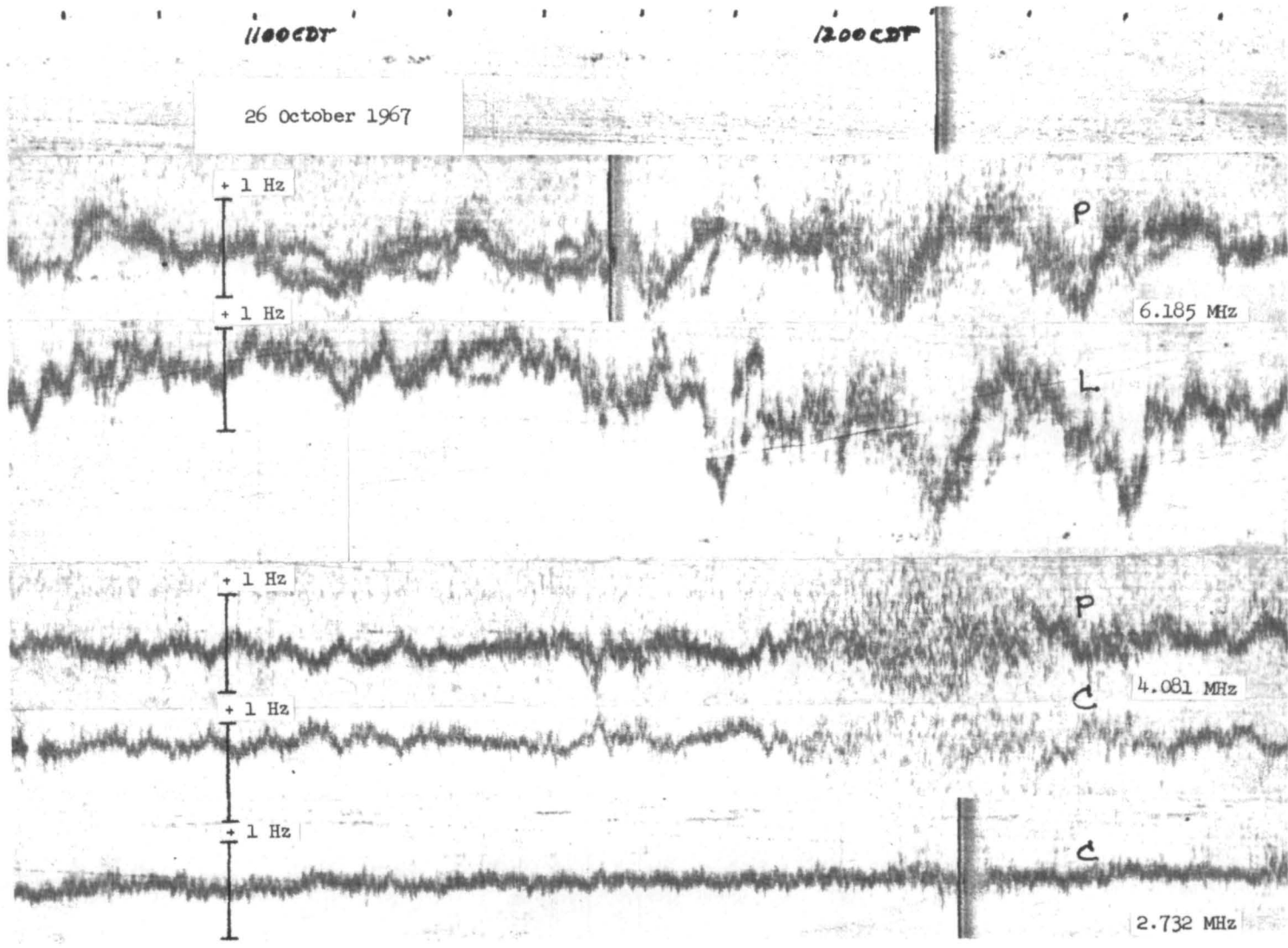
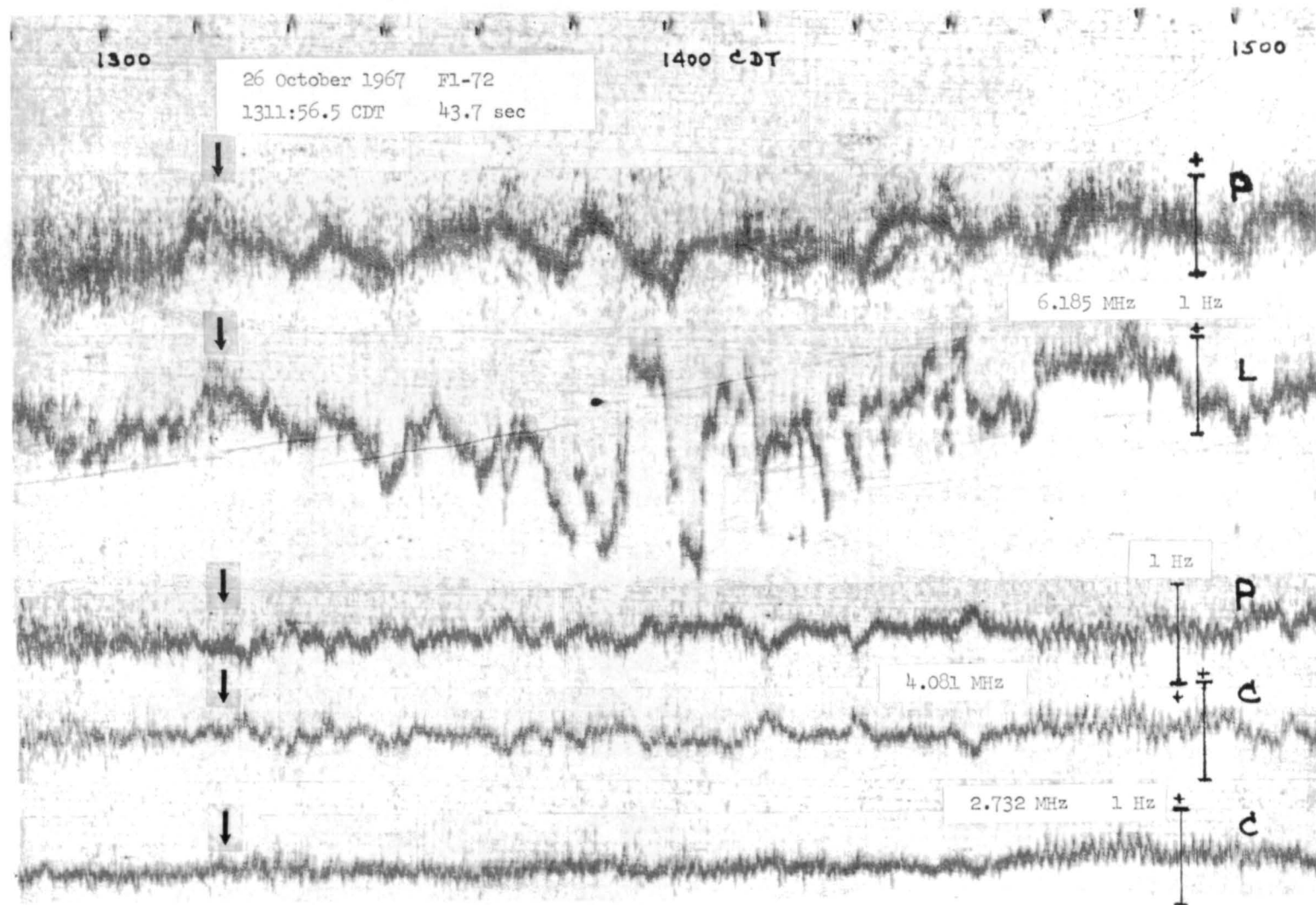


Figure 25: Doppler data record, 19 October 1967: Huntsville, Alabama



-64-

Figure 26 (a): Doppler data record, 26 October 1967: Huntsville, Alabama



-65-

Figure 26 (b): Doppler data record, 26 October 1967: Huntsville, Alabama

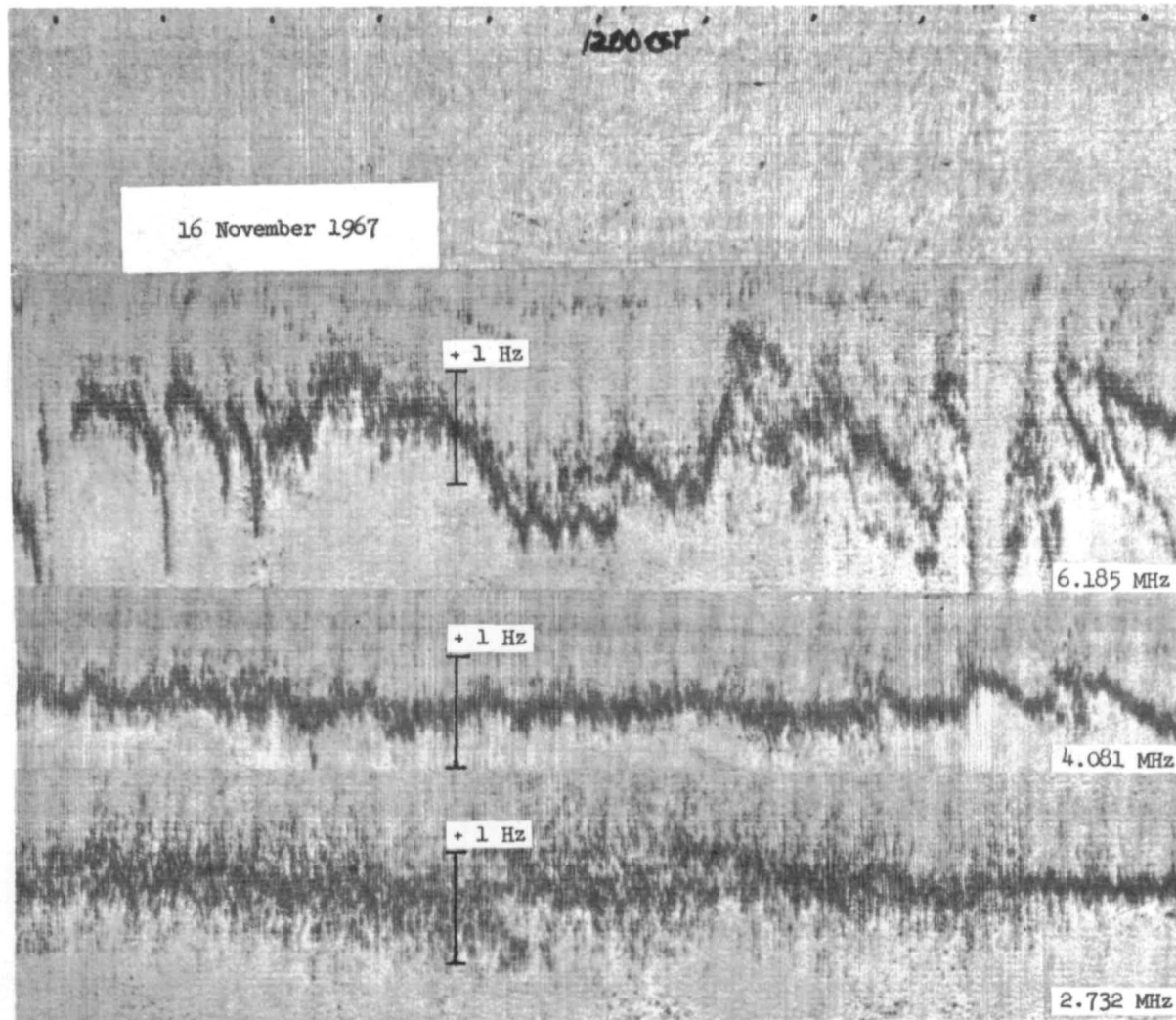


Figure 27 (a): Doppler data record, 16 November 1967: Huntsville, Alabama

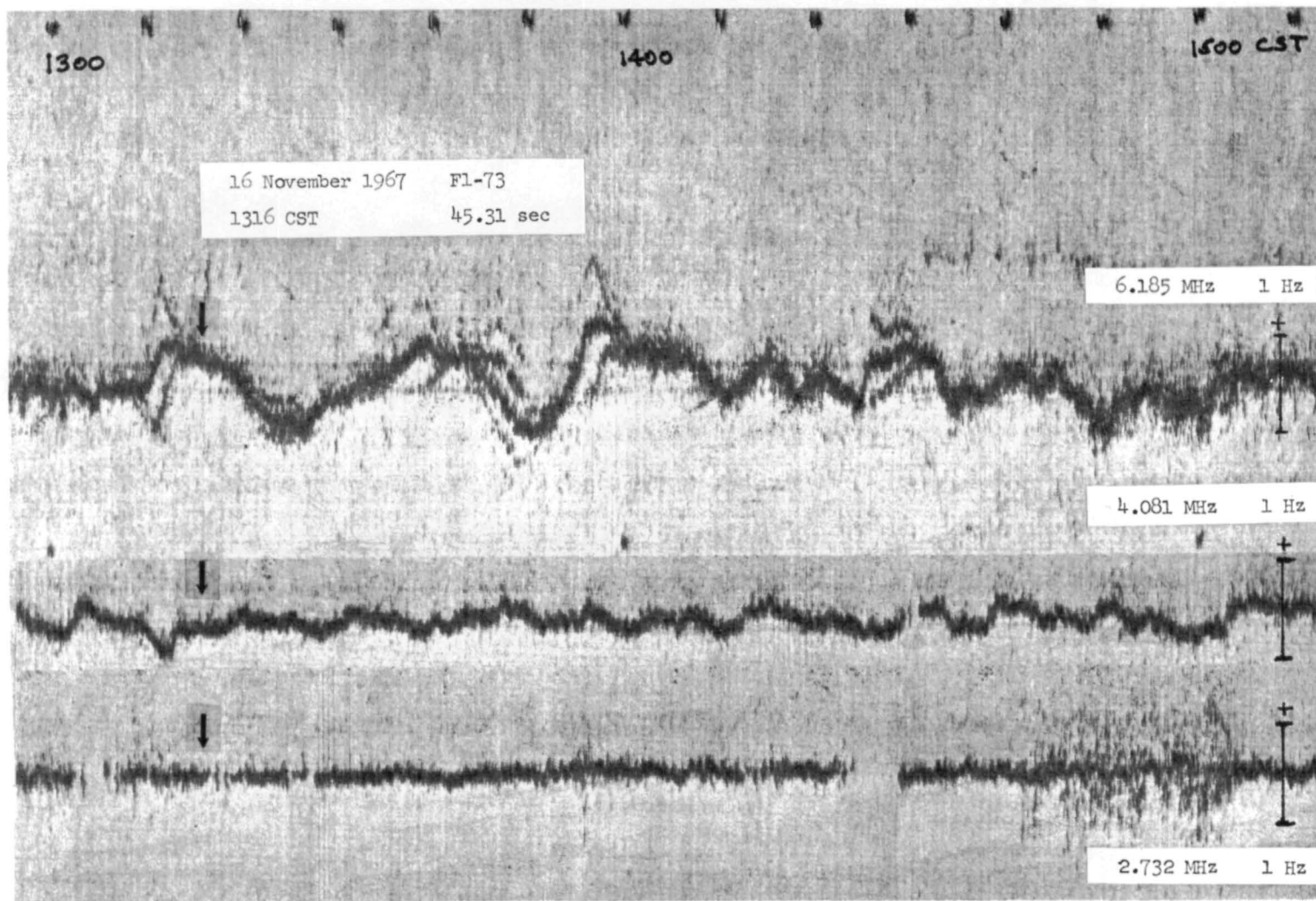


Figure 27 (b): Doppler data record, 16 November 1967: Huntsville, Alabama

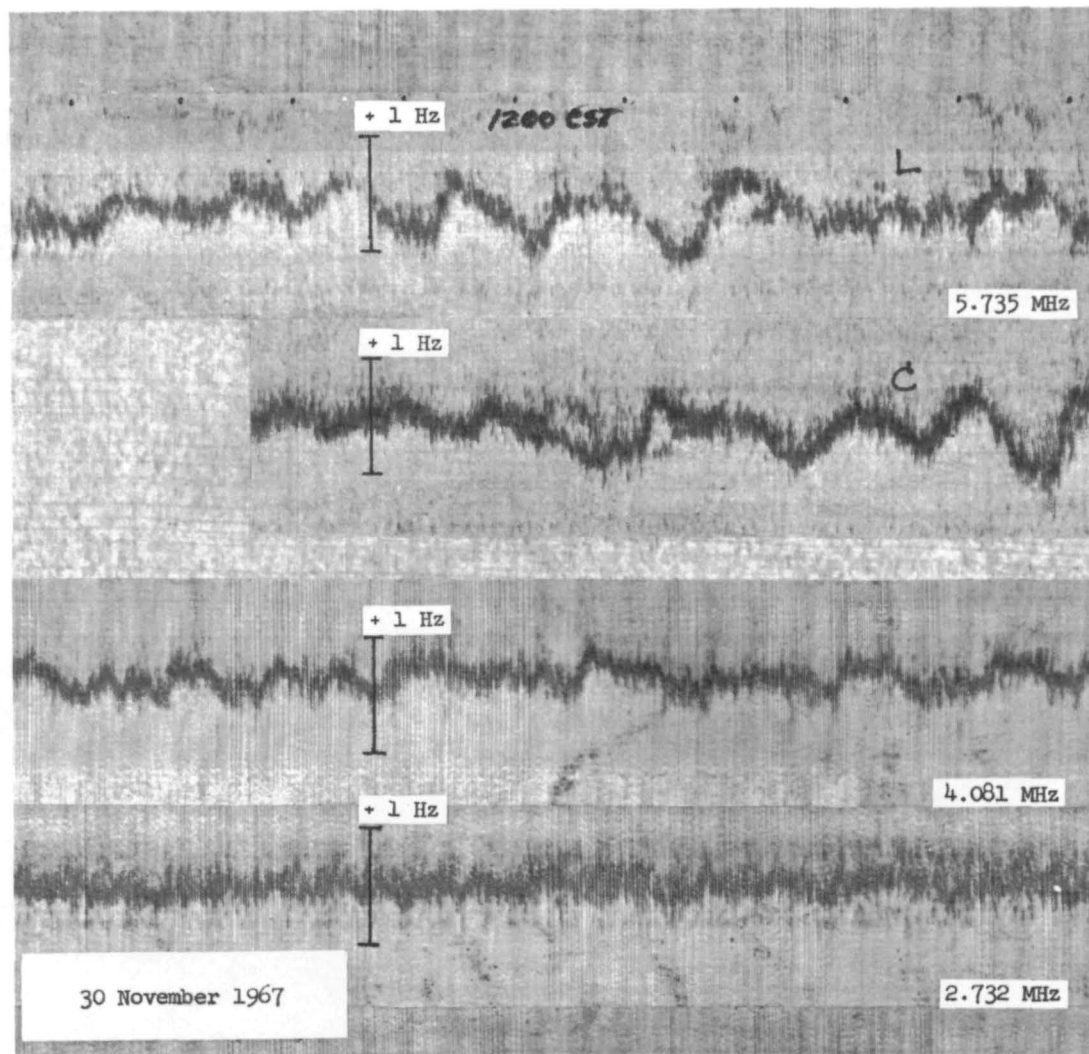


Figure 28 (a): Doppler data record, 30 November 1967: Huntsville, Alabama

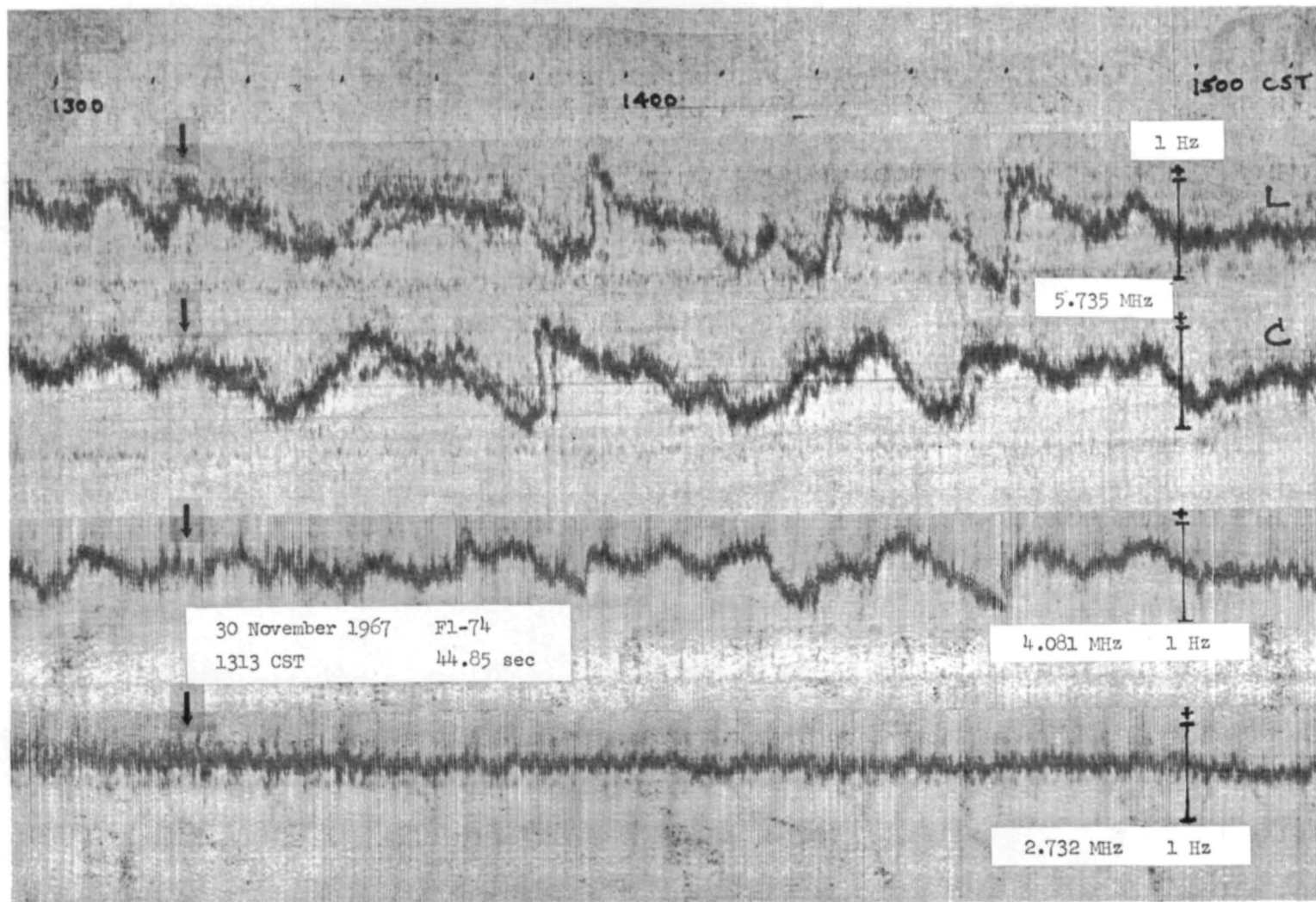


Figure 28 (b): Doppler data record, 30 November 1967: Huntsville, Alabama

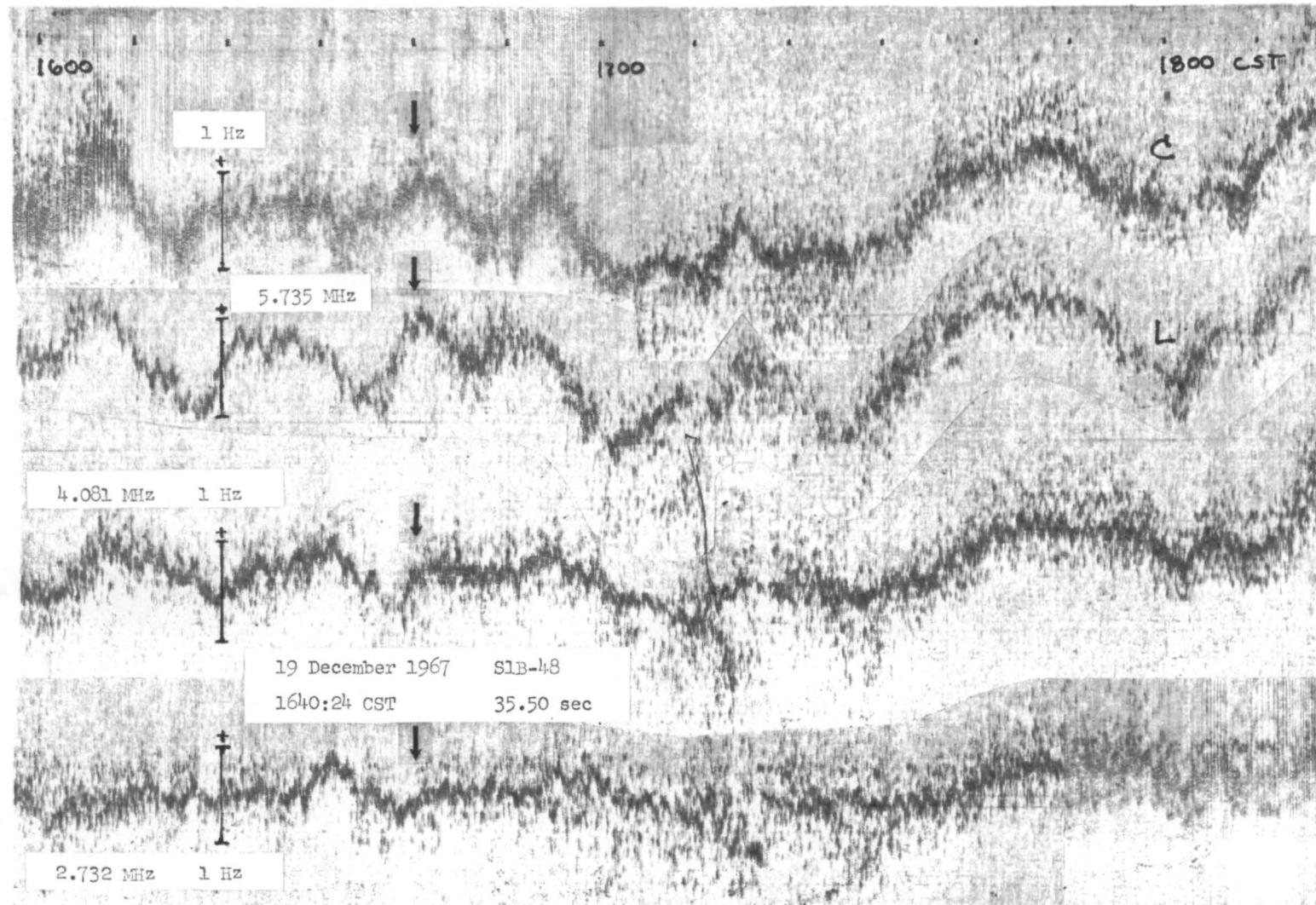


Figure 29: Doppler data record, 19 December 1967: Huntsville, Alabama

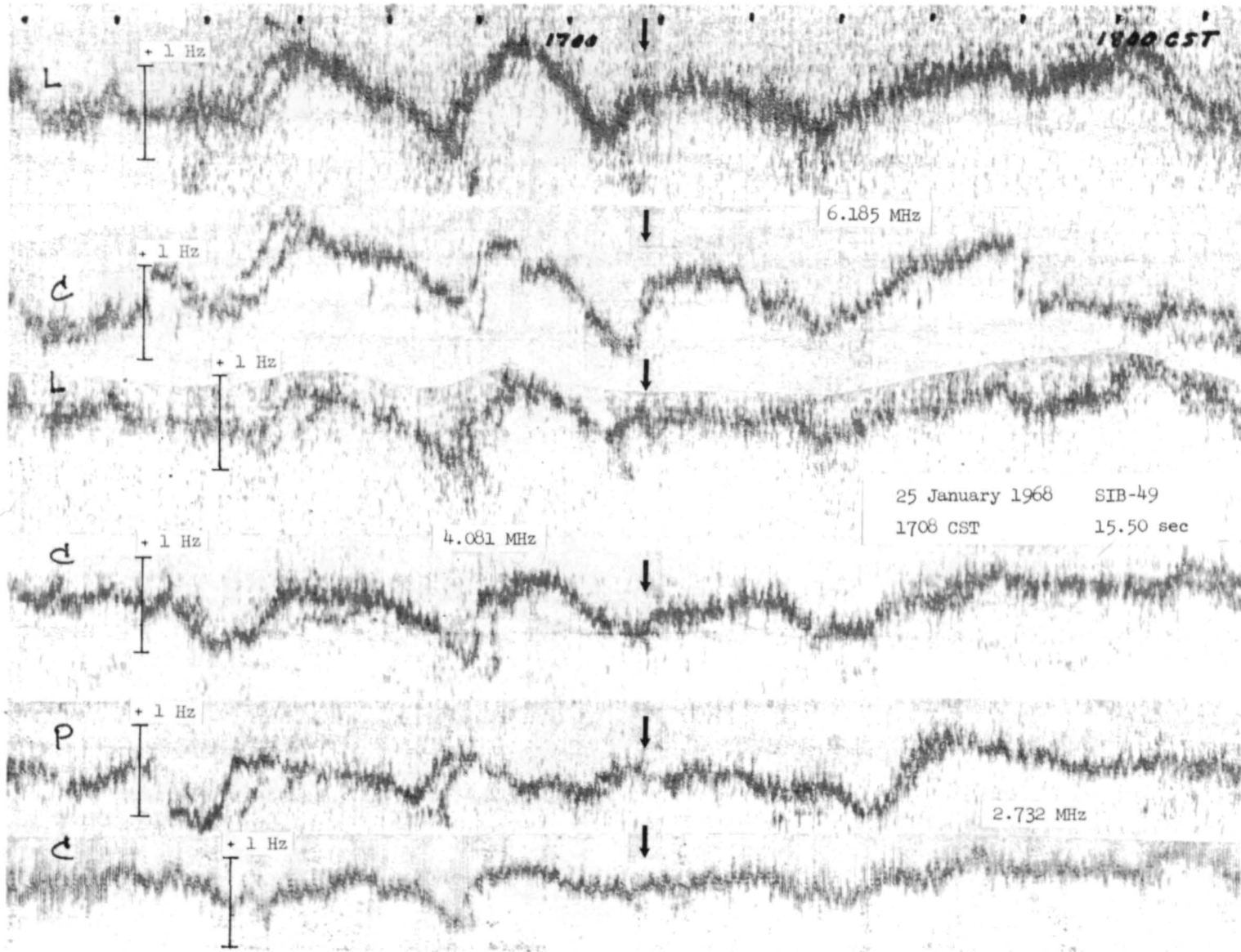


Figure 30: Doppler data record, 25 January 1968: Huntsville, Alabama

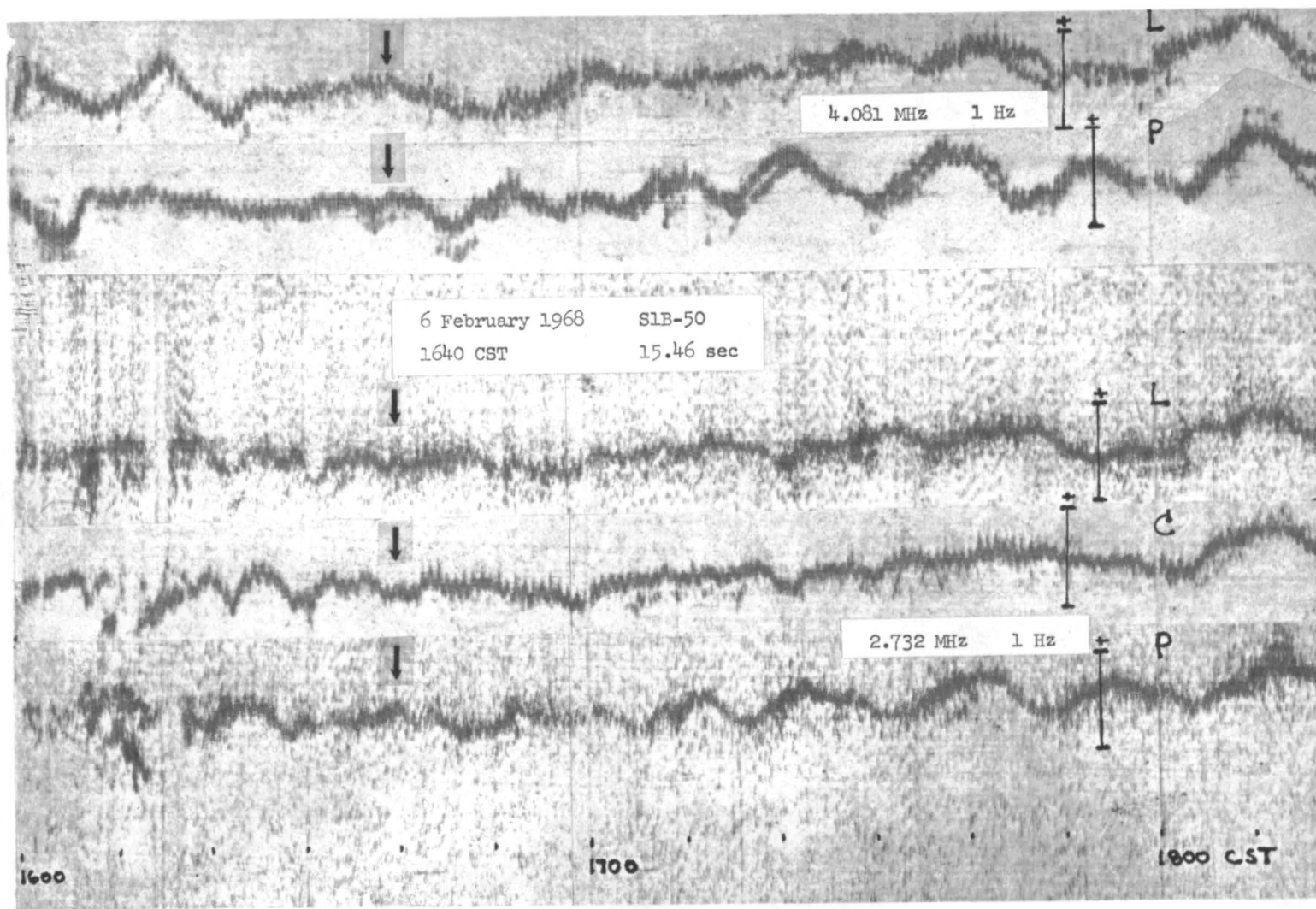


Figure 31 (a): Doppler data record, 6 February 1968: Huntsville, Alabama

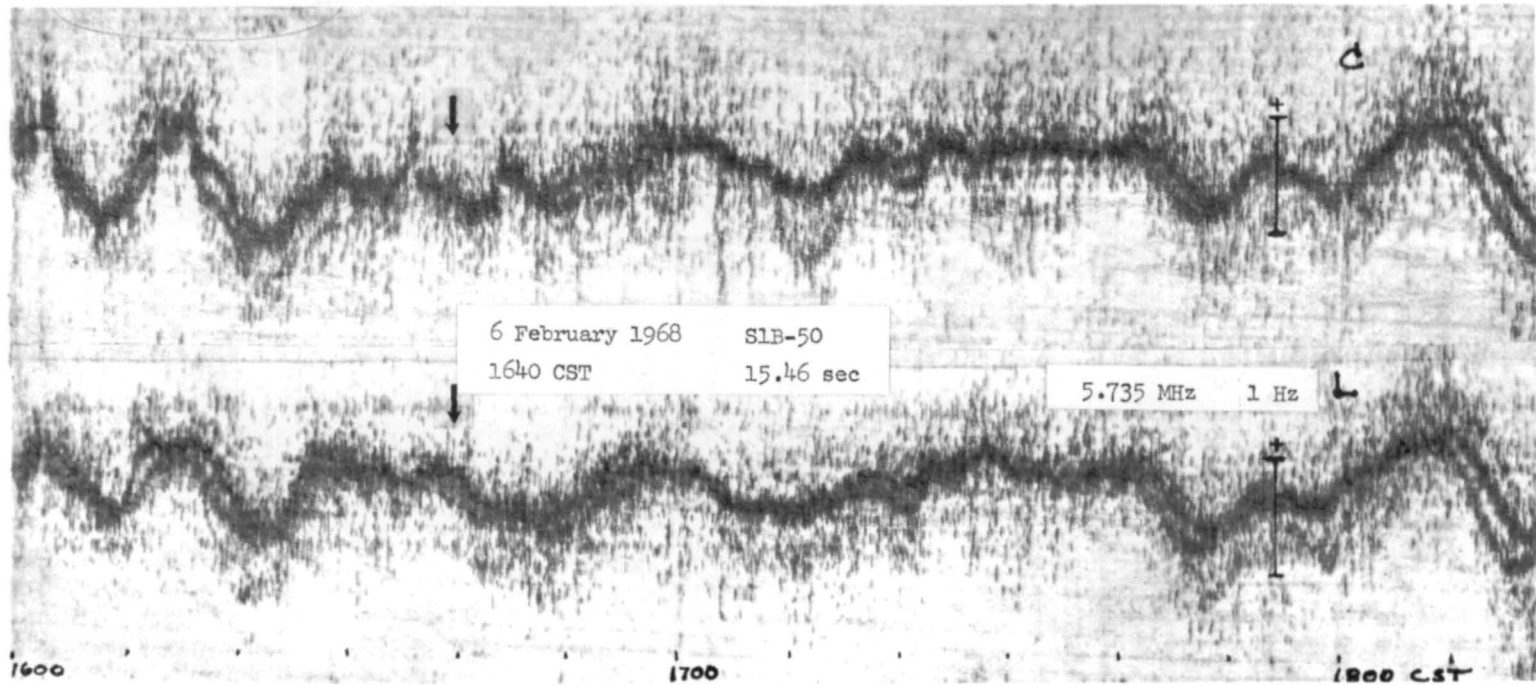


Figure 31 (b): Doppler data record, 6 February 1968: Huntsville, Alabama

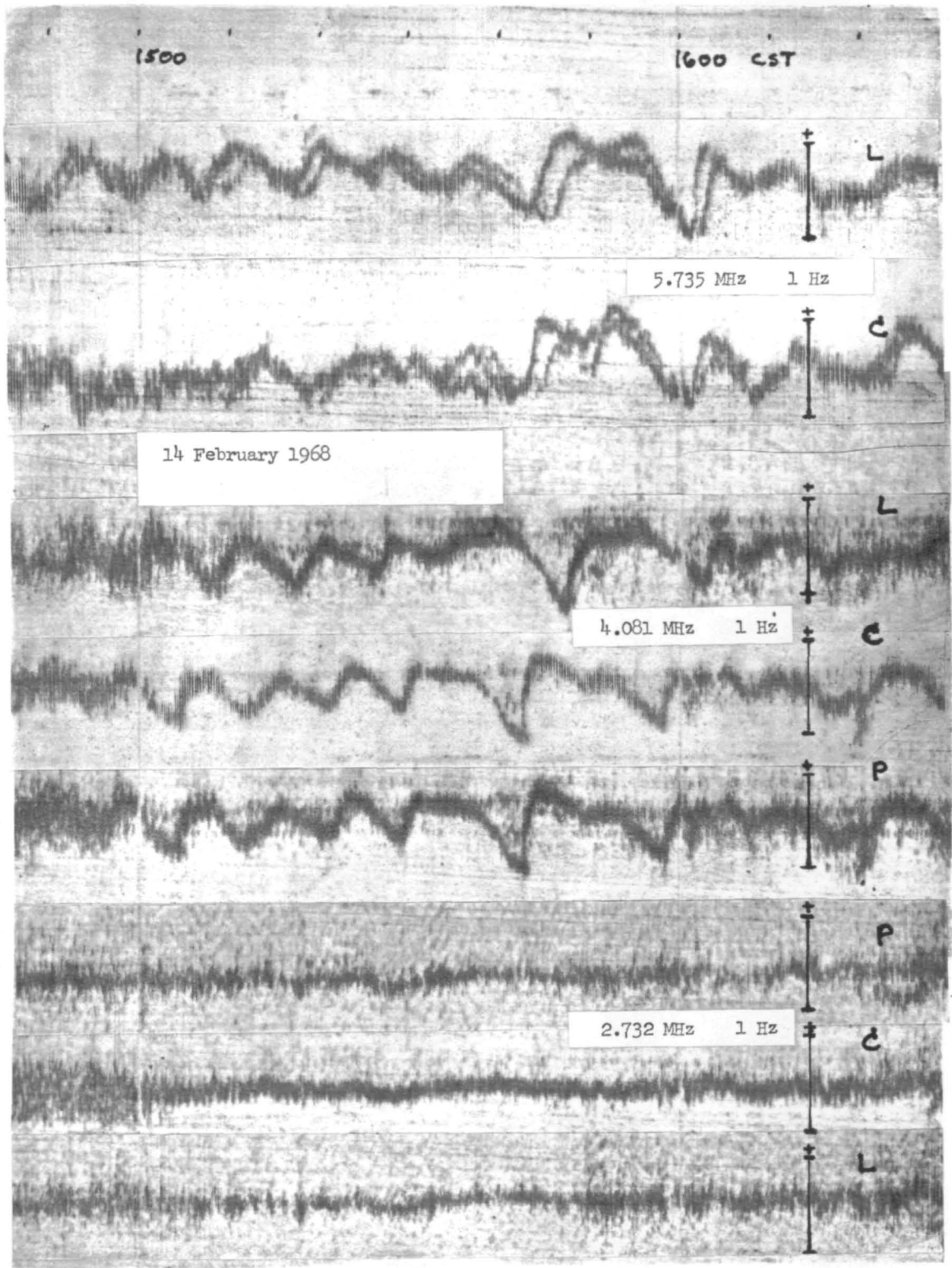


Figure 32 (a): Doppler data record,
14 February 1968: Huntsville, Alabama

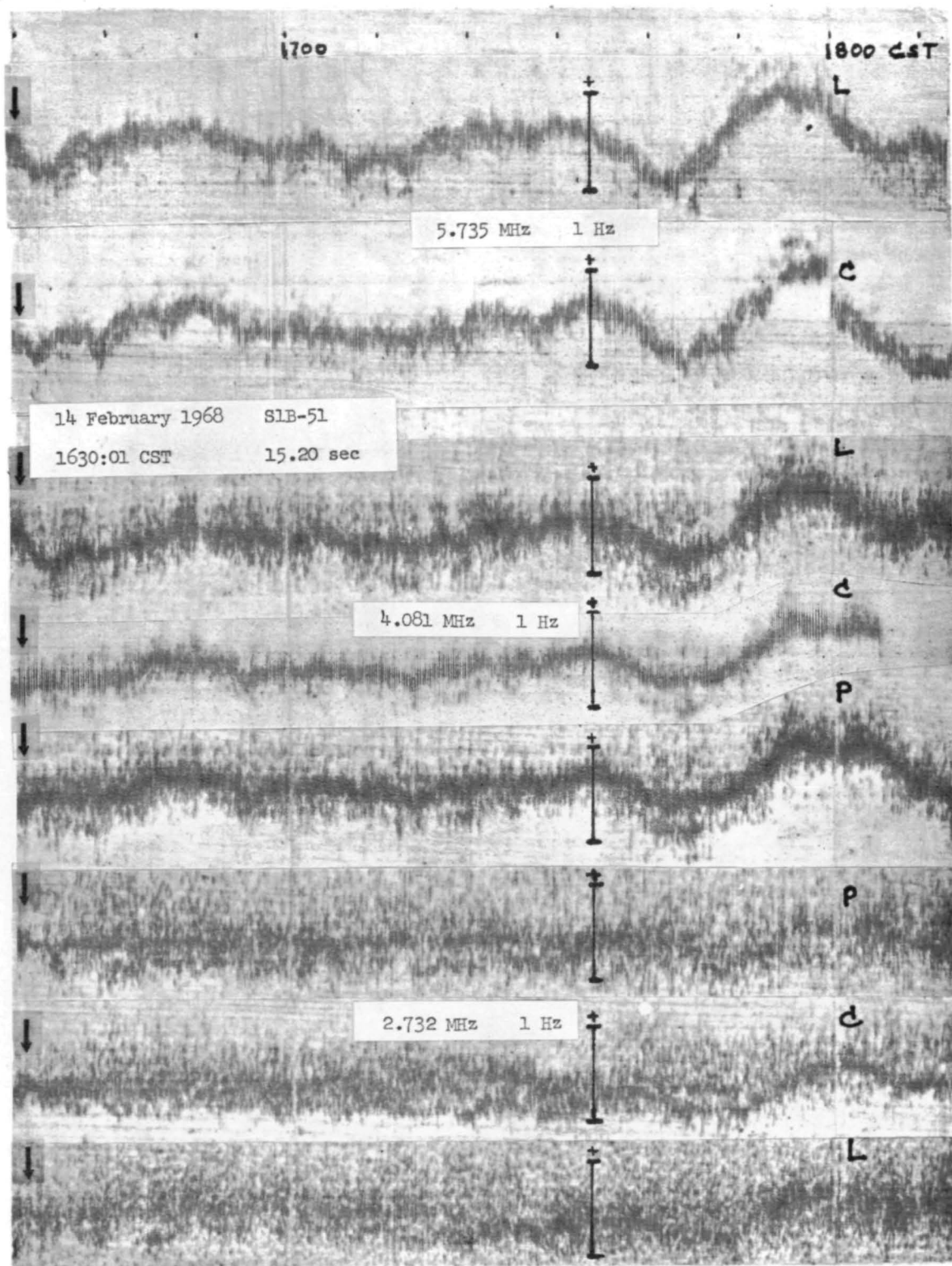


Figure 32 (b): Doppler data record,
14 February 1968: Huntsville, Alabama

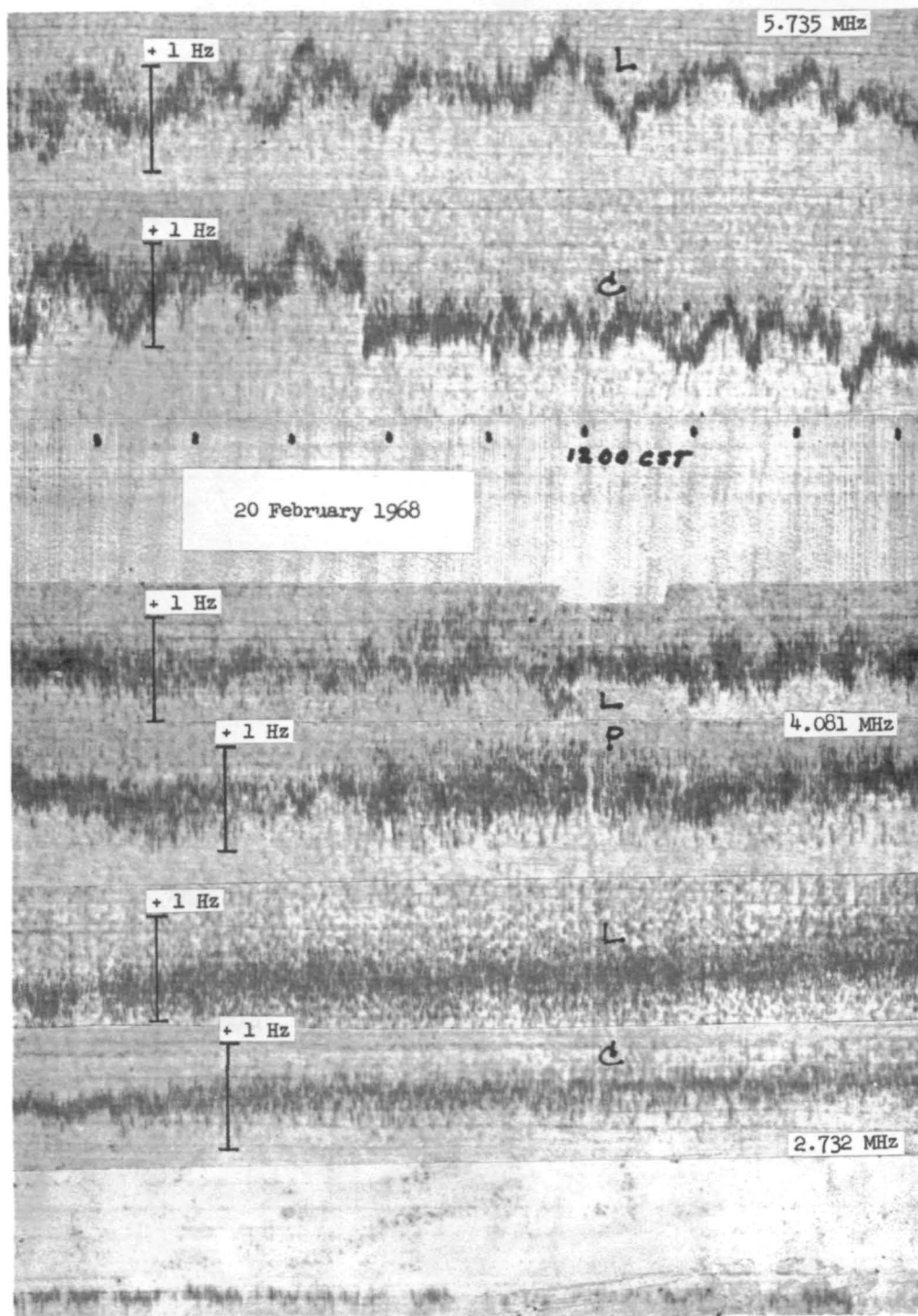


Figure 33 (a): Doppler data record,
20 February 1968: Huntsville, Alabama

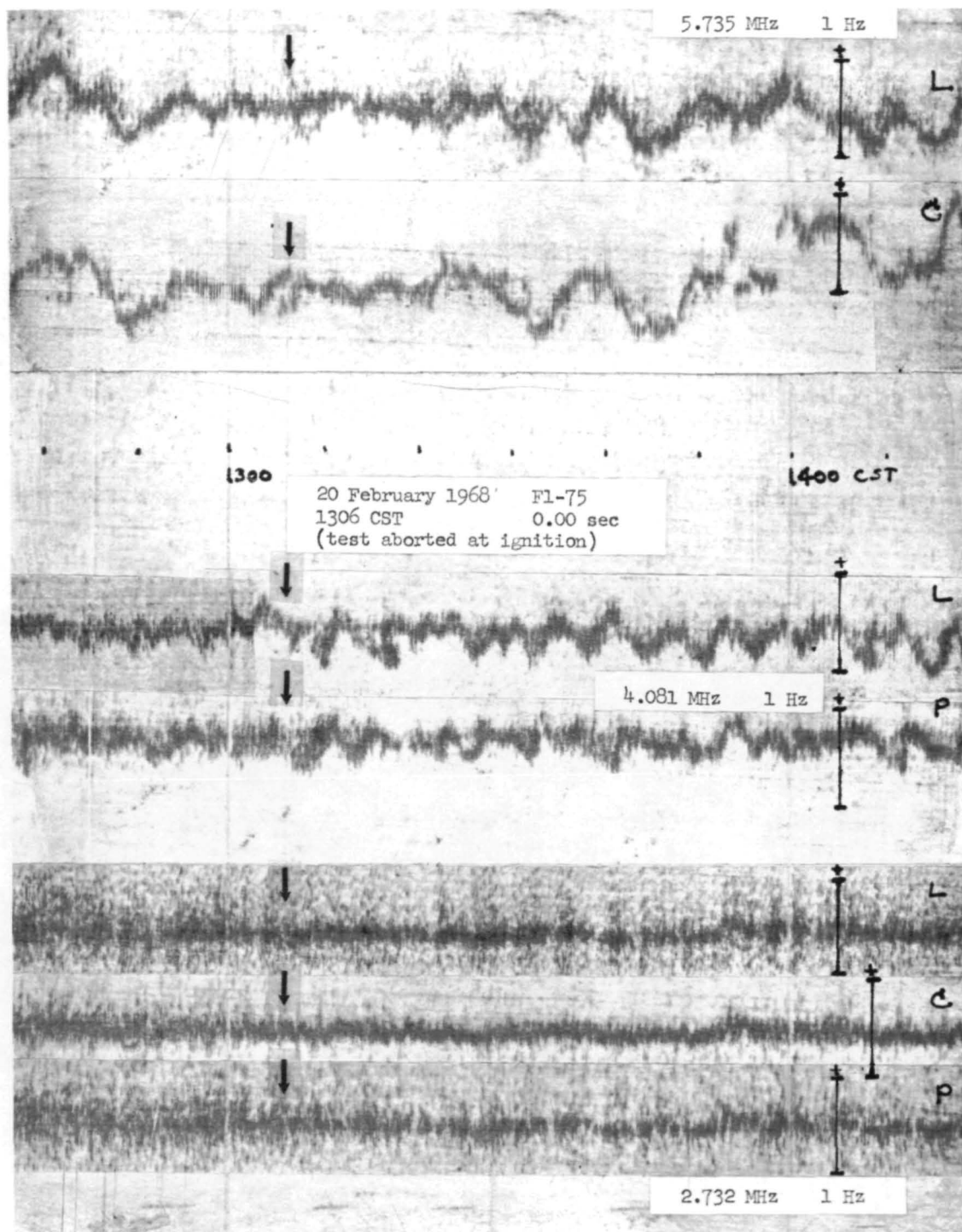


Figure 33 (b): Doppler data record,
20 February 1968: Huntsville, Alabama

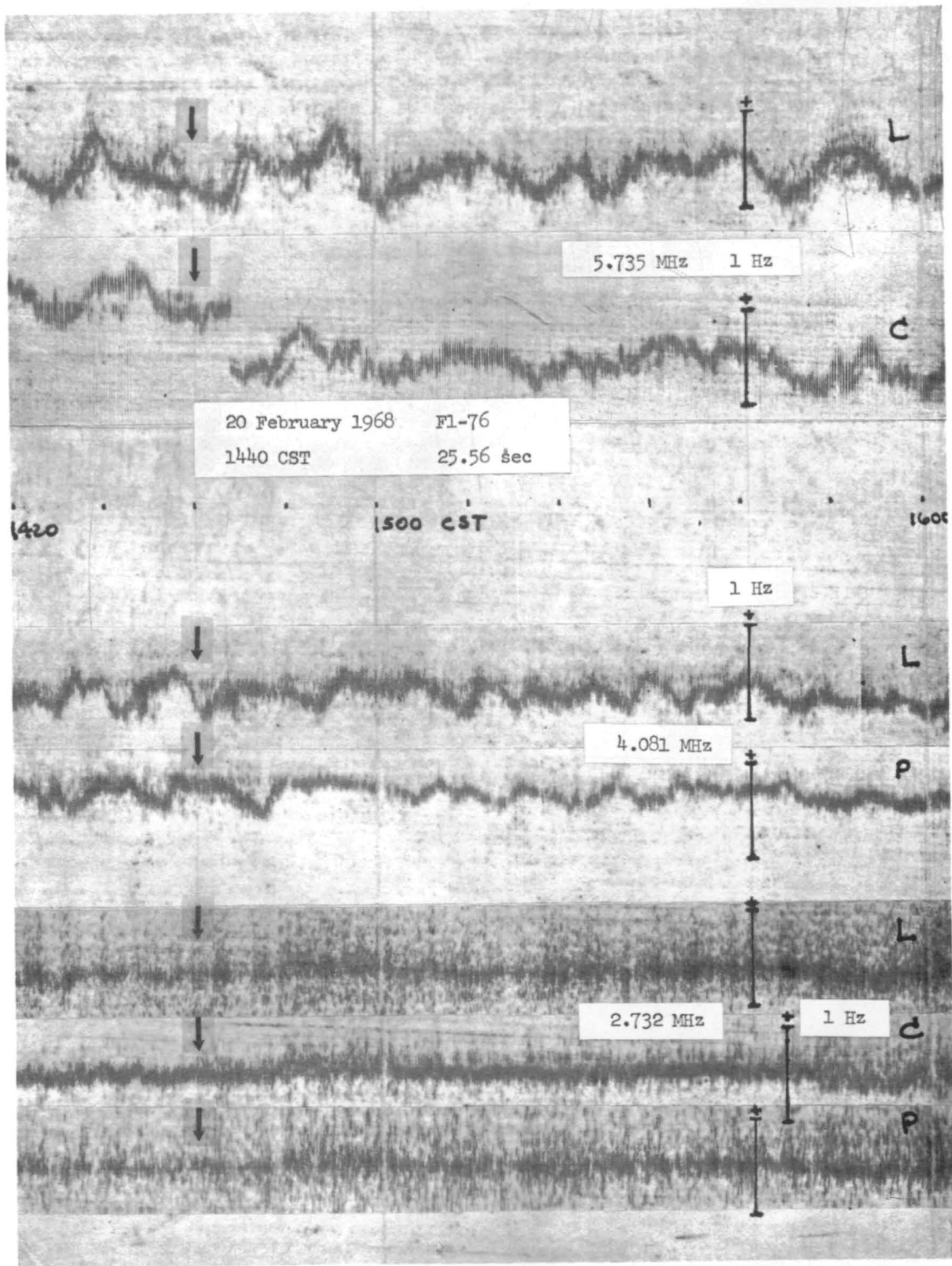


Figure 33 (c): Doppler data record,
20 February 1968: Huntsville, Alabama

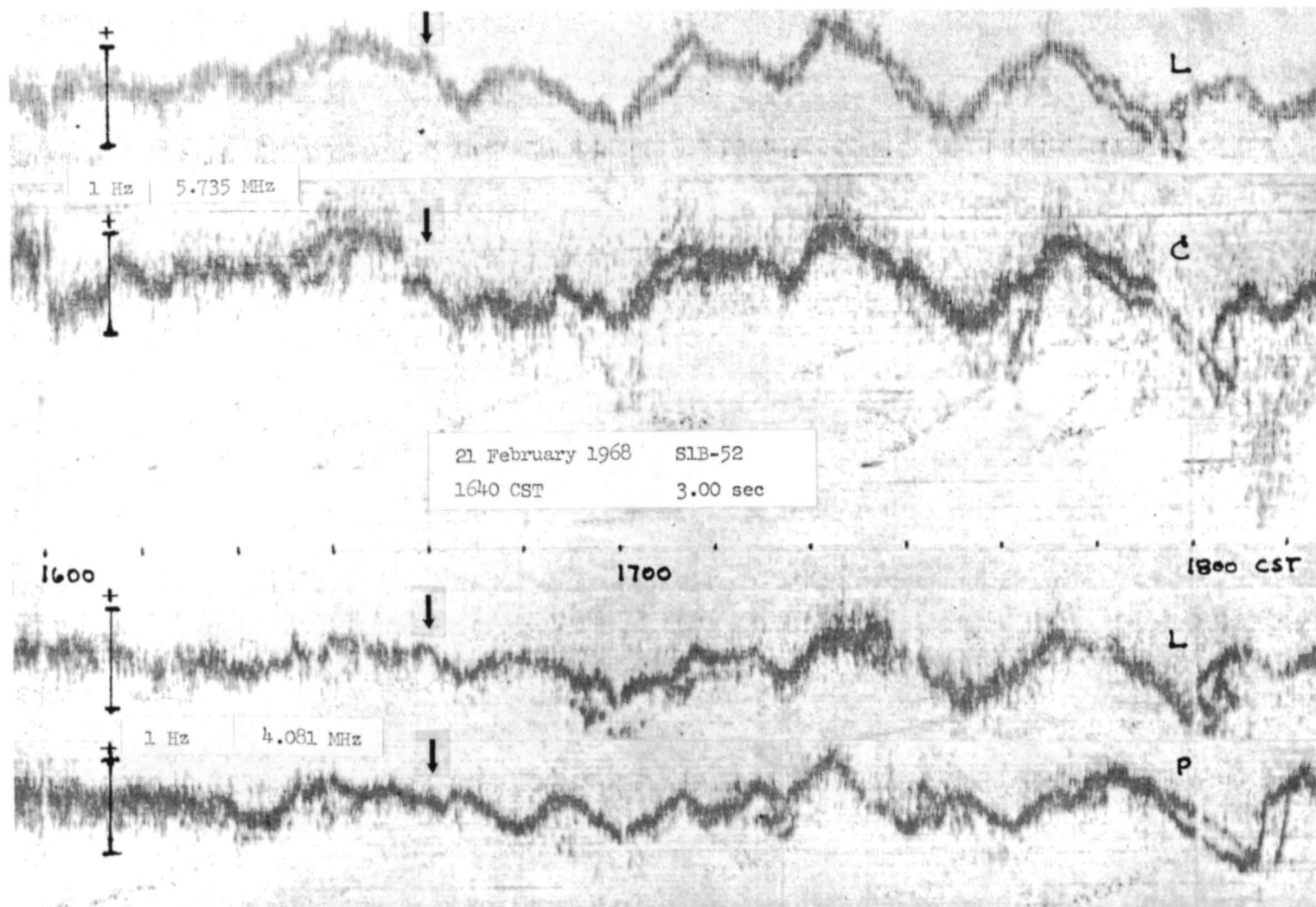


Figure 34 (a): Doppler data record, 21 February 1968: Huntsville, Alabama

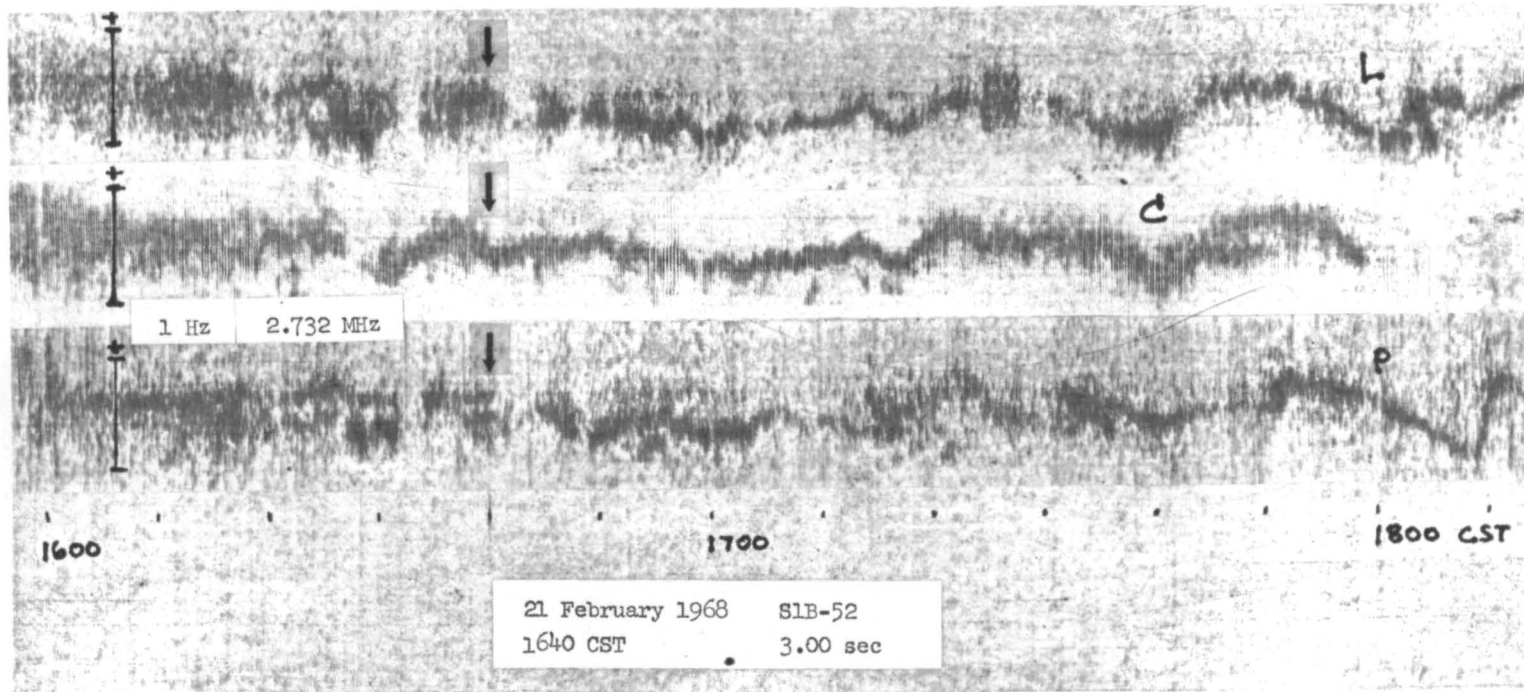


Figure 34 (b): Doppler data record, 21 February 1968: Huntsville, Alabama

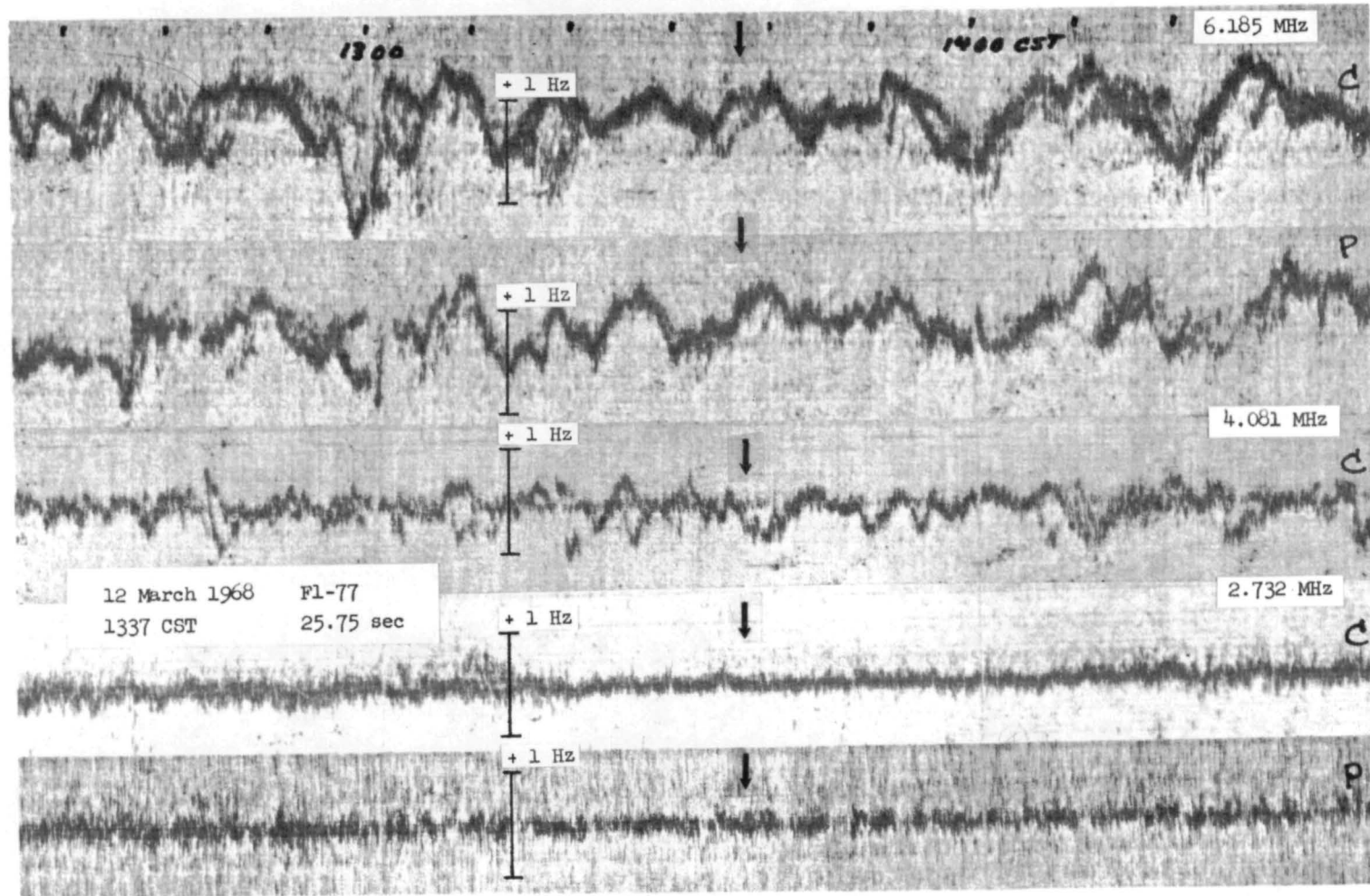


Figure 35: Doppler data record, 12 March 1968: Huntsville, Alabama

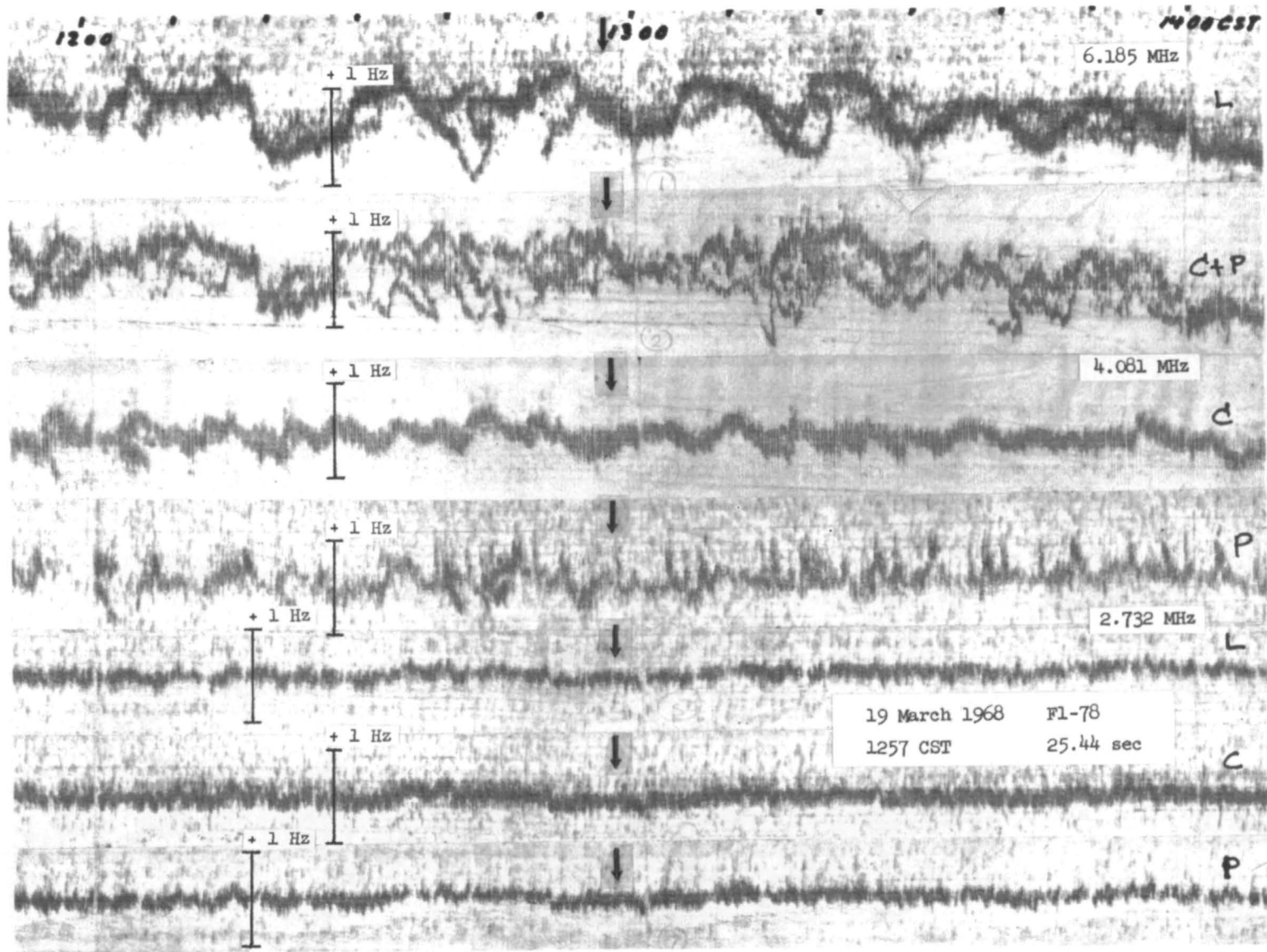


Figure 36: Doppler data record, 19 March 1968: Huntsville, Alabama

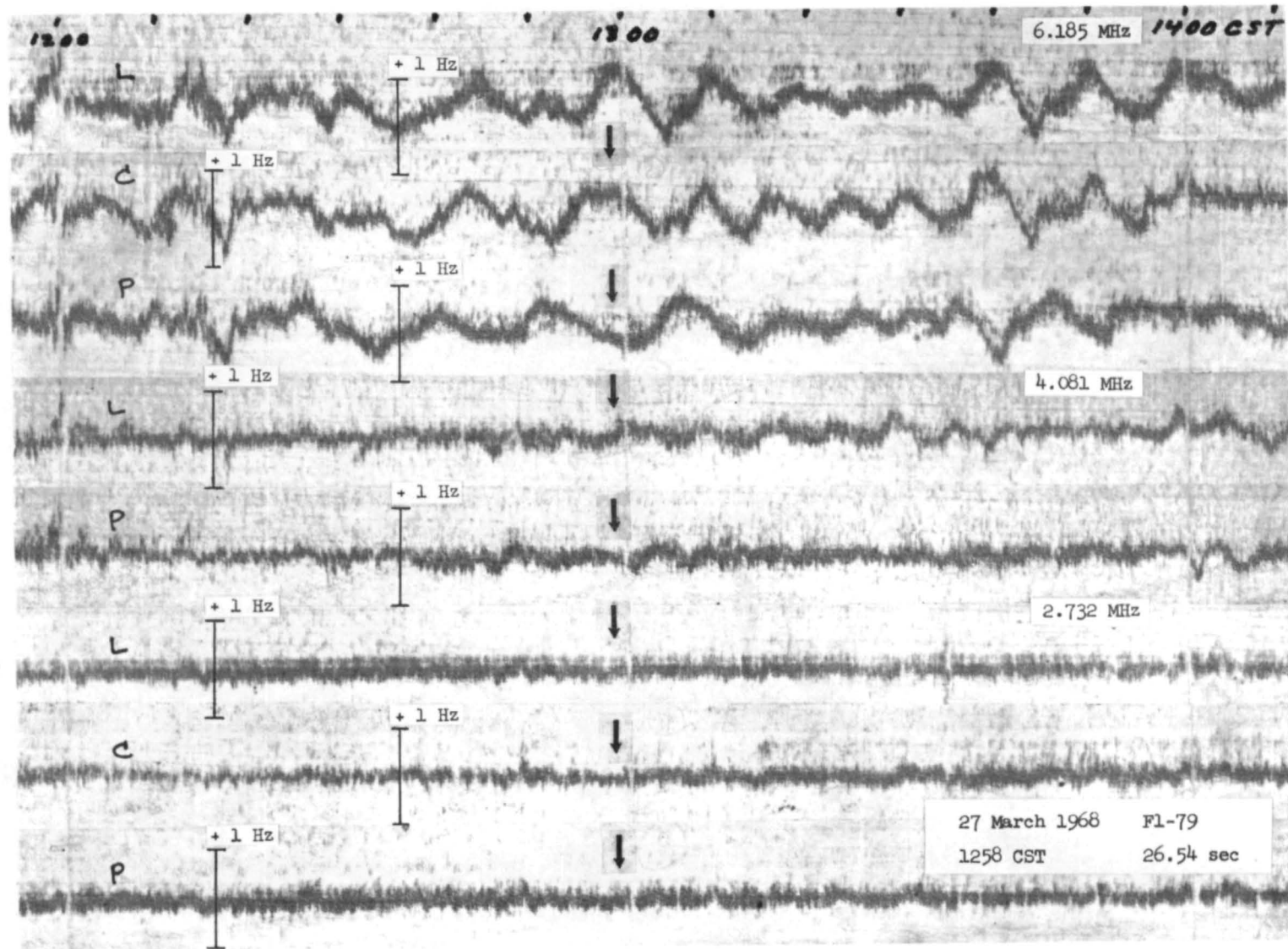


Figure 37: Doppler data record, 27 March 1968: Huntsville, Alabama

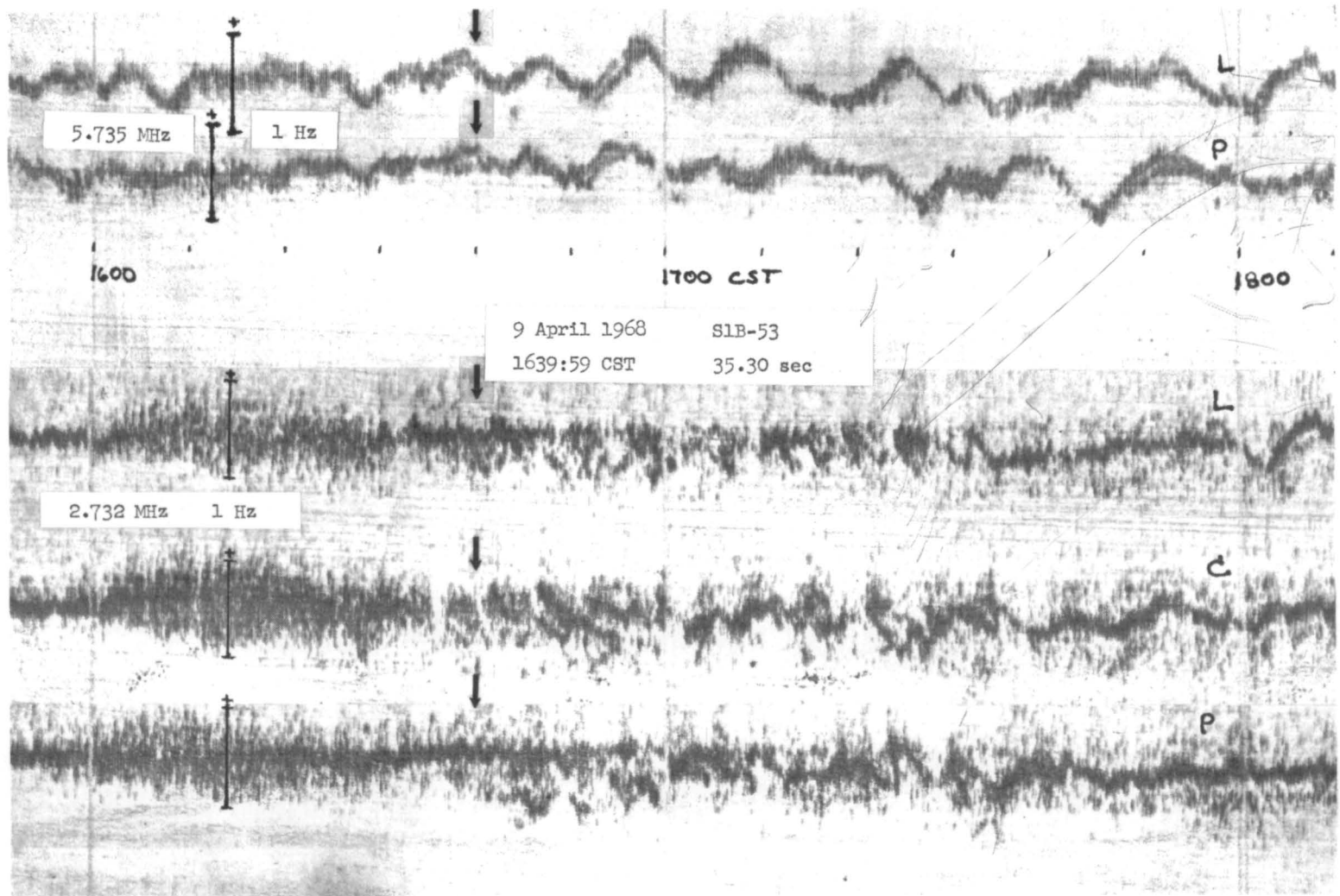


Figure 38 (a): Doppler data record, 9 April 1968: Huntsville, Alabama

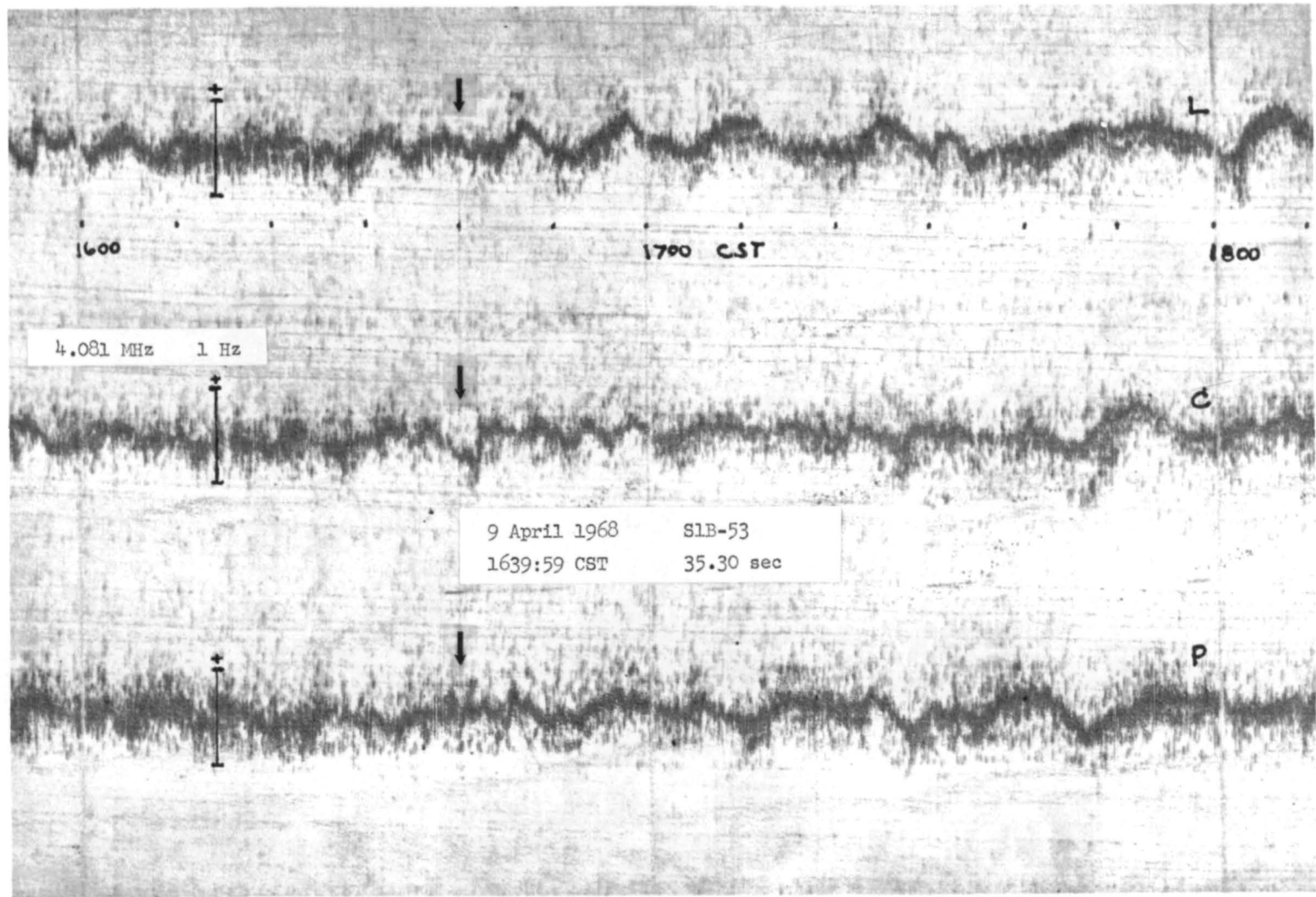


Figure 38 (b): Doppler data record, 9 April 1968: Huntsville, Alabama

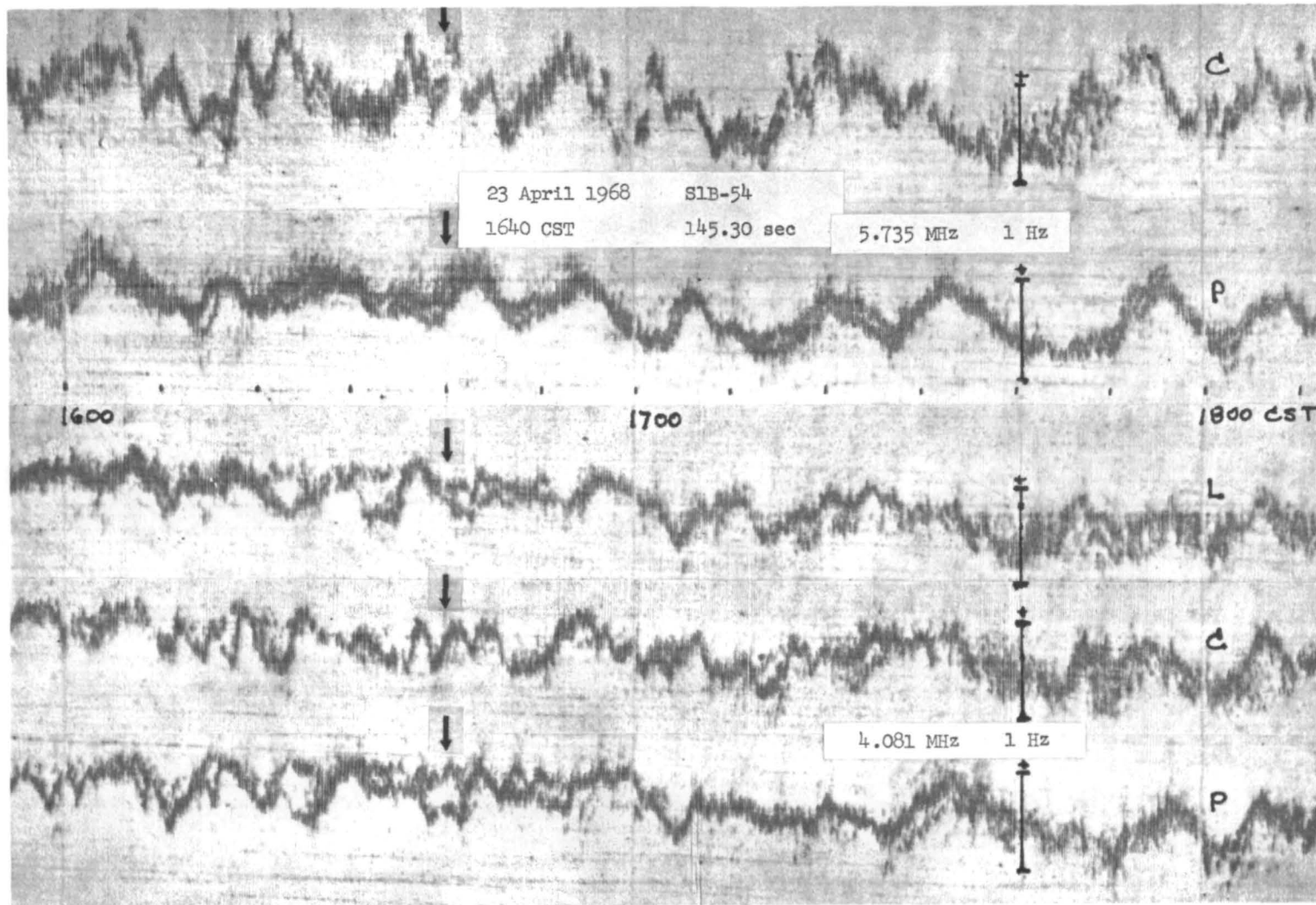


Figure 39 (a): Doppler data record, 23 April 1968: Huntsville, Alabama

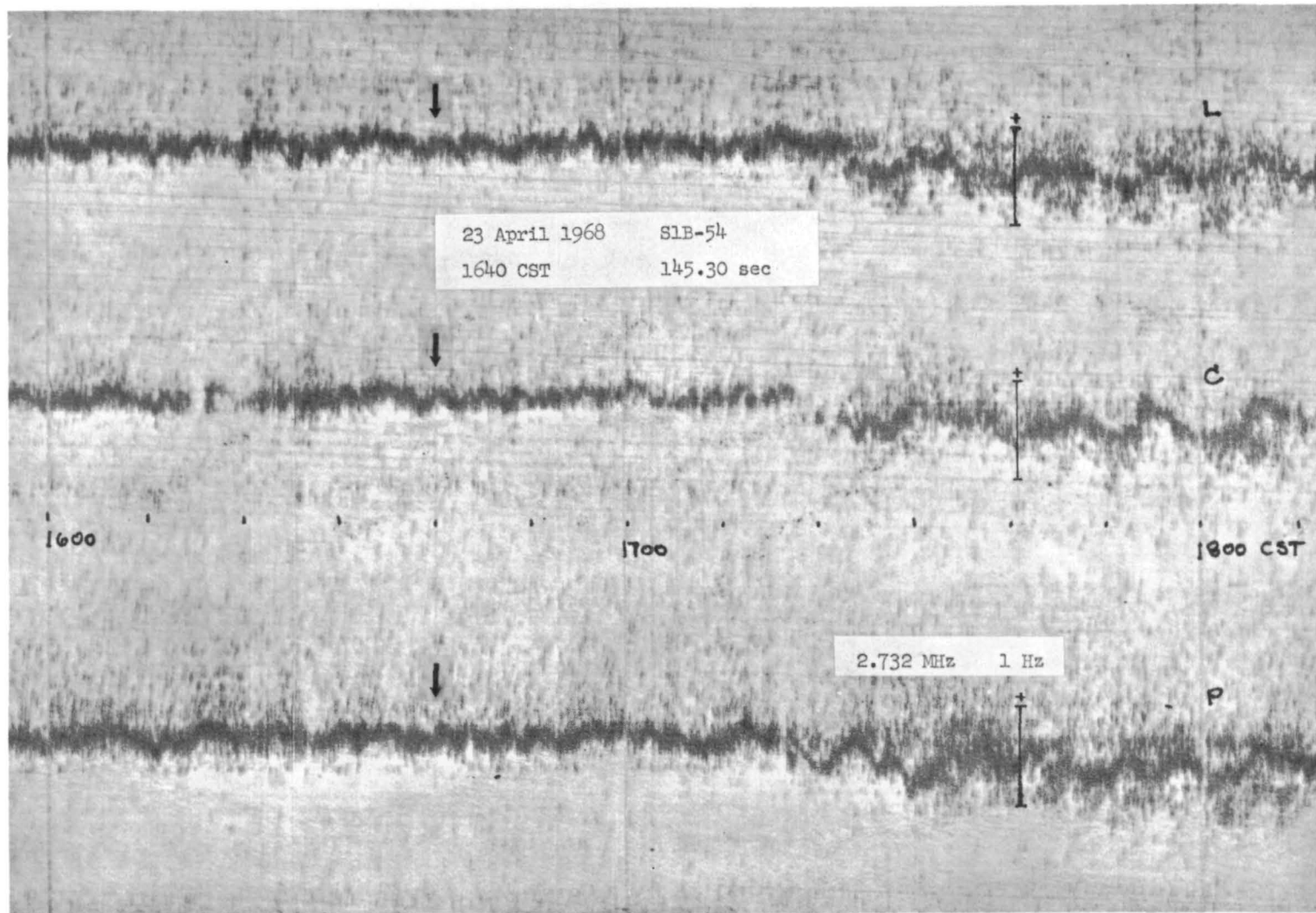


Figure 39 (b): Doppler data record, 23 April 1968: Huntsville, Alabama

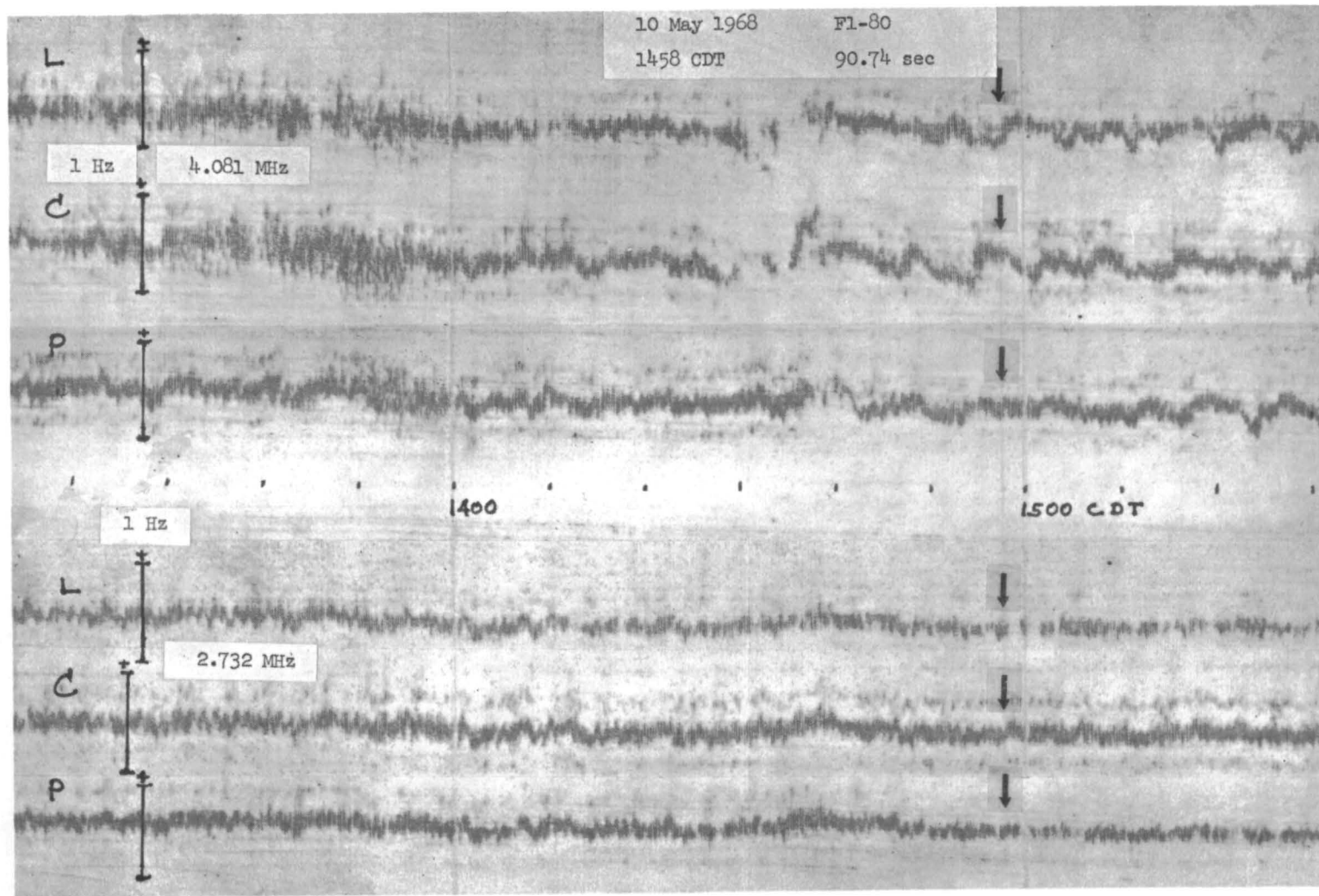


Figure 40 (a): Doppler data record, 10 May 1968: Huntsville, Alabama

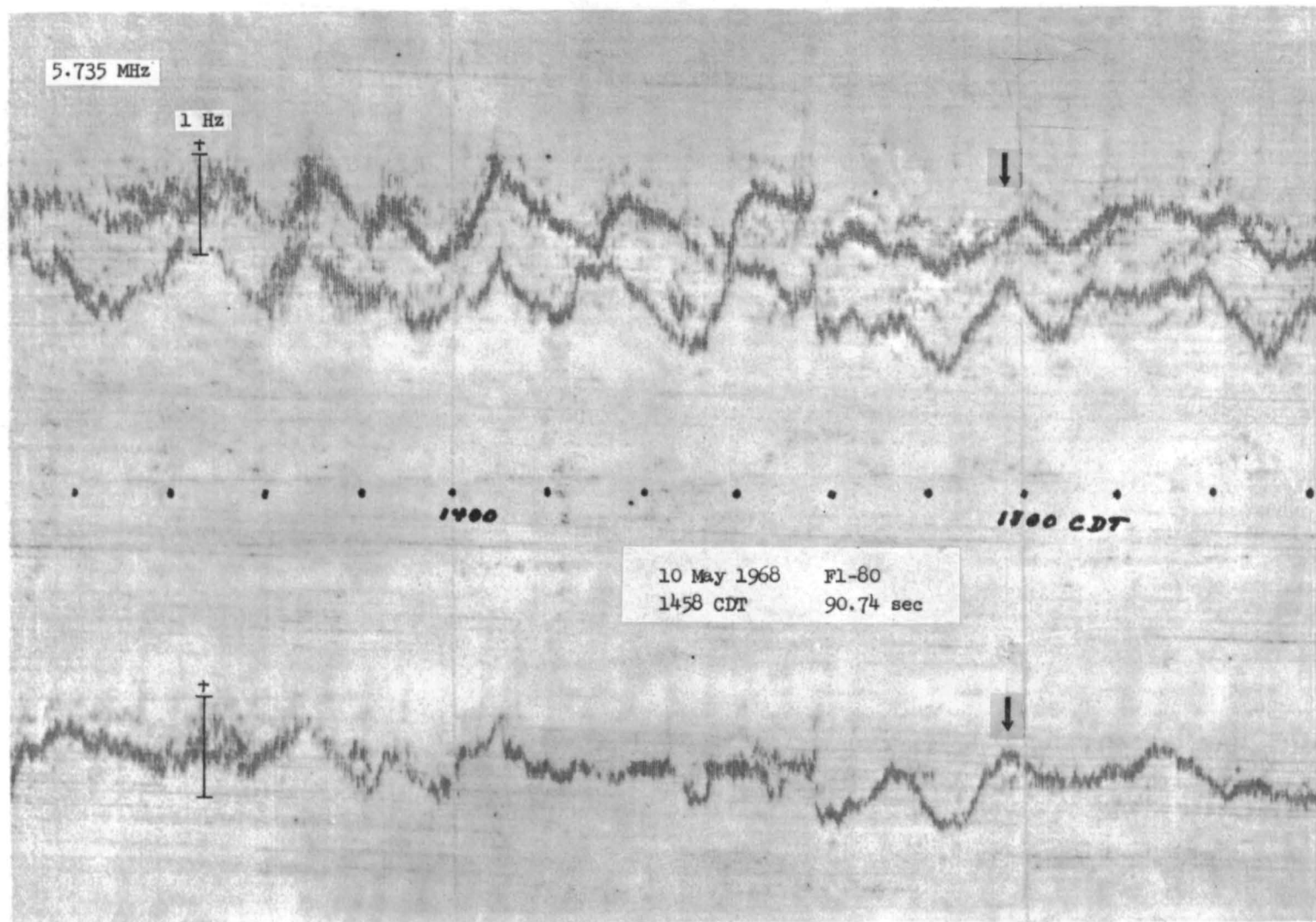


Figure 40 (b): Doppler data record, 10 May 1968: Huntsville, Alabama
processed with low analyzer gain

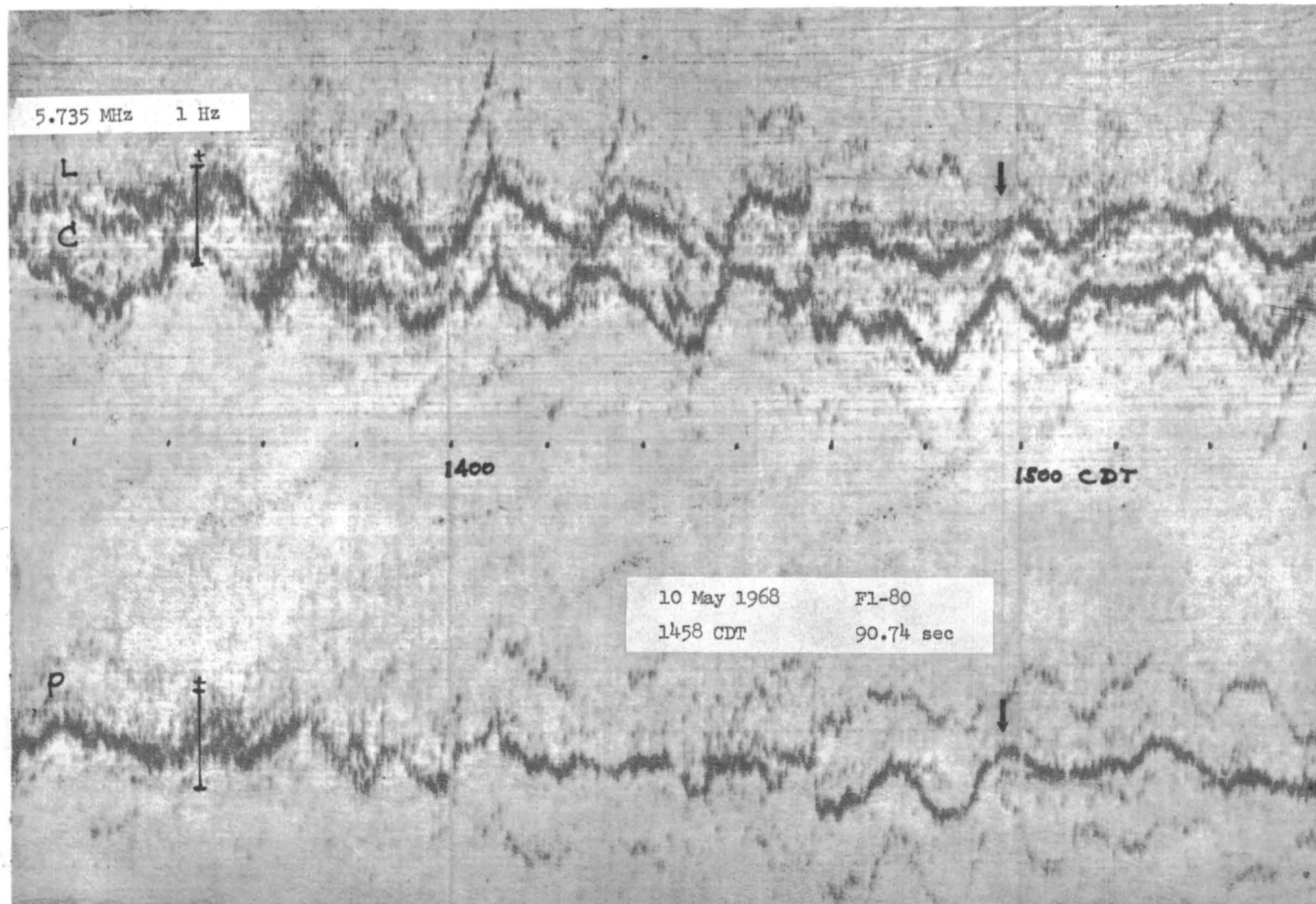


Figure 40 (c): Doppler data record, 10 May 1968: Huntsville, Alabama processed with intermediate analyzer gain

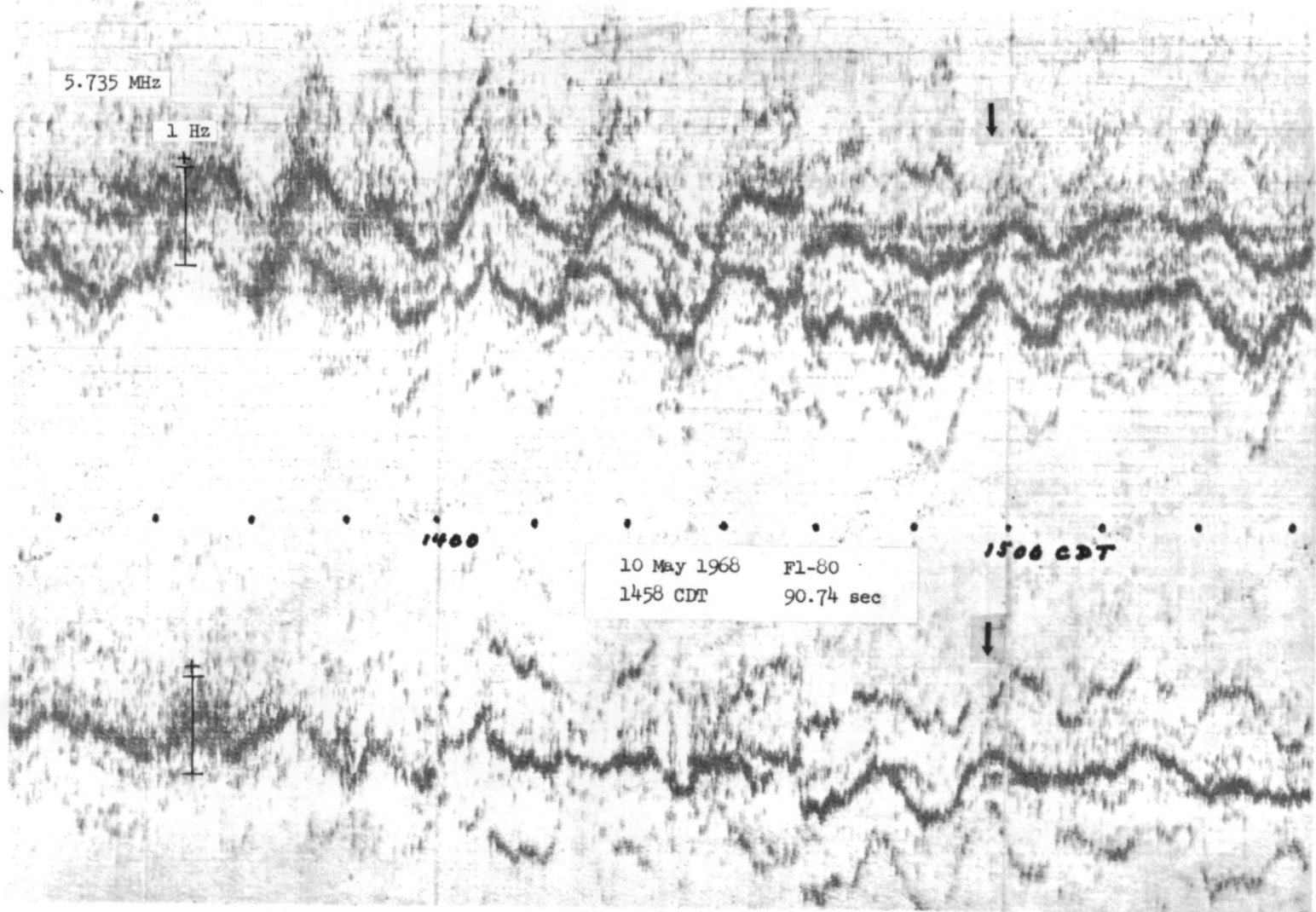


Figure 40 (d): Doppler data record, 10 May 1968: Huntsville, Alabama processed with high analyzer gain

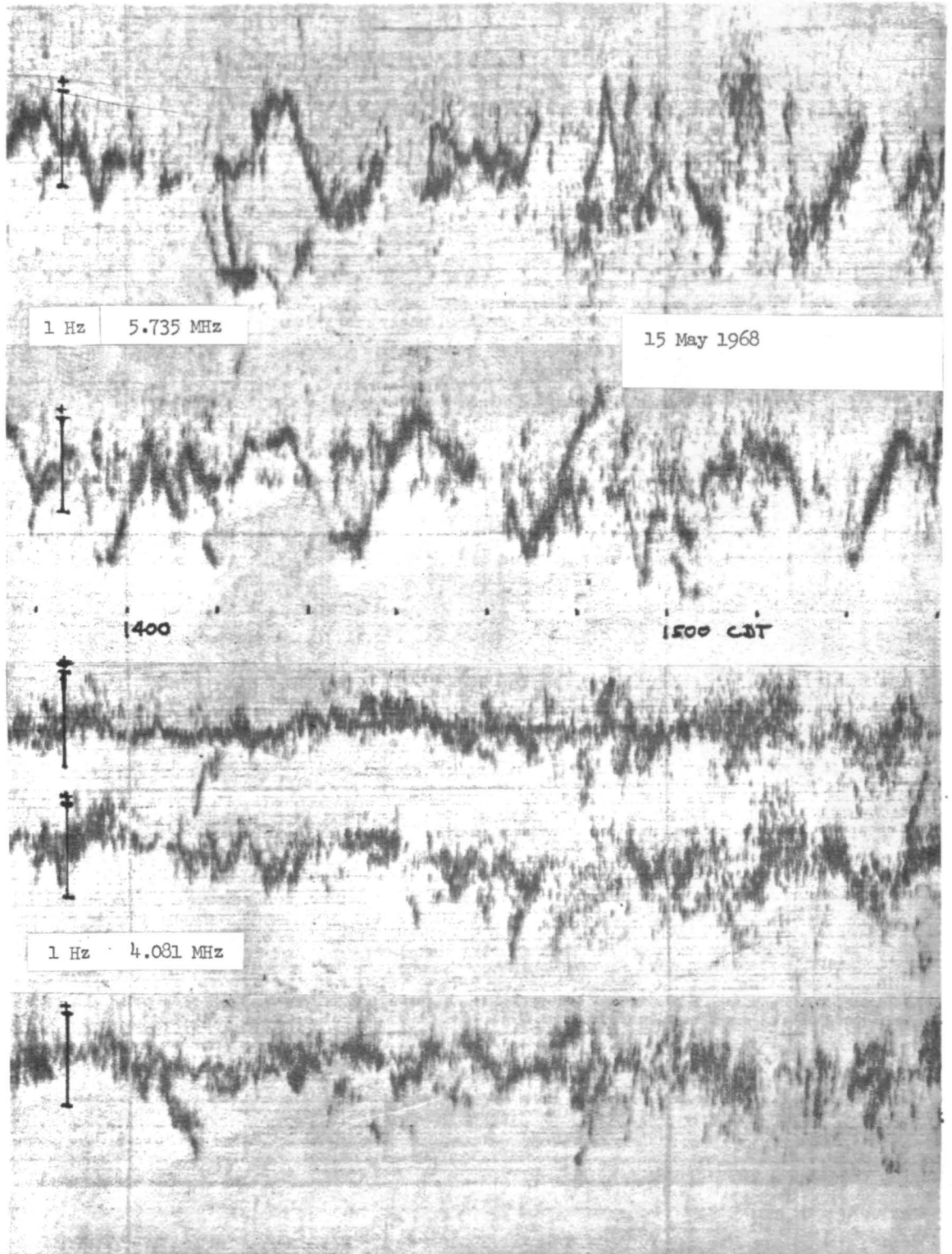


Figure 41 (a): Doppler data record,
15 May 1968: Huntsville, Alabama

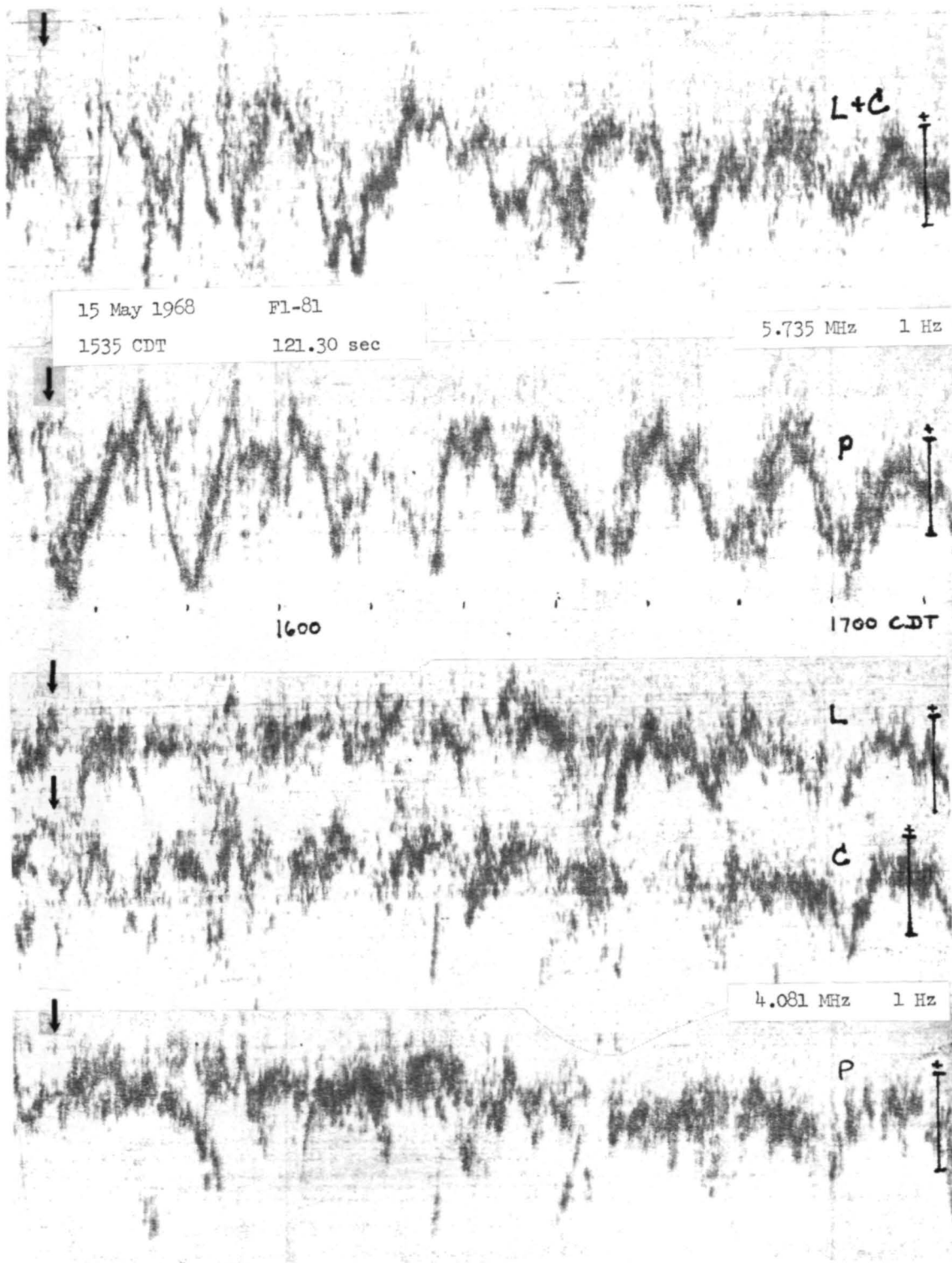


Figure 41 (b): Doppler data record,
 15 May 1968: Huntsville, Alabama

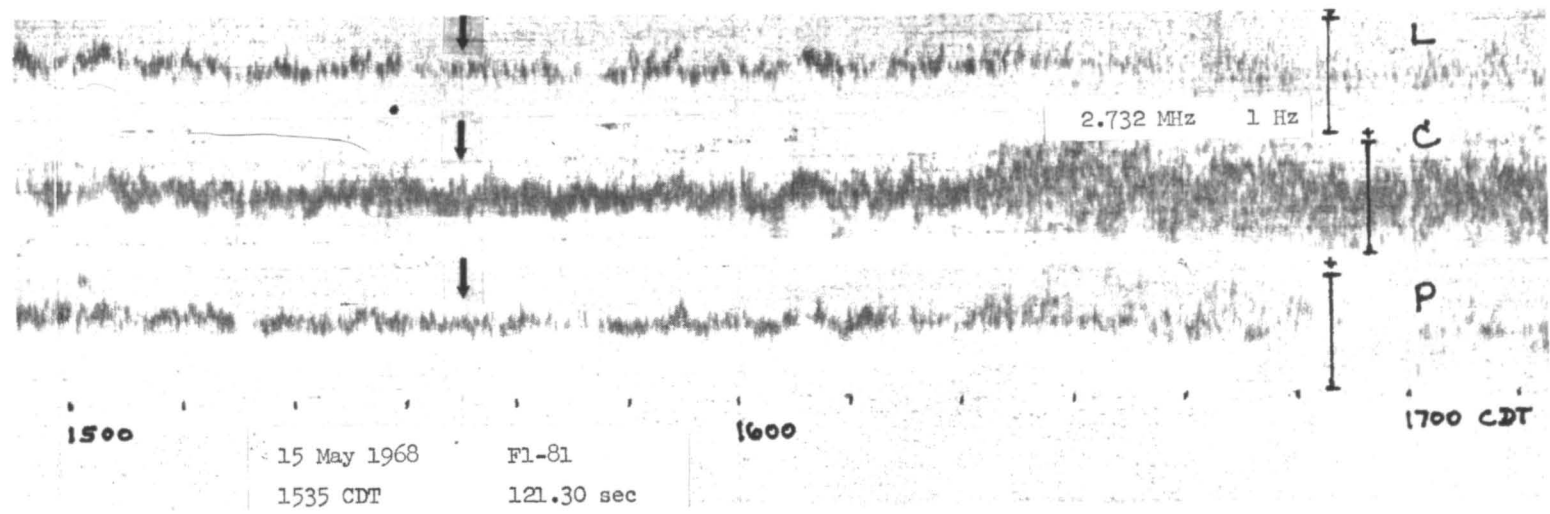
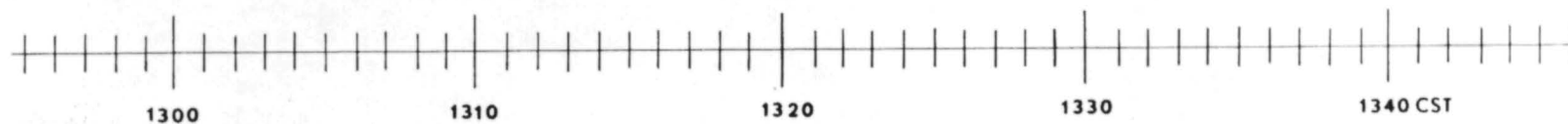
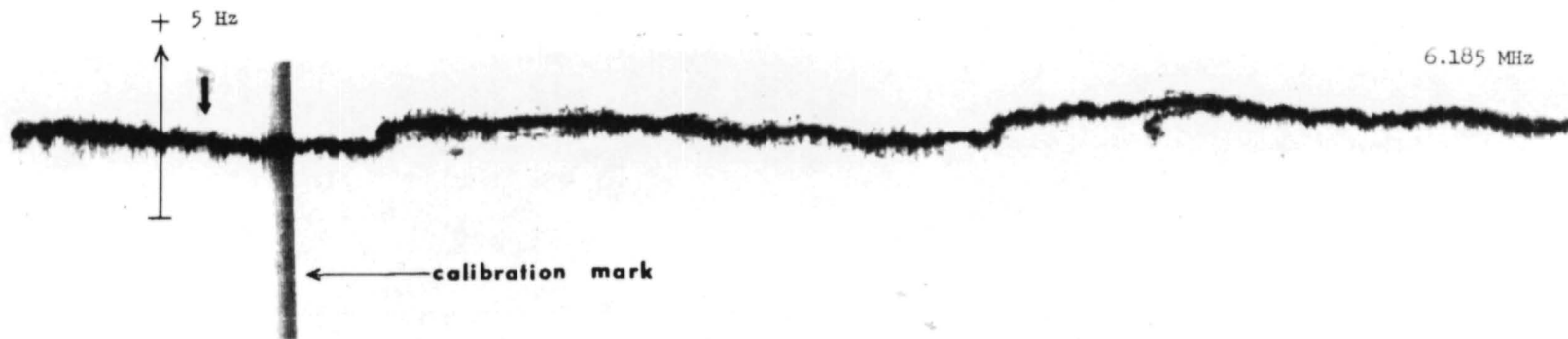


Figure 41 (c): Doppler data record, 15 May 1968: Huntsville, Alabama



-95-

20 April 1967 Fl-61
1301 CST 40 sec

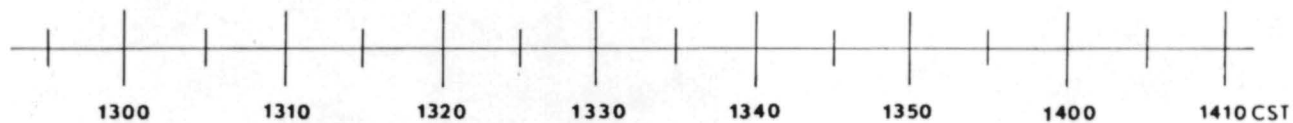
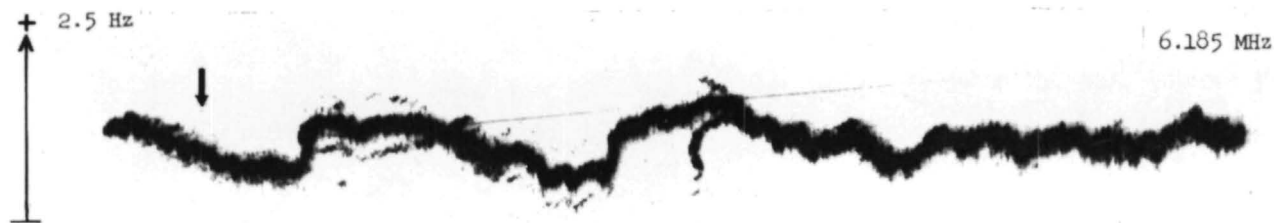
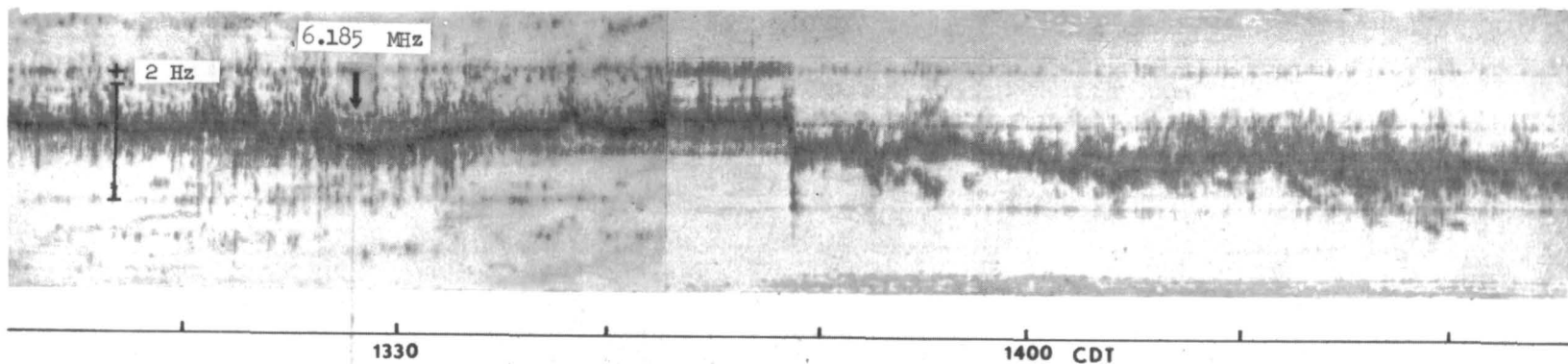


Figure 42: Doppler data record, 20 April 1967: Huntsville, Alabama



19 May 1967	F1-62
1328:06 CDT	25.004 sec

-96-

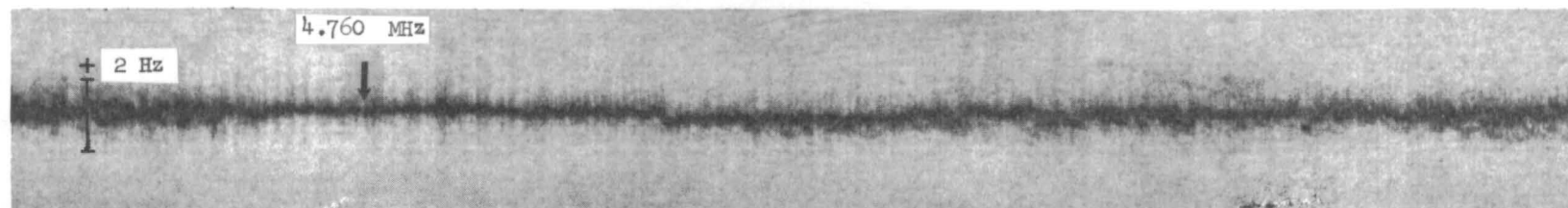
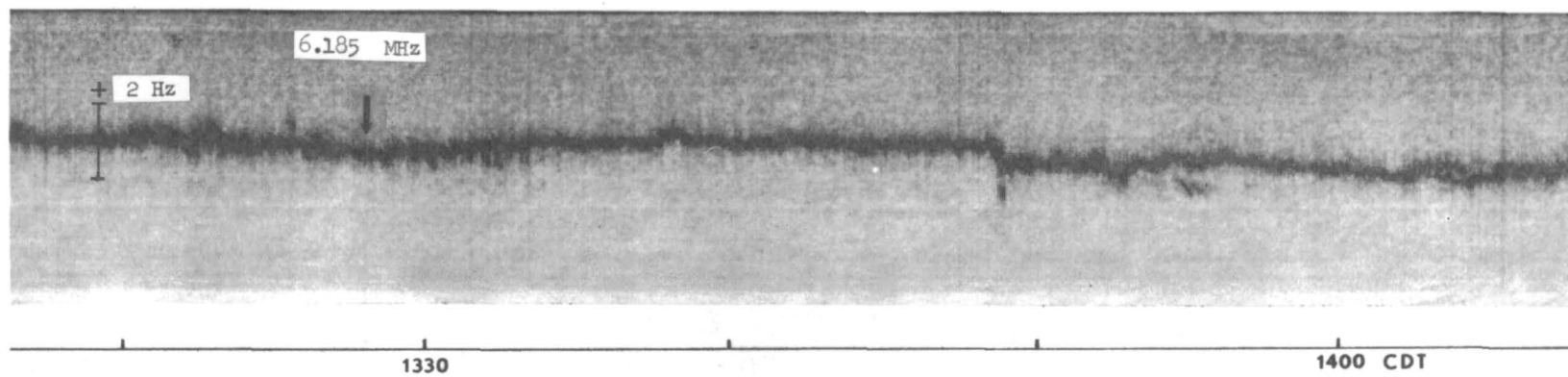
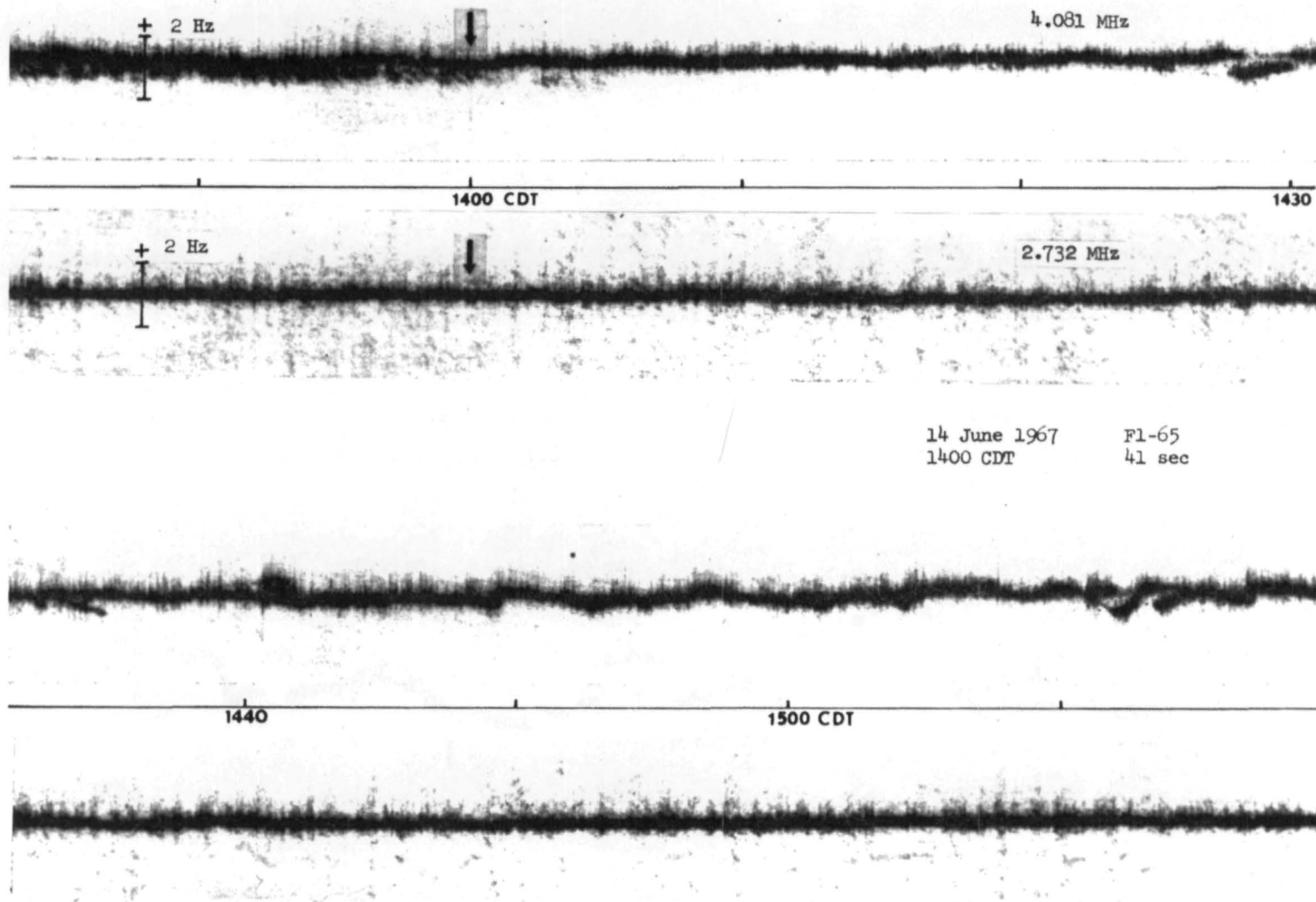


Figure 43: Doppler data record, 19 May 1967: Huntsville, Alabama



-97-

Figure 44: Doppler data record, 14 June 1967: Huntsville, Alabama

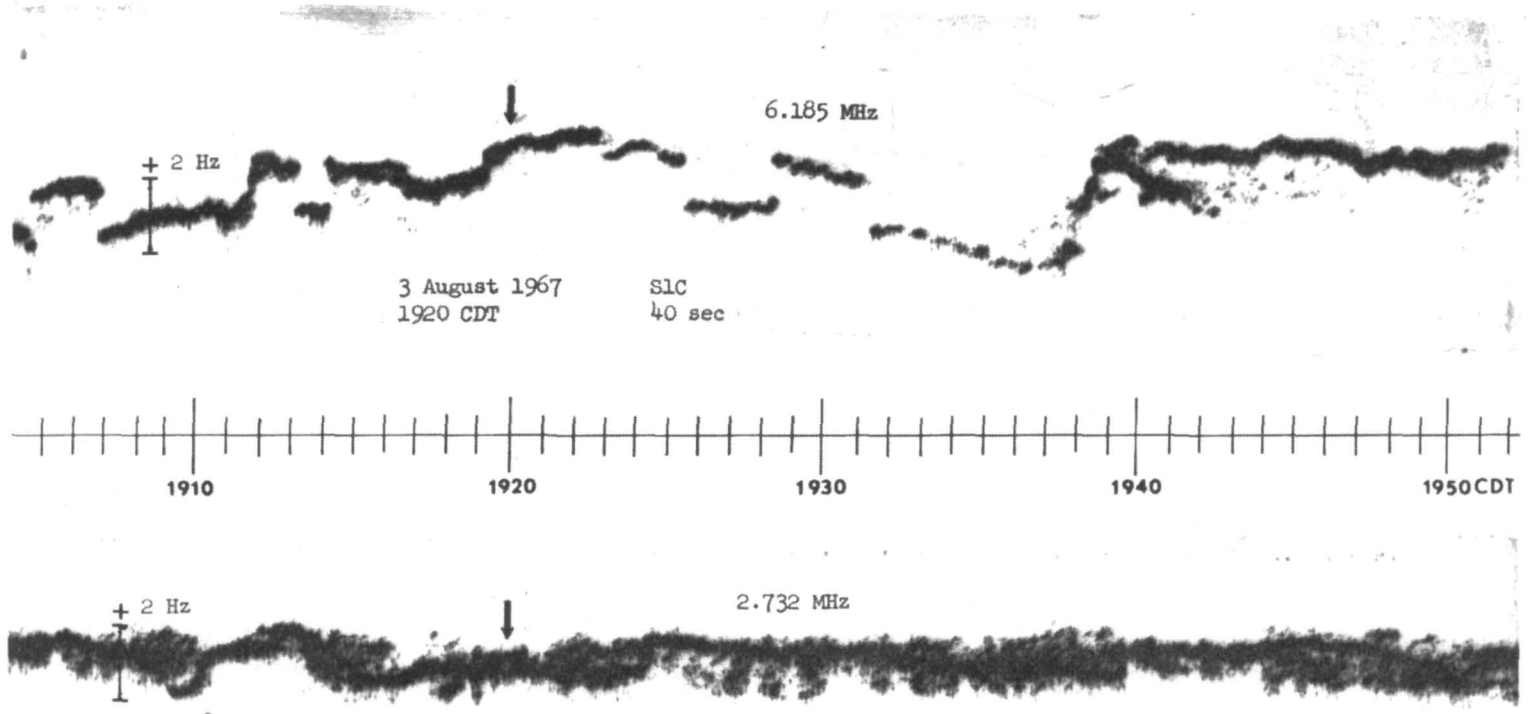


Figure 45: Doppler data record, 3 August 1967: Huntsville, Alabama

Phase Path Variation
2.732 MHz 3 August 1967
Huntsville, Alabama

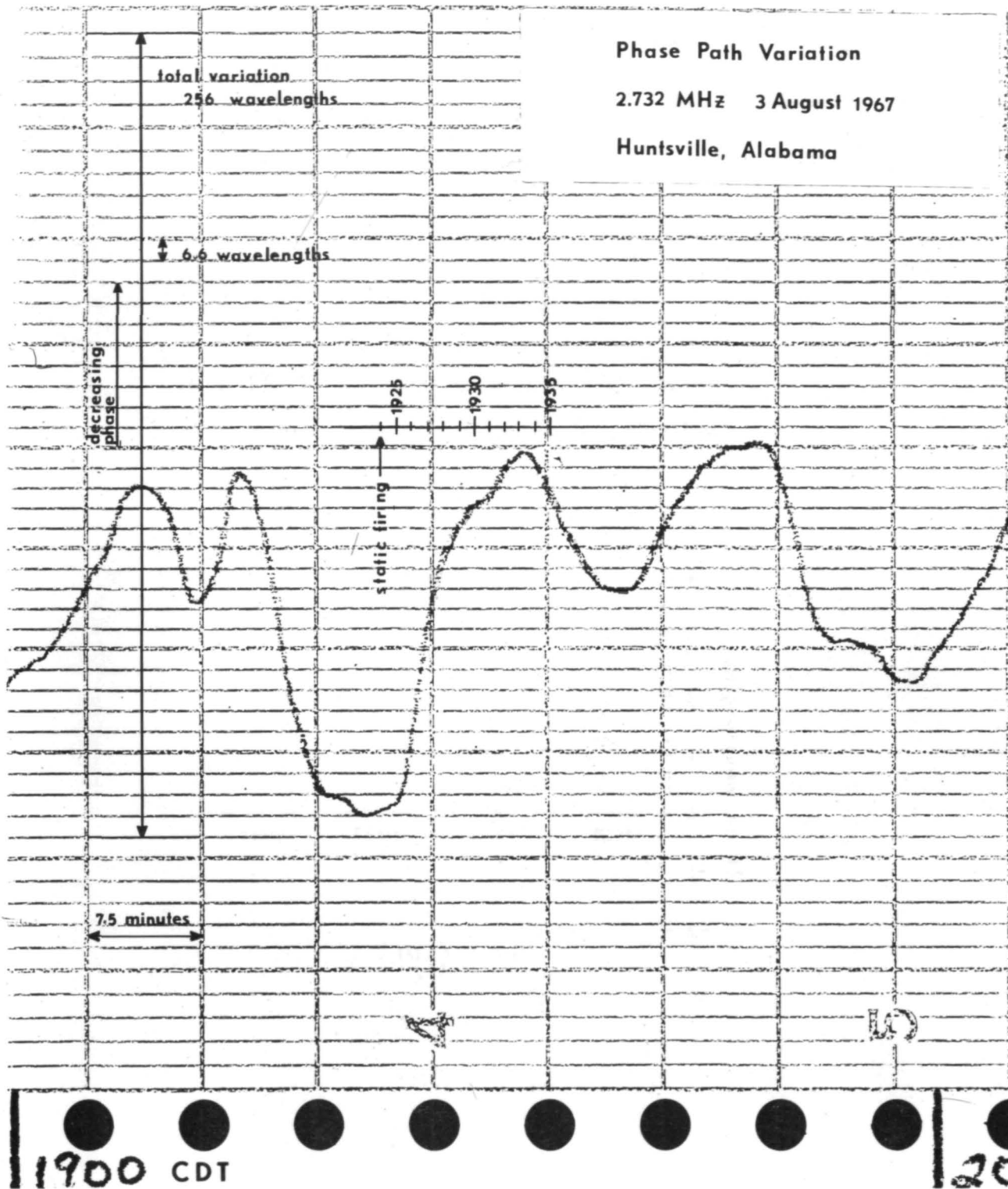


Figure 46: Phase-locked loop data record,
3 August 1967: Huntsville, Alabama

Phase Path Perturbation 2.732 MHz
Huntsville, Alabama 3 August 1967

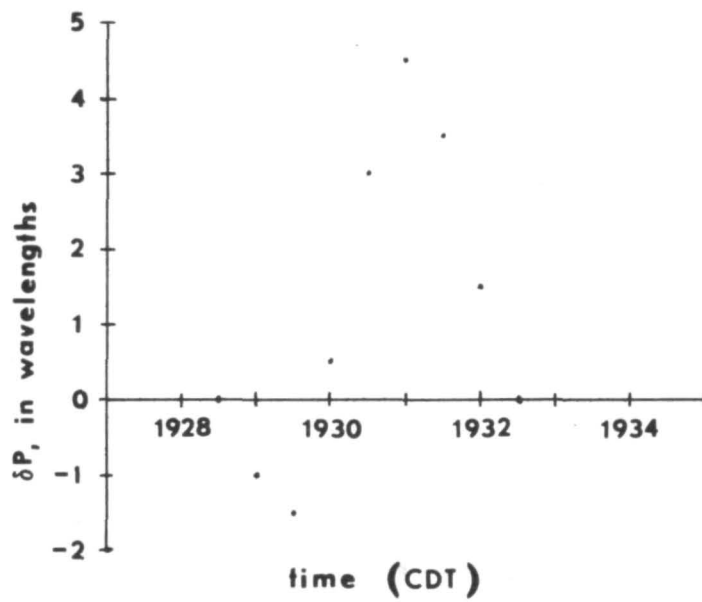
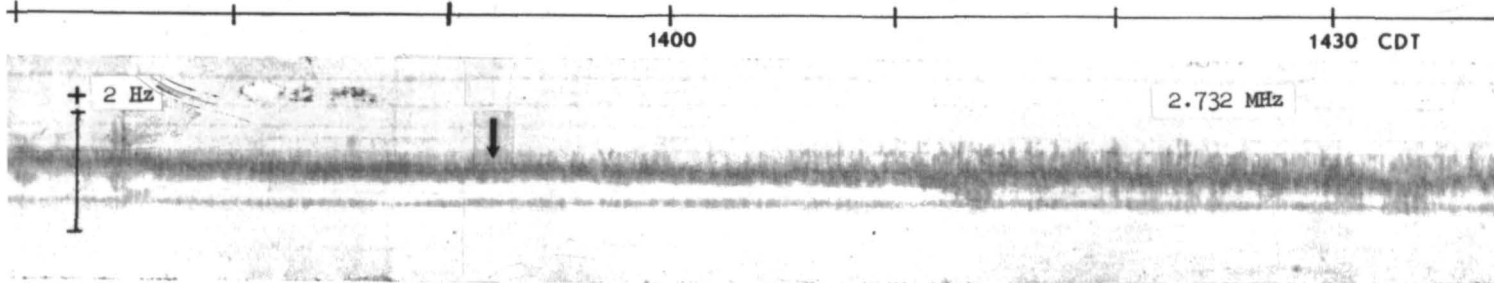
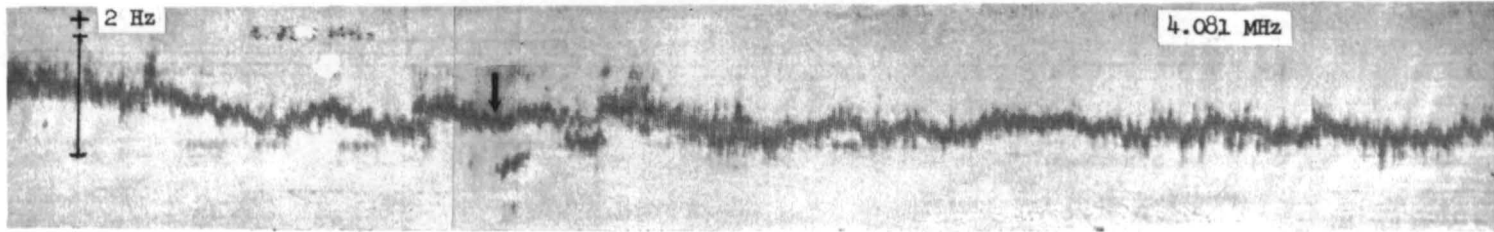
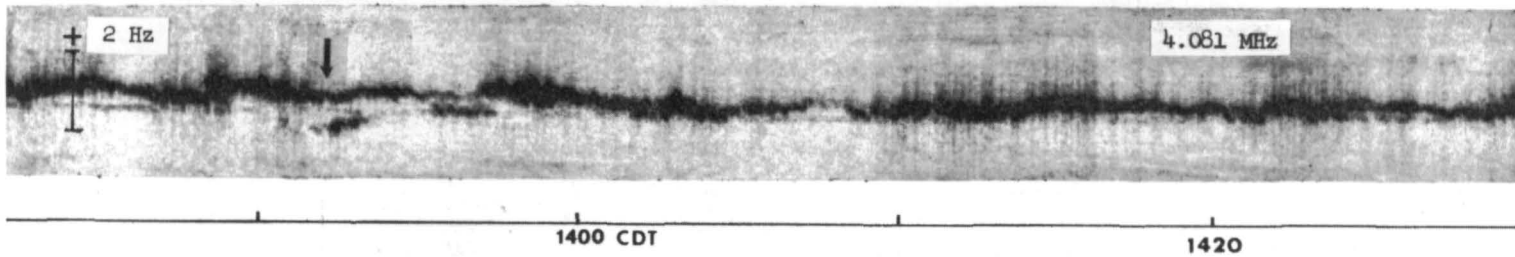


Figure 47
Phase path perturbation extracted from Figure 46



16 August 1967 F1-68
 1352 CDT 41 sec



-101-

Figure 48: Doppler data record, 16 August 1967: Huntsville, Alabama

APPENDIX D

THE PROPAGATION OF ACOUSTIC-GRAVITY WAVES
THROUGH THE MIDDLE ATMOSPHERE

(prepared by Charles Moo, Avco/SSD)

The propagation of acoustic-gravity waves to ionospheric heights from the troposphere is complicated by the presence of temperature and wind gradients in the intervening medium. These serve to extract energy from the incident wave, depending on wave frequency ω and the wind velocity and temperature profiles. The mean atmospheric density decreases with height, and the wave amplitude is inversely proportional to the square root of the mean density, so that if energy per unit volume is the same at two heights, the amplitude will be correspondingly larger at higher altitudes. Hines²¹ has estimated that vertical energy fluxes of the order of $1 \text{ erg cm}^{-2} \text{ sec}^{-1}$ are required to obtain waves of the sort typically observed in the ionosphere. Gossard²² and Pierce and Coroniti¹⁵ computed fluxes leaving the troposphere of the order of $100 \text{ ergs cm}^{-2} \text{ sec}^{-1}$, orders of magnitude above that required for observation at ionospheric heights if the waves were free of dissipation and reflection through the intervening atmosphere. Thus extensive and significant mechanisms for attenuation must obtain.

Viscosity and thermal conduction²³ dissipate atmospheric gravity waves at thermospheric heights, especially at the high frequency end of the spectrum. More important for troposphere-ionosphere coupling are the roles of thermal reflection and wind shear filtering. Hines²⁴ and Friedman²⁵ show that although thermal reflections at mesospheric heights reduce the energy coupled to the ionosphere, a major portion of the wave spectrum of acoustic-gravity waves would pass through to the lower ionosphere.

Of apparent major importance in restricting troposphere-ionosphere coupling is the possible occurrence of "critical layers", in which the wave frequency is Doppler shifted to zero, as measured in the reference frame moving with the background wind of the layer^{26, 27, 28}. Under the conditions in which WKB approximations can be applied (i. e. for large Richardson number

$$R = \omega_b^2 / V^2$$

where ω_b is the Brunt frequency and V the horizontal wind speed) Bretherton showed that, for a travelling wave group with dominant frequency ω and horizontal wave number k_h , there is a critical level at which the Doppler shifted frequency

$$\Omega = \omega - k_h V$$

vanishes, and the wave in effect is not propagated above this level. Furthermore, the total wave energy of a wave packet is not conserved but is proportional to Ω . "Changes in the wave energy occur because an upward propagating internal wave is associated with a vertical transfer of horizontal momentum, and in a shear flow there is a continual transfer of energy between the mean flow and the wave, as the momentum is transferred up or down the mean velocity gradient (Eliassen and Palm²⁹)".²⁶

APPENDIX E

ACOUSTIC RAY-TRACING PROGRAM

(prepared by Sheldon Weinstein, Avco/SSD)

A three-dimensional acoustic ray-tracing computer program, originally developed by Pierce²⁰ at Avco/SSD, has been modified slightly and re-written in a format suitable for general purpose usage. The principal change incorporated into Pierce's skeleton code was the replacement of his rather simple numerical integration method by a standard Adams-Moulton integration routine with error checking and variable step size. This was required in order to reduce the errors accumulated when integrating along a raypath with steps of fixed incremental length.

The following is a brief, user-oriented description in outline form of the essence of the program, the required input data, and its outputs for operation on the Avco IBM 360/75 computer, utilizing the SC-4020 digital microfilm plotter. Details of the mathematical approach and its computer implementation are found in Pierce's report.

1. Purpose

Integration of the three-dimensional atmospheric acoustics ray-tracing equations in a temperature and wind stratified atmosphere, winds being considered two-dimensionally within each stratum.

2. Equations

$$\frac{dt}{dz} = \frac{\frac{\rho}{c^2}}{k_z} \quad (1)$$

$$\frac{dx}{dz} = \frac{k_x + v_x \frac{\rho}{c^2}}{k_z} \quad (2)$$

$$\frac{dy}{dz} = \frac{k_y + v_y \frac{\rho}{c^2}}{k_z} \quad (3)$$

$$\rho = 1 - k_x v_x - k_y v_y \quad (4)$$

$$k_z^2 = \frac{\rho^2}{c^2} - k_x^2 - k_y^2 \quad (5)$$

$$k_x = \frac{\sin \theta \cos \phi}{c} \quad (6)$$

$$k_y = \frac{\sin \theta \sin \phi}{c} \quad (7)$$

$$c = \sqrt{\frac{1.4 \times 8.3144 \times 10^{-3}}{29} \times (T + 273)} \quad (8)$$

where (see Figure 49)

- t dependent variable time (sec)
- $\left. \begin{matrix} x \\ y \end{matrix} \right\}$ dependent variables - horizontal distances (km)
- z independent variable height (km)
- $\left. \begin{matrix} v_x \\ v_y \end{matrix} \right\}$ horizontal wind velocity components (km/sec)
- T air temperature ($^{\circ}\text{C}$)
- c sound velocity (km/sec)
- θ elevation angle, measured down from the vertical
- ϕ azimuth angle, measured clockwise from north

3. Numerical Integration Method

The solution of the set of three differential equations, (1), (2), and (3), is performed by Adams-Moulton integration. The method is implemented with a standard computer library predictor-corrector integration routine, using a four-point Runge-Kutta corrector scheme. Integration steps (in height) are of variable length, selected by the predictor-corrector procedure so as to bring the difference between the predicted and corrected values of t, x, and y to within error tolerance limits specified by the program user.

The advantage of this approach is maintenance of the required accuracy of the dependent variables, by checking the differences between the extrapolated and interpolated results for each incremental step and changing the step size of the independent variable to control accuracy while optimizing program speed. Operationally acceptable error limits have been chosen by requiring the ground-to-reflection and reflection-to-ground halves of the height vs. time raypaths to be symmetric about their reflection points, a condition which can be invoked from the physics of the process. The integration error tolerance limits thusly

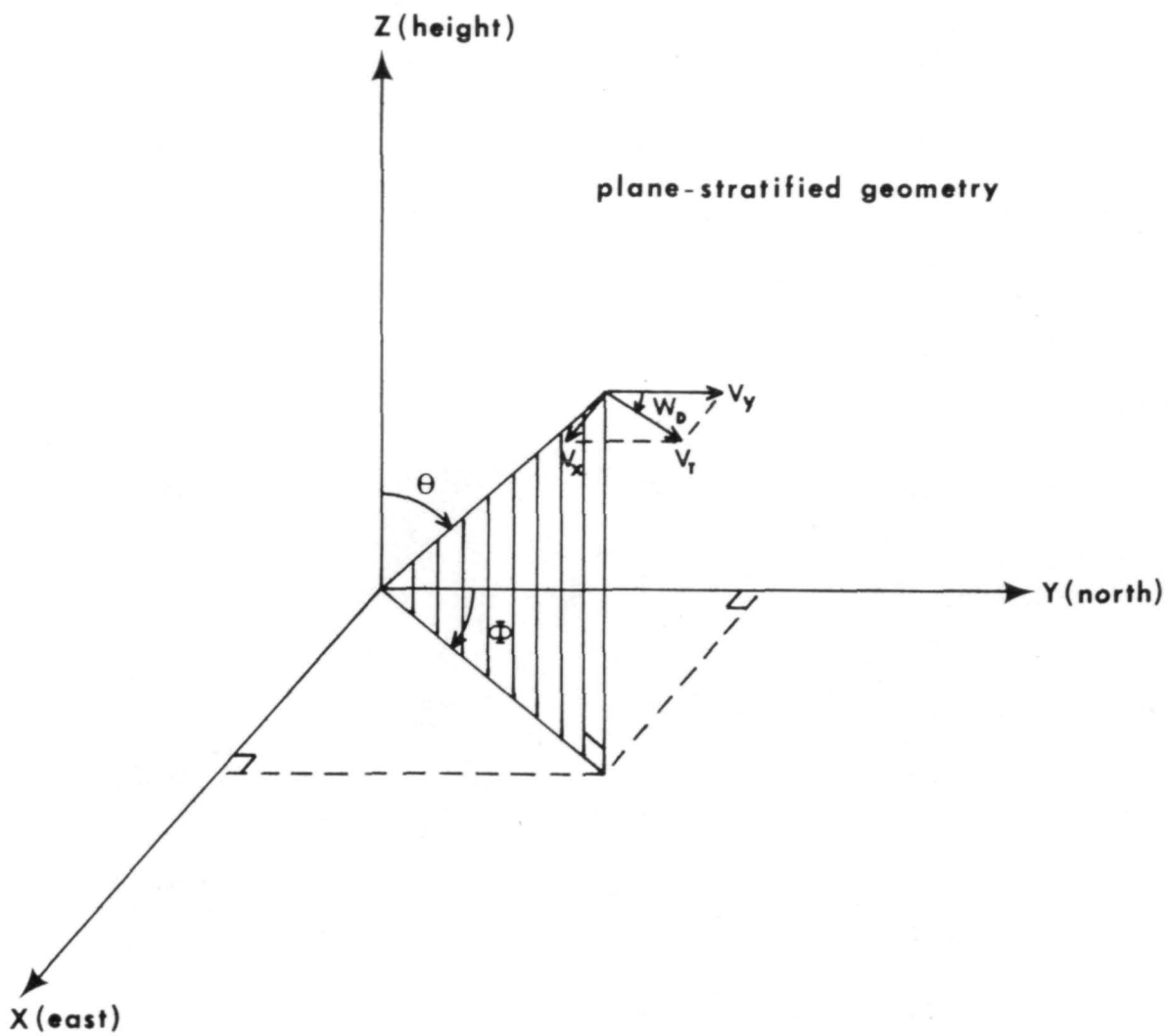


Figure 49: Ray-tracing program geometry

derived are currently preset in the program in UPBND and DNBND as follows:

$$\text{UPBND} = 10^{-2}, 1, 1 \quad (\text{upper bound on errors in } t, x, y)$$

$$\text{DNBND} = 10^{-4}, 10^{-2}, 10^{-2} \quad (\text{lower bound on errors in } t, x, y)$$

If the errors in any of the variables exceed UPBND, the step size is decreased to improve accuracy. If the predicted and corrected values of all the functions differ by less than DNBND, the step size is increased to reduce computer time.

4. Input Data

4.1 Atmospheric Profile

4.1.1 Title Card

Any information in columns 1 - 72.

4.1.2 Profile Data Cards (300 maximum)

<u>Column</u>	<u>Contents</u>	<u>Remarks</u>
2-11	Height (km)	Real - Decimal Point/F10.0
12-21	X component of wind velocity (km/sec)	++
22-31	Y ++	++
32-41	Temperature (°C)	++

4.1.3 End of Profile Data

<u>Column</u>	<u>Contents</u>	<u>Remarks</u>
1	9	This card signifies the end of the Profile Data.

4.1.4 Parameter Cards

The following parameters are input via Variable Field Input. The parameter name followed by its value is punched in columns 2 - 72. A blank is the delimiter between parameters and between parameters and their values.

<u>Parameter</u>	<u>Description</u>	<u>Preset Value*</u>
ITHETAI	Initial value of Elevation Angle (Degrees)	1
ITHETAF	Final ++	89
ITHETAST	Step ++	1
PHI	Azimuth angle (Degrees)	45
ZS	Initial Height (km)	0
TS	Initial Time (sec)	100
XS } YS }	Initial horizontal coordinates (km) (km)	0 0
TMARK	Increment for Time Tic marks (sec) on summary graphs	100

* Note: If parameter is not input, this value is used.

4.1.5 End of Parameters

<u>Column</u>	<u>Contents</u>	<u>Remarks</u>
1	Any integer	This card signifies the end of parameter input.

4.1.6 End Card*

<u>Column</u>	<u>Contents</u>	<u>Remarks</u>
1-3	END	This card signifies the end of all data.

* Note: Additional cases consisting of items 4.1.4 and 4.1.5 may be placed before the End Card.

5. Output

- 5.1 Atmospheric Profile Table
- 5.2 Input Parameter Table
- 5.3 Ray Table for each specified elevation angle
- 5.4 Plots of Atmospheric Profile
- 5.5 Plots of Ray Variables
- 5.6 Summary Plots of Ray Variables

Figures 50-55 show program-produced plots of sample input temperature and wind data, as well as vertical profiles of orthogonal wind components and sound speed derived therefrom. The particular temperature and wind profiles represented here were synthesized from the following sources, using free-hand extrapolations where required.

WINDS

Height Regime	Data Source
0-16.3 km	MSFC balloon release ³⁰ , 1901 UT, 20 April 1967
25-70	White Sands MRN ³¹ mean wind direction and vector speed values for April
85-170	Average midlatitude ionospheric meridional and zonal wind patterns, after Rosenberg ³²
above 170	Mid-latitude upper atmospheric wind regimes, after Smith and Weidner ³³

TEMPERATURE

Height Regime	Data Source
0-16.3 km	MSFC balloon release ³⁰ , 1901 UT, 20 April 1967
25-120	Standard atmosphere ³⁴ , mid- latitude spring/fall
120-300	Model atmosphere ³⁴ , spring/ fall, exospheric temperature of 800°K.

Figures 56-61 show computer drawn summary output plots of raypaths traced at an azimuth of 45°, using the above data, through a series of elevation angle between 1° and 81°, in 10° steps. (The small numbers at the ends of the ray trajectories give the launching elevation angle for the particular raypath.)

WIND PROFILE 1A, 20 APRIL 1967, HUNTSVILLE

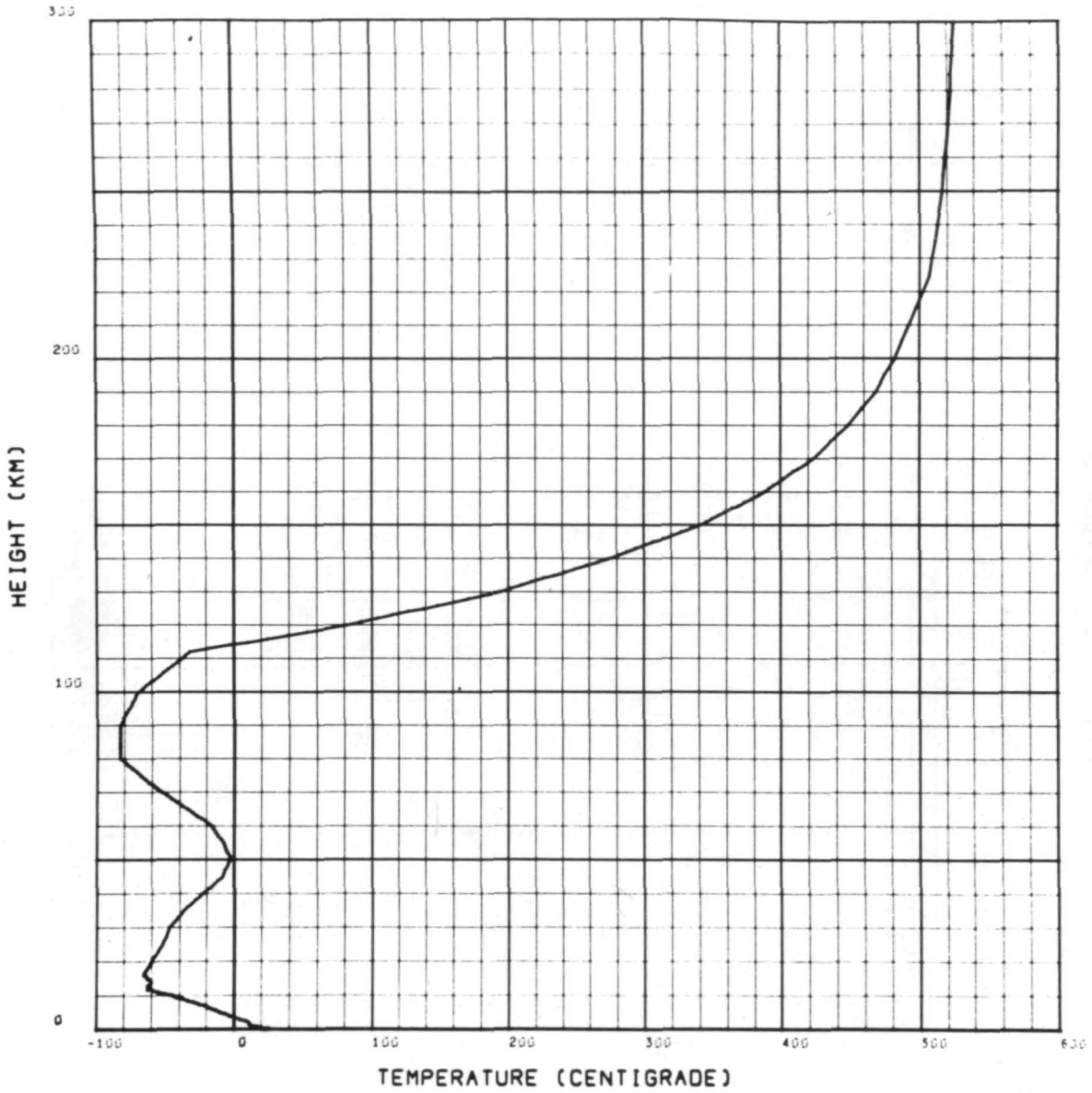


Figure 50: Acoustic ray-tracing input data:
height vs. temperature

WIND PROFILE 1A, 20 APRIL 1967, HUNTSVILLE

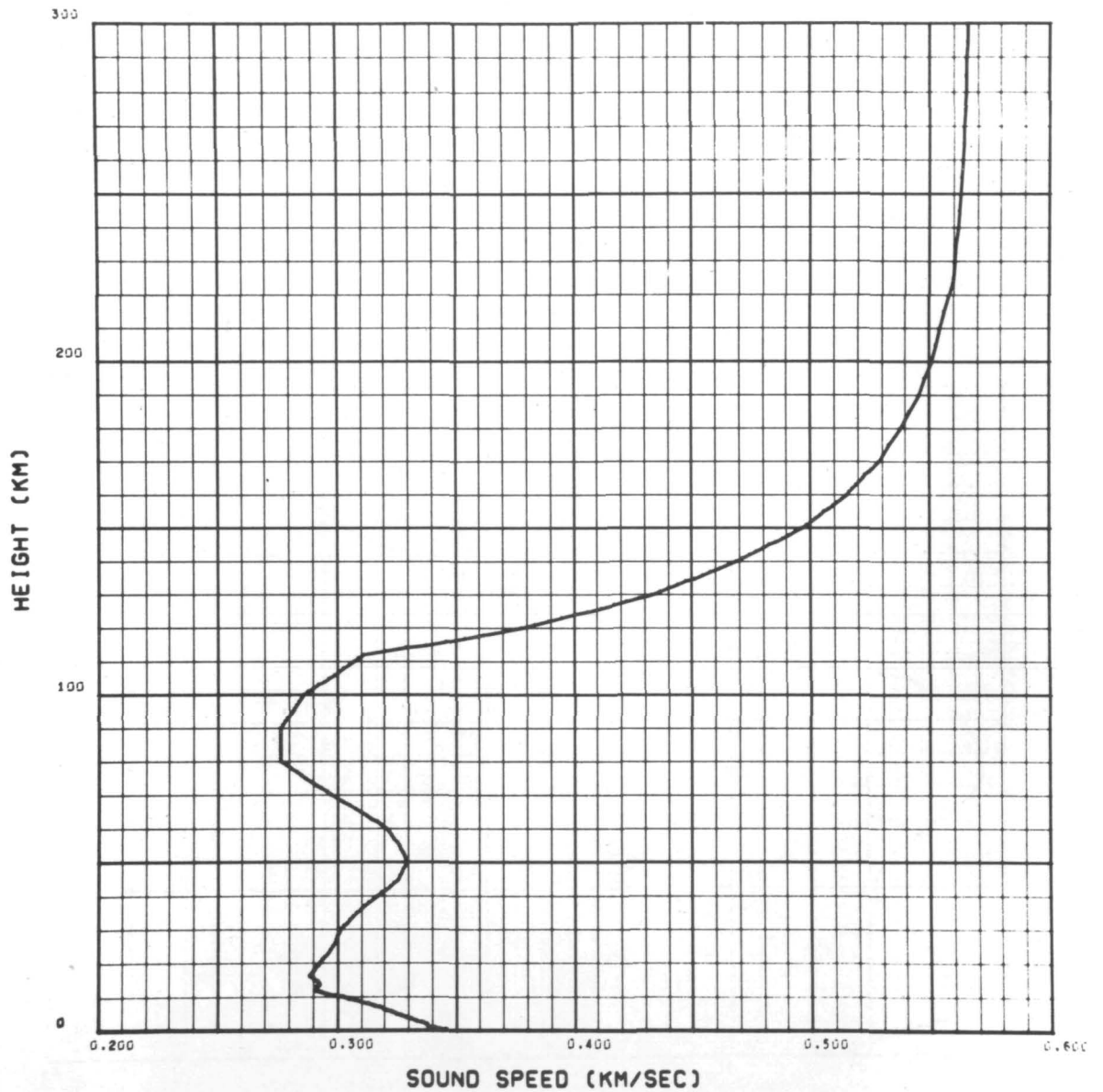


Figure 51: Acoustic ray-tracing input data:
height vs. sound speed

WIND PROFILE 1A, 20 APRIL 1967, HUNTSVILLE

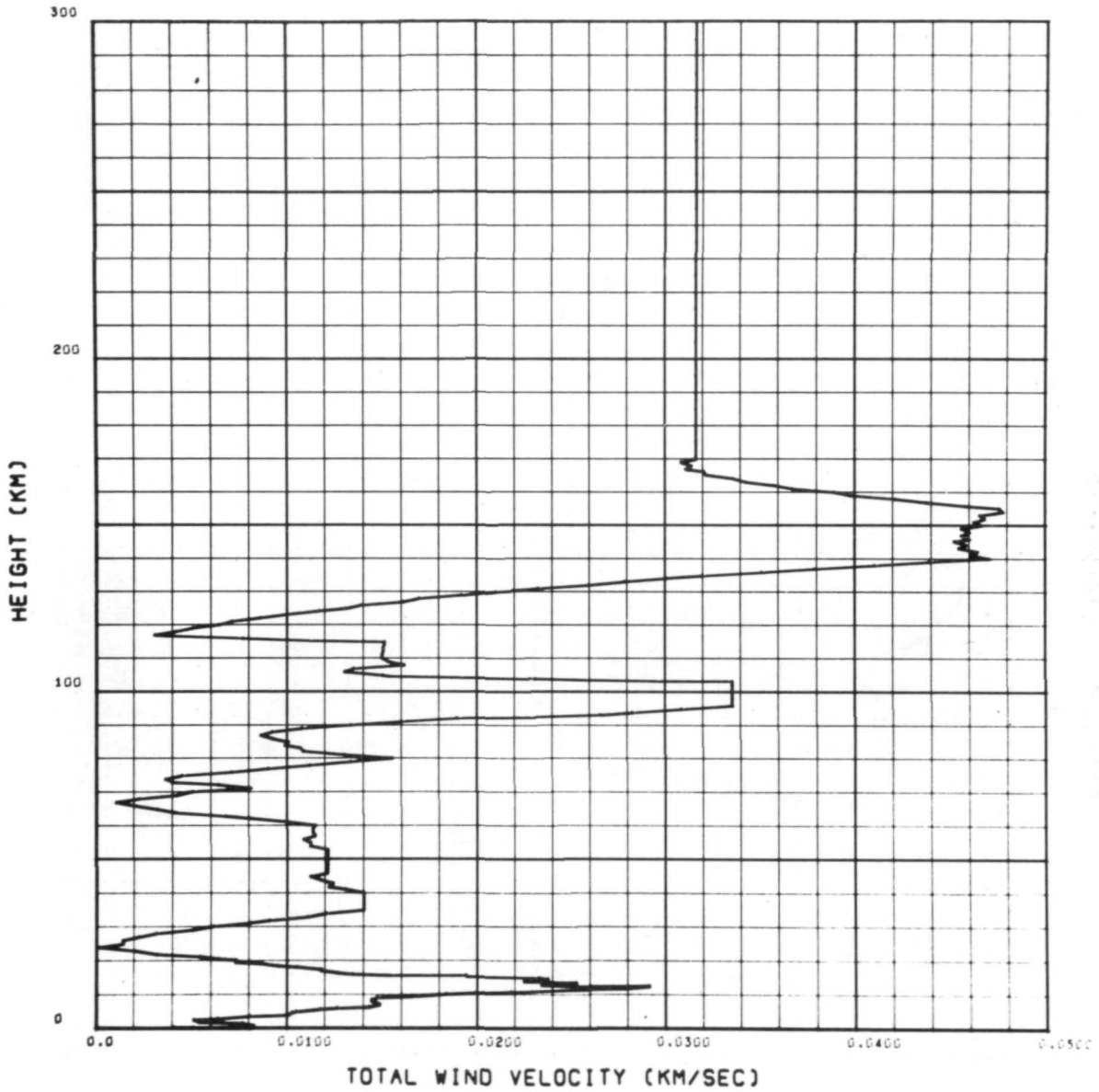


Figure 52: Acoustic ray-tracing input data:
height vs. total wind velocity

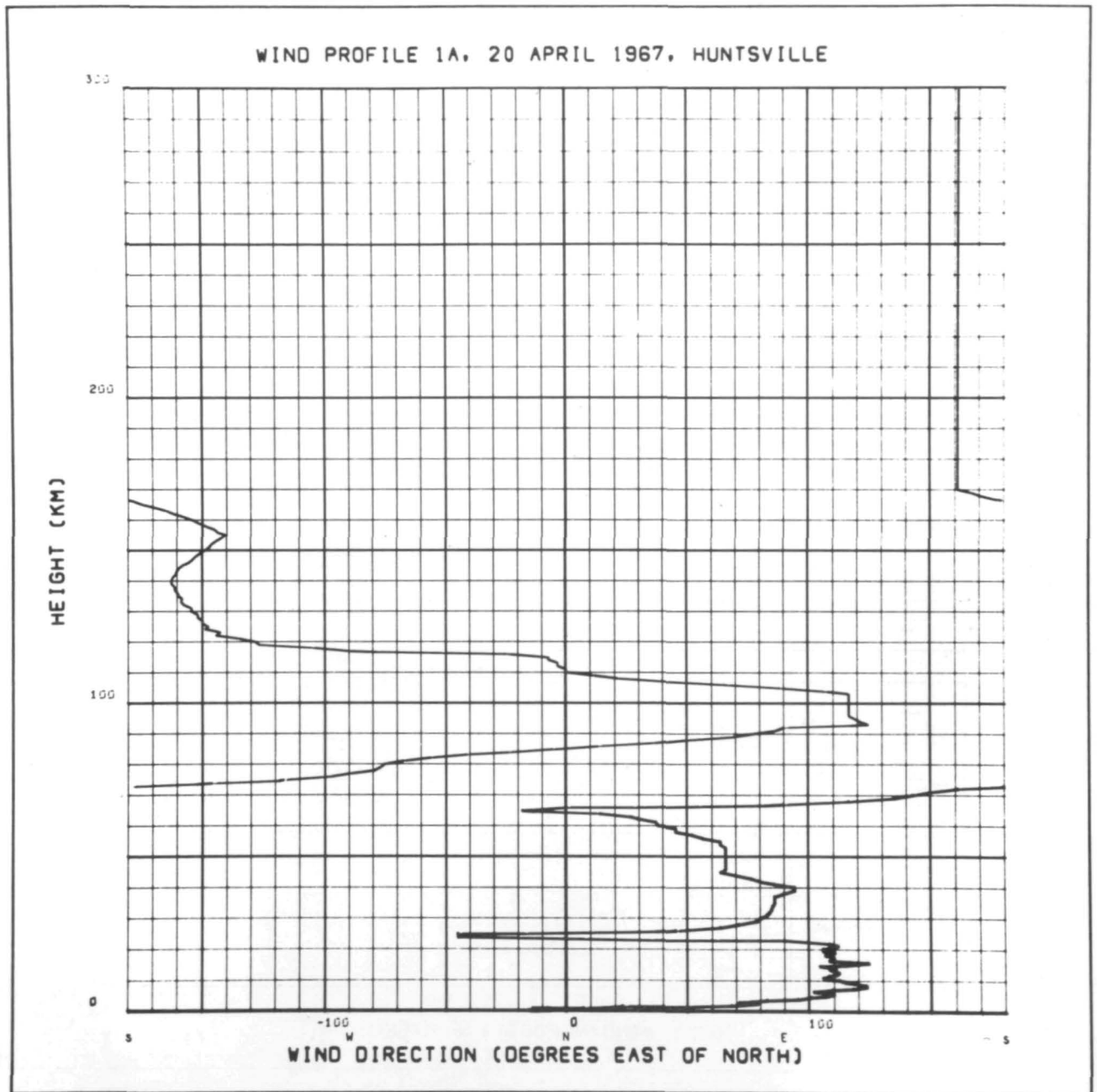


Figure 53: Acoustic ray-tracing input data:
height vs. wind direction

WIND PROFILE 1A, 20 APRIL 1967, HUNTSVILLE

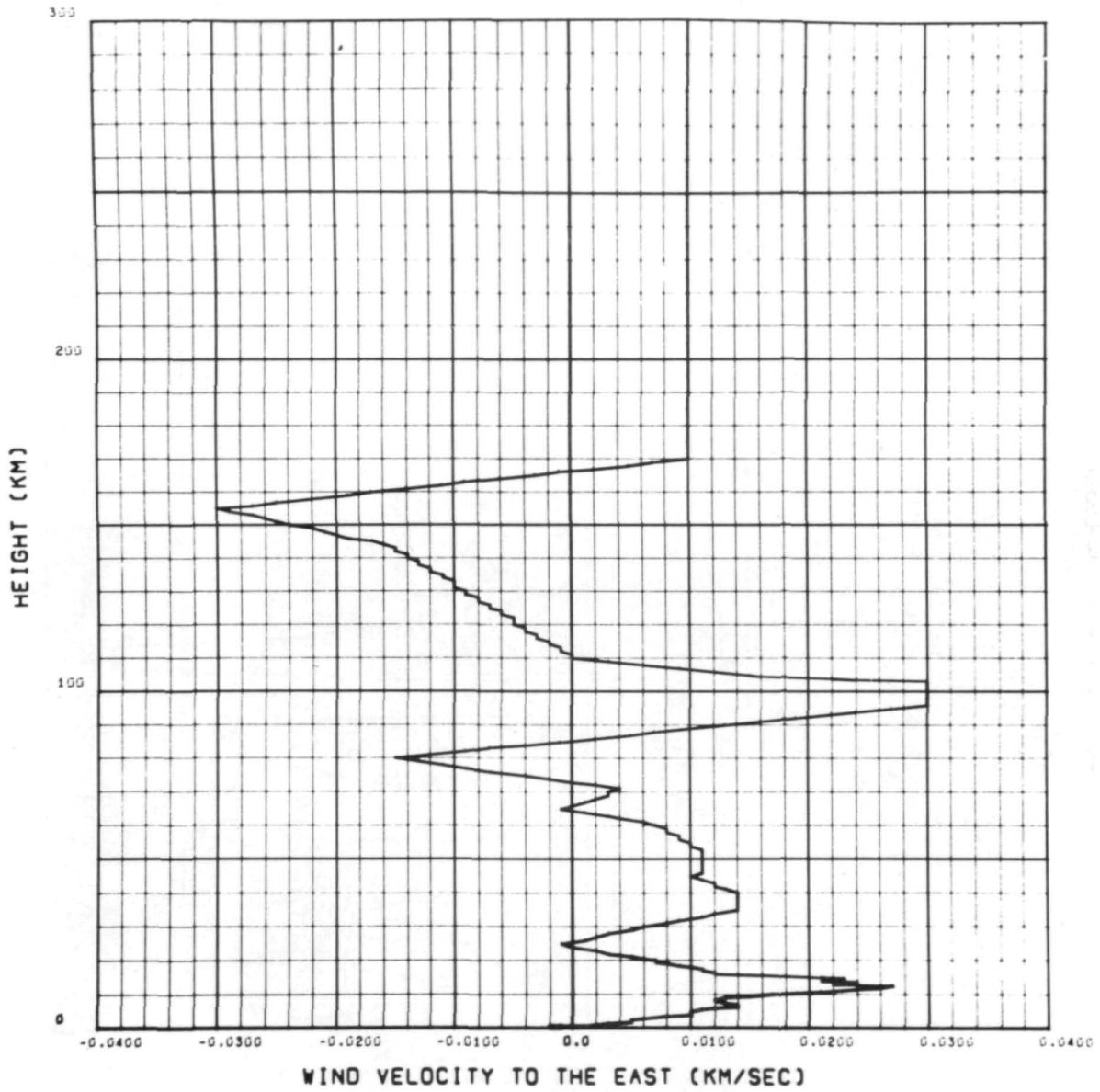


Figure 54: Acoustic ray-tracing input data:
height vs. x-component of wind velocity

WIND PROFILE 1A, 20 APRIL 1967, HUNTSVILLE

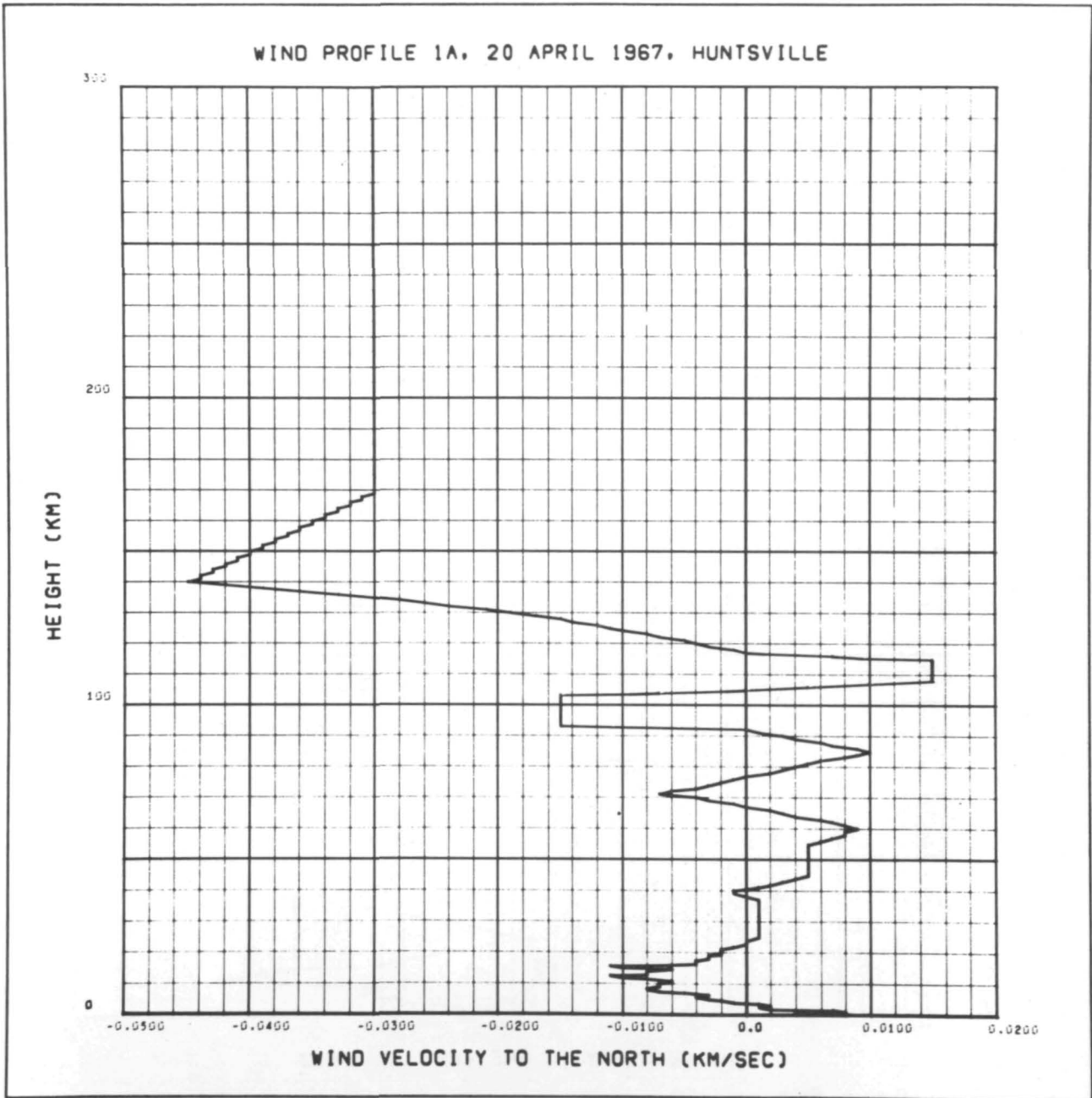


Figure 55: Acoustic ray-tracing input data:
height vs. y-component of wind velocity

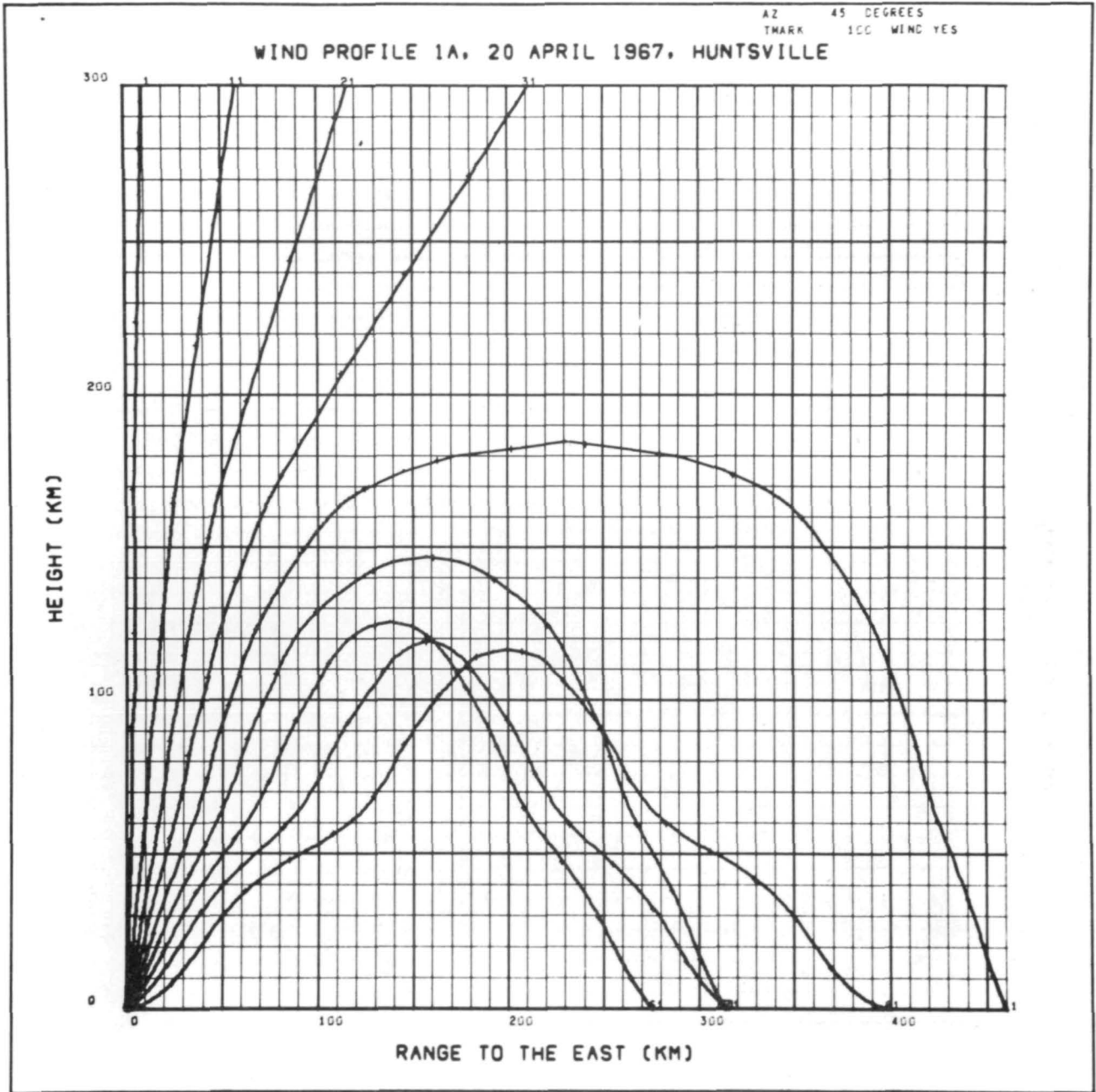


Figure 56: Acoustic ray-tracing output data:
height vs. x-distance

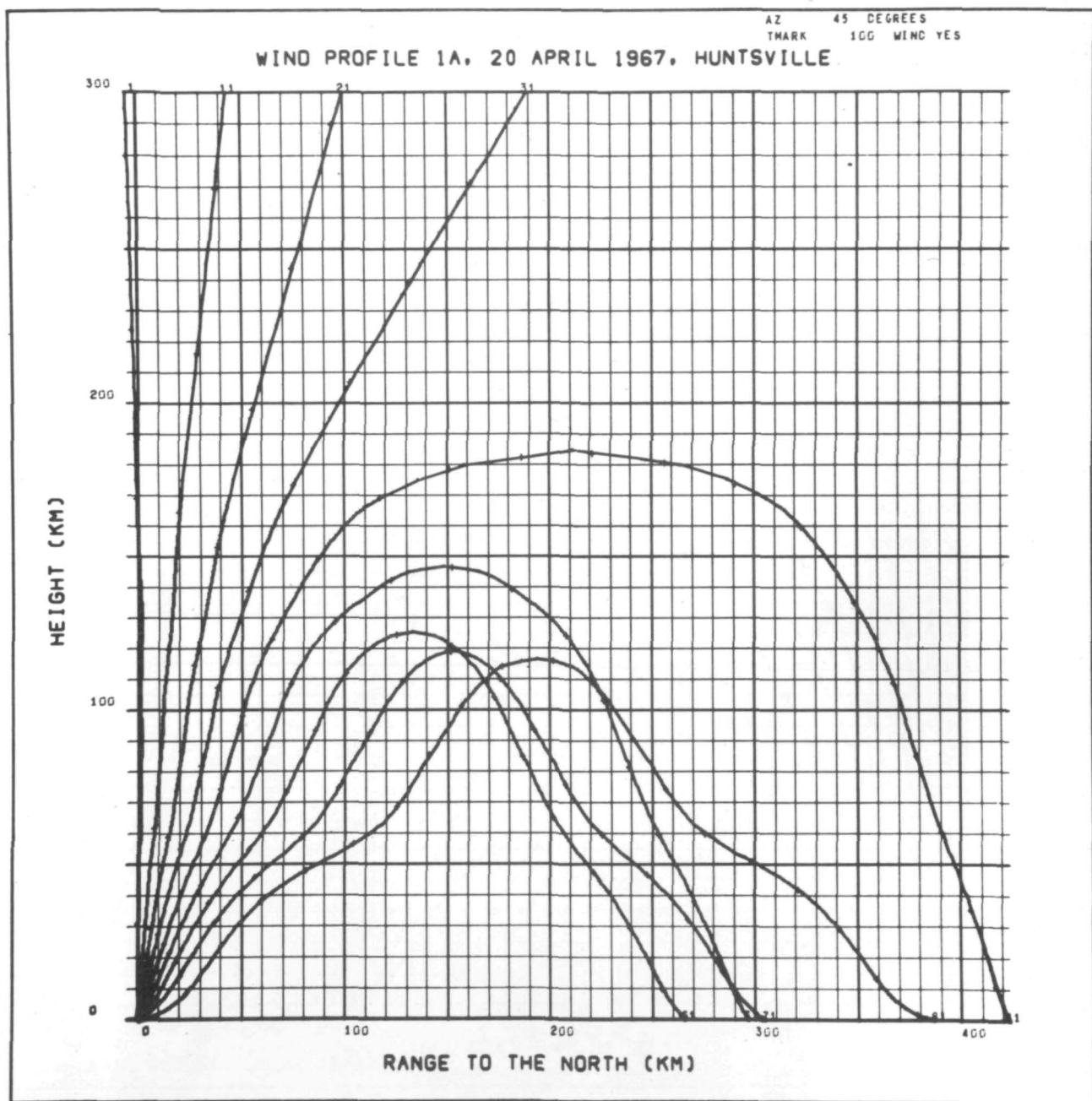


Figure 57: Acoustic ray-tracing output data:
height vs. y-distance

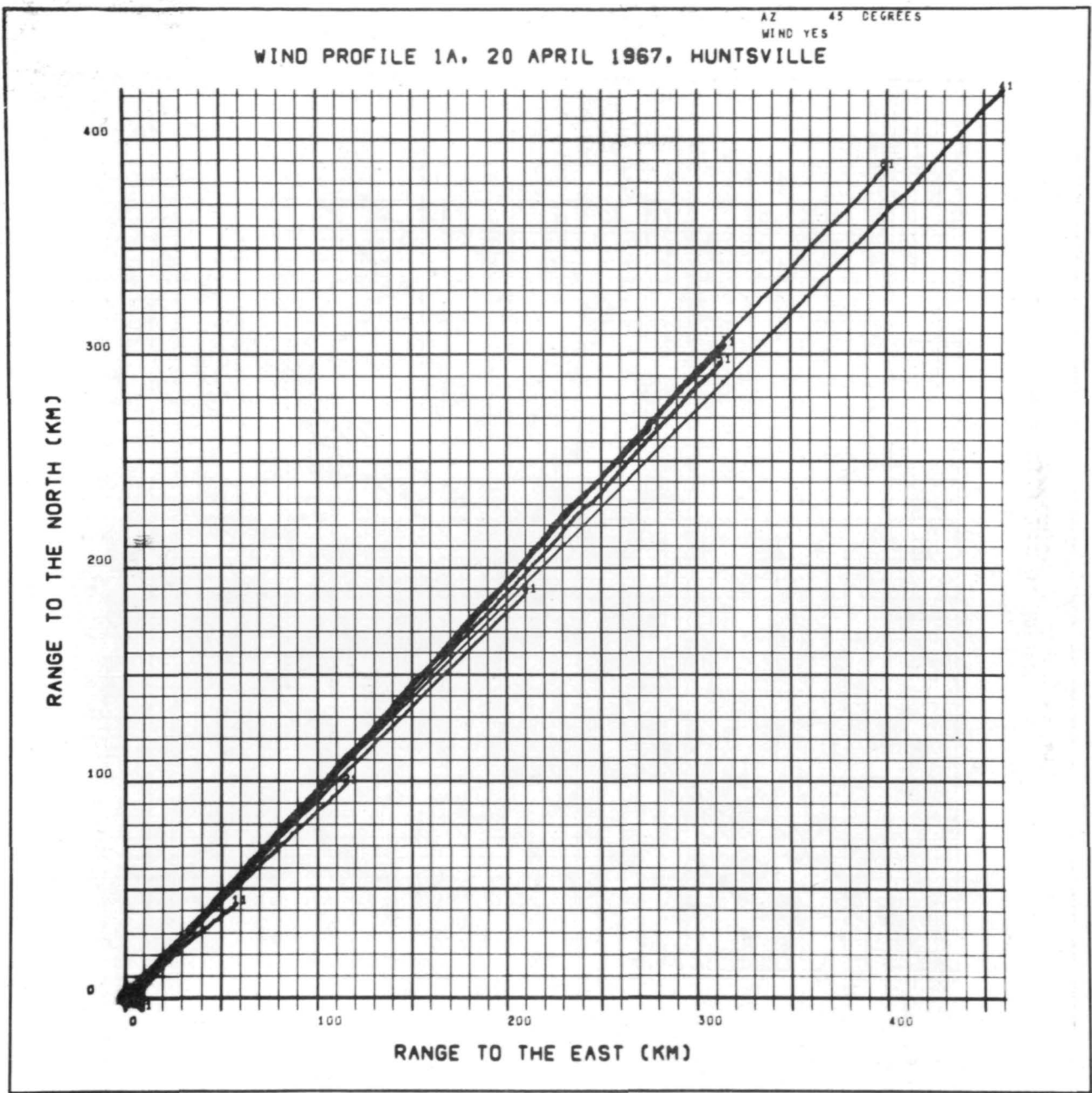


Figure 58: Acoustic ray-tracing output data:
y-distance vs. x-distance

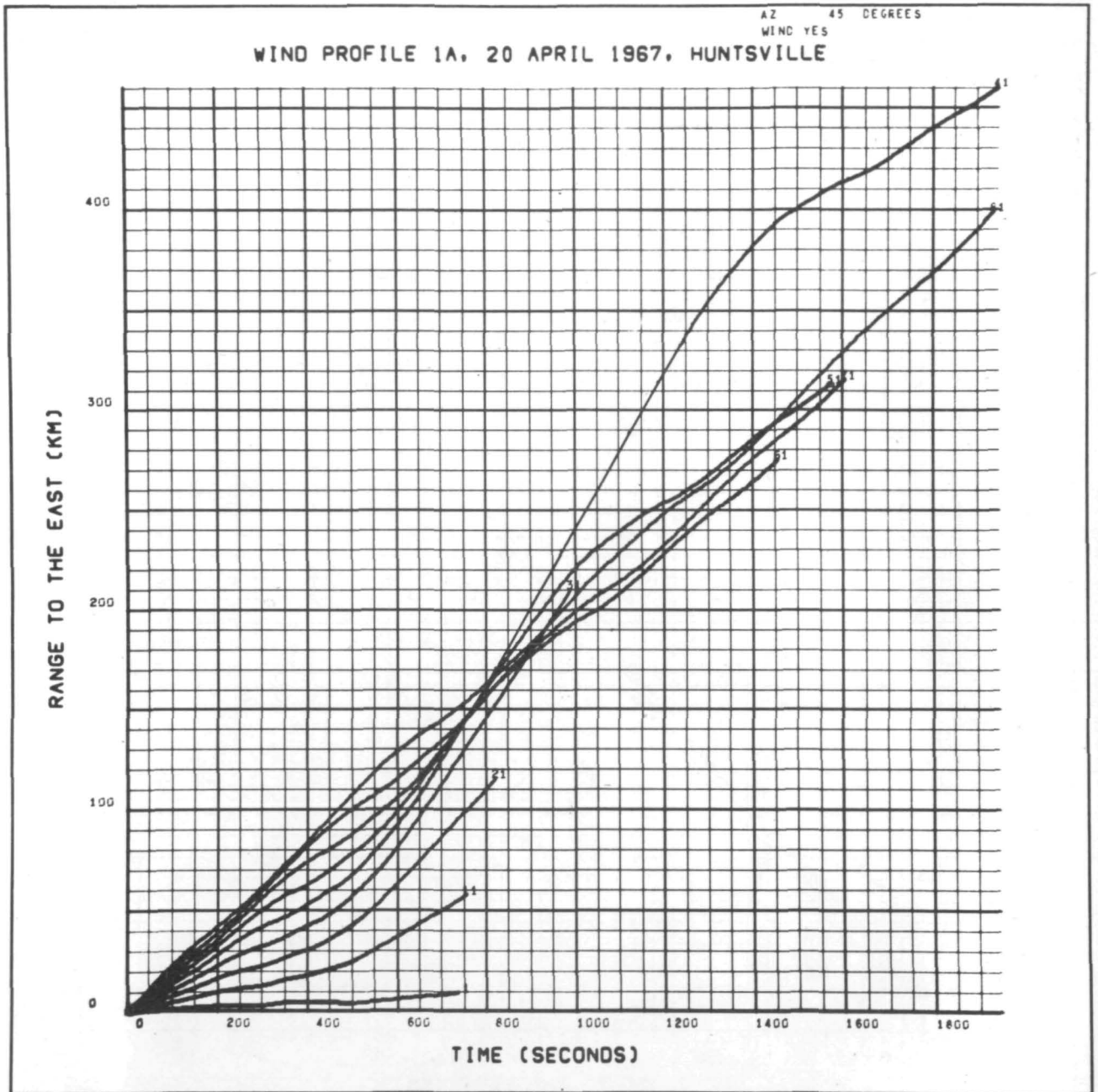


Figure 59: Acoustic ray-tracing output data:
x-distance vs. time

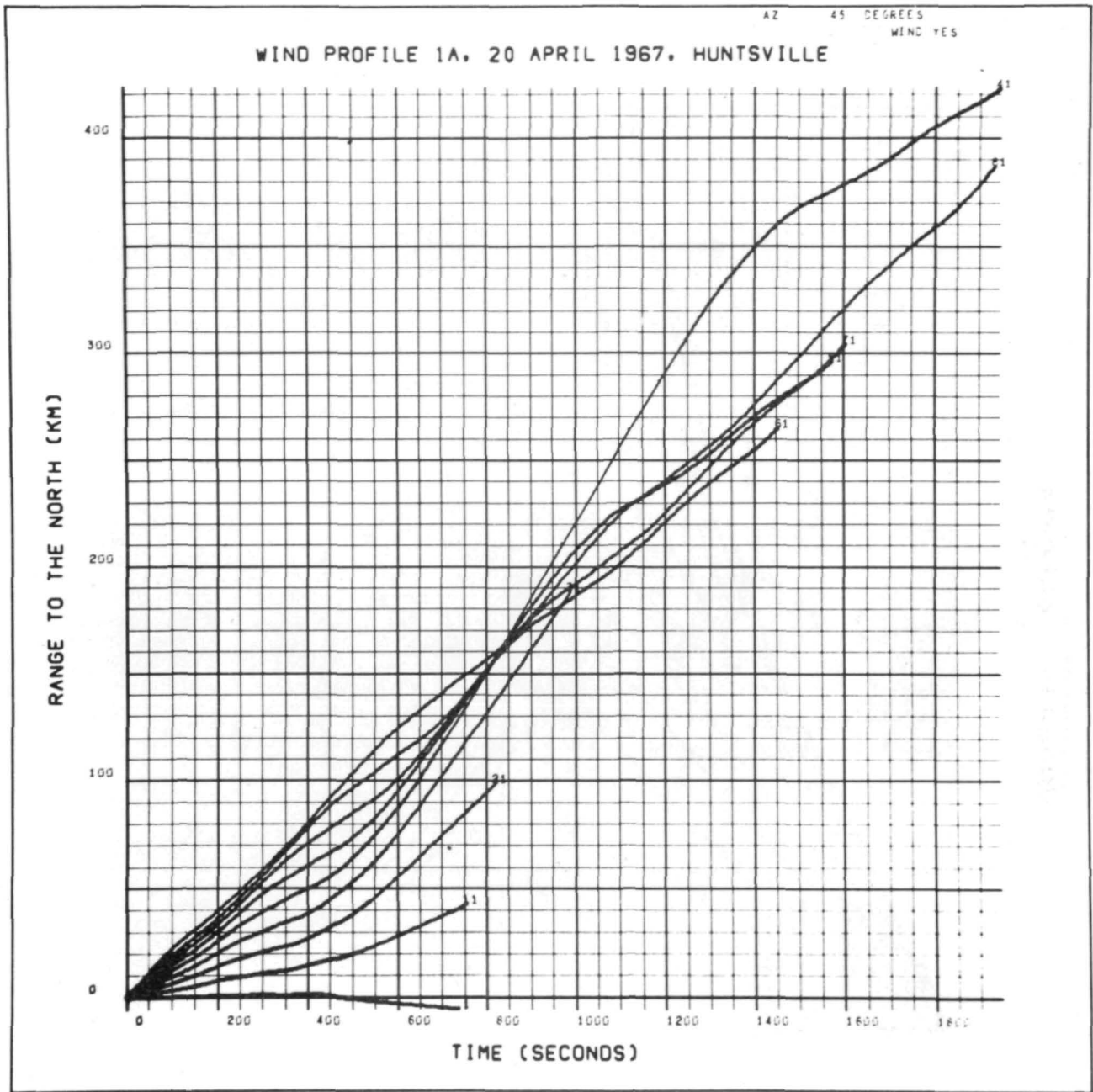


Figure 60: Acoustic ray-tracing output data:
y-distance vs. time

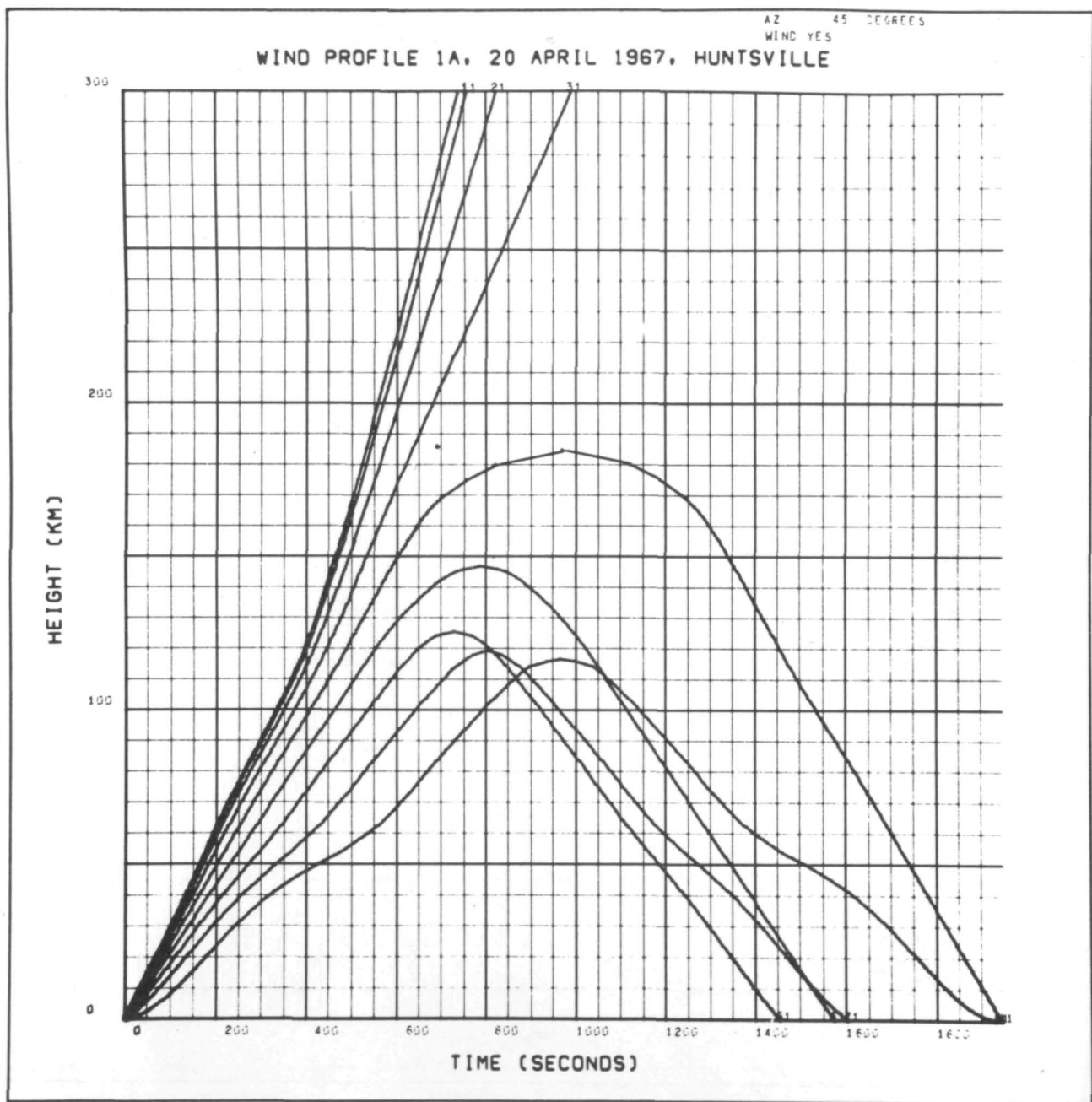


Figure 61: Acoustic ray-tracing output data:
height vs. time

All the plots shown in Figures 50-61 are drawn and annotated automatically by the SC-4020 plotter. Detailed tabular printouts of the raypath trajectories are also optionally available.

6. Computer Program

A Fortran IV listing of the program for the Avco IBM 360/75 computer and detailed flow charts of each section of the program are included at the end of this appendix.

FORTAN IV LISTING OF
ACOUSTIC RAY-TRACING COMPUTER PROGRAM

IMPLICIT REAL *8(A-H,O-Z)	MAN00010
ACOUSTIC RAY-TRACING	MAN00020
L8074 R1748210000 Z230 DFTERT/WEINSTEIN 1/68	MAN00030
MOD. OF L8032	MAN00040
REF- GEOMETRICAL ACOUSTICS' THEORY OF WAVES FROM A POINT SOURCE	MAN00050
IN A TEMPERATURE AND WIND-STRATIFIED ATMOSPHERE	MAN00060
BY ALLAN PIERCE AVSSD-0135-66-CR 2AUG66	MAN00070
	MAN00080
	MAN00090
	MAN00100
SUBROUTINES	MAN00110
	MAN00120
PARAM	MAN00130
DNDIST	MAN00140
SKDIST	MAN00150
ARTLU	MAN00160
DEREQ	
ADM4RK	
	MAN00170
	MAN00180
COMMON/FAYE/GI(300),VXI(300),VYI(300),ZI(300),PLXT(600),PLYZ(600),	MAN00190
1 PLYX(600),PLYZ(600)	MAN00200
COMMON/JANET/NMAX,NPLT	MAN00210
COMMON/PEARL/ZTOP,ITOP,XTOP,YTOP,T2,X2,Y2	MAN00220
DIMENSION TITLE(9),VTIX(600),VTI(300),WDI(300),PLDCDZ(300)	MAN00230
DIMENSION TEMQ(300),ORDTM(9)	MAN00240
EQUIVALENCE (VTIX(1),VTI(1)),(VTIX(301),TEMQ(1))	MAN00250
DIMENSION ABSCP(9),ORDPX(9),ORDPY(9),ORDPT(9),ORDPC(9),ABSCT(9),	MAN00260
1 ORDZZ(9),ORDXX(9),ORDYY(9),ABWD(9),ABVT(9),ABK(9),ORDC(9)	MAN00270
REAL *4 INTABQ(300)	MAN00280
	MAN00290
CALL MIBCOM	MAN00300
CALL IDFRMV('S.WEINSTEIN ','P1','L8074')	MAN00310
REWIND 13	MAN00320
	MAN00330
DATA ABSCP/2*' ','Z' ','6*' '/'	MAN00340
DATA ORDTM/2*' ','TEMP' ','6*' '/'	MAN00350
DATA ORDPX/2*' ','VX' ','6*' '/'	MAN00360
DATA ORDPY/2*' ','VY' ','6*' '/'	MAN00370
DATA ORDPC/2*' ','C' ','6*' '/'	MAN00380
DATA ABSCT/2*' ','TIME' ','6*' '/'	MAN00390
DATA ORDZZ/2*' ','Z' ','6*' '/'	MAN00400
DATA ORDYY/2*' ','Y' ','6*' '/'	MAN00410
DATA ORDXX/2*' ','X' ','6*' '/'	MAN00420
DATA ABK /2*' ','K' ','6*' '/'	MAN00430
DATA ABWD/2*' ','WD' ','6*' '/'	MAN00440
DATA ABVT/2*' ','VT' ','6*' '/'	MAN00450
DATA ORDC/2*' ','DC/DZ' ','6*' '/'	MAN00460
DATA KXP,KYP,NDP,NVP,NSP,NCP,NGP,NXDP,NYDP/	MAN00470
1 0, 0, 1, 2, 1, 42, 1, 1, 1/	MAN00480
DATA INCOL1/8888/	MAN00490
TMARK = 1.0D&2	MAN00500
ITEST=0	MAN00510
CCONST=1.4D0*8.3144D-3/29.0D0	MAN00520
NCARDS=1	MAN00530
DEGRAD=0.01745329D0	MAN00540
RADDEG=57.2957795D0	MAN00550
TCK=273.0D0	MAN00560

```

NTAB=1
ITHETI=1
ITHETF=80
ITHETS=1
NOPTN=1
LD=1
LS=1
PHI=45.000
ZS=0.000
TS=0.000
XS=0.000
YS=0.000
CALL WHEREF(INTABO)
C
CALL SETUP(8HITHEAI ,4,ITHETI )
CALL SETUP(8HITHEAF ,4,ITHETF )
CALL SETUP(8HITHEAST,4,ITHETS )
CALL SETUP(8HPHI ,8,PHI )
CALL SETUP(8HZS ,8,ZS )
CALL SETUP(8HTS ,8,TS )
CALL SETUP(8HXS ,8,XS )
CALL SETUP(8HYS ,8,YS )
CALL SETUP(8HNOPTN ,4,NOPTN )
CALL SETUP(8HTMARK ,8,TMARK )
C
C READ AND WRITE INPUT TABLE
C
WRITE(6,1)
READ(5,2) TITLE
WRITE(6,3) TITLE
C
110 READ(5,4) ITEST,ZI(NCARDS),VXI(NCARDS),VYI(NCARDS),TEMQ(NCARDS)
IF(ITEST.EQ.9) GO TO 130
C
CI(NCARDS)=DSORT(CCONST*(TEMQ(NCARDS) & TCK))
VXISQ = VXI(NCARDS)*VXI(NCARDS)
VYISQ = VYI(NCARDS)*VYI(NCARDS)
VTI(NCARDS) = SORT(VXISQ & VYISQ)
WDI(NCARDS) = DATAN2(VXI(NCARDS),VYI(NCARDS)) *RADDEG
WRITE(6,5) NCARDS,ZI(NCARDS),VXI(NCARDS),VYI(NCARDS),
1 TEMQ(NCARDS),CI(NCARDS)
NCARDS=NCARDS & 1
IF(NCARDS.LE.300) GO TO 110
C
WRITE(6,6)
GO TO 1000
C
130 NCARDS=NCARDS - 1
C
DO 120 I=2,NCARDS
J = I - 1
PLDCDZ(J) = (-CI(J) & CI(I))/(ZI(I) - ZI(J))
120 CONTINUE
C
PLDCDZ(NCARDS) = PLDCDZ(NCARDS - 1)
C
NMAX=NCARDS
C

```

NPP=NMAX	MAN01150
NFP=1	MAN01160
DCXP=16.CDD	MAN01170
DCYP=16.CDD	MAN01180
CALL AICRT3(KXP,KYP, VXi, ZI,NPP,NDP,NVP,NSP,NCP, TITLE,	MAN01190
\$ DRDPX, ABSCP,NFP,NGP,DCXP,DCYP,NXOP,XLP,XUP,NYOP,YLP,YUP)	MAN01200
CALL AICRT3(KXP,KYP, VYI, ZI,NPP,NDP,NVP,NSP,NCP, TITLE,	MAN01210
\$ DRDPY, ABSCP,NFP,NGP,DCXP,DCYP,NXOP,XLP,XUP,NYOP,YLP,YUP)	MAN01220
CALL AICRT3(KXP,KYP, CI, ZI,NPP,NDP,NVP,NSP,NCP, TITLE,	MAN01230
\$ DRDPC, ABSCP,NFP,NGP,DCXP,DCYP,NXOP,XLP,XUP,NYOP,YLP,YUP)	MAN01240
CALL AICRT3(KXP,KYP, VTI, ZI,NPP,NDP,NVP,NSP,NCP, TITLE,	MAN01250
\$ ABVT, ABSCP,NFP,NGP,DCXP,DCYP,NXOP,XLP,XUP,NYOP,YLP,YUP)	MAN01260
CALL AICRT3(KXP,KYP, WOI, ZI,NPP,NDP,NVP,NSP,NCP, TITLE,	MAN01270
\$ ABWD, ABSCP,NFP,NGP,DCXP,DCYP,NXOP,XLP,XUP,NYOP,YLP,YUP)	MAN01280
CALL AICRT3(KXP,KYP, ZI,PLDCDZ,NPP,NDP,NVP,NSP,NCP, TITLE,	MAN01290
\$ ABSCP, DRDC, NFP,NGP,DCXP,DCYP,NXOP,XLP,XUP,NYOP,YLP,YUP)	MAN01300
CALL AICRT3(KXP,KYP, TEMQ, ZI,NPP,NDP,NVP,NSP,NCP, TITLE,	MAN01310
\$ DRDTM,DRDZZ, NFP,NGP,DCXP,DCYP,NXOP,XLP,XUP,NYOP,YLP,YUP)	MAN01320
2000 CONTINUE	MAN01330
WRITE(6,7)	MAN01340
CALL READIN(INC011,\$1000)	MAN01350
PHI=PHI*DEGRAD	MAN01360
LOOP FOR INCREMENTED THETA	MAN01370
DO 150 I=ITHETI,ITHETF,ITHETS	MAN01380
AI=I*DEGRAD	MAN01390
CALL ARTLU(NTAB,ZS,ZI,CZ,CI)	MAN01400
AKX=DSIN(AI)*DCOS(PHI)/CZ	MAN01410
AKY=DSIN(AI)*DSIN(PHI)/CZ	MAN01420
LS=1	MAN01430
NPLT=0	MAN01440
CALL SKDIST(NOPTN,ZS,TS,XS,YS,AKX,AKY,TTOTS,XTOTS,YTOTS,LS)	MAN01450
IF(LS.LT.0) GO TO 132	MAN01460
ZSDN = PLYZ(NPLT)	MAN01470
NPLT = NPLT & 1	MAN01480
PLYZ(NPLT) = ZTOP	MAN01490
PLXT(NPLT) = TTOT	MAN01500
PLYX(NPLT) = XTOT	MAN01510
PLYZ(NPLT) = YTOT	MAN01520
NPLT = NPLT & 1	MAN01530
PLYZ(NPLT) = ZSDN	MAN01540
PLXT(NPLT) = TTOTS	MAN01550
PLYX(NPLT) = XTOTS	MAN01560
PLYZ(NPLT) = YTOTS	MAN01570
L=LS	MAN01580
AKR=AKX	MAN01590
AKS=AKY	MAN01600
CALL DNDIST(NOPTN, ZSDN,TTOTS,XTOTS,YTOTS,AKR,AKS,TTOTS,XTOTS	MAN01610
\$,YTOTS,L)	MAN01620
	MAN01630
	MAN01640
	MAN01650
	MAN01660
	MAN01670
	MAN01680
	MAN01690
	MAN01700
	MAN01710
	MAN01720

132 CONTINUE

THETA=I
WRITE(6,9) THETA,PHII,TTOTS,XTOTS,YTOTS

C

NPP=NPLT
DPLT=I
CALL AICRT3(KXP,KYP, PLXT, PLYZ,NPP,NDP,NVP,NSP,NCP, TITLE,
\$ ABSCT, ORDZZ,NFP,NGP,DCXP,DCYP,NXDP,XLP,XUP,NYDP,YLP,YUP)
CALL PRINTV(3,'EL ',718,1015)
CALL LABLV(DPLT,750,1015,6,1,4)
CALL PRINTV(8,' DEGREES',806,1015)
CALL PRINTV(3,'AZ ',718, 999)
CALL LABLV(PHII,750,999,6,1,4)
CALL PRINTV(8,' DEGREES',806, 999)

C

CALL AICRT3(KXP,KYP, PLXT, PLYX,NPP,NDP,NVP,NSP,NCP, TITLE,
\$ ABSCT, ORDXX,NFP,NGP,DCXP,DCYP,NXDP,XLP,XUP,NYDP,YLP,YUP)
CALL PRINTV(3,'EL ',718,1015)
CALL LABLV(DPLT,750,1015,6,1,4)
CALL PRINTV(8,' DEGREES',806,1015)
CALL PRINTV(3,'AZ ',718, 999)
CALL LABLV(PHII,750,999,6,1,4)
CALL PRINTV(8,' DEGREES',806, 999)

C

CALL AICRT3(KXP,KYP, PLXT, PLYY,NPP,NDP,NVP,NSP,NCP, TITLE,
\$ ABSCT, ORDYY,NFP,NGP,DCXP,DCYP,NXDP,XLP,XUP,NYDP,YLP,YUP)
CALL PRINTV(3,'EL ',718,1015)
CALL LABLV(DPLT,750,1015,6,1,4)
CALL PRINTV(8,' DEGREES',806,1015)
CALL PRINTV(3,'AZ ',718, 999)
CALL LABLV(PHII,750,999,6,1,4)
CALL PRINTV(8,' DEGREES',806, 999)

C

CALL AICRT3(KXP,KYP, PLYX, PLYY,NPP,NDP,NVP,NSP,NCP, TITLE,
\$ ORDXX, ORDYY,NFP,NGP,DCXP,DCYP,NXDP,XLP,XUP,NYDP,YLP,YUP)

C

CALL PRINTV(3,'EL ',718,1015)
CALL LABLV(DPLT,750,1015,6,1,4)
CALL PRINTV(8,' DEGREES',806,1015)
CALL PRINTV(3,'AZ ',718, 999)
CALL LABLV(PHII,750,999,6,1,4)
CALL PRINTV(8,' DEGREES',806, 999)

C

CALL AICRT3(KXP,KYP, PLYX, PLYZ,NPP,NDP,NVP,NSP,NCP, TITLE,
\$ ORDXX, ORDZZ,NFP,NGP,DCXP,DCYP,NXDP,XLP,XUP,NYDP,YLP,YUP)

C

CALL PRINTV(3,'EL ',718,1015)
CALL LABLV(DPLT,750,1015,6,1,4)
CALL PRINTV(8,' DEGREES',806,1015)
CALL PRINTV(3,'AZ ',718, 999)
CALL LABLV(PHII,750,999,6,1,4)
CALL PRINTV(8,' DEGREES',806, 999)

C

CALL AICRT3(KXP,KYP, PLYY, PLYZ,NPP,NDP,NVP,NSP,NCP, TITLE,
\$ ORDYY, ORDZZ,NFP,NGP,DCXP,DCYP,NXDP,XLP,XUP,NYDP,YLP,YUP)
CALL PRINTV(3,'EL ',718,1015)
CALL LABLV(DPLT,750,1015,6,1,4)
CALL PRINTV(8,' DEGREES',806,1015)

CALL PRINTV(3,'AZ ',718, 999)	MAN02310
CALL LABLV(PHII,750,999,6,1,4)	MAN02320
CALL PRINTV(8,' DEGREES',806, 999)	MAN02330
	MAN02340
DO 133 IIQ=1,NPLT	MAN02350
PLYXSQ = PLYX(IIQ)*PLYX(IIQ)	MAN02360
PLYYSQ = PLYY(IIQ)*PLYY(IIQ)	MAN02370
VTIX(IIQ) = SQRT(PLYXSQ & PLYYSQ)	MAN02380
133 CONTINUE	MAN02390
	MAN02400
CALL ATCRT3(KXP,KYP, VTIX, PLYZ,NPP,NDP,NVP,NSP,NCP, TITLE,	MAN02410
\$ ABK, ORDZZ,NFP,NGP,DCXP,DCYP,NXOP,XLP,XUP,NYOP,YLP,YUP)	MAN02420
	MAN02430
CALL PRINTV(3,'EL ',718,1015)	MAN02440
CALL LABLV(DPLT,750,1015,6,1,4)	MAN02450
CALL PRINTV(8,' DEGREES',806,1015)	MAN02460
CALL PRINTV(3,'AZ ',718, 999)	MAN02470
CALL LABLV(PHII,750,999,6,1,4)	MAN02480
CALL PRINTV(8,' DEGREES',806, 999)	MAN02490
	MAN02500
	MAN02510
	MAN02520
IF(I.NE.ITHETI) GO TO 135	MAN02530
	MAN02540
PLYZMX = PLYZ(1)	MAN02550
PLYXMX = PLYX(1)	MAN02560
PLYYMX = PLYY(1)	MAN02570
PLYVMX = VTIX(1)	MAN02580
PLYZMN = PLYZ(1)	MAN02590
PLYXMN = PLYX(1)	MAN02600
PLYYMN = PLYY(1)	MAN02610
PLYVMN = VTIX(1)	MAN02620
XTMAX = PLXT(NPP)	MAN02630
XTMIN = PLXT(1)	MAN02640
GO TO 137	MAN02650
	MAN02660
135 CONTINUE	MAN02670
XTMAX = DMAX1(XTMAX,PLXT(NPP))	MAN02680
XTMIN = DMIN1(XTMIN,PLXT(1))	MAN02690
	MAN02700
137 CONTINUE	MAN02710
	MAN02720
DO 140 II=1,NPP	MAN02730
PLYZMX = DMAX1(PLYZ(II),PLYZMX)	MAN02740
PLYXMX = DMAX1(PLYX(II),PLYXMX)	MAN02750
PLYYMX = DMAX1(PLYY(II),PLYYMX)	MAN02760
PLYVMX = DMAX1(VTIX(II),PLYVMX)	MAN02770
PLYZMN = DMIN1(PLYZ(II),PLYZMN)	MAN02780
PLYXMN = DMIN1(PLYX(II),PLYXMN)	MAN02790
PLYYMN = DMIN1(PLYY(II),PLYYMN)	MAN05210
PLYVMN = DMIN1(VTIX(II),PLYVMN)	MAN05220
140 CONTINUE	MAN05230
	MAN05240
WRITE(13) NPP,PLXT,PLYZ,PLYX,PLYY,VTIX	MAN05250
	MAN05260
150 CONTINUE	MAN05270
	MAN05280
	MAN05290

C	PLOT COMPOSIT GRAPHS	MAN053
C		MAN053
	END FILE 13	MAN053
	REWIND 13	MAN053
	NFP=1	MAN053
C		MAN053
	NXOP=2	MAN053
	NYOP=2	MAN053
	XLP = XTMIN	MAN053
	XUP = XTMAX	MAN053
	YLP = PLYZMN	MAN054
	YUP = PLYZMX	MAN054
C		MAN054
	DO 200 I=ITHETI,ITHETF,ITHETS	MAN054
	IF(I.GT.ITHETI) NFP=2	MAN054
	READ(13) NPP,PLXT,PLYZ,PLYX,PLY,VTIX	MAN054
	CALL AICRT3(KXP,KYP, PLXT, PLYZ,NPP,NDP,NVP,NSP,NCP, TITLE,	MAN054
	\$ ABSCT, DRDZZ,NFP,NGP,DCXP,DCYP,NXOP,XLP,XUP,NYOP,YLP,YUP)	MAN054
	200 CONTINUE	MAN054
C		MAN054
	REWIND 13	MAN055
	CALL PRINTV(3,'AZ ',718,1015)	MAN055
	CALL LABLV(PHII,750,1015,6,1,4)	MAN055
	CALL PRINTV(8,' DEGREES',806,1015)	MAN055
C		MAN055
	NFP=1	MAN055
	YLP = PLYXMN	MAN055
	YUP = PLYXMX	MAN055
C		MAN055
	DO 210 I=ITHETI,ITHETF,ITHETS	MAN055
	IF(I.GT.ITHETI) NFP=2	MAN056
	READ(13) NPP,PLXT,PLYZ,PLYX,PLY,VTIX	MAN056
	CALL AICRT3(KXP,KYP, PLXT, PLYX,NPP,NDP,NVP,NSP,NCP, TITLE,	MAN056
	\$ ABSCT, DRDXX,NFP,NGP,DCXP,DCYP,NXOP,XLP,XUP,NYOP,YLP,YUP)	MAN056
	210 CONTINUE	MAN056
C		MAN056
	REWIND 13	MAN056
	CALL PRINTV(3,'AZ ',718,1015)	MAN056
	CALL LABLV(PHII,750,1015,6,1,4)	MAN056
	CALL PRINTV(8,' DEGREES',806,1015)	MAN056
C		MAN057
	NFP=1	MAN057
	YLP=PLYMNM	MAN057
	YUP=PLYMX	MAN057
C		MAN057
	DO 220 I=ITHETI,ITHETF,ITHETS	MAN057
	IF(I.GT.ITHETI) NFP=2	MAN057
	READ(13) NPP,PLXT,PLYZ,PLYX,PLY,VTIX	MAN057
	CALL AICRT3(KXP,KYP, PLXT, PLYY,NPP,NDP,NVP,NSP,NCP, TITLE,	MAN057
	\$ ABSCT, DRDYY,NFP,NGP,DCXP,DCYP,NXOP,XLP,XUP,NYOP,YLP,YUP)	MAN057
	220 CONTINUE	MAN057
C		MAN057
	REWIND 13	MAN057
	CALL PRINTV(3,'AZ ',718,1015)	MAN057
	CALL LABLV(PHII,750,1015,6,1,4)	MAN057
	CALL PRINTV(8,' DEGREES',806,1015)	MAN057
C		MAN057
	NFP=1	MAN057

YLP = PLYZMN	MAN05880
YUP = PLYZMX	MAN05890
XLP = PLYXMN	MAN05900
XUP = PLYXMX	MAN05910
	MAN05920
DO 230 I=ITHETI,ITHETE,ITHETS	MAN05930
IF(I.GT.ITHETI) NFP=2	MAN05940
READ(13) NPP,PLXT,PLYZ,PLYX,PLYY,VTIX	MAN05950
CALL AICRT3(KXP,KYP, PLYX, PLYZ,NPP,NDP,NVP,NSP,NCP, TITLE,	MAN05960
\$ ORDX, ORDZZ,NFP,NGP,DCXP,DCYP,NXOP,XLP,XUP,NYOP,YLP,YUP)	MAN05970
TMARKQ = PLXT(NPP)	MAN05980
TMARKX = TMARK	MAN05990
234 IF(TMARKX.GE.TMARKQ) GO TO 236	MAN06000
CALL ARTLU(2,TMARKX,PLXT,YMARK,PLYZ,XMARK,PLYX)	MAN06010
CALL PLOTV(NXV(XMARK),NYV(YMARK),16)	MAN06020
TMARKX = TMARKX & TMARK	MAN06030
GO TO 234	MAN06040
236 CONTINUE	MAN06050
230 CONTINUE	MAN06060
	MAN06070
REWIND 13	MAN06080
CALL PRINTV(3,'AZ ',718,1015)	MAN06090
CALL LABLV(PHII,750,1015,6,1,4)	MAN06100
CALL PRINTV(8,' DEGREES ',806,1015)	MAN06110
CALL PRINTV(6,'TMARK ',718,999)	MAN06120
CALL LABLV(TMARK,774,999,6,1,4)	MAN06130
	MAN06140
	MAN06150
NFP=1	MAN06160
XLP = PLYYMN	MAN06170
XUP = PLYYMX	MAN06180
	MAN06190
DO 240 I=ITHETI,ITHETE,ITHETS	MAN06200
IF(I.GT.ITHETI) NFP=2	MAN06210
READ(13) NPP,PLXT,PLYZ,PLYX,PLYY,VTIX	MAN06220
CALL AICRT3(KXP,KYP, PLYY, PLYZ,NPP,NDP,NVP,NSP,NCP, TITLE,	MAN06230
\$ ORDYY, ORDZZ,NFP,NGP,DCXP,DCYP,NXOP,XLP,XUP,NYOP,YLP,YUP)	MAN06240
TMARKQ = PLXT(NPP)	MAN06250
TMARKX = TMARK	MAN06260
244 IF(TMARKX.GE.TMARKQ) GO TO 246	MAN06270
CALL ARTLU(2,TMARKX,PLXT,YMARK,PLYZ,XMARK,PLYY)	MAN06280
CALL PLOTV(NXV(XMARK),NYV(YMARK),16)	MAN06290
TMARKX = TMARKX & TMARK	MAN06300
GO TO 244	MAN06310
246 CONTINUE	MAN06320
240 CONTINUE	MAN06330
	MAN06340
REWIND 13	MAN06350
CALL PRINTV(3,'AZ ',718,1015)	MAN06360
CALL LABLV(PHII,750,1015,6,1,4)	MAN06370
CALL PRINTV(8,' DEGREES ',806,1015)	MAN06380
CALL PRINTV(6,'TMARK ',718,999)	MAN06390
CALL LABLV(TMARK,774,999,6,1,4)	MAN06400
	MAN06410
	MAN06420
NFP=1	MAN06430
XLP = PLYVMN	MAN06440
XUP = PLYVMX	MAN06450

```

C MAN06460
C DO 250 I=ITHETI,ITHEIF,IHETS MAN06470
C IF(I.GT.ITHETI) NFP=2 MAN06480
C READ(13) NPP,PLXT,PLYZ,PLYX,PLYY,VTIX MAN06490
C CALL AICRT3(KXP,KYP,VTIX,PLYZ,NPP,NDP,NVP,NSP,NCP,TITLE, MAN06500
C $ ABK,ORDZZ,NFP,NGP,DCXP,DCYP,NXQP,XLP,XUP,NYQP,YLP,YUP) MAN06510
C 250 CONTINUE MAN06520
C MAN06530
C REWIND 13 MAN06540
C CALL PRINTV(3,'AZ ',Z18,1015) MAN06550
C CALL LABLV(PHII,750,1015,6,1,4) MAN06560
C CALL PRINTV(8,' DEGREES ',806,1015) MAN06570
C MAN06580
C NFP = 1 MAN06590
C XLP = PLYXMN MAN06600
C XUP = PLYXMX MAN06610
C YLP = PLYYMN MAN06620
C YUP = PLYYMX MAN06630
C MAN06640
C DO 260 I=IITHETI,IITHEIF,IIHETS MAN06650
C IF(I.GT.IITHETI) NFP=2 MAN06660
C READ(13) NPP,PLXT,PLYZ,PLYX,PLYY,VTIX MAN06670
C CALL AICRT3(KXP,KYP,PLYX,PLYY,NPP,NDP,NVP,NSP,NCP,TITLE, MAN06680
C $ ORDXX,ORDYY,NFP,NGP,DCXP,DCYP,NXQP,XLP,XUP,NYQP,YLP,YUP) MAN06690
C 260 CONTINUE MAN06700
C MAN06710
C REWIND 13 MAN06720
C CALL PRINTV(3,'AZ ',Z18,1015) MAN06730
C CALL LABLV(PHII,750,1015,6,1,4) MAN06740
C CALL PRINTV(8,' DEGREES ',806,1015) MAN06750
C MAN06760
C GO TO 2000 MAN06770
C MAN06780
C 1000 CONTINUE MAN06790
C CALL FRAMEV(0) MAN06800
C CALL PLTND MAN06810
C MAN06820
C 1 FORMAT('ACOUSTIC RAY-TRACING',/' ') MAN06830
C 2 FORMAT(9A8) MAN06840
C 3 FORMAT('C',9A8,/' I',7X,'ZI',8X,'VXI',7X,'VYI',5X,'TEMP',8X,'CI' MAN06850
C $ ,/' ') MAN06860
C 4 FORMAT(I1,4E10.0) MAN06870
C 5 FORMAT(1X,I3,F10.1,3F10.3,F10.4) MAN06880
C 6 FORMAT(// '** TOO MANY CARDS FOR TABLE') MAN06890
C 7 FORMAT('1') MAN06900
C 8 FORMAT('C ITHETA ',F10.1,/ MAN06910
C 1 ' PHI ',F10.1,/ MAN06920
C 2 ' TOTAL TIME ',F10.1,/ MAN06930
C 3 ' TOTAL X ',F10.1,/ MAN06940
C 4 ' TOTAL Y ',F10.1) MAN06950
C MAN06960
C STOP MAN06970
C END MAN06980
C IMPLICIT REAL*8 (A-H,O-Z) PAR000
C SUBROUTINE PARAM(AKX,AKY,C,VX,VY,DTUP,DXUP,DYUP,AKZSQ) PAR000
C BOM=1.0-AKX*VX-AKY*VY PAR000
C DTUP=BOM/C**2 PAR000
C DXUP=AKX&VX*DTUP PAR000

```

DYUP=AKY&VY*DTUP	PAR00060
AKZSQ=BOM*DTUP-AKX**2-AKY**2	PAR00070
RETURN	PAR00080
END	PAR00090
IMPLICIT REAL*8 (A-H,O-Z)	SKD00010
SUBROUTINE SKDIST(NOPTN,ZS,TS,XS,YS,AKX,AKY,TTOT,XTOT,YTOT,L)	SKD00020
	SKD00030
	SKD00040
MODIFIED FOR PREDICTOR CORRECTOR	SKD00050
COMMON/FAYE/CI(300),VXI(300),VYI(300),ZI(300),PLXT(600),PLYZ(600),	SKD00060
1 PLYX(600),PLYY(600)	SKD00070
COMMON/JANET/NMAX,NPLT	SKD00080
COMMON/PEARL/ZTOP,TTOP,XTOP,YTOP,T2,X2,Y2	SKD00090
DIMENSION VALUE(3),DERN(3),UPBND(3),DNBND(3)	SKD00100
COMMON/JULIA/QAKX,QAKY	SKD00110
RADDEG = 57.295779513100	SKD00130
AKXKY = AKX*AKX & AKY*AKY	SKD00140
QAKX = AKX	SKD00150
QAKY = AKY	SKD00160
	SKD00170
IF(ZS.LT.ZI(NMAX)) GO TO 110	SKD00180
WRITE(6,1) ZS,ZI(NMAX)	SKD00190
CALL EXIT	SKD00200
	SKD00210
110 CONTINUE	SKD00220
	SKD00230
DO 120 I=2,NMAX	SKD00240
IF(ZS.LE.ZI(I))GO TO 130	SKD00250
120 CONTINUE	SKD00260
	SKD00270
130 IF(ZS.EQ.ZI(I)) I=I&1	SKD00280
IXX=I	SKD00290
IF(ZS.GT.ZI(I)) GO TO 135	SKD00300
VX = VXI(I)	SKD00310
VY = VYI(I)	SKD00320
C = CI(I)	SKD00330
GO TO 136	SKD00340
135 CONTINUE	SKD00350
CALL ARTLU(3,ZS,ZI,VX,VXI,VY,VYI,C,CI)	SKD00360
136 CONTINUE	SKD00370
TM1 = (1.000 - AKX*VX - AKY*VY)/C	SKD00380
AKISQ = TM1*TM1 - AKXKY	SKD00390
	SKD00400
IF(AKISQ.GT.0.000) GO TO 140	SKD00410
WRITE(6,2) ZI	SKD00420
L=-1	SKD00440
RETURN	SKD00450
	SKD00460
140 WRITE(6,7) AKX,AKY	SKD00470
WRITE(6,3)	SKD00480
	SKD00490
INITIAL CONDITIONS	SKD00500
	SKD00510
NEQ = 3	SKD00520
DATA UPBND/1.00-2,2*1.000/	SKD00530
DNBND(1) = 1.00-4	SKD00540
DNBND(2) = 1.00-2	SKD00550
DNBND(3) = 1.00-2	SKD00560

	FACTOR = .500	SKD00570
	ZIND = ZS	SKD00580
	DELMIT = 0.000	SKD00590
	VALUE(1) = IS	SKD00600
	VALUE(2) = XS	SKD00610
	VALUE(3) = YS	SKD00620
	WRITE(6,4) ZIND,VALUE	SKD00630
C		SKD00640
	DD 160 I=IXX,NMAX	SKD00650
	HLIMIT = ZI(I)	SKD00660
	DEL = DABS(HLIMIT-ZIND) * 1.0D-1	SKD00670
	FREQ = 10.000*DEL	SKD00680
	LQX = 1	SKD00690
	IF(HLIMIT.GT.ZI(1)) GO TO 145	SKD00700
	VX = VXI(1)	SKD00710
	VY = VYI(1)	SKD00720
	C = CI(1)	SKD00730
	GO TO 146	SKD00740
145	CONTINUE	SKD00750
	CALL ARTLU(3,HLIMIT,ZI,VX,VXI,VY,VYI,C,CI)	SKD00760
146	CONTINUE	SKD00770
	TM1 = (1.000 - AKX*VX - AKY*VY)/C	SKD00780
	AK2SQ = TM1*TM1 - AKXKY	SKD00790
	IF(AK2SQ.LE.0.000) GO TO 180	SKD00800
150	CONTINUE	SKD00810
155	CALL ADM4RK(NEQ,DEL,VALUE,DERN,UPBND,DNBND,FACTOR,FREQ,HLIMIT,	SKD00820
	1 LQX,ZIND,DELMIT)	SKD00830
	GO TO(155,155,157,157,155,156),LQX	SKD00840
156	WRITE(6,9) DEL	SKD00850
	L = -1	SKD00860
	RETURN	SKD00870
C		SKD00880
157	CONTINUE	SKD00890
	NPLT = NPLT & 1	SKD00900
	PLXT(NPLT) = VALUE(1)	SKD00910
	PLYX(NPLT) = VALUE(2)	SKD00920
	PLYY(NPLT) = VALUE(3)	SKD00930
	PLYZ(NPLT) = ZIND	SKD00940
	CALL ARTLU(2,ZIND,ZI,VX,VXI,VY,VYI)	SKD00950
	VT = DSORT(VX*VX & VY*VY)	SKD00960
	WD = 0.000	SKD00970
	VYVT = VY/VT	SKD00980
	IF(VYVT.LT.1.000) WD = DARCOS(VYVT) * RADDEG	SKD00990
	WRITE(6,4) ZIND,VALUE,VT,WD,AK1SQ,AK2SQ	SKD01000
	AK1SQ = AK2SQ	SKD01010
160	CONTINUE	SKD01020
C		SKD01030
	WRITE(6,5)	SKD01040
	TTOT = VALUE(1)	SKD01050
	XTOT = VALUE(2)	SKD01060
	YTOT = VALUE(3)	SKD01070
	L = -1	SKD01080
	RETURN	SKD01090
C		SKD01100
180	CONTINUE	SKD01110
	CALL INTERP(AK1SQ,AK2SQ,ZI(I-1),ZI(I),AKX,AKY,VALUE)	SKD01120
C		SKD01130
	TTOT = T2	SKD01140

XTOT = X2	SKD01120
YTOT = Y2	SKD01130
L=1	SKD01140
CALL ARTLU(2,ZTOP,ZI,VXTOP,VXI,VYTOP,VYI)	SKD01150
VT=DSORT(VXTOP*VXTOP & VYTOP*VYTOP)	SKD01160
WD=0.000	SKD01170
VYVT = VY/VT	SKD01180
IF(VYVT.LT.1.000) WD=DARCOS(VYVT)*RADDEG	SKD01190
WRITE(6,10)ZTOP,TTOP,XTOP,YTOP,VT,WD	SKD01200
1 FORMAT(' ** Z0 = ',G15.5,2X,'ZMAX = ',G15.5)	SKD01210
2 FORMAT(' ** NO RAY AT ALTITUDE OF ',G15.5)	SKD01220
3 FORMAT('0',9X,'HEIGHT',11X,'TIME',10X,'XDIST',10X,'YDIST',	SKD01230
1 11X,'VT',13X,'WD',9X,'KZ1SQ',10X,'KZ2SQ',/' ')	SKD01240
4 FORMAT(' ',6F15.4,2G15.5)	SKD01250
5 FORMAT(' ** NOT ENOUGH DATA')	SKD01260
6 FORMAT(' ** DELZ = ',G15.5)	SKD01270
7 FORMAT('1',12X,'RAY PARAMETERS - KX = ',F12.4,2X,'KY = ',F12.4)	SKD01280
8 FORMAT(' ** SUB DHPCG - IHLF = ',I4)	SKD01290
9 FORMAT(' ** DEL Z TOO SMALL - DEL Z = ',G15.5)	SKD01300
10 FORMAT('0',6F15.4,2X,'REFLECTION',/' ')	SKD01310
RETURN	SKD01320
END	SKD01330
IMPLICIT REAL*8 (A-H,O-Z)	SKD01340
	DND00010
	DND00020
SUBROUTINE DNDIST(NOPIN,ZS,IS,XS,YS,AKX,AKY,TTOT,XTOT,YTOT,L)	DND00030
	DND00040
MODIFIED FOR PREDICTOR CORRECTOR	DND00050
	DND00060
COMMON/FAVE/CI(300),VXI(300),VYI(300),ZI(300),PLXT(600),PLYZ(600),	DND00070
1 PLYX(600),PLYZ(600)	DND00080
COMMON/JANET/NMAX,NPLT	DND00090
COMMON/PEARL/ZTOP,TTOP,XTOP,YTOP	DND00100
DIMENSION VALUE(3),DERN(2),UPBND(3),DNBND(3)	DND00110
COMMON/JULIA/QAKX,QAKY	DND00120
	DND00140
	DND00150
RADDEG = 57.295779513100	DND00160
AKXKY = AKX*AKX & AKY*AKY	DND00170
QAKX = AKX	DND00180
QAKY = AKY	DND00190
	DND00200
IF(ZS.LT.ZI(NMAX)) GO TO 110	DND00210
WRITE(6,1) ZS,ZI(NMAX)	DND00220
CALL EXIT	DND00230
	DND00240
110 CONTINUE	DND00250
	DND00260
DO 120 I=2,NMAX	DND00270
IF(ZS.LE.ZI(I)) GO TO 130	DND00280
120 CONTINUE	DND00290
	DND00300
130 CONTINUE	DND00310
ITX = I-1	DND00320
	DND00330
CALL ARTLU(3,ZS,ZI,VX,VXI,VY,VYI,C,CT)	DND00340
	DND00350
TM1 = (1.000 - AKX*VX - AKY*VY)/C	DND00360
AK1SQ = TM1*TM1 - AKXKY	

C	IF(AK1SQ.GT.0.000) GO TO 140	DND00370
	WRITE(4,2) Z1	DND00380
	L = -1	DND00390
	RETURN	DND00400
C	140 CONTINUE	DND00430
C	INITIAL CONDITIONS	DND00440
C	NEQ = 3	DND00450
	DATA UPBND/1.0D-2,2*1.0D0/	DND00460
	DATA DNBND/1.0D-4,2*1.0D-2/	DND00470
	FACTOR = .5D0	DND00480
	ZIND = ZS	DND00490
	DELMIT = 0.0D0	DND00500
	VALUE(1) = TS	DND00510
	VALUE(2) = XS	DND00520
	VALUE(3) = YS	DND00530
	T1 = TS	DND00540
	X1 = XS	DND00550
	Y1 = YS	DND00560
	JZ = IXX & 1	DND00570
	WRITE(6,5) ZIND,VALUE	DND00580
C	DO 160 I = 1,IXX	DND00590
	JZ = JZ - 1	DND00600
	HLIMIT = ZI(JZ)	DND00610
	DEL = (HLIMIT-ZIND)*1.0D-1	DND00620
	FREQ = 10.0D0*DEL	DND00630
	LQX = 1	DND00640
	IF(HLIMIT.GT.ZI(1)) GO TO 145	DND00650
	VX = VXI(1)	DND00660
	VY = VYI(1)	DND00670
	C = CI(1)	DND00680
	GO TO 146	DND00690
145	CONTINUE	DND00700
	CALL ARTLU(3,HLIMIT,ZI,VX,VXI,VY,VYI,C,CI)	DND00710
146	CONTINUE	DND00720
	TM1 = (1.0D0 - AKX*VX - AKY*VY)/C	DND00730
	AK2SQ = TM1*TM1 - AKXKY	DND00740
	IF(AK2SQ.LE.0.0D0) GO TO 180	DND00750
C	155 CALL ADM4RK(NEQ,DEL,VALUE,DERN,UPBND,DNBND,FACTOR,FREQ,HLIMIT,	DND00760
	1 LQX,ZIND,DELMIT)	DND00770
	GO TO(155,155,157,157,155,156),LQX	DND00780
C	156 WRITE(6,4)	DND00790
	L = -1	DND00800
	RETURN	DND00810
C	157 CONTINUE	DND00820
	NPLT = NPLT & 1	DND00830
	T1 = T1 & (T1 - VALUE(1))	DND00840
	X1 = X1 & (X1 - VALUE(2))	DND00850
	Y1 = Y1 & (Y1 - VALUE(3))	DND00860
	VALUE(1) = T1	DND00870
	VALUE(2) = X1	DND00880


```

VALUE(3) = Y1
PLXT(NPLT) = VALUE(1)
PLYX(NPLT) = VALUE(2)
PLYY(NPLT) = VALUE(3)
PLYZ(NPLT) = ZIND
IF(ZIND.GT.7I(1)) GO TO 158
VX = VXI(1)
VY = VYI(1)
GO TO 159
158 CONTINUE
CALL ARTLU(2,ZIND,ZI,VX,VXI,VY,VYI)
159 CONTINUE
VT = DSQRT(VX*VX & VY*VY)
WD = 0.000
VYVT = VY/VT
IF(VYVT.LT.1.000) WD = DARCOS(VYVT) * RADDEG
WRITE(6,5) ZIND,VALUE,VT,WD,AK1SQ,AK2SQ
AK1SQ = AK2SQ
160 CONTINUE

TTOT = VALUE(1)
XTOT = VALUE(2)
YTOT = VALUE(3)
L = 1
RETURN

80 WRITE(6,6) AK2SQ,HLIMIT
1 FORMAT(' ** Z0 = ',G15.5,2X,'ZMAX = ',G15.5)
2 FORMAT(' ** NO RAY AT ALTITUDE OF ',G15.5)
4 FORMAT(' ** DEL Z TOO SMALL')
5 FORMAT(' ',6F15.4,2G15.5)
6 FORMAT(' ** K2SQ NEGATIVE - K2SQ = ',G15.5,' Z = ',G15.5)
RETURN
END
IMPLICIT REAL*8 (A-H,O-Z)

SUBROUTINE INTERP(AK1SQ,AK2SQ,Z1,Z2,AKX,AKY,VALUE)
COMMON/FAYE/CI(300),VXI(300),VYI(300),ZI(300),PLXT(600),PLYZ(600),
1 PLYX(600),PLYY(600)
COMMON/JANET/NMAX,NPLT
COMMON/PFARL/ZTOP,ITOP,XTOP,YTOP,T2,X2,Y2
DIMENSION VALUE(1)

T1 = VALUE(1)
X1 = VALUE(2)
Y1 = VALUE(3)
CALL ARTLU(3,Z1,ZI,C,CI,VX,VXI,VY,VYI)
CALL PAPAM(AKX,AKY,C,VX,VY,TUP1,XUP1,YUP1,AK1SQ)
CALL ARTLU(3,Z2,ZI,C,CI,VX,VXI,VY,VYI)
CALL PARAM(AKX,AKY,C,VX,VY,TUP2,XUP2,YUP2,AK2SQ)
PLUS = -1.000
DSIG = TUP1*(Z2-Z1)
IF(DSIG.GT.0.000) PLUS = 1.000
AK1 = PLUS* SORT(AK1SQ)
DENOM = AK1SQ-AK2SQ
ENUM = AK2SQ & AK1SQ/3.000
RAT = ENUM/DENOM

```

```

DND00960
DND00970
DND00980
DND00990
DND01000
DND01010
DND01020
DND01030
DND01040
DND01050
DND01060
DND01070
DND01080
DND01090
DND01100
DND01110
DND01120
DND01130
DND01140
DND01150
DND01160
DND01170
DND01180
DND01190
DND01200
DND01210
DND01220
DND01240
DND01250
DND01260
DND01270
DND01280
DND28880
DND28890
INT00010
INT00020
INT00030
INT00040
INT00050
INT00060
INT00070
INT00080
INT00090
INT00100
INT00110
INT00120
INT00130
INT00140
INT00150
INT00160
INT00170
INT00180
INT00190
INT00200
INT00210
INT00220
INT00230
INT00240

```

```

TUPAV = 0.500*(TUP1 & TUP2) - .500*(TUP1-TUP2)*RAT      INT0025
XUPAV = 0.500*(XUP1 & XUP2) - .500*(XUP1-XUP2)*RAT      INT0026
YUPAV = 0.500*(YUP1 & YUP2) - .500*(YUP1-YUP2)*RAT      INT0027
EQU = 4.000*AK1*(Z2-Z1)/DENOM                             INT0028
ZTOP = Z1 & (AK1SQ*(Z2-Z1)/DENOM)                         INT0029
TTOP = T1 & .500*EQU*TUPAV                                INT0030
XTOP = X1 & .500*EQU*XUPAV                                INT0031
YTOP = Y1 & .500*EQU*YUPAV                                INT0032
T2 = T1 & EQU*TUPAV                                        INT0033
X2 = X1 & EQU*XUPAV                                        INT0034
Y2 = Y1 & EQU*YUPAV                                        INT0035
IF(T2-T1) 110,120,120                                     INT0036
110 WRITE(6,1) TUP1,TUPAV                                  INT0037
1 FORMAT(' ** TIME REVERSAL IN INTERP',6X,'TUP1 = ',F12.4,3X,'TUPAV',
1,F12.4)                                                  INT0039
T2=T1 & DABS(EQU*TUPAV)                                    INT0040
120 CONTINUE                                              INT0041
RETURN                                                    INT0042
END                                                        INT0043
IMPLICIT REAL*8 (A-H,O-Z)                                  DER0001
C                                                         DER0002
SUBROUTINE DEREQ(VALUE,ZIND,DERY,LQX)                       DER0003
C                                                         DER0004
DIMENSION VALUE(1),DERY(1)                                DER0005
COMMON/JULIA/AKX,AKY                                       DER0006
COMMON/FAYE/CI(300),VXI(300),VYI(300),ZI(300),PLXT(600),PLYZ(600),
1 PLYX(600),PLY(600)                                       DER0008
IF(ZIND.GT.ZI(1)) GO TO 100                                DER0009
VX = VXI(1)                                                DER0010
VY = VYI(1)                                                DER0011
C = CI(1)                                                  DER0012
GO TO 110                                                  DER0013
100 CONTINUE                                              DER0014
CALL ARTLU(3,ZIND,ZI,VX,VXI,VY,VYI,C,CI)                  DER0015
110 CONTINUE                                              DER0016
OMEGA = 1.000 - AKX*VX - AKY*VY                            DER0017
TUP = OMEGA/C**2                                           DER0018
XUP = AKX & VX*TUP                                         DER0019
YUP = AKY & VY*TUP                                         DER0020
AKZSQ = OMEGA*TUP - AKX*AKX - AKY*AKY                     DER0021
AKZ = DSQRT(AKZSQ)                                         DER0022
DERY(1) = TUP/AKZ                                          DER0023
DERY(2) = XUP/AKZ                                          DER0024
DERY(3) = YUP/AKZ                                          DER0025
RETURN                                                    DER0026
END                                                        DER0027

```

FLOW CHARTS OF ACOUSTIC
RAY-TRACING COMPUTER PROGRAM

IMPLICIT REAL *8 (A-H, O-Z)

C ACOUSTIC RAY-TRACING
C L8074 R1748210000 Z230 DETERT/WEINSTEIN 1/68
C MOD. OF L8032
C REF- GEOMETRICAL ACOUSTICS' THEORY OF WAVES FROM A POINT SOURCE
C IN A TEMPERATURE AND WIND-STRATIFIED ATMOSPHERE
C BY ALLAN PIERCE AVSSD-0135-66-CR 2AUG66
C SUBROUTINES
C PARAM

C DNDIST
C SKDIST
C ARTLU
C DEREQ
C ADM4AK

COMMON/FAYE/CI (300), VXI (300), VYI (300), ZI (300), PLXT (600), PLYZ (600),
PLYX (600), PLYY (600)

COMMON /JANET/ NMAX, NPLT, IPATX
COMMON/PEARL/ZTOP, TTOP, XTOP, YTOP, T2, X2, Y2
DIMENSION TITLE (9), VTIX (600), VTI (300), WDI (300), PLOC0Z (300)
DIMENSION TEM0 (300), ORDTM (9)
EQUIVALENCE (VTIX (1), VTI (1)), (VTIX (301), TEM0 (1))

DIMENSION ABSCP (9), ORDPX (9), ORDPY (9), ORDPT (9), ORDPC (9), ABSCT (9),
ORDZZ (9), ORDXX (9), ORDYY (9), ABWD (9), ABVT (9), ABK (9), ORDC (9)

DIMENSION IDFRMZ (3)
REAL *4 INTAB0 (300)



IPRTX = 0
DATA WINDY /'WIND YES'/
DATA WINDN /'WIND NO '/
TMARK = 1.00+2
ITEST=0
CCONST=1.400*8.31440-3/29.000
NCARDS=1
DEGRAD=0.0174532900

RADDEG=57.295779500
TCK=273.000
NTAB=1
ITHETI=1
ITHETF=89
ITHETS=1
NOPTN=1
LD=1

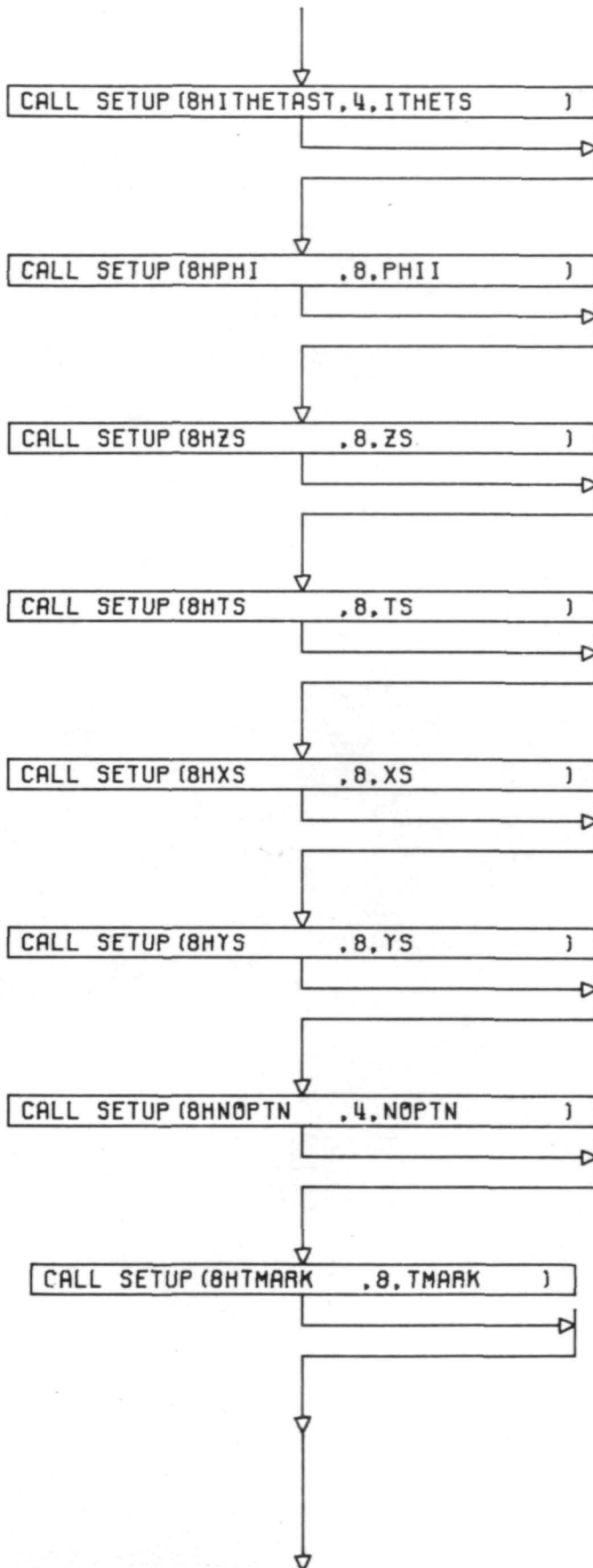
LS=1
PHI1=45.000
ZS=0.000
TS=0.000
XS=0.000
YS=0.000

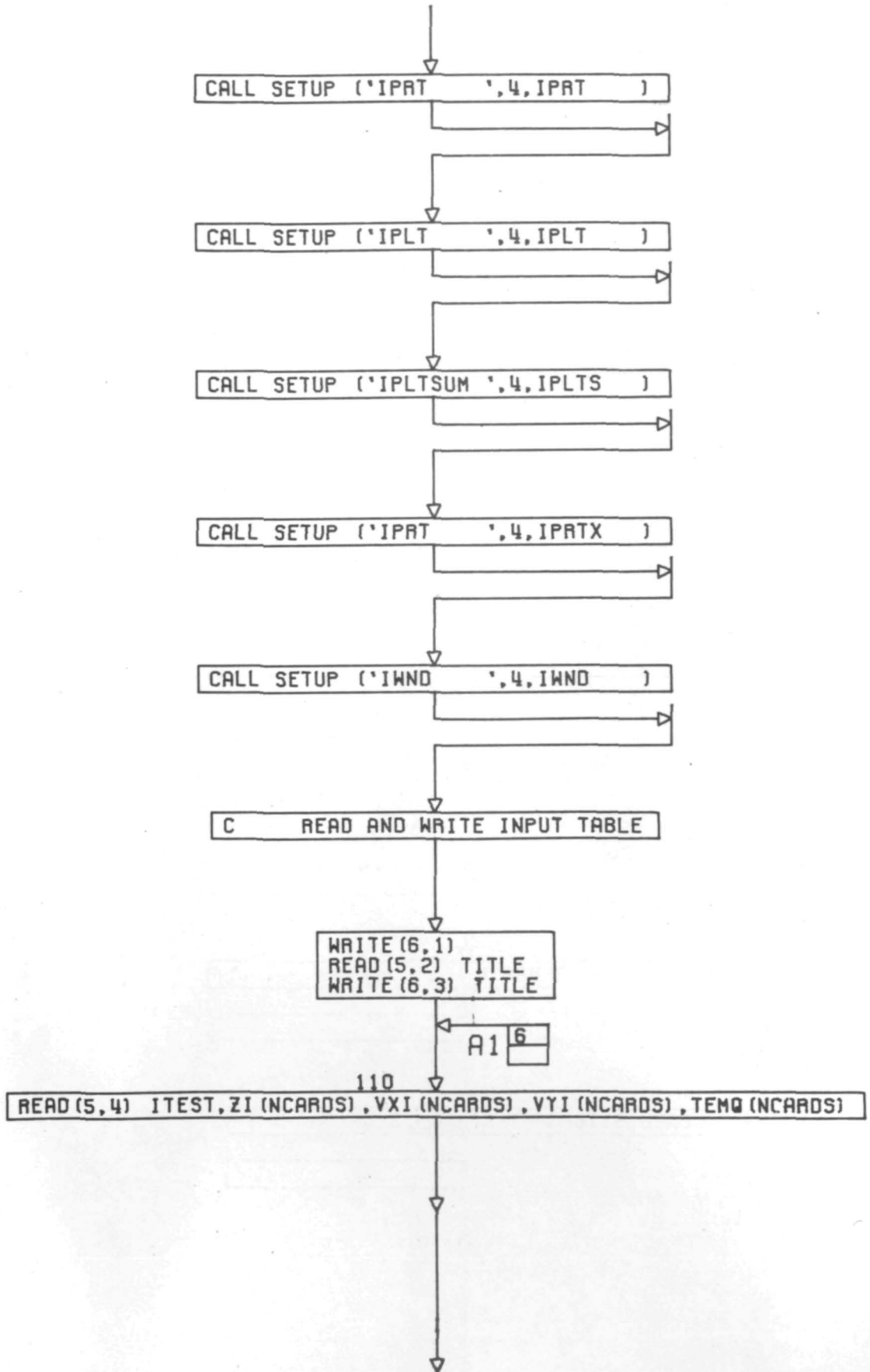
CALL WHERE (INTABQ)

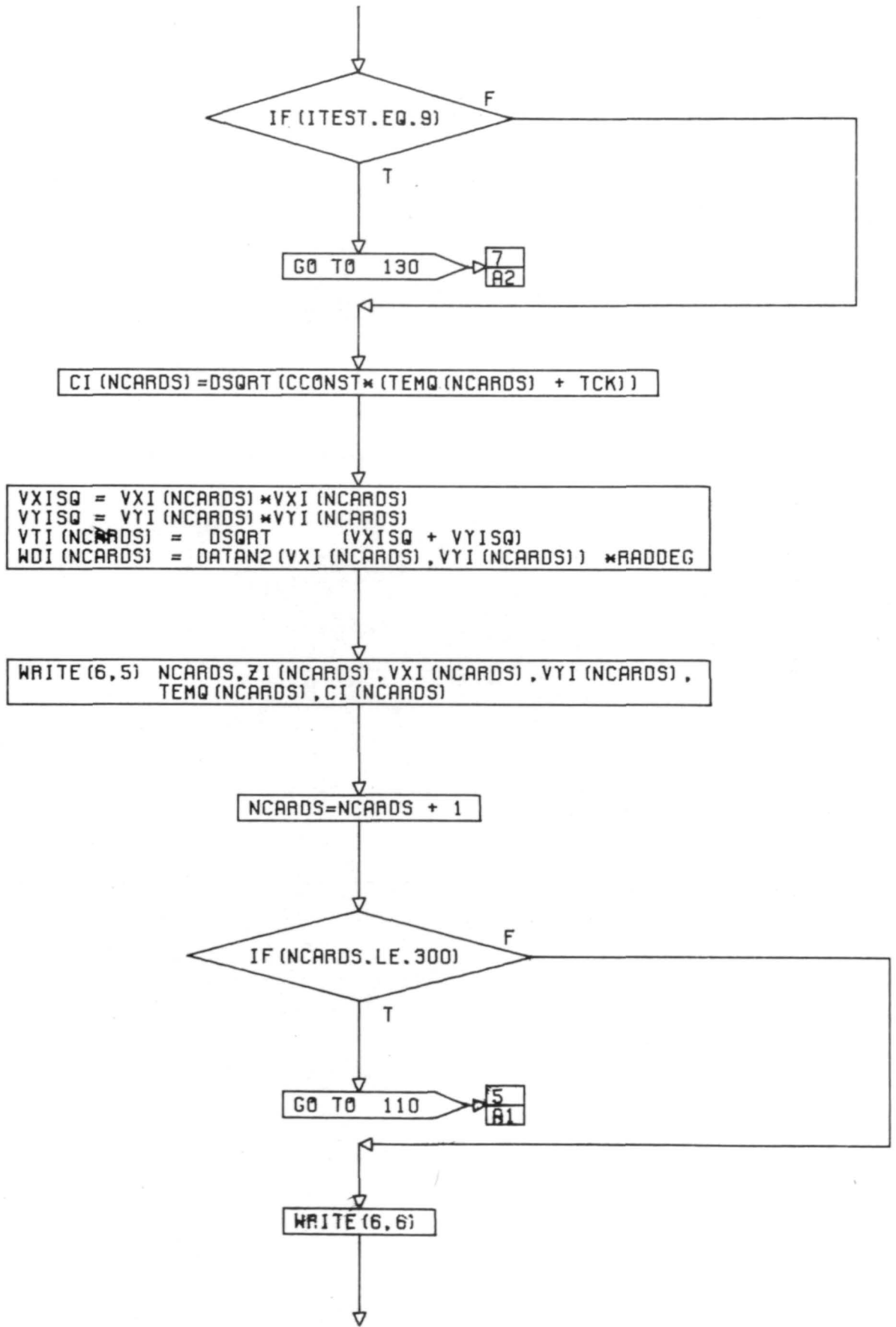
CALL SETUP (8HITHETAI ,4, ITHETI)

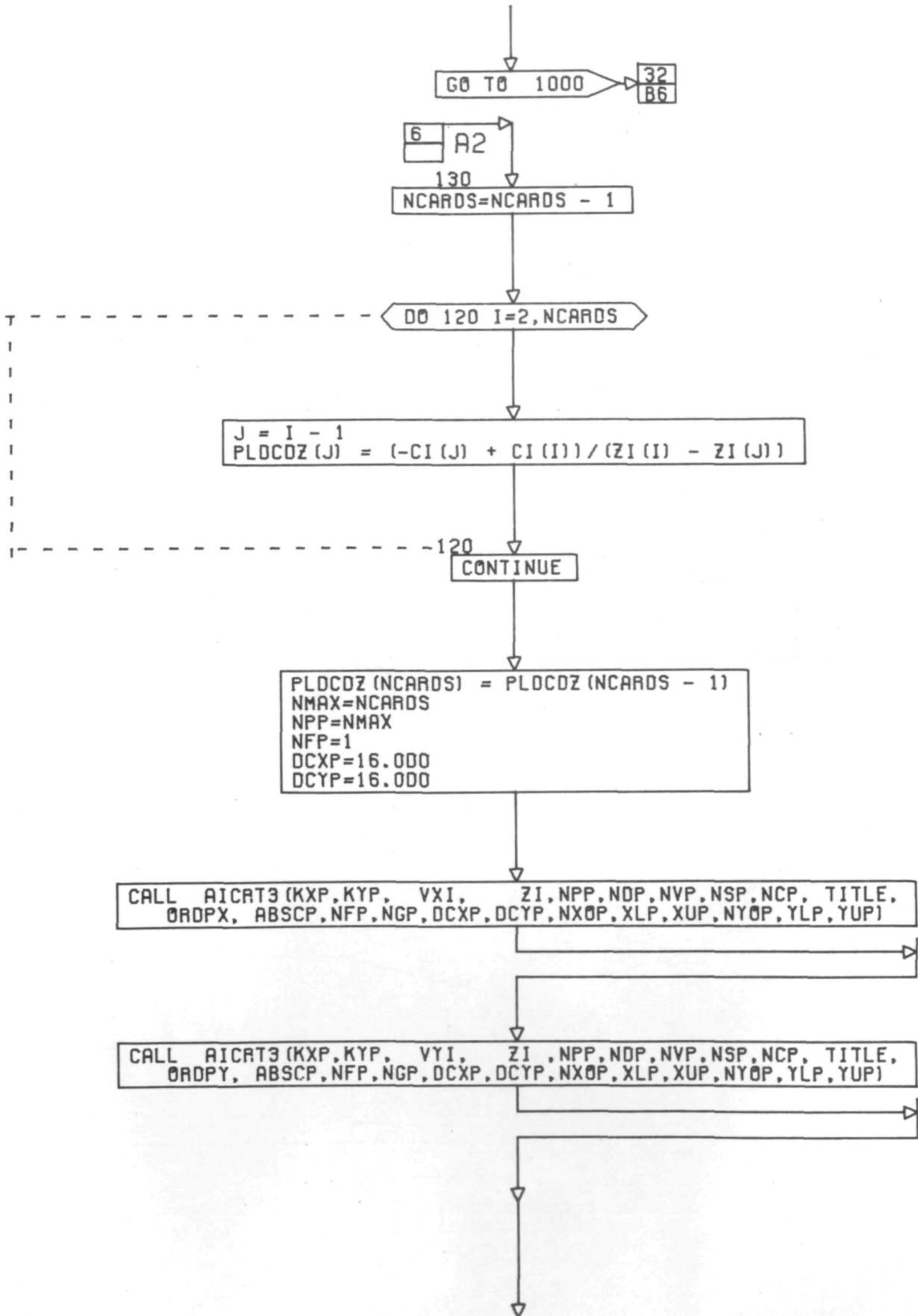
CALL SETUP (8HITHETAF ,4, ITHETF)

CONT. ON PG 4









CONT. ON PG 8

CALL AICRT3(KXP,KYP, CI, ZI,NPP,NOP,NVP,NSP,NCP, TITLE,
ORDPC, ABSCP,NFP,NGP,DCXP,DCYP,NXOP,XLP,XUP,NYOP,YLP,YUP)

CALL AICRT3(KXP,KYP, VTI, ZI,NPP,NOP,NVP,NSP,NCP, TITLE,
ABVT, ABSCP,NFP,NGP,DCXP,DCYP,NXOP,XLP,XUP,NYOP,YLP,YUP)

CALL AICRT3(KXP,KYP, WDI, ZI,NPP,NOP,NVP,NSP,NCP, TITLE,
ABWD, ABSCP,NFP,NGP,DCXP,DCYP,NXOP,XLP,XUP,NYOP,YLP,YUP)

CALL AICRT3(KXP,KYP, ZI,PLDCOZ,NPP,NOP,NVP,NSP,NCP, TITLE,
ABSCP, ORDC, NFP,NGP,DCXP,DCYP,NXOP,XLP,XUP,NYOP,YLP,YUP)

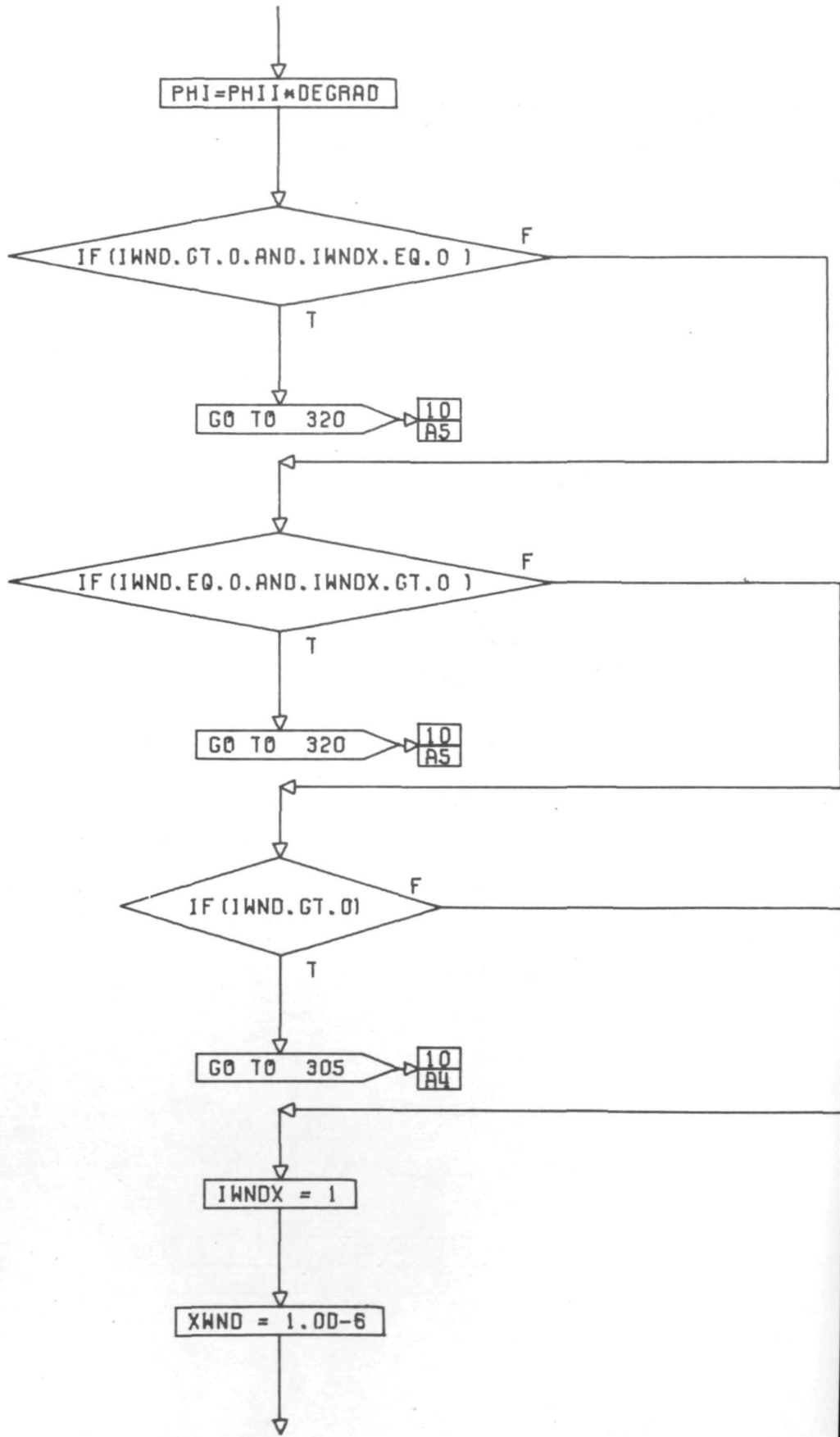
CALL AICRT3(KXP,KYP, TEMQ, ZI,NPP,NOP,NVP,NSP,NCP, TITLE,
ORDTM,ORDZZ, NFP,NGP,DCXP,DCYP,NXOP,XLP,XUP,NYOP,YLP,YUP)

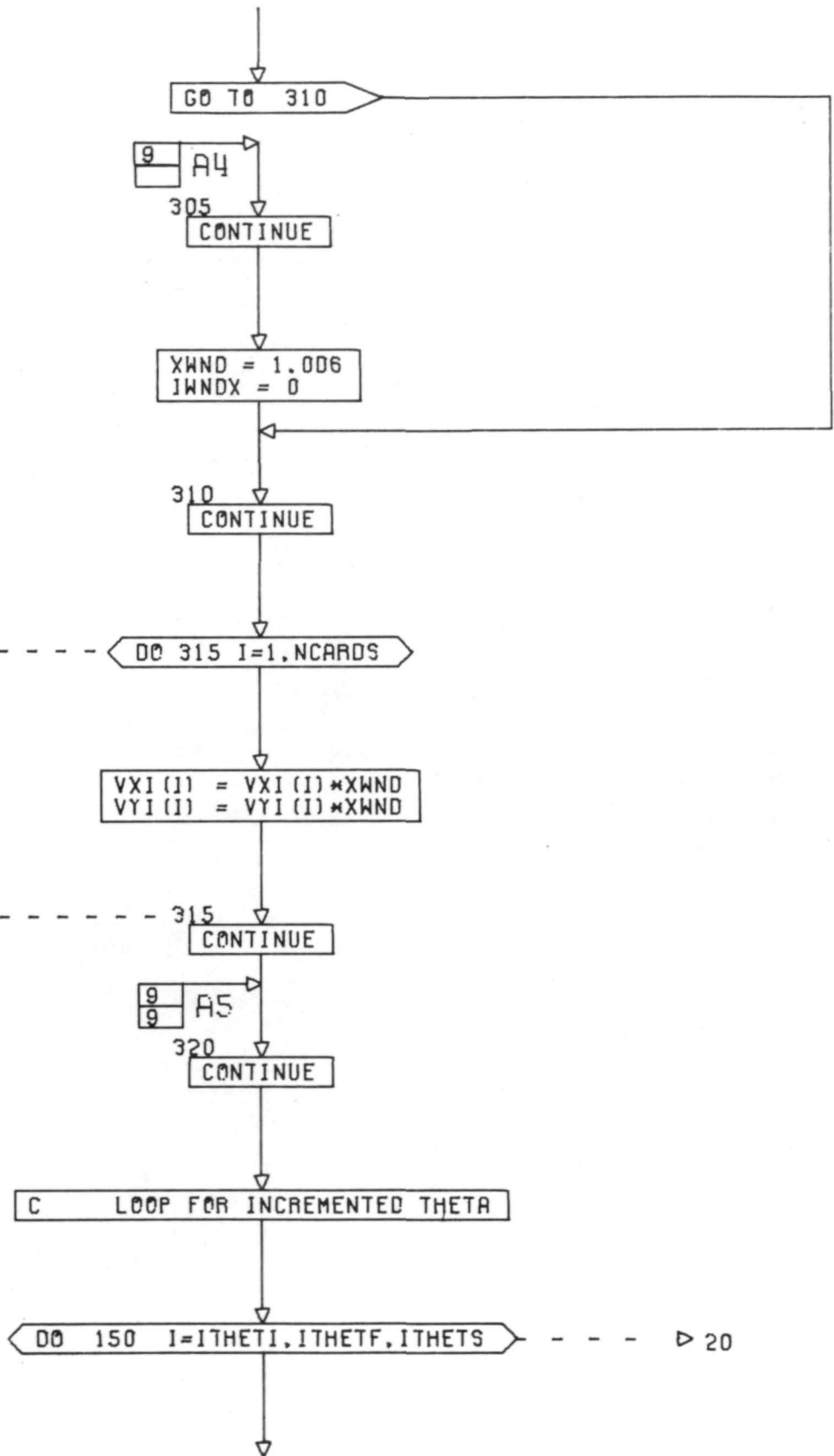
A3 21
31

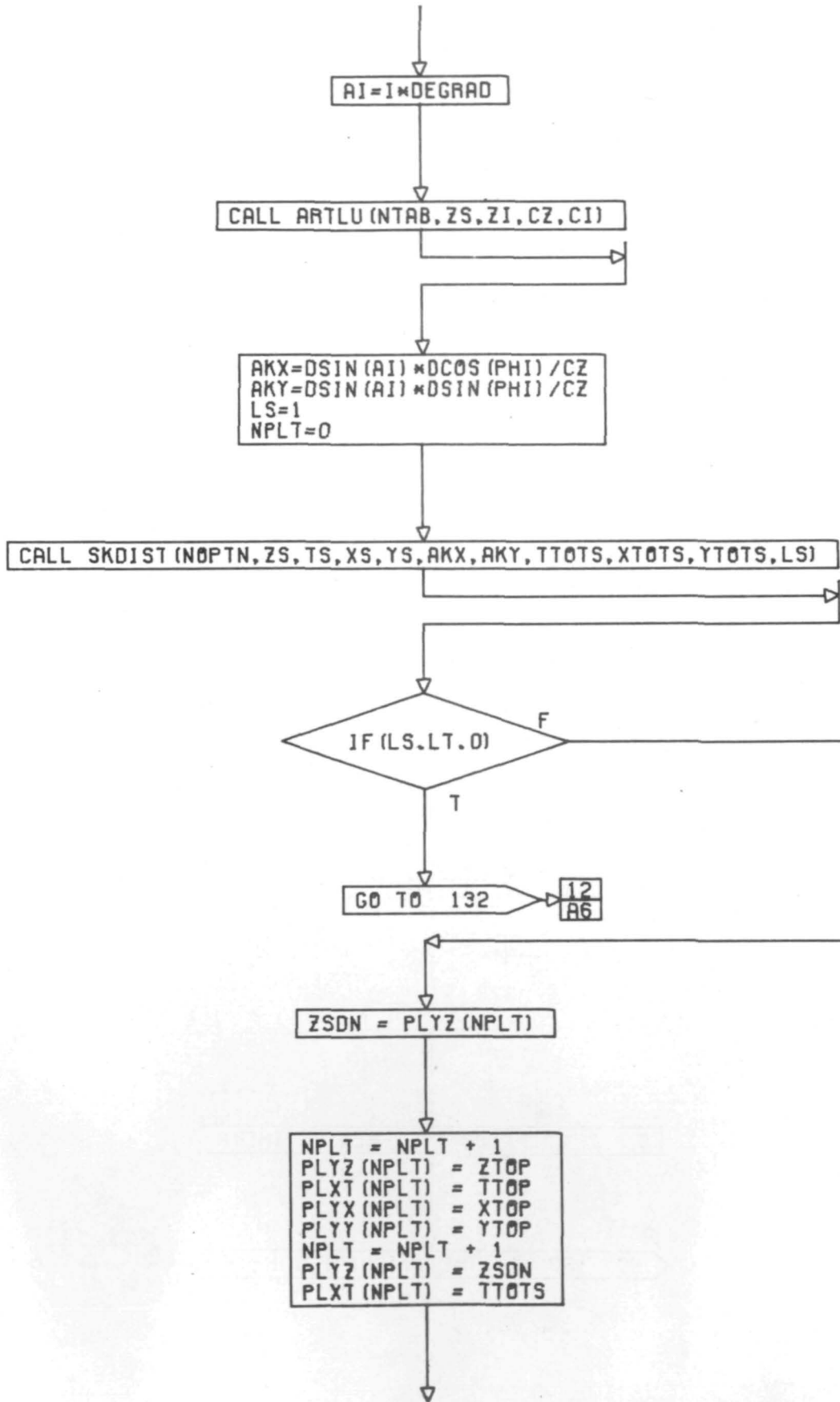
2000
CONTINUE

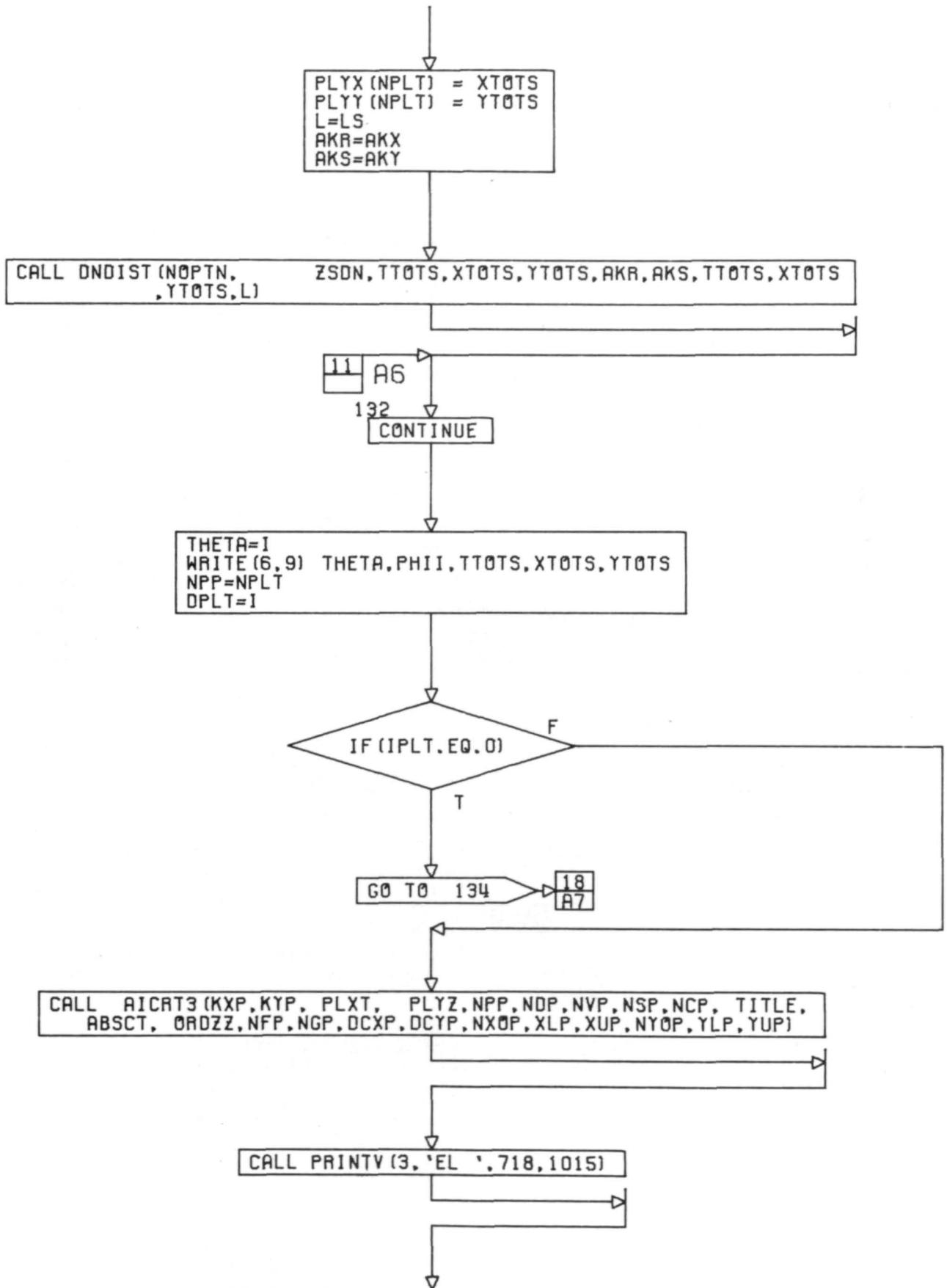
WRITE(6,7)

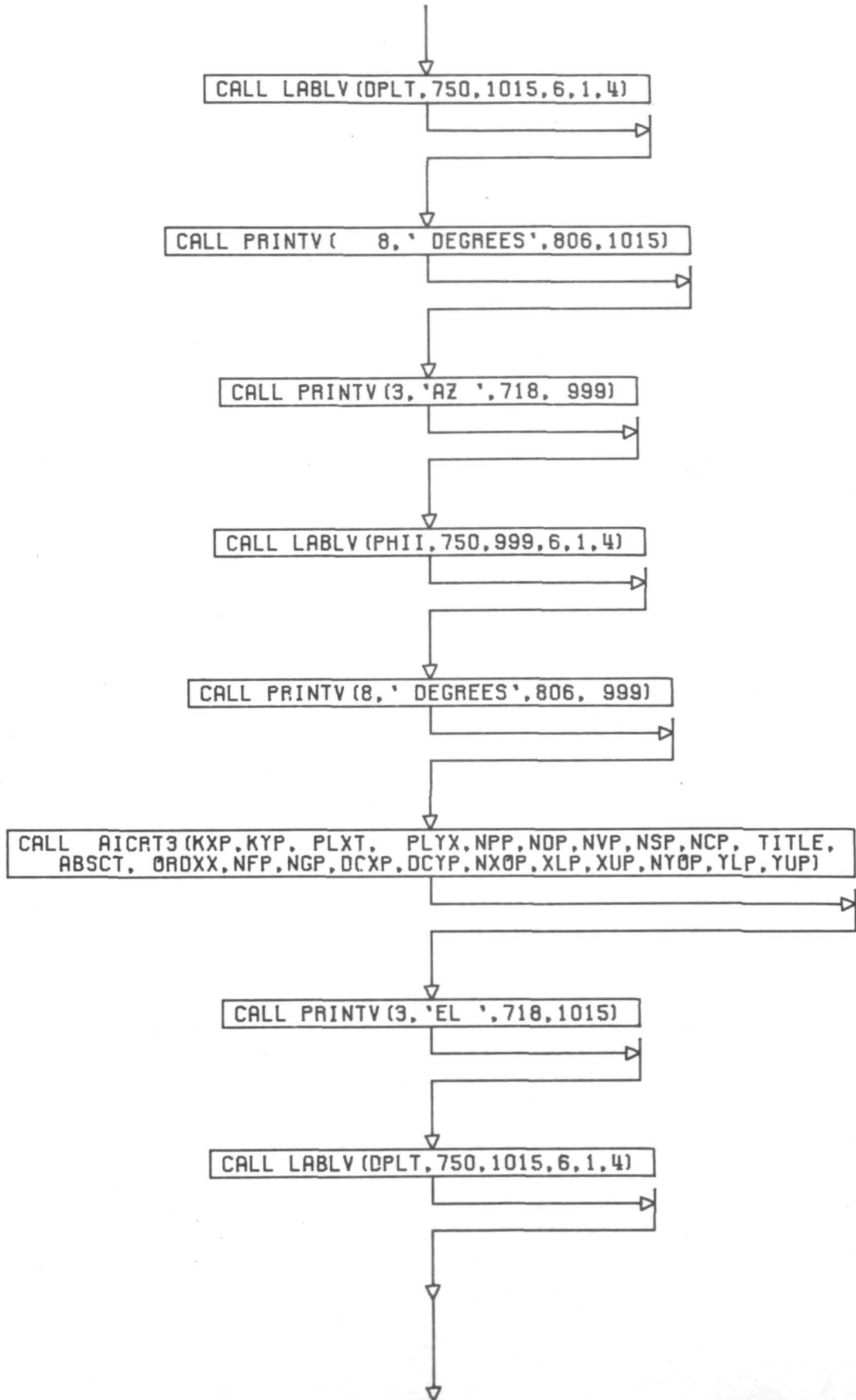
CALL READIN(INCOL1,\$1000)

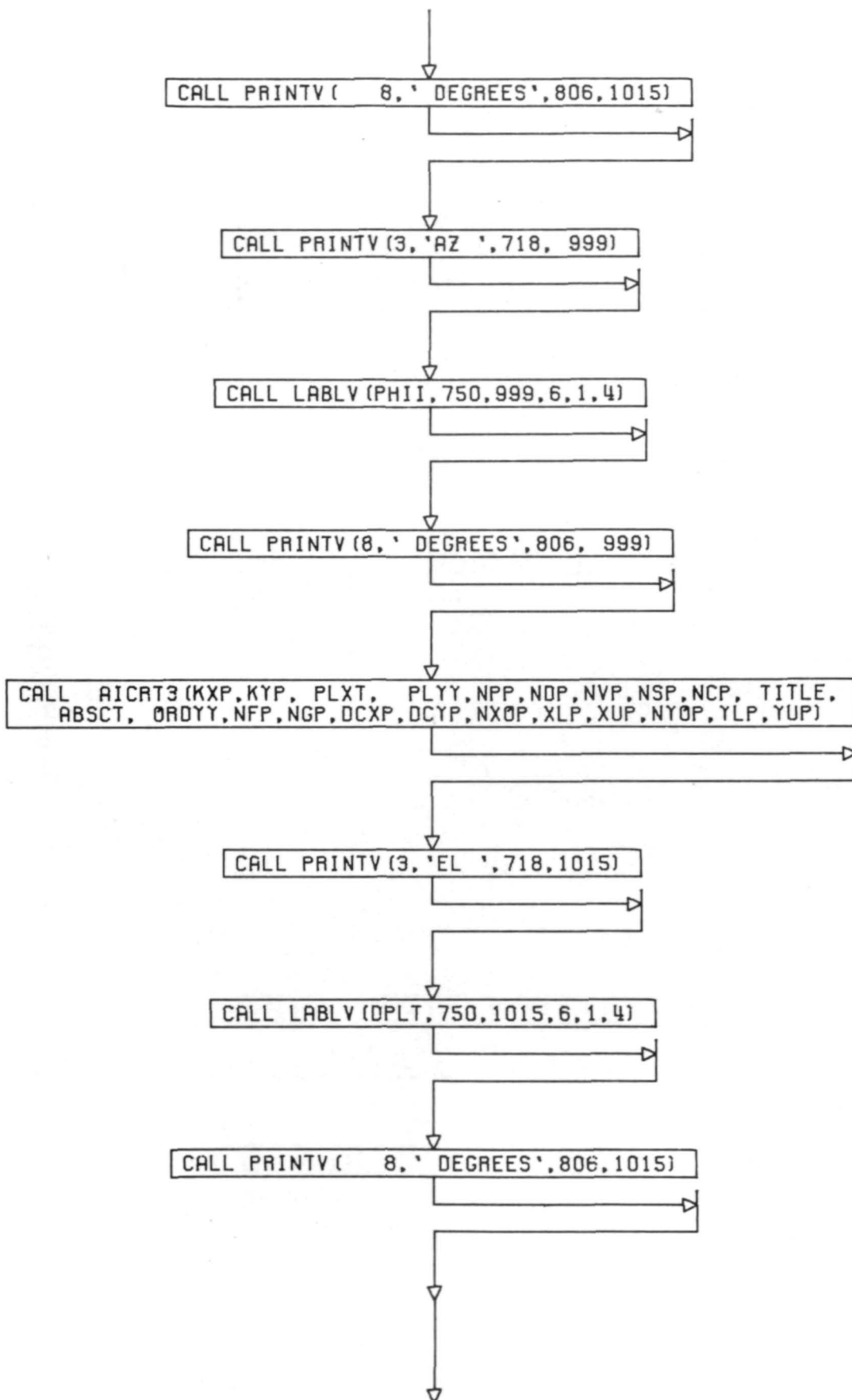


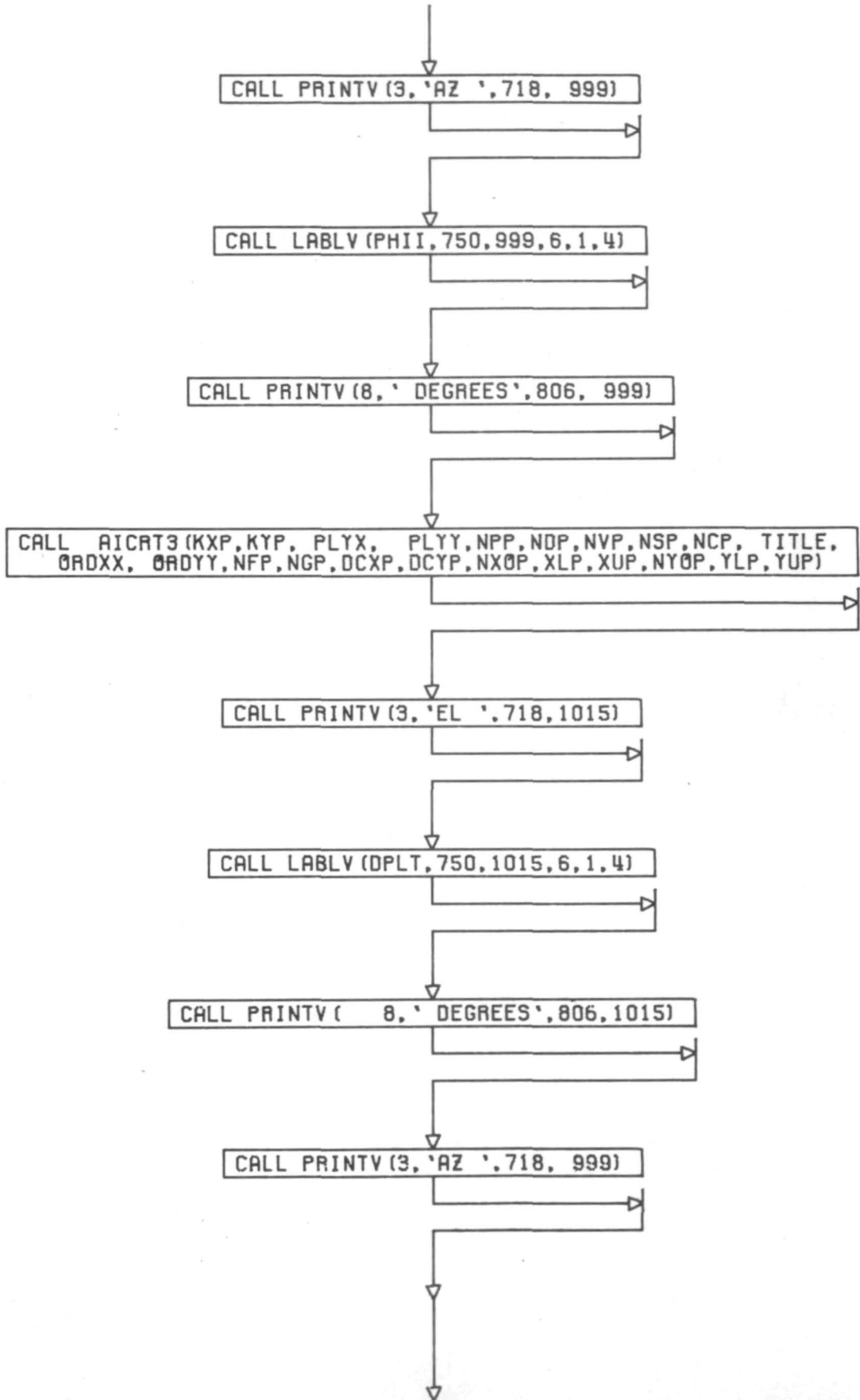


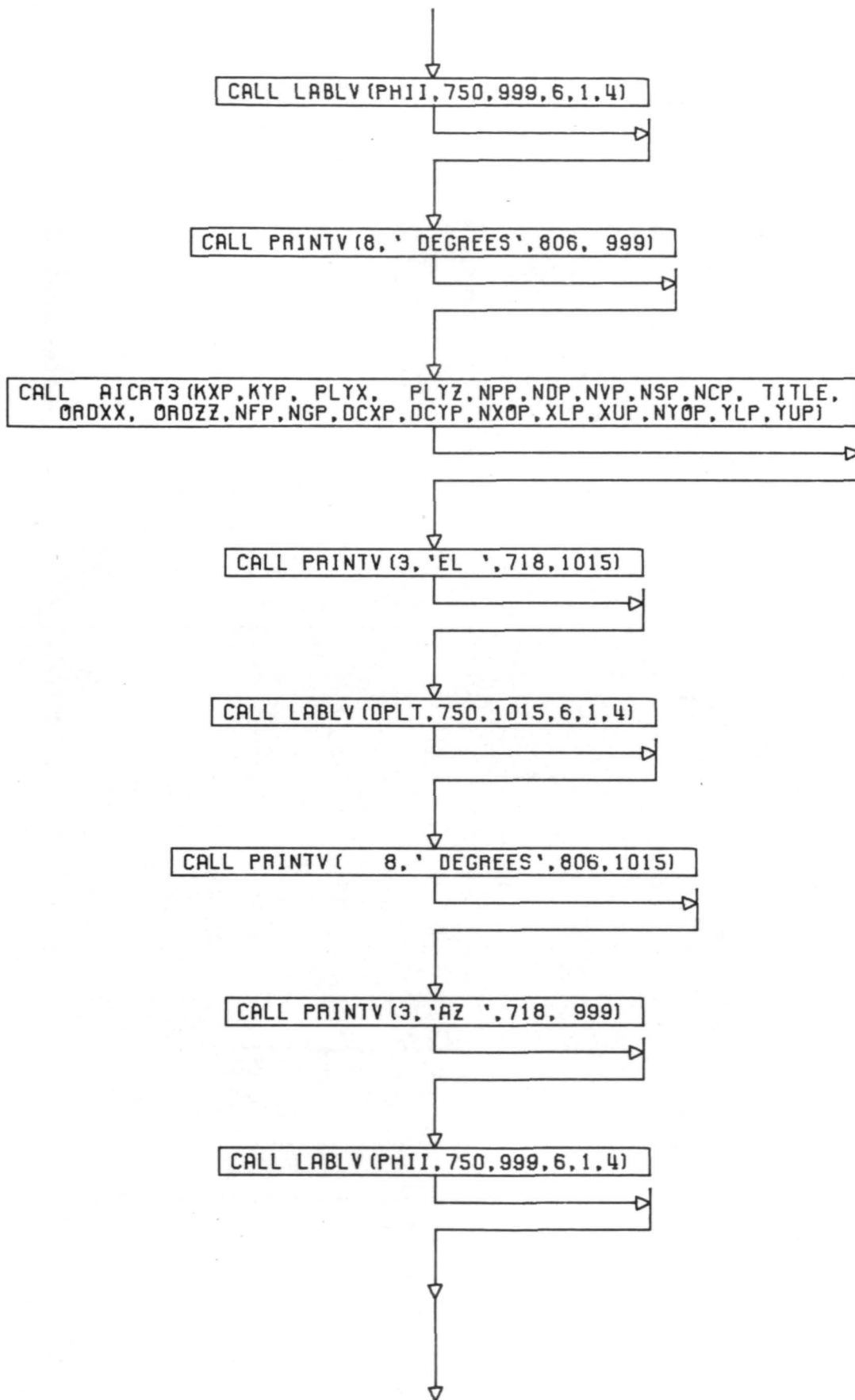


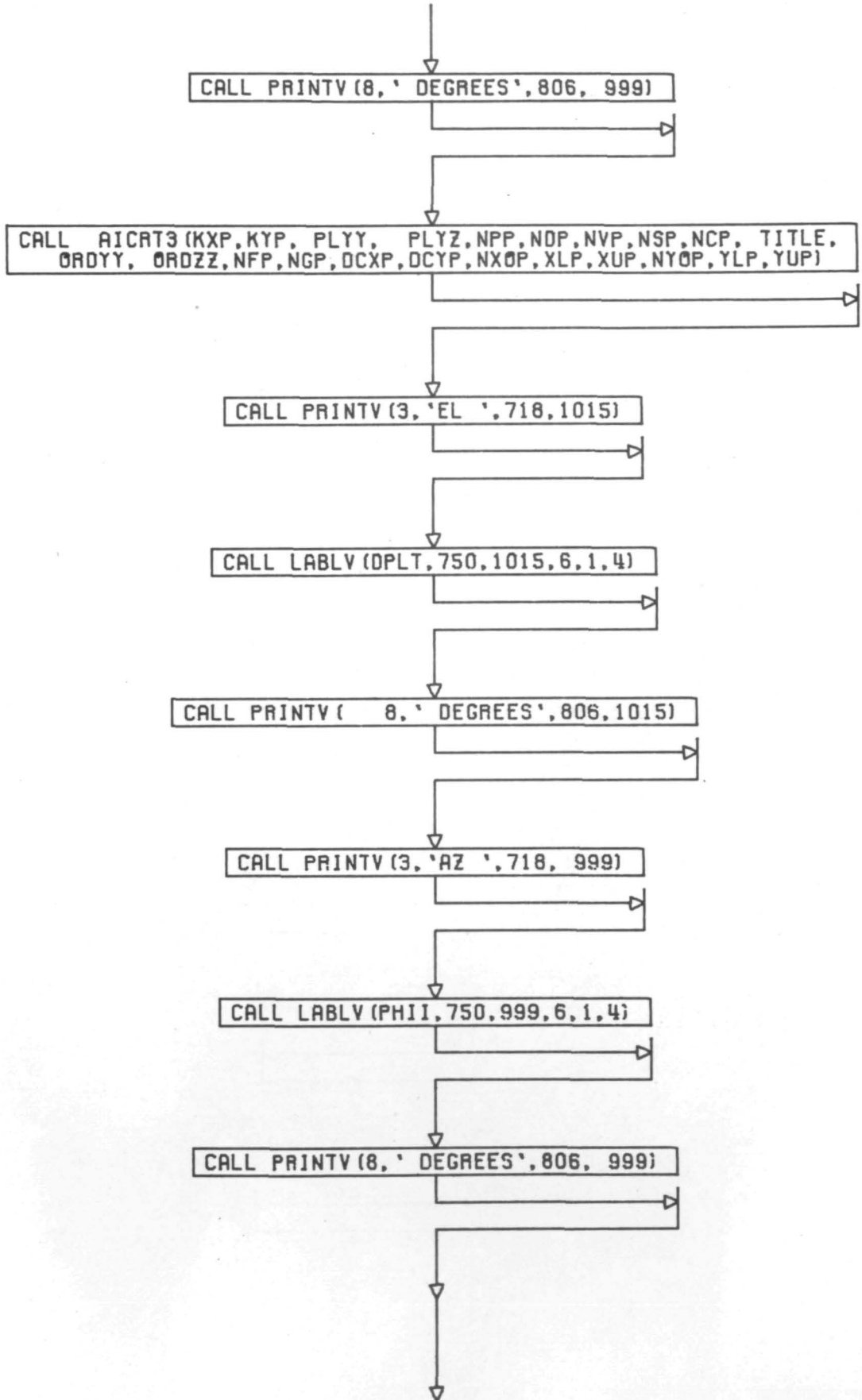












DO 133 IIQ=1,NPLT

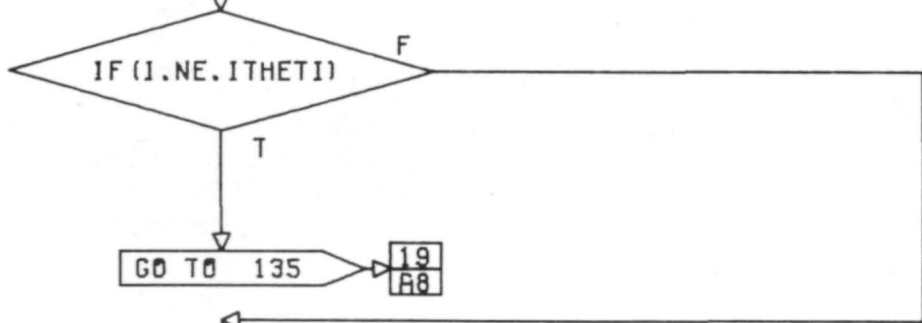
PLYXSQ = PLYX (IIQ) * PLYX (IIQ)
PLYYSQ = PLYY (IIQ) * PLYY (IIQ)
VTIX (IIQ) = DSQRT (PLYXSQ + PLYYSQ)

133
CONTINUE

```
C CALL AICRT3 (KXP, KYP, VTIX, PLYZ, NPP, NDP, NVP, NSP, NCP, TITLE,  
C $ ABK, ORDZZ, NFP, NGP, DCXP, DCYP, NXOP, XLP, XUP, NYOP, YLP, YUP)  
C CALL PRINTV (3, 'EL ', 718, 1015)  
C CALL LABLV (DPLT, 750, 1015, 6, 1, 4)  
C CALL PRINTV ( 8, ' DEGREES ', 806, 1015)  
C CALL PRINTV (3, 'AZ ', 718, 999)  
C CALL LABLV (PHI1, 750, 999, 6, 1, 4)  
C CALL PRINTV (8, ' DEGREES ', 806, 999)
```

12 A7

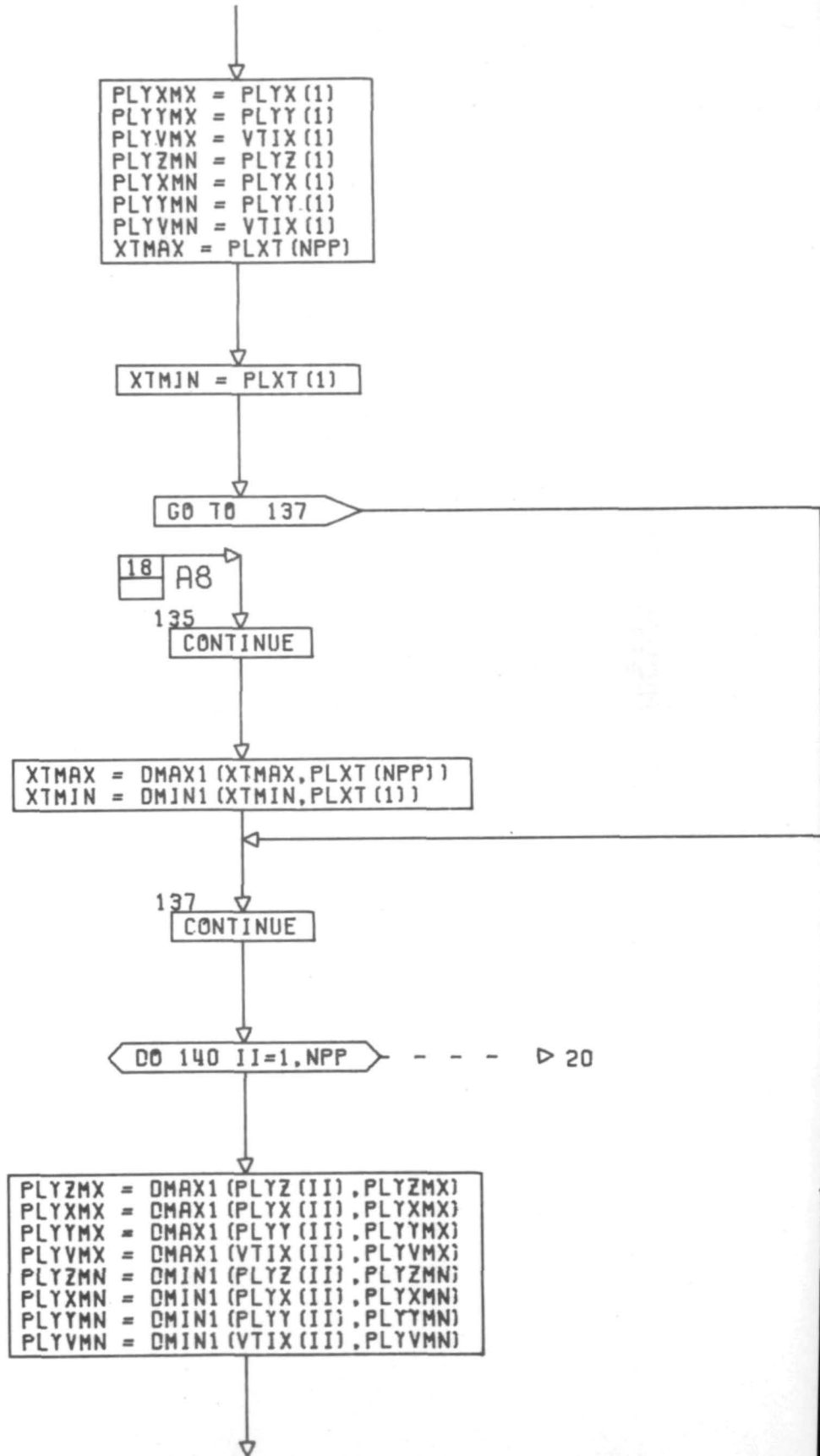
134
CONTINUE

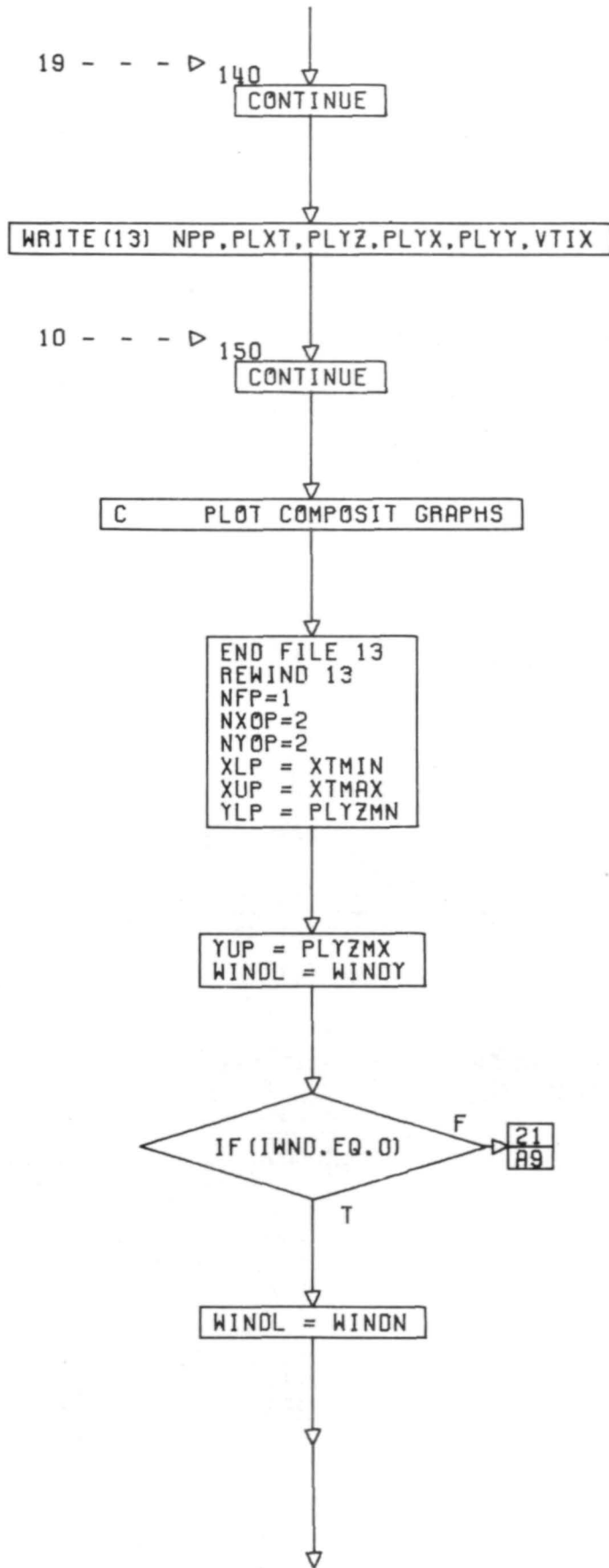


GO TO 135

19
A8

PLYZMX = PLYZ (1)

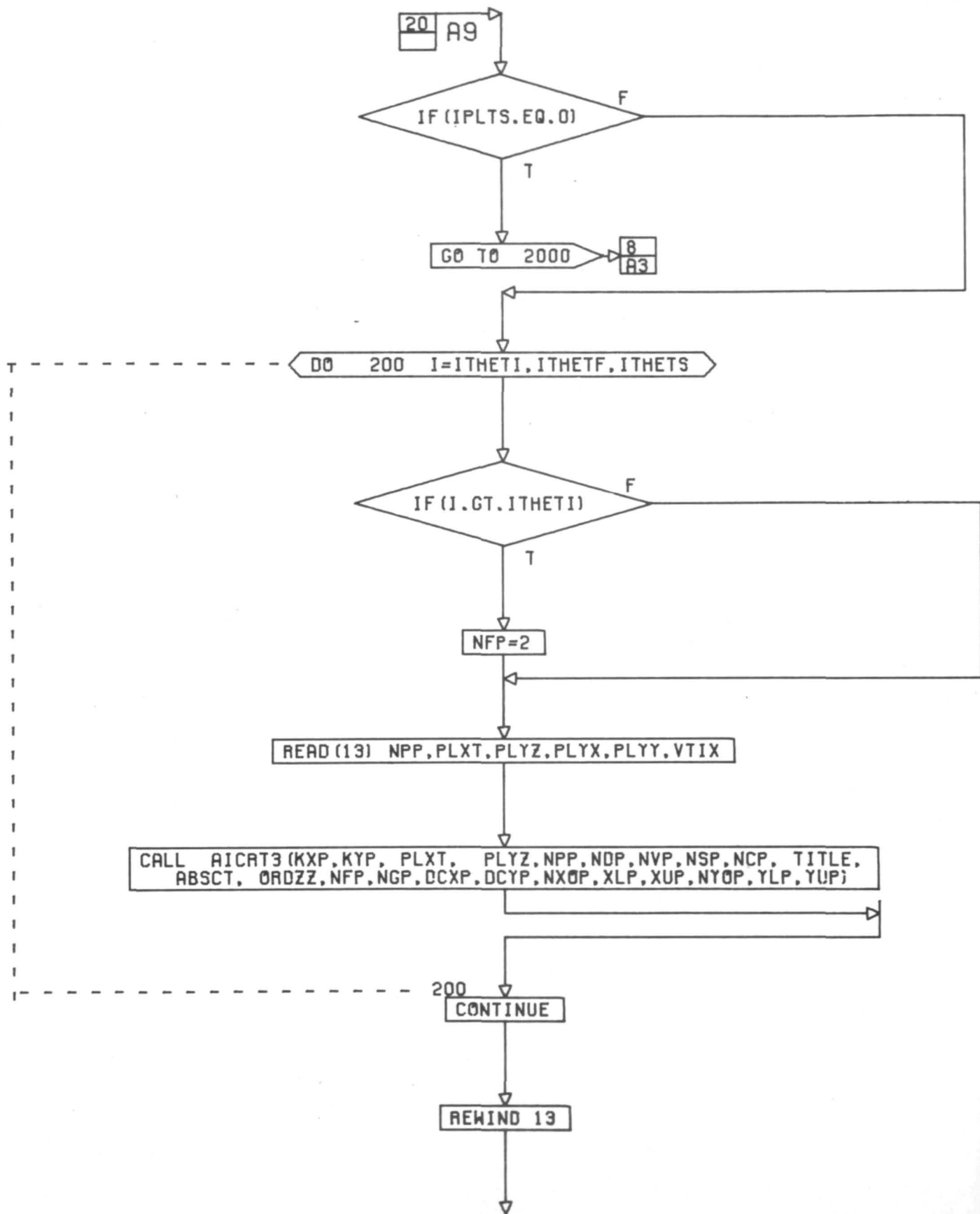


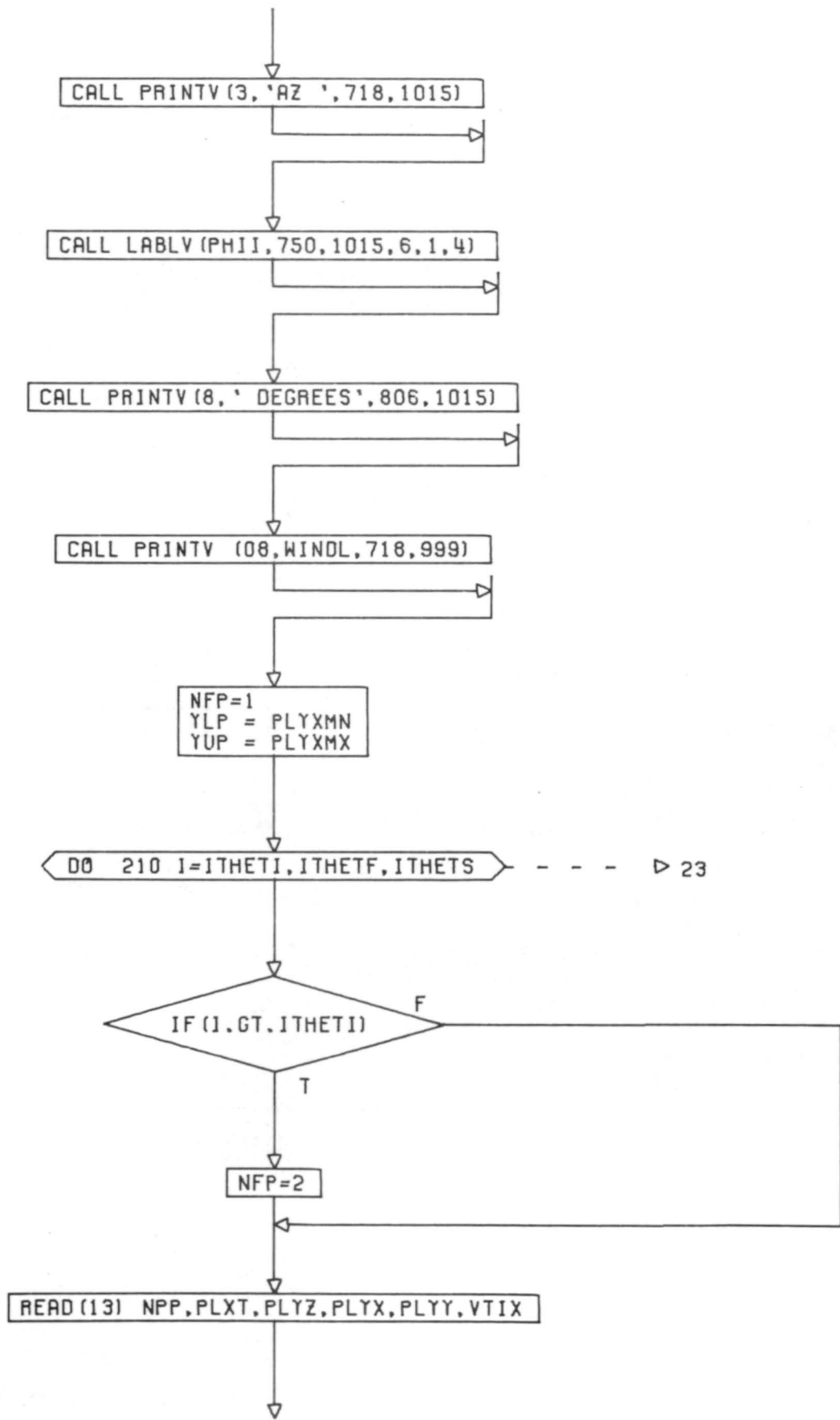


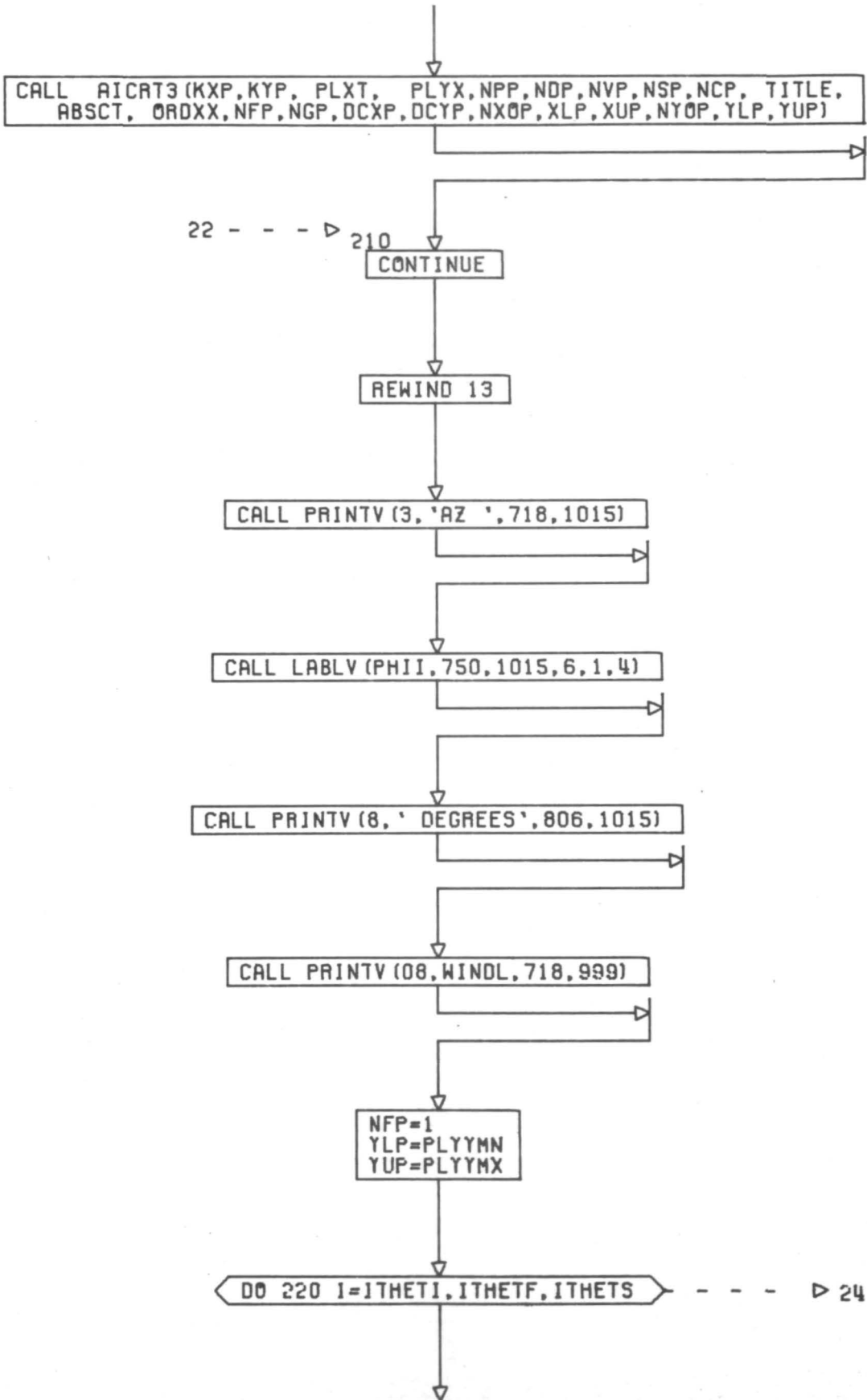
19 - - - - ▷ 140

10 - - - - ▷ 150

F ▷ 21
19

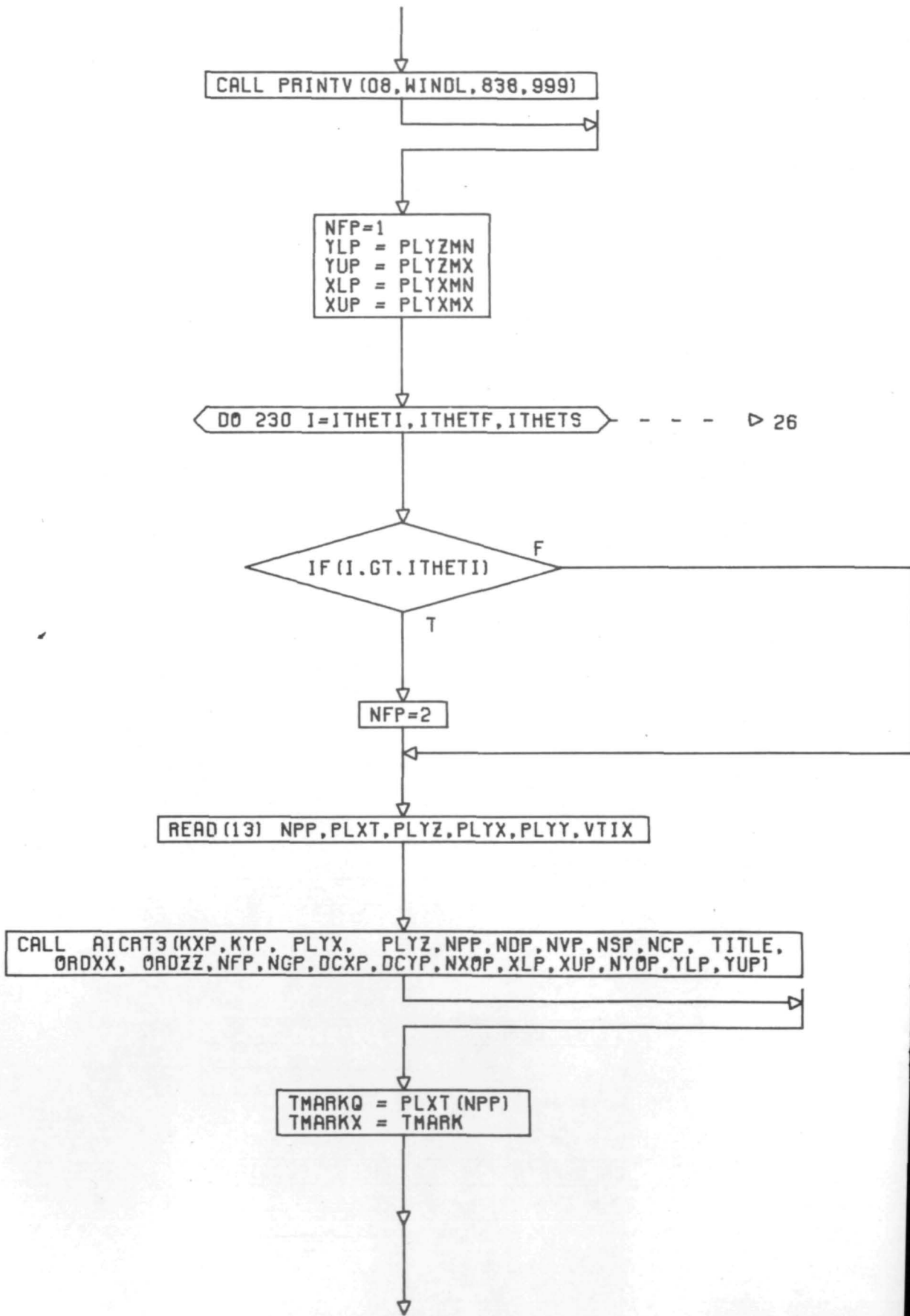


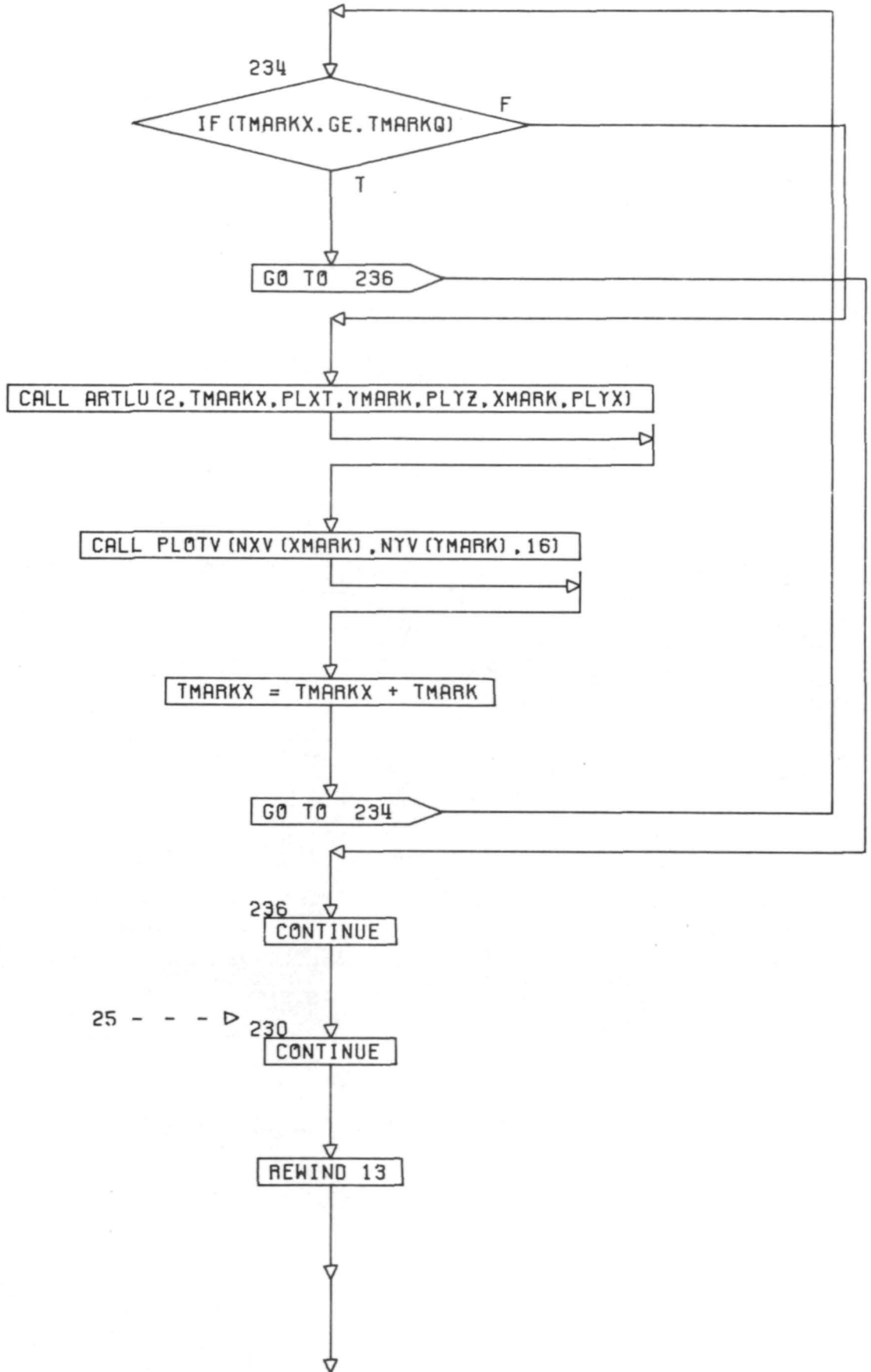




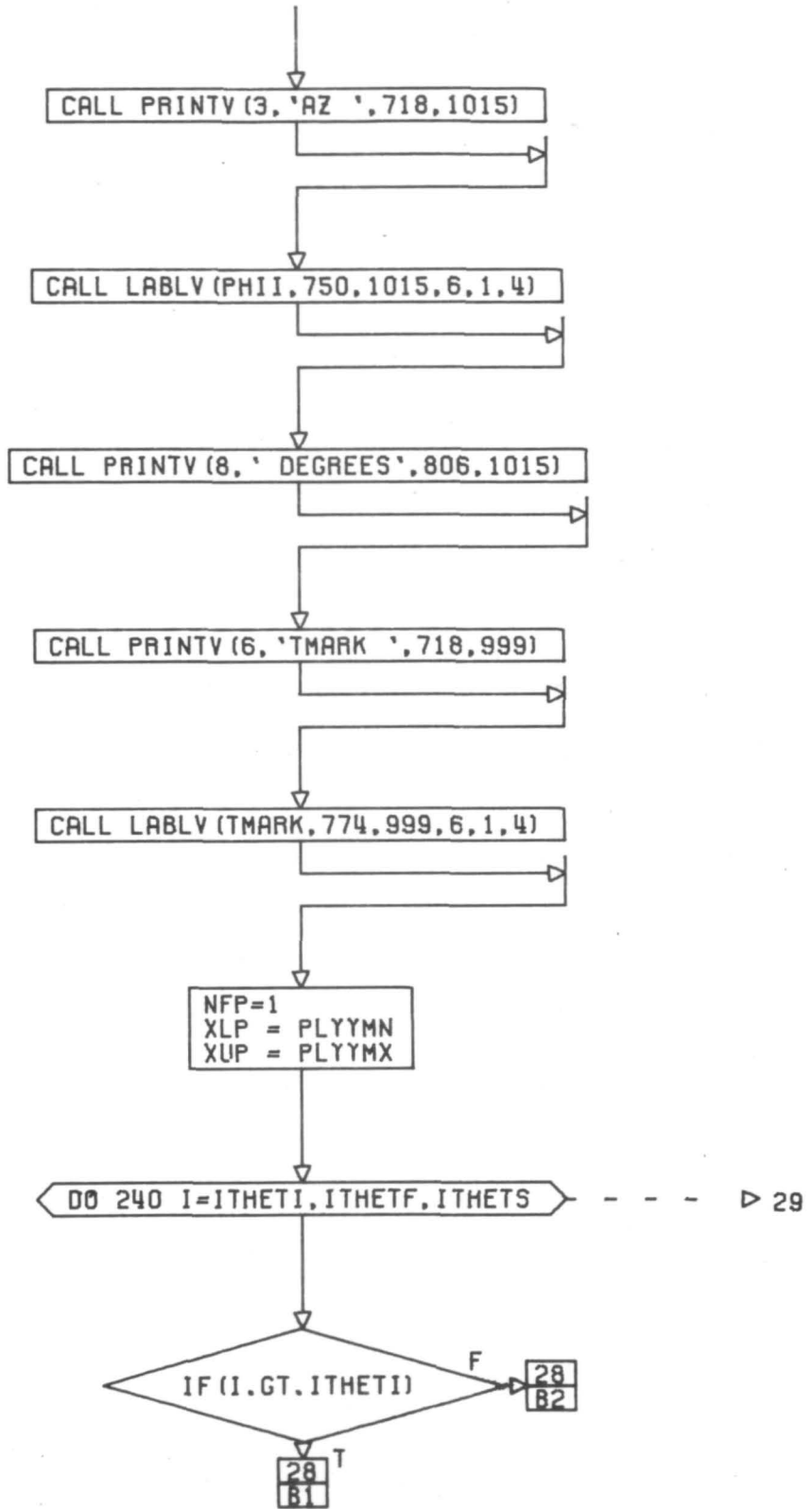
22 - - - - ▷ 210

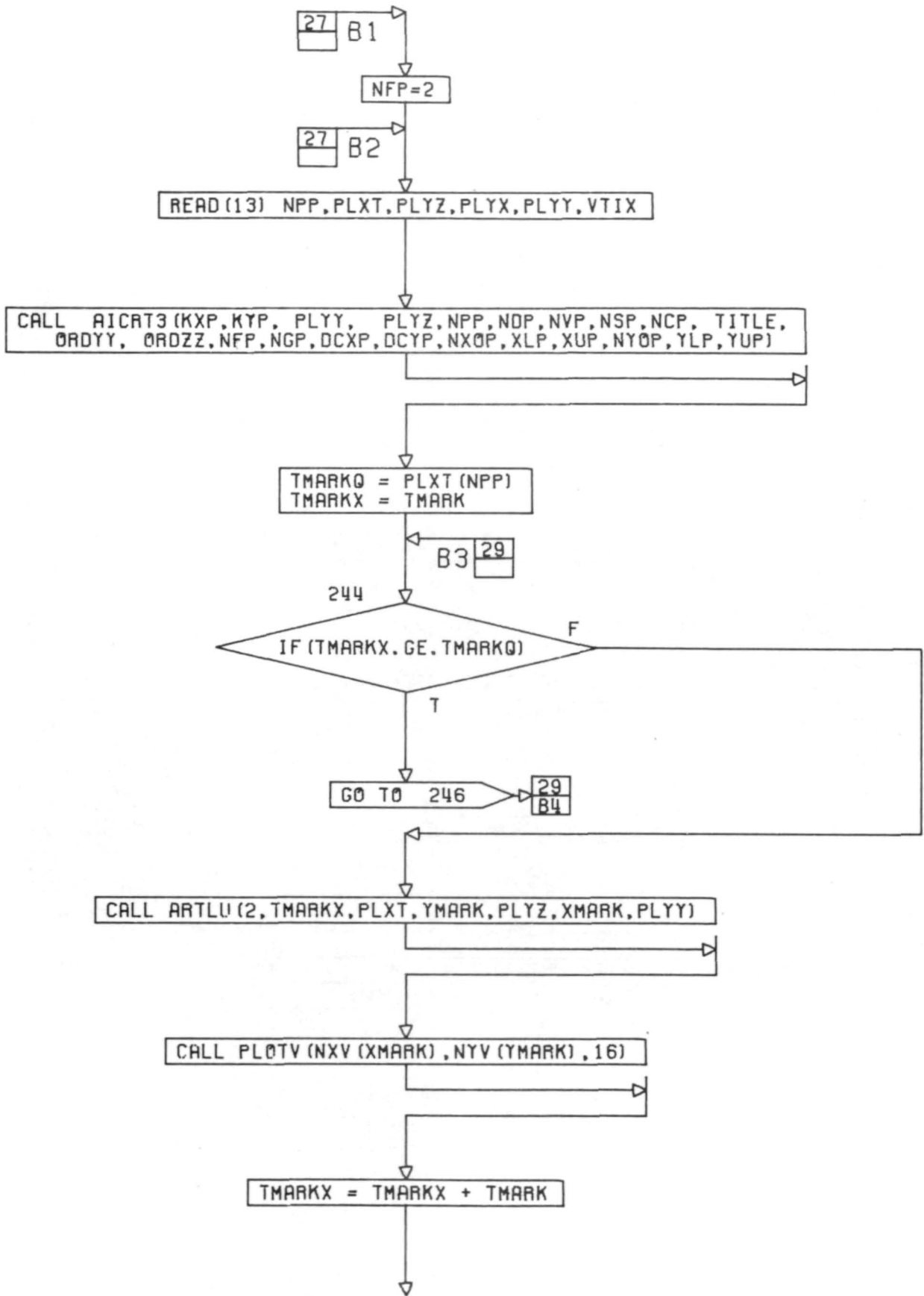
- - - - ▷ 24

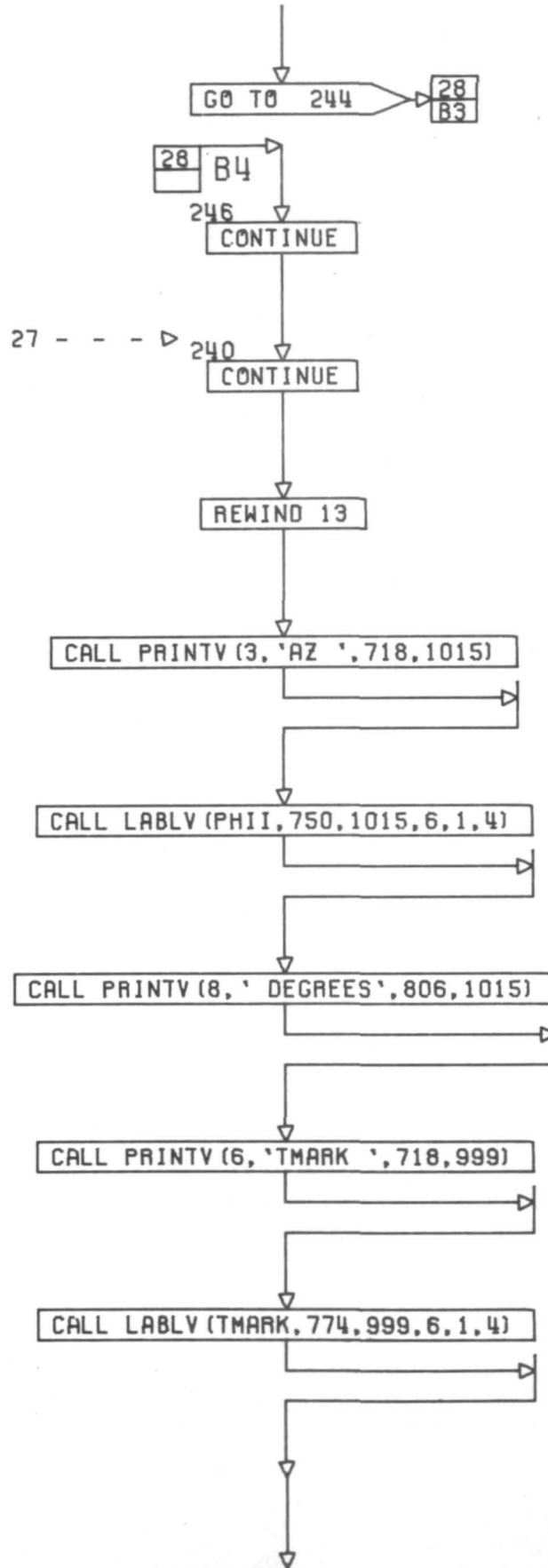




25 - - - - ▷







CONT. ON PG 30

CALL PRINTV (08,WINDL,838,999)

```
C NFP=1
C XLP = PLYVMN
C XUP = PLYVMX
C DO 250 I=ITHETI,ITHETF,ITHETS
C IF (I.GT.ITHETI) NFP=2
C READ (13) NPP,PLXT,PLYZ,PLYX,PLY,VTIX
C CALL AICAT3(KXP,KYP,VTIX, PLYZ,NPP,NDP,NVP,NSP,NCP, TITLE,
C $ ABK, ORDZZ,NFP,NGP,DCXP,DCYP,NXOP,XLP,XUP,NYOP,YLP,YUP)
```

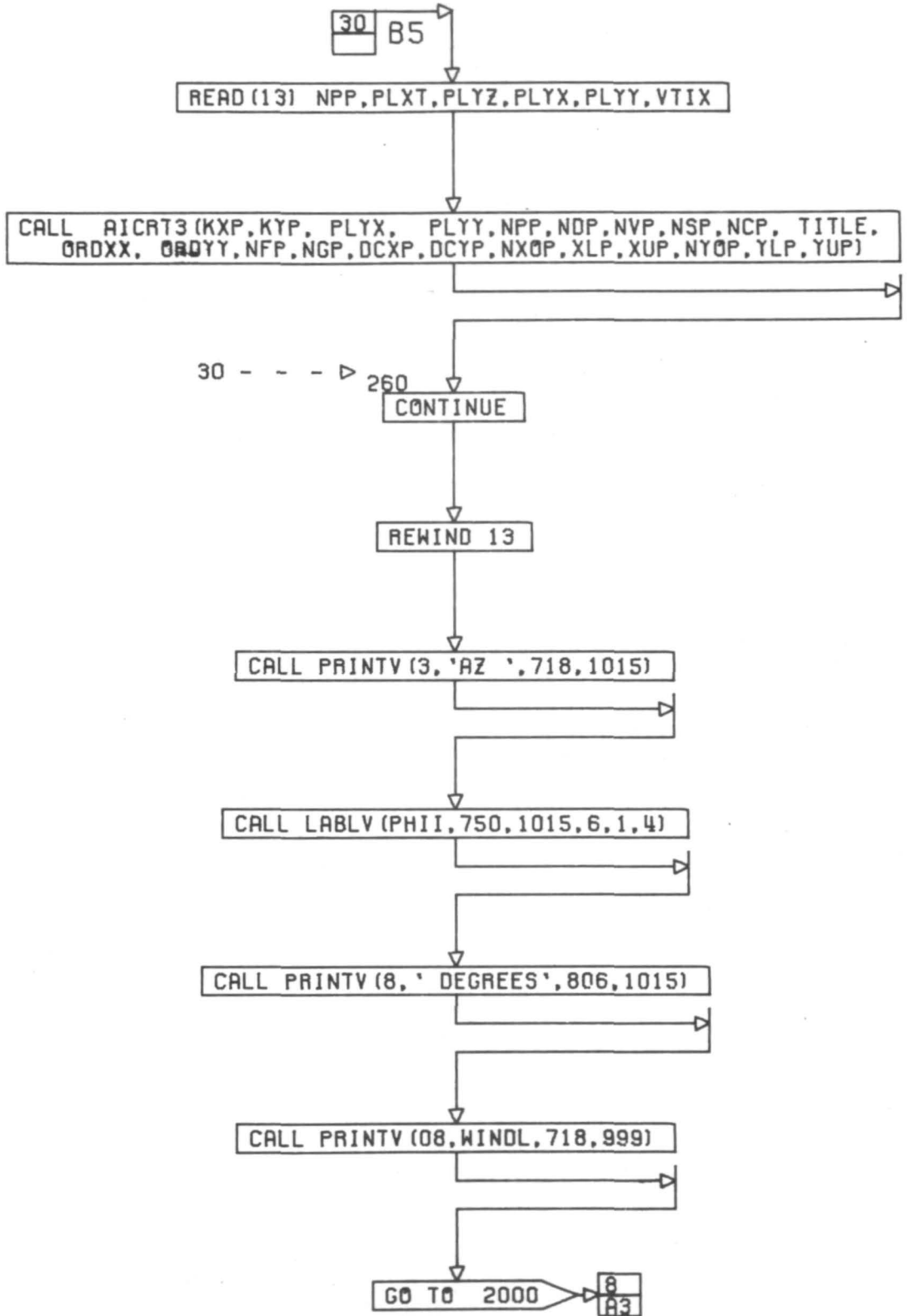
```
C 250 CONTINUE
C REWIND 13
C CALL PRINTV (3,'AZ ',718,1015)
C CALL LABLV (PHI,750,1015,6,1,4)
C CALL PRINTV (8,' DEGREES ',806,1015)
```

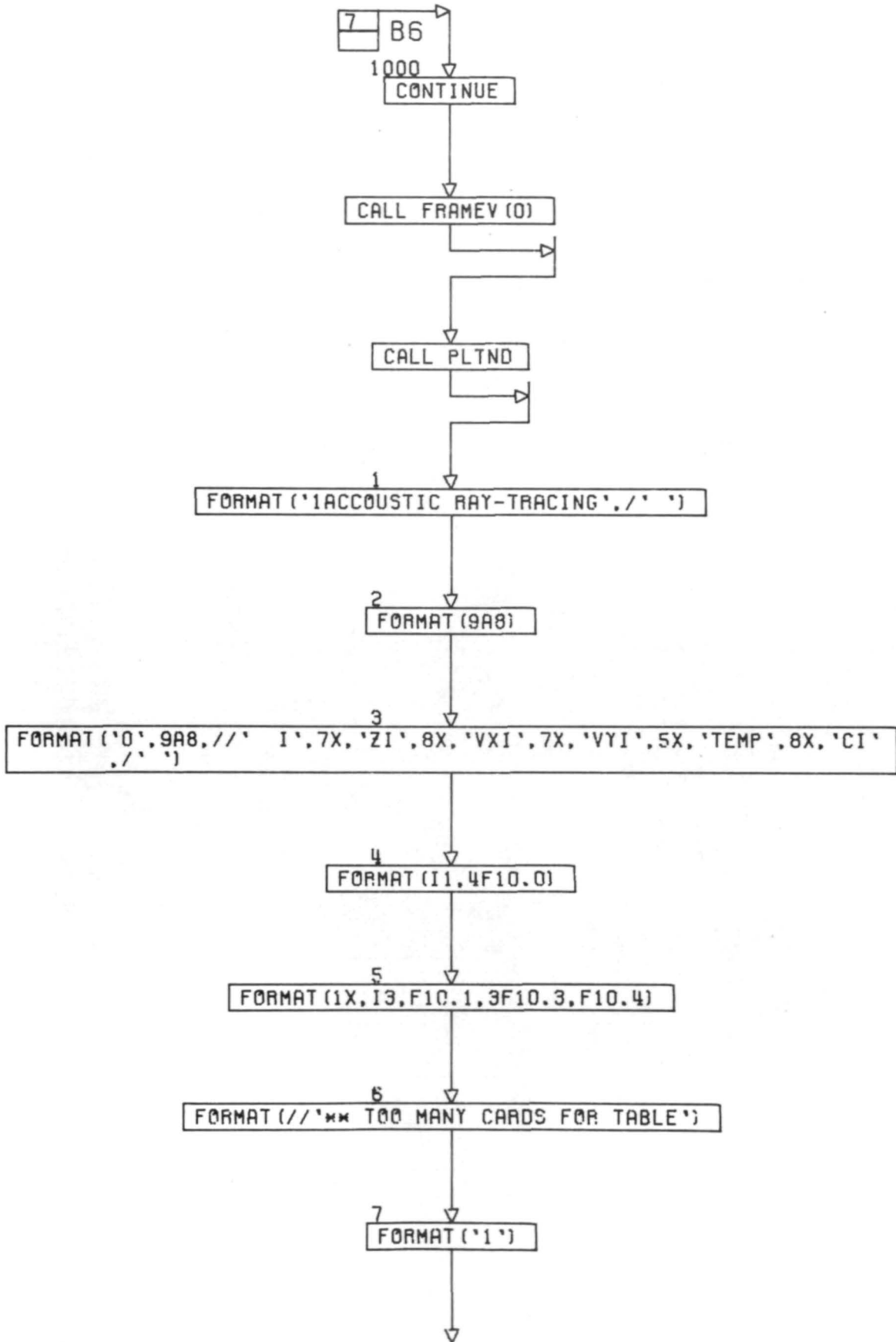
```
NFP = 1
XLP = PLYXMN
XUP = PLYXMX
YLP = PLYYMN
YUP = PLYYMX
```

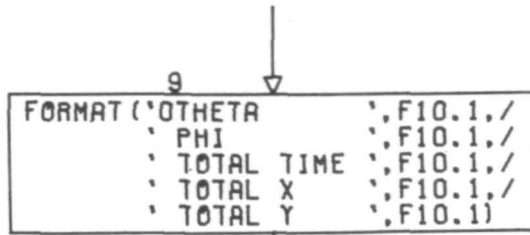
DO 260 I=ITHETI,ITHETF,ITHETS - - - - > 31

IF (I.GT.ITHETI) F 31/85

NFP=2







STOP

END

IMPLICIT REAL*8 (A-H,O-Z)
SUBROUTINE SKDIST (N0PTN,ZS,TS,XS,YS,AKX,AKY,TTOT,XTOT,YTOT,L)

C MODIFIED FOR PREDICTOR CORRECTOR

COMMON/FAYE/CI(300),VXI(300),VYI(300),ZI(300),PLXT(600),PLYZ(600),
PLYX(600),PLY(600)

COMMON /JANET/ NMAX,NPLT,IPATX
COMMON/PEARL/ZTOP,TTOP,XTOP,YTOP,T2,X2,Y2
DIMENSION VALUE(3),DEAN(3),UPBND(3),DNBND(3)
COMMON/JULIA/QAKX,QAKY
RADDEG = 57.295779513100
AKXKY = AKX*AKX + AKY*AKY
QAKX = AKX
QAKY = AKY

IF (ZS.LT.ZI (NMAX))

F

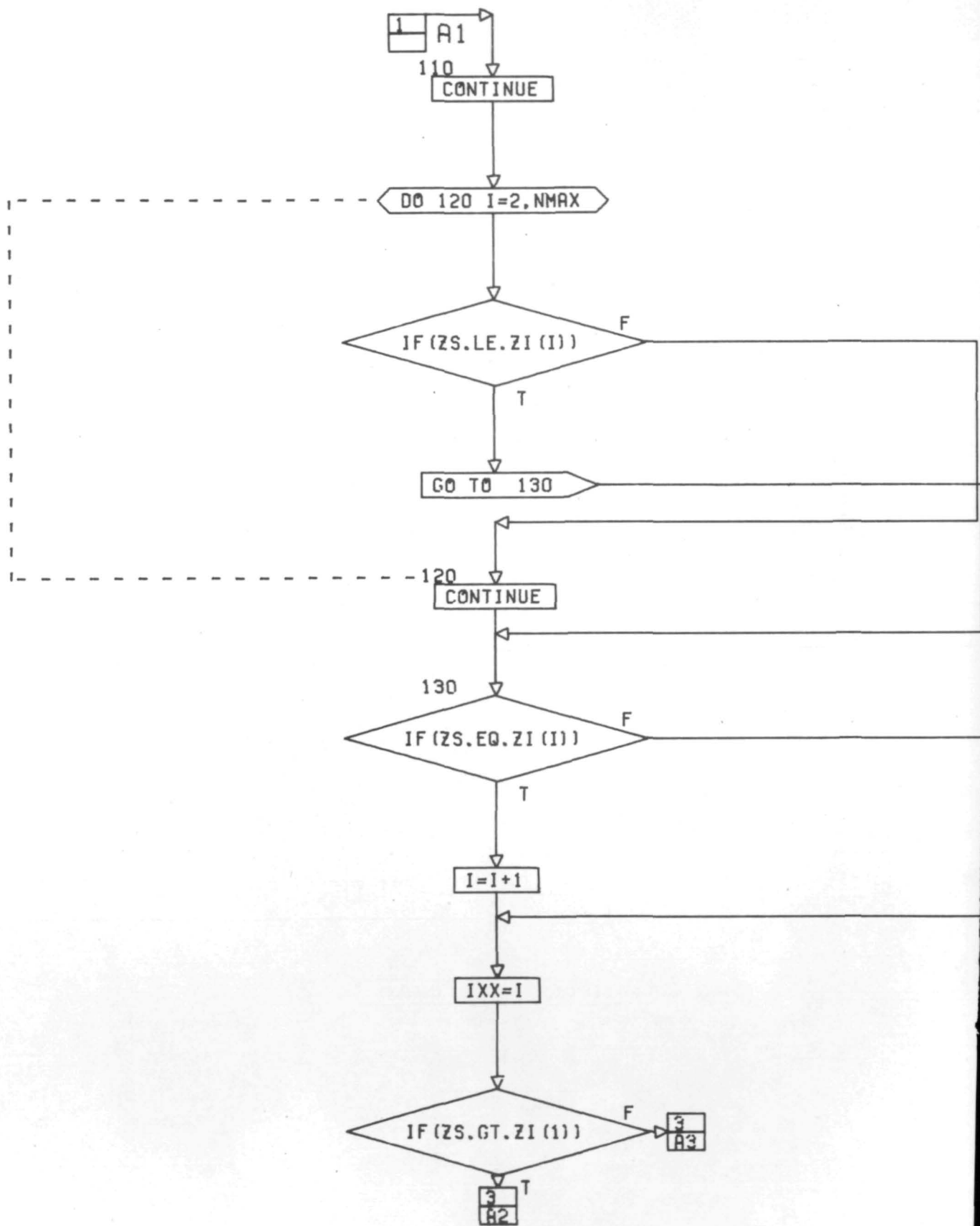
T

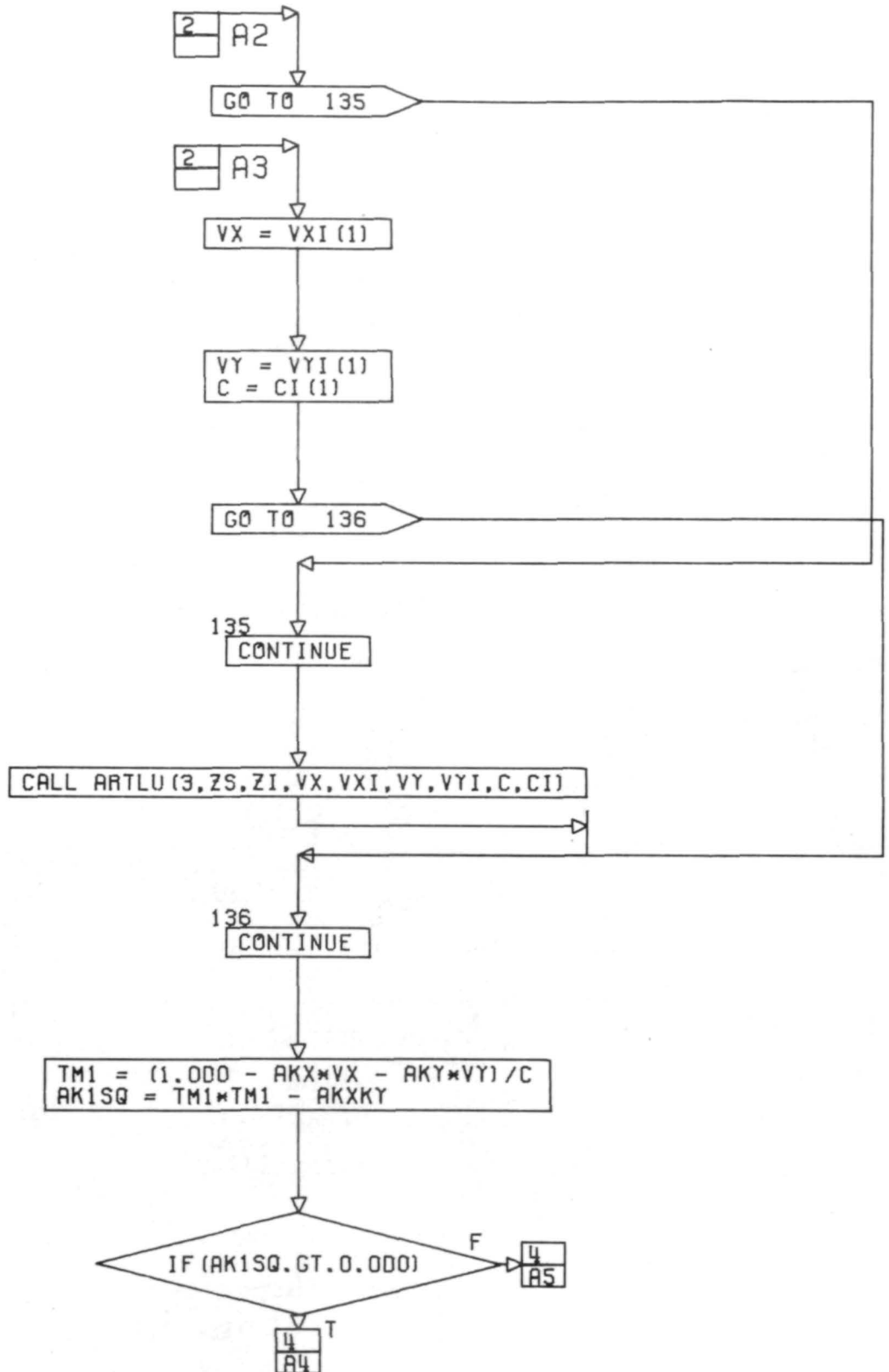
GO TO 110

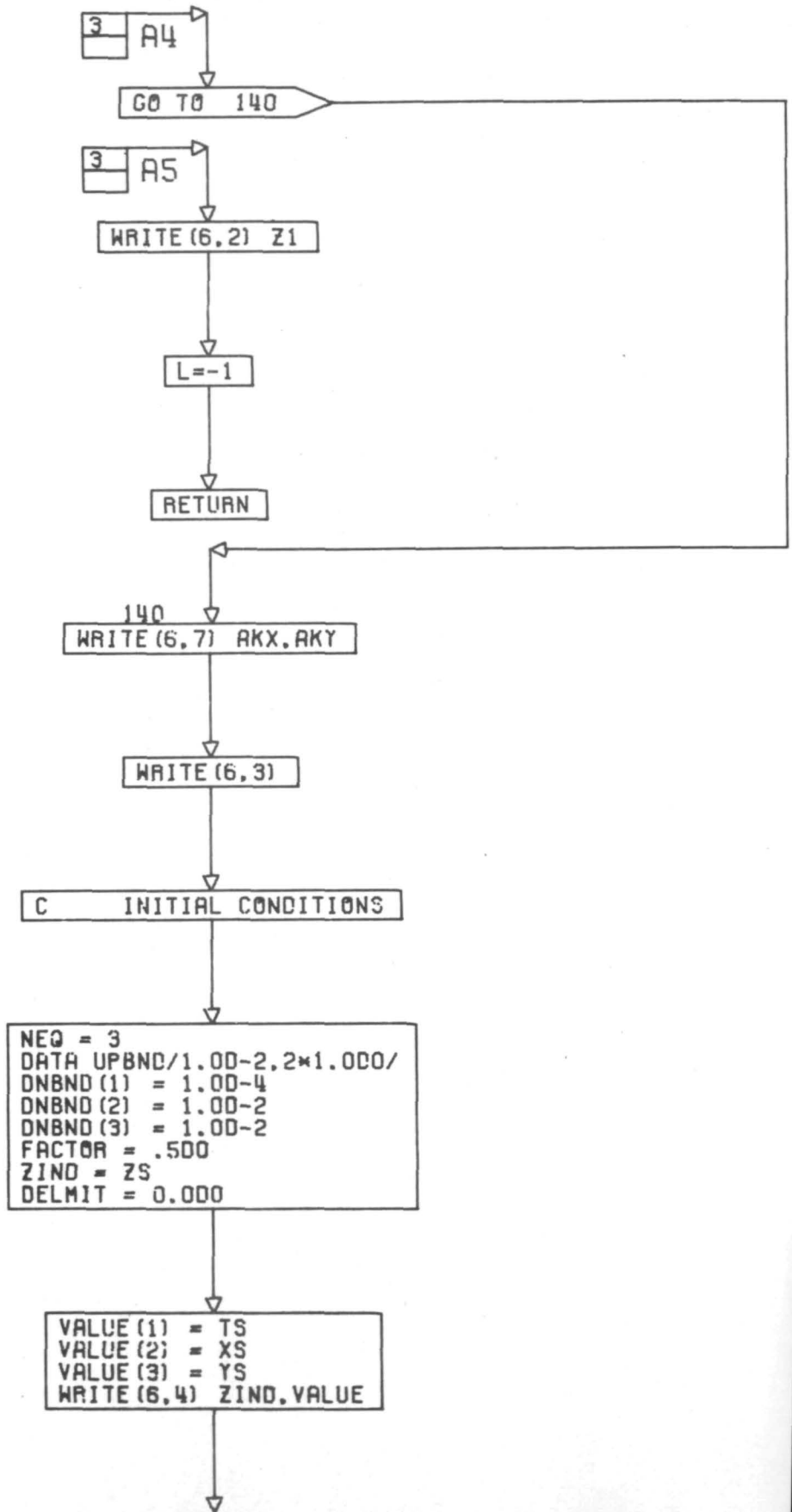
2
A1

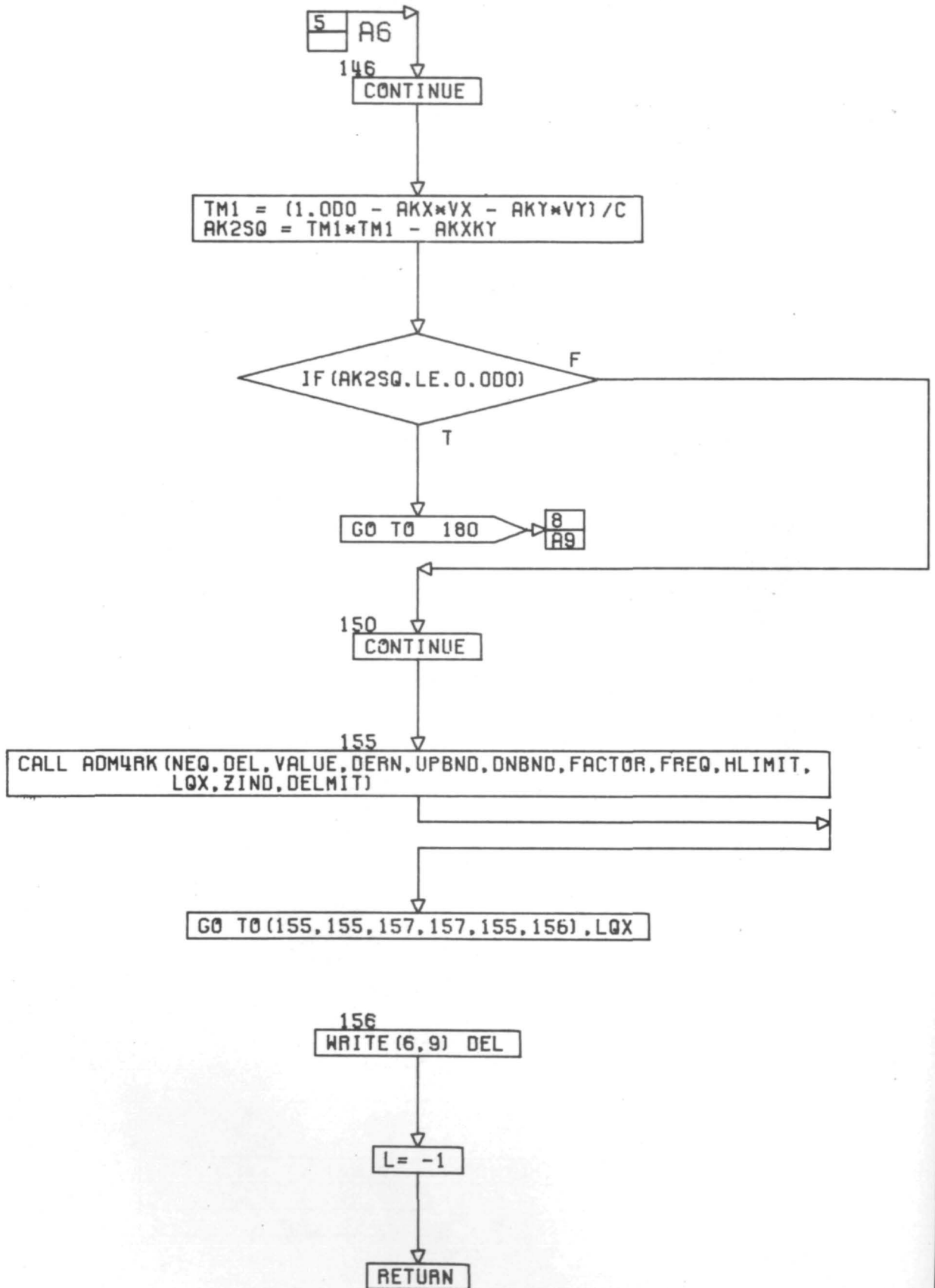
WRITE (6,1) ZS,ZI (NMAX)

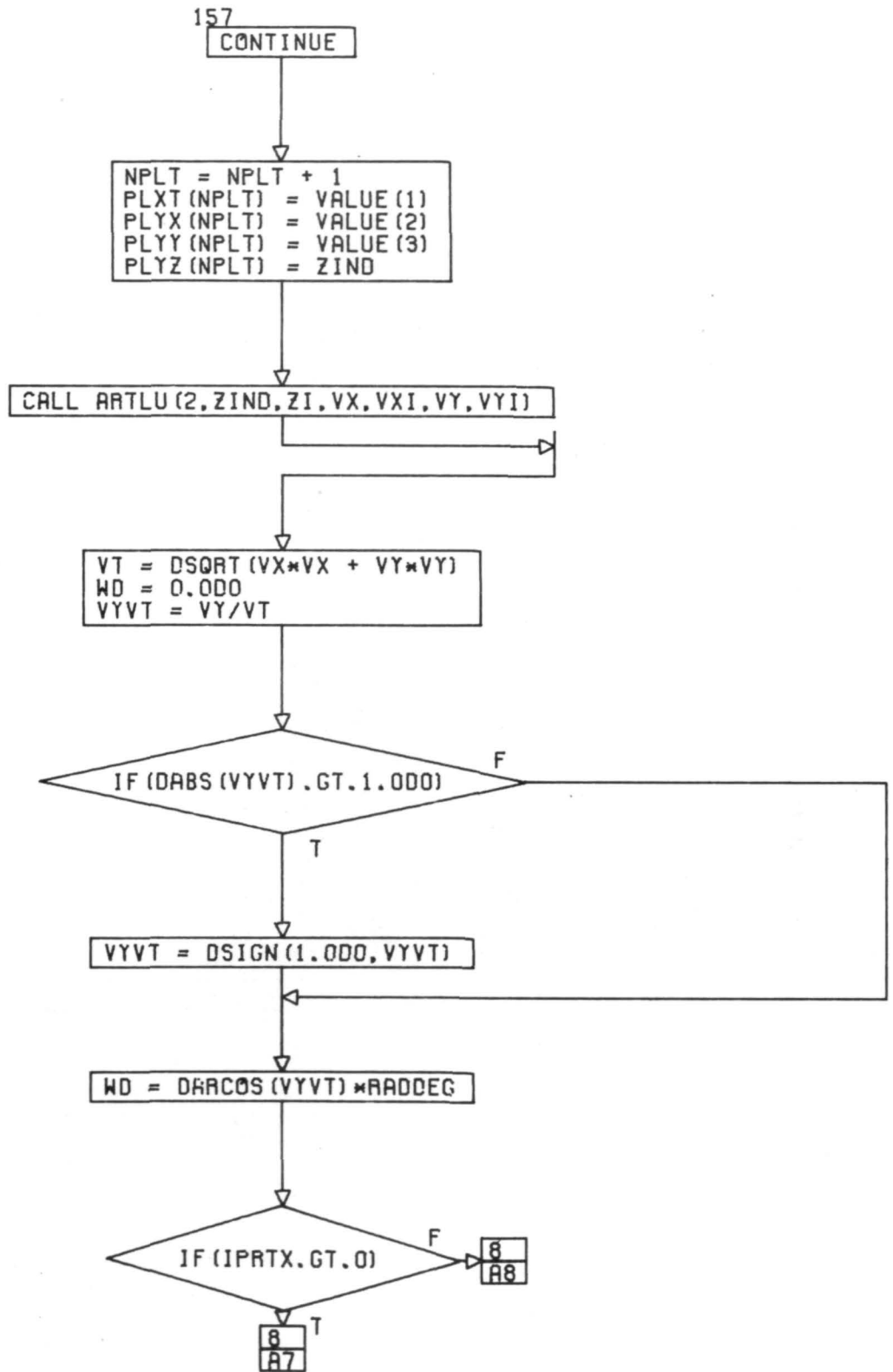
CALL EXIT

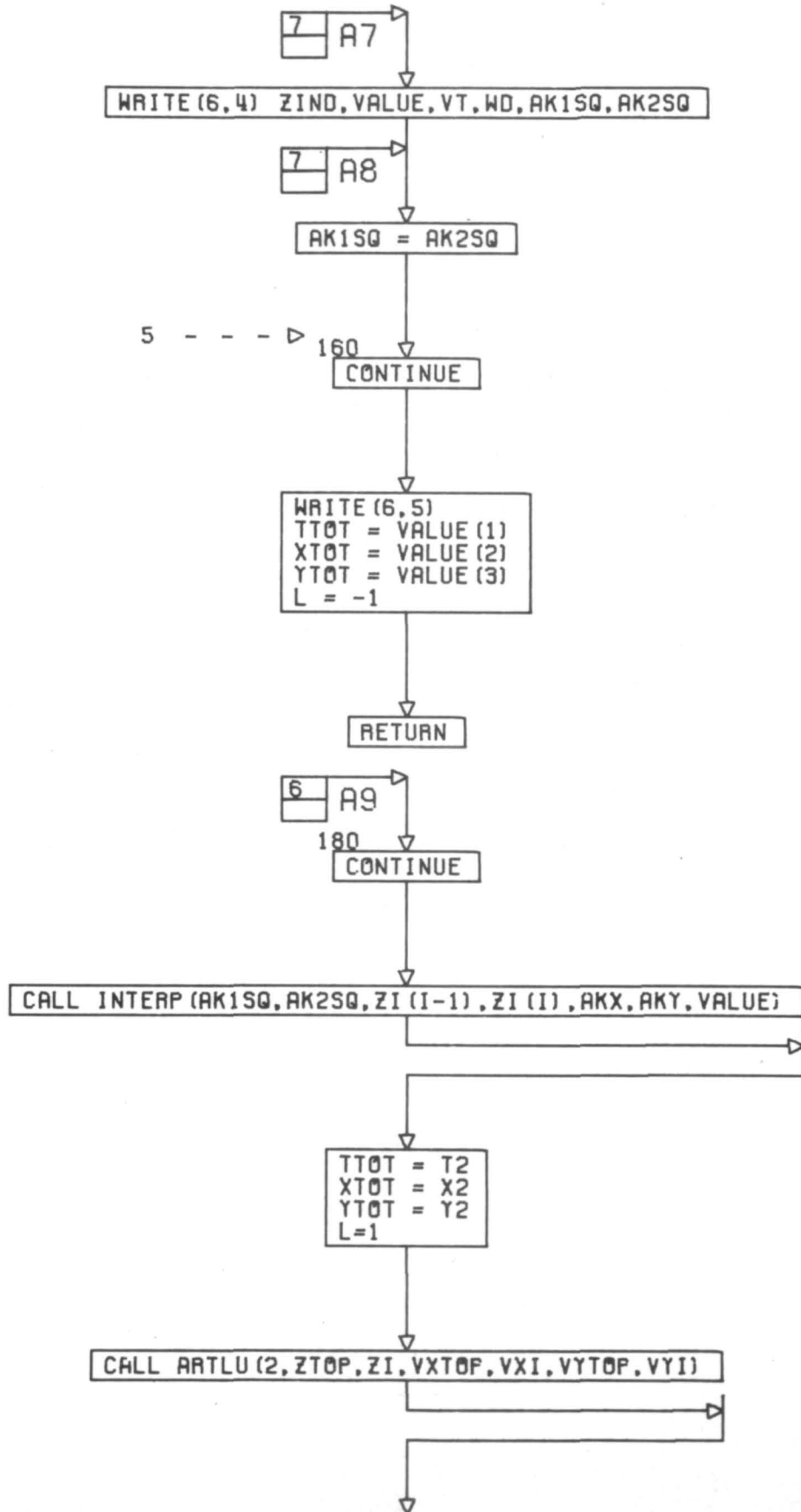


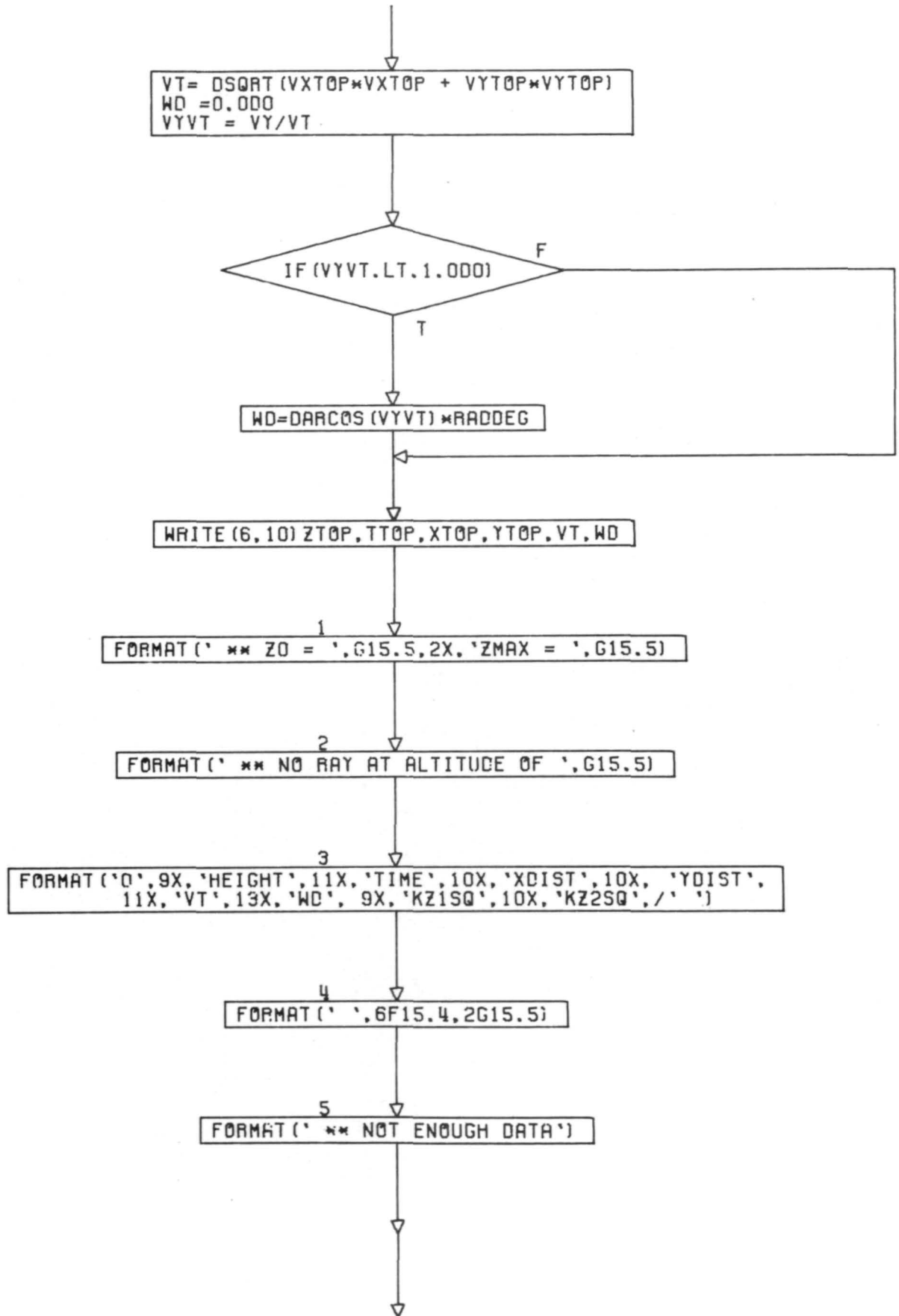


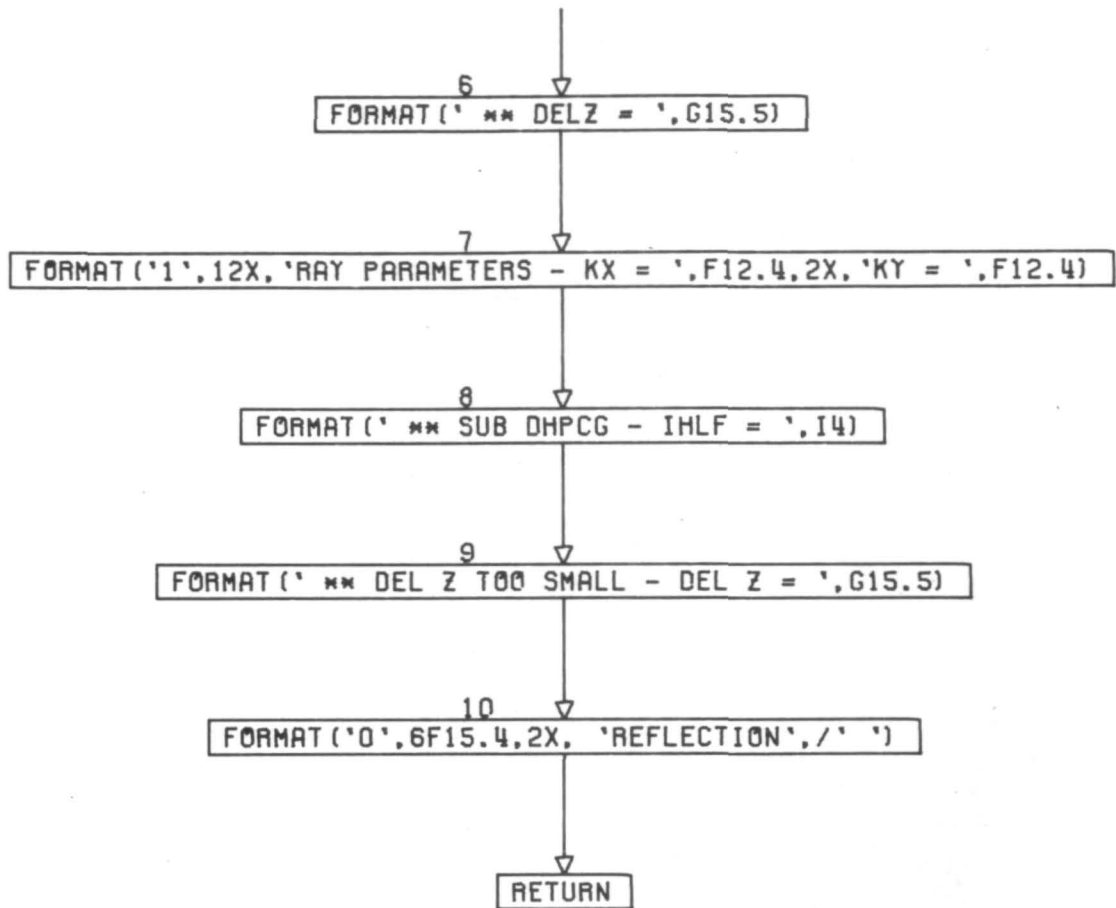












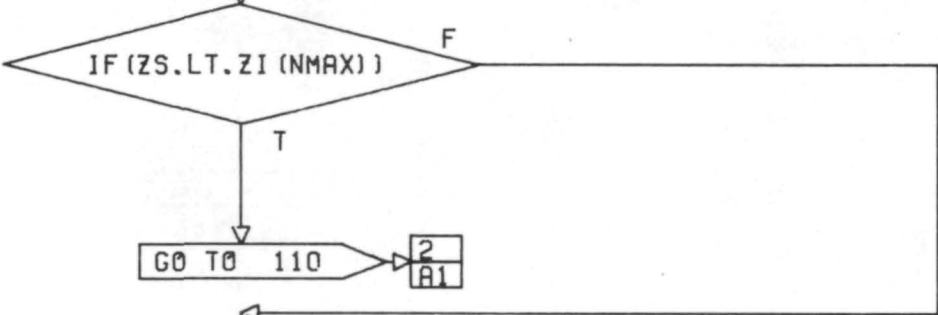
END

```
IMPLICIT REAL*8 (A-H, O-Z)  
SUBROUTINE DNDIST (NOPIN, ZS, TS, XS, YS, AKX, AKY, TTOT, XTOT, YTOT, L)
```

```
C      MODIFIED FOR PREDICTOR CORRECTOR
```

```
COMMON/FAYE/CI (300), VXI (300), VYI (300), ZI (300), PLXT (600), PLYZ (600),  
      PLYX (600), PLYY (600)
```

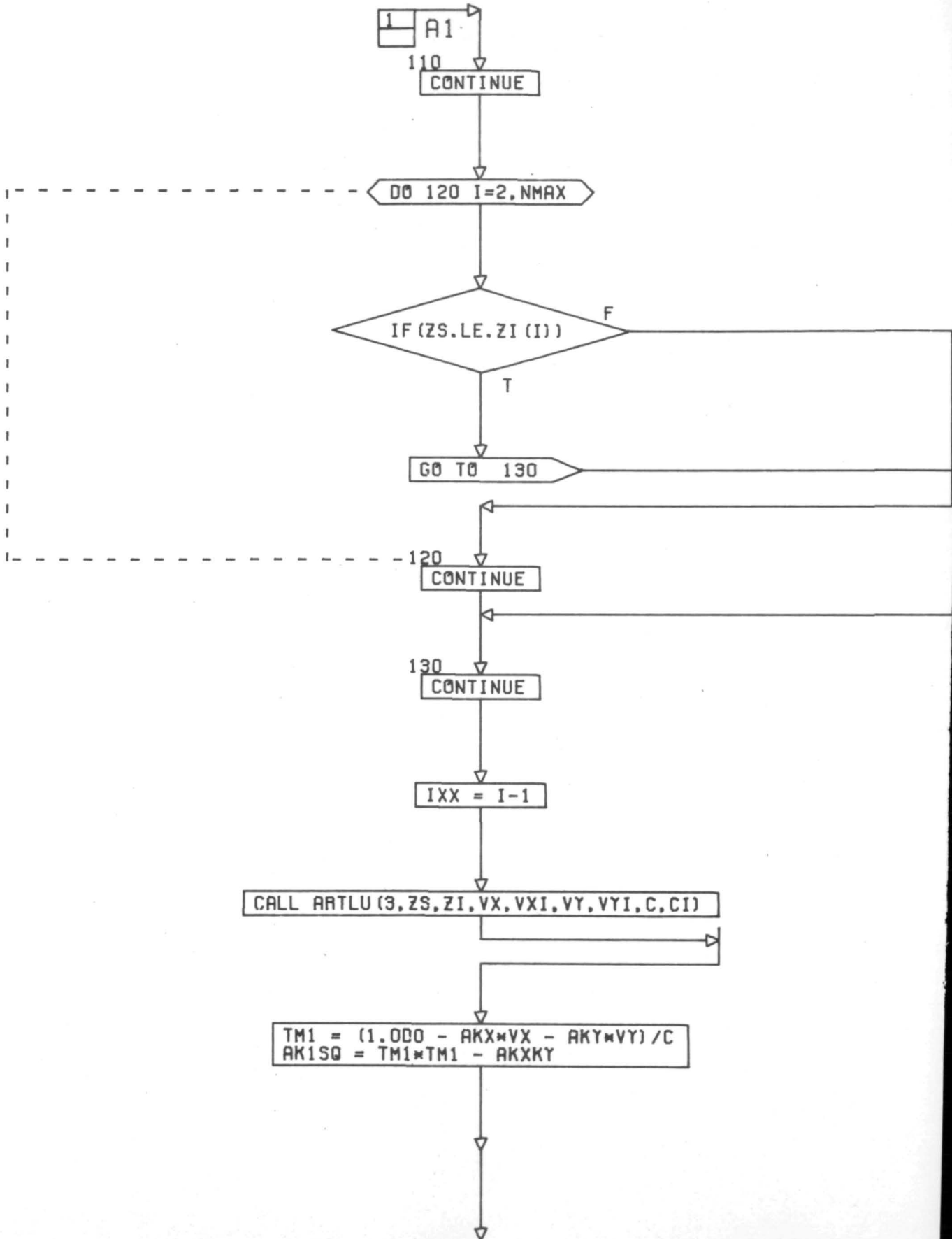
```
COMMON /JANET/ NMAX, NPLT, IPRTX  
COMMON/PEARL/ZTOP, TTOP, XTOP, YTOP  
DIMENSION VALUE (3), DEAN (3), UPBND (3), DNBND (3)  
COMMON/JULIA/QAKX, QAKY  
RADDEG = 57.295779513100  
AKXKY = AKX*AKX + AKY*AKY  
QAKX = AKX  
QAKY = AKY
```

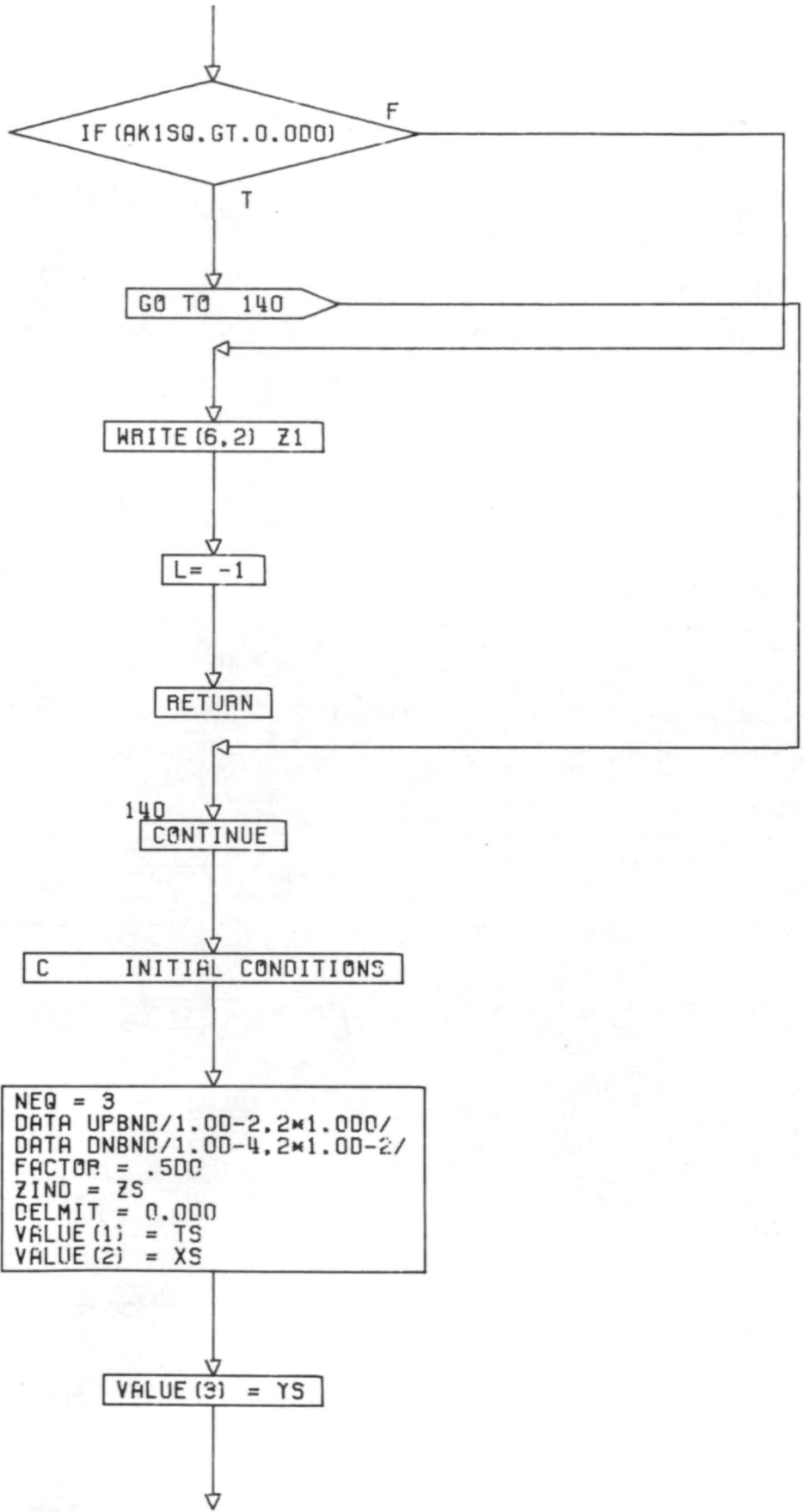


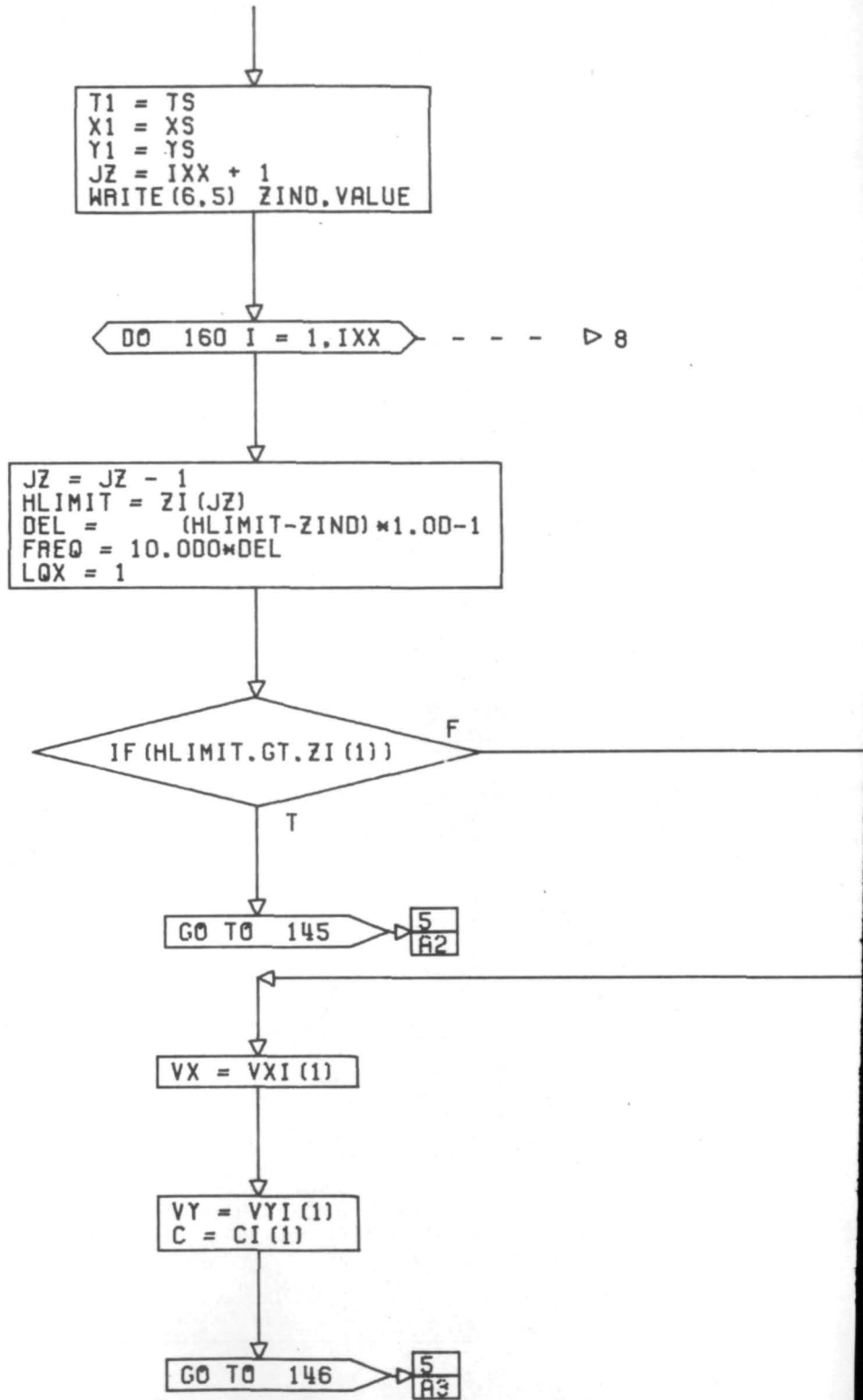
```
GO TO 110
```

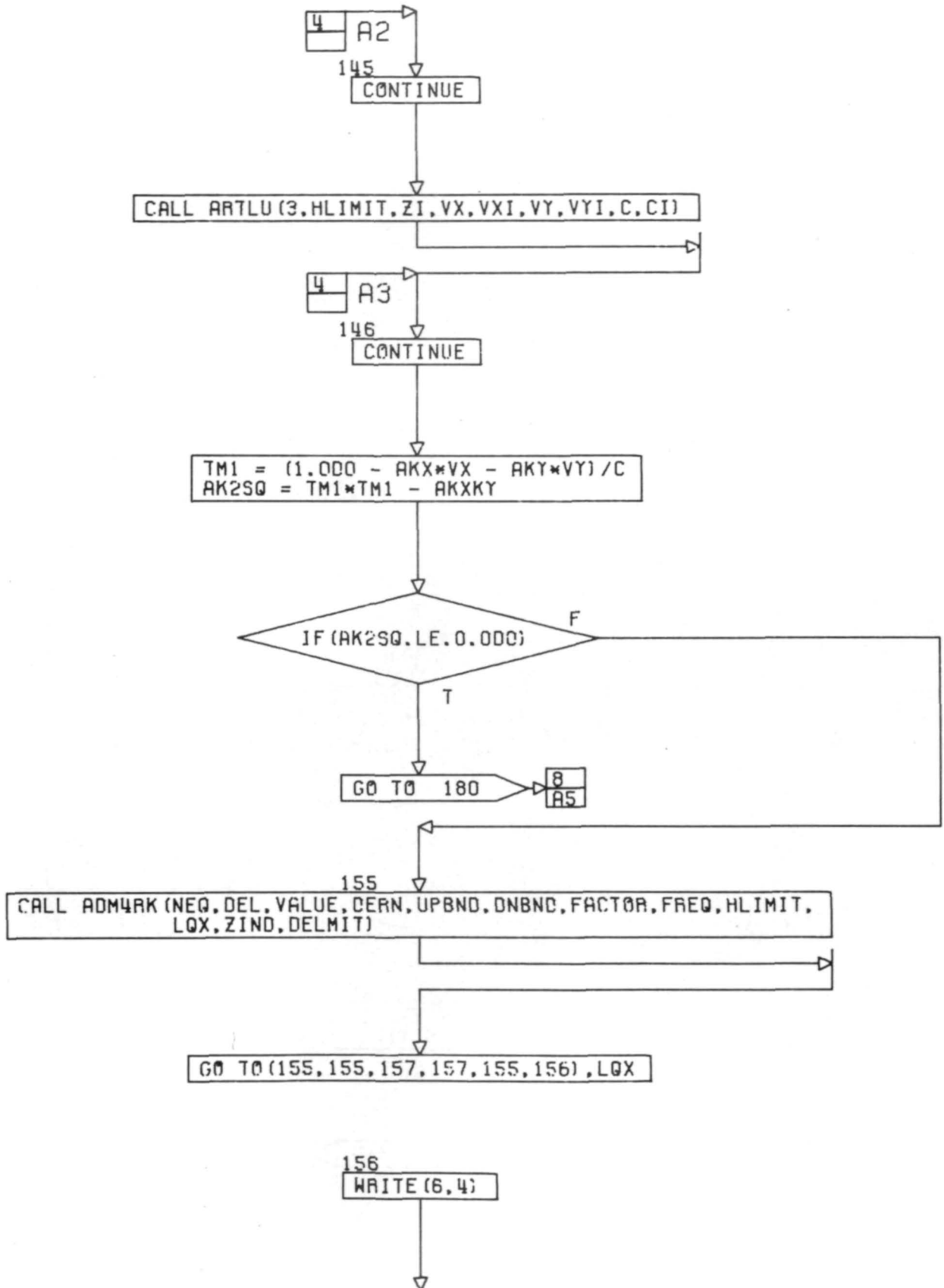
```
WRITE (6, 1) ZS, ZI (NMAX)
```

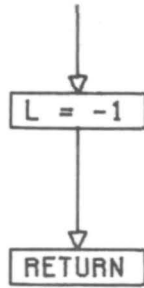
```
CALL EXIT
```











157
CONTINUE

```
NPLT = NPLT + 1  
T1 = T1 + (T1 - VALUE (1))  
X1 = X1 + (X1 - VALUE (2))  
Y1 = Y1 + (Y1 - VALUE (3))  
VALUE (1) = T1  
VALUE (2) = X1  
VALUE (3) = Y1  
PLXT (NPLT) = VALUE (1)
```

```
PLYX (NPLT) = VALUE (2)  
PLY Y (NPLT) = VALUE (3)  
PLY Z (NPLT) = ZIND
```

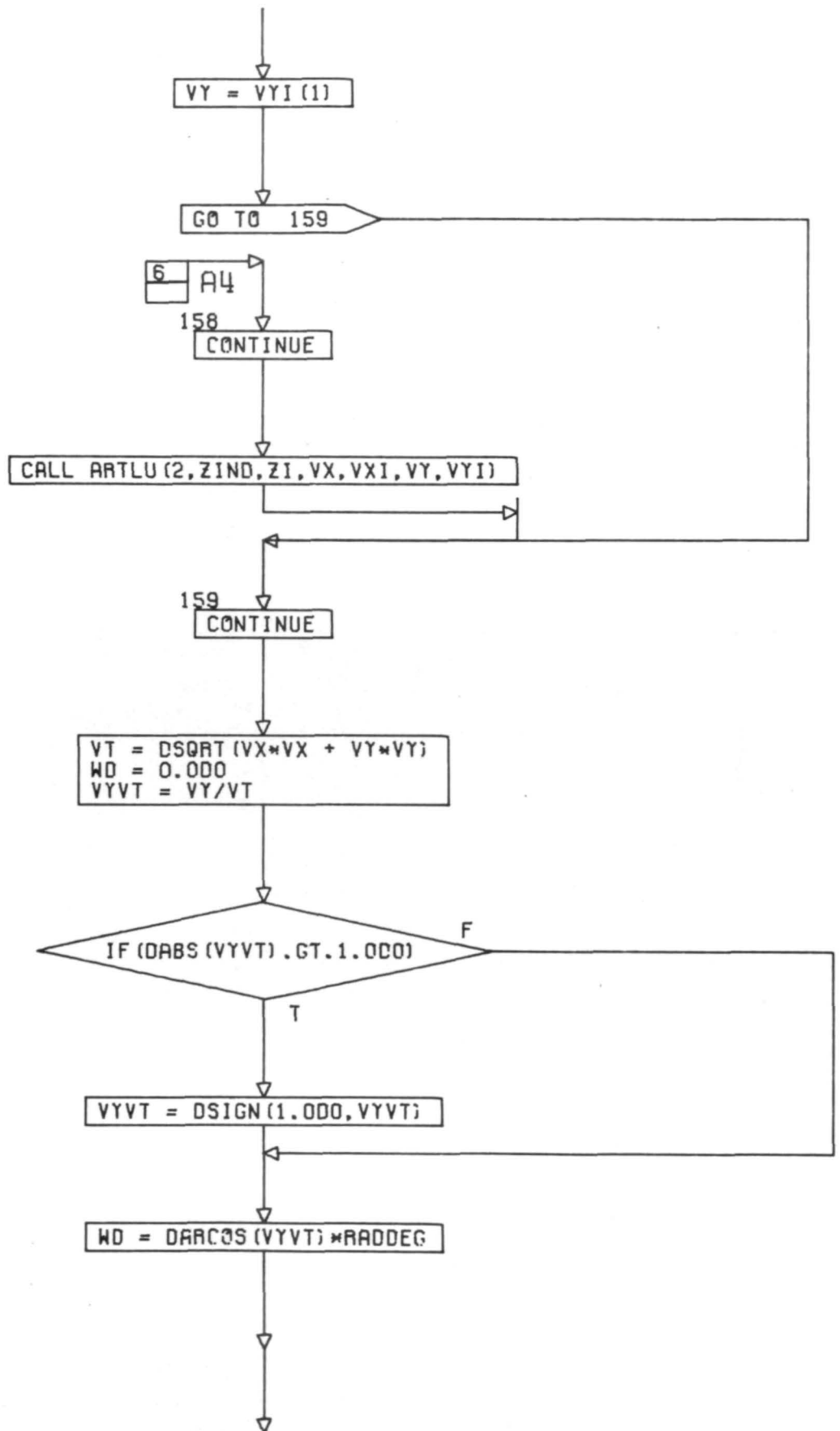


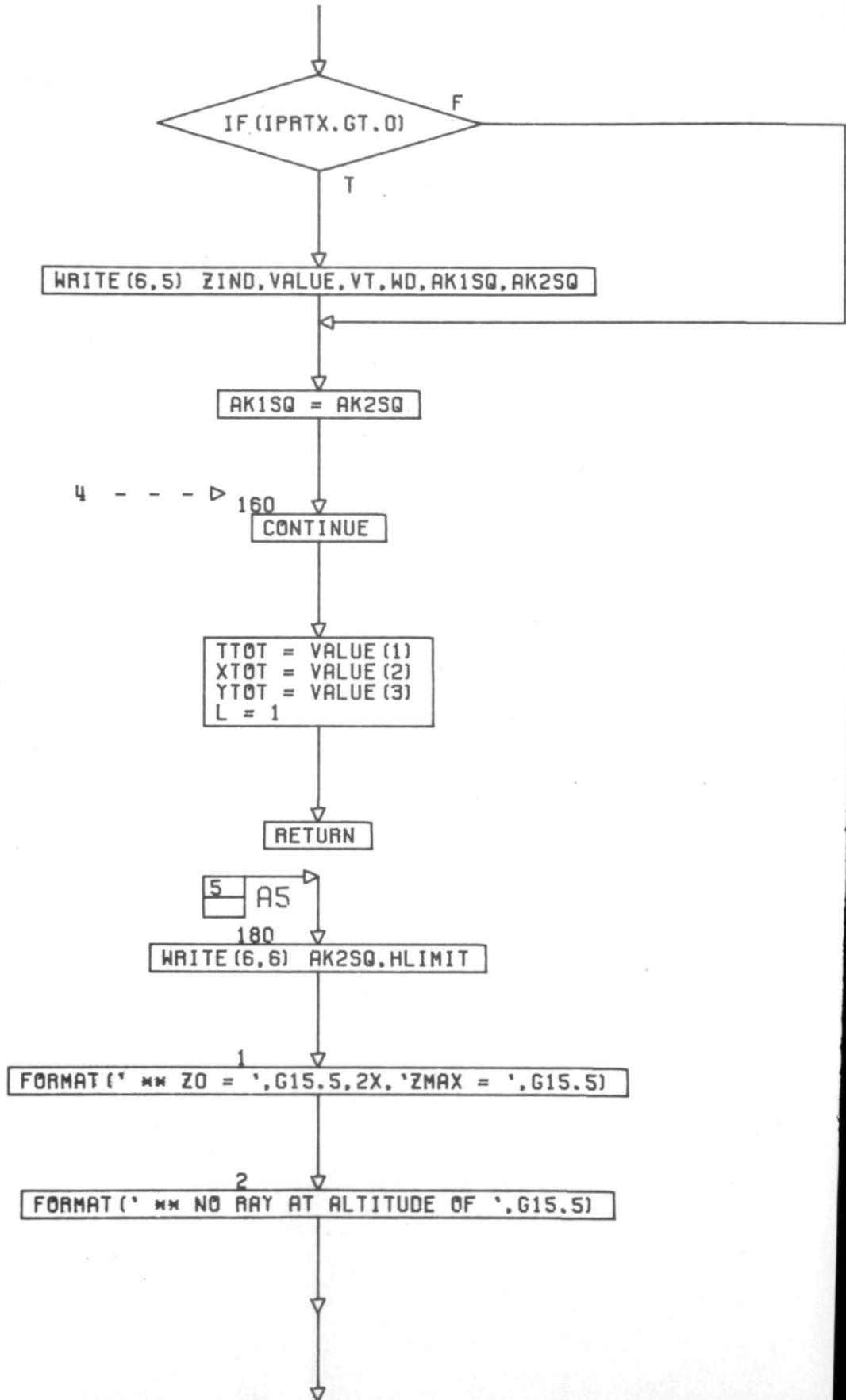
GO TO 158

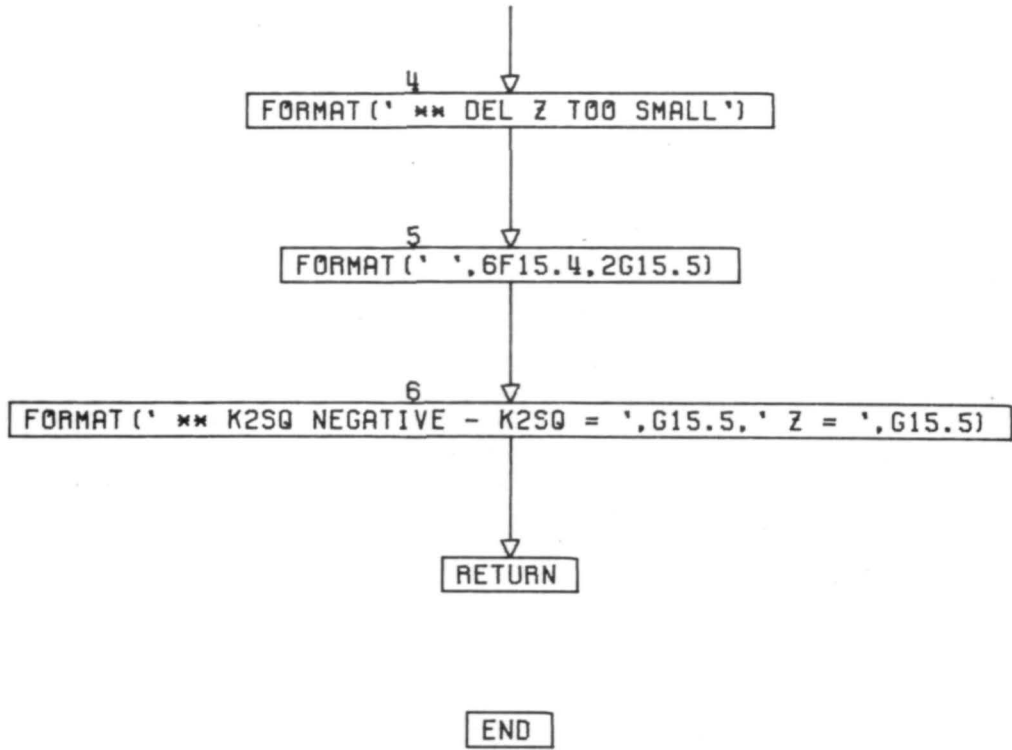
7
A4

VX = VXI (1)

CONT. ON PG 7







IMPLICIT REAL*8 (A-H,O-Z)
SUBROUTINE INTERP (AK1SQ,AK2SQ,Z1,Z2,AKX,AKY,VALUE)

COMMON/FAYE/CI (300),VXI (300),VYI (300),ZI (300),PLXT (600),PLYZ (600),
PLYX (600),PLY (600)

COMMON/JANET/NMAX,NPLT
COMMON/PEARL/ZTOP,TTOP,XTOP,YTOP,T2,X2,Y2
DIMENSION VALUE (1)
T1 = VALUE (1)
X1 = VALUE (2)
Y1 = VALUE (3)

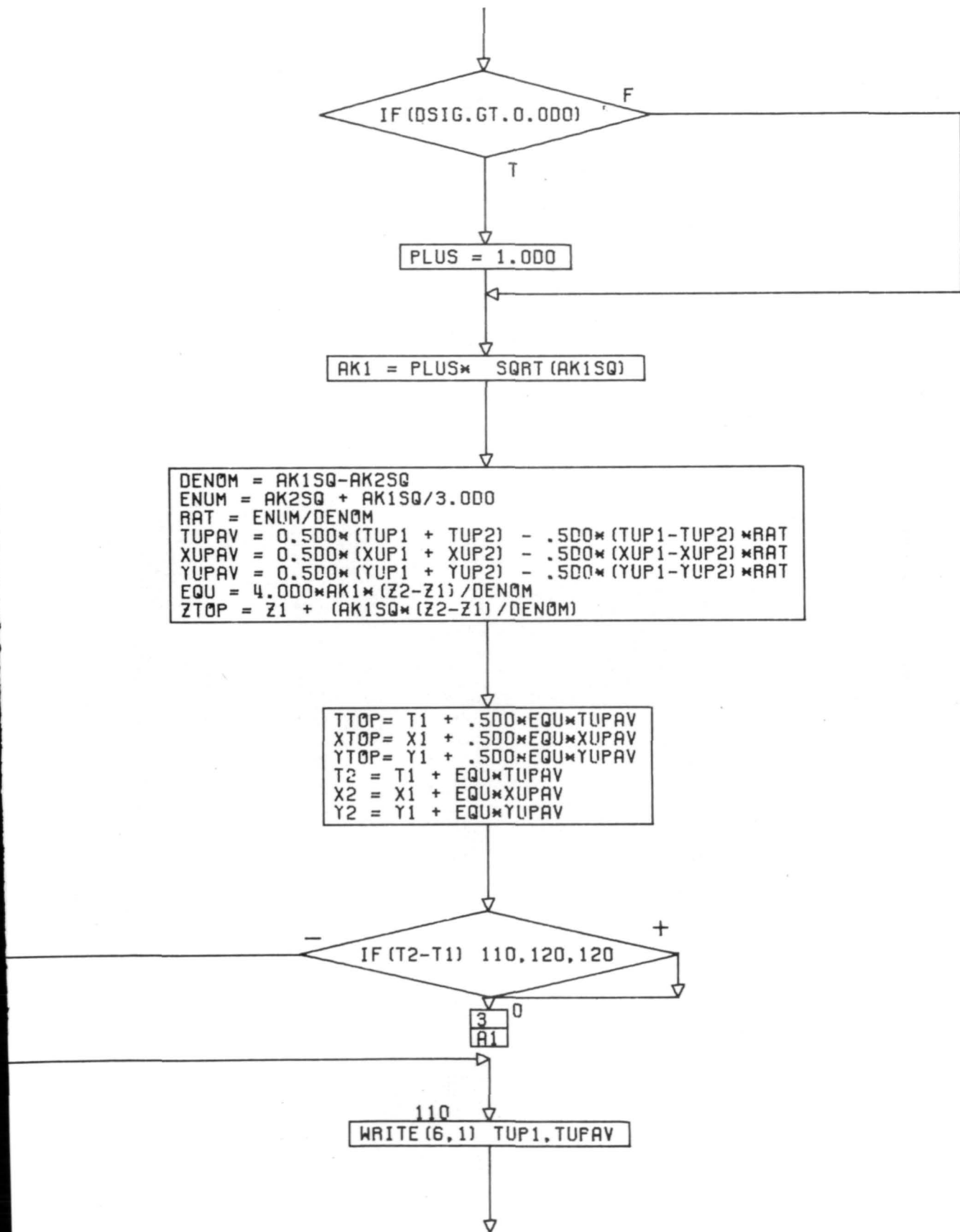
CALL ARTLU (3,Z1,ZI,C,CI,VX,VXI,VY,VYI)

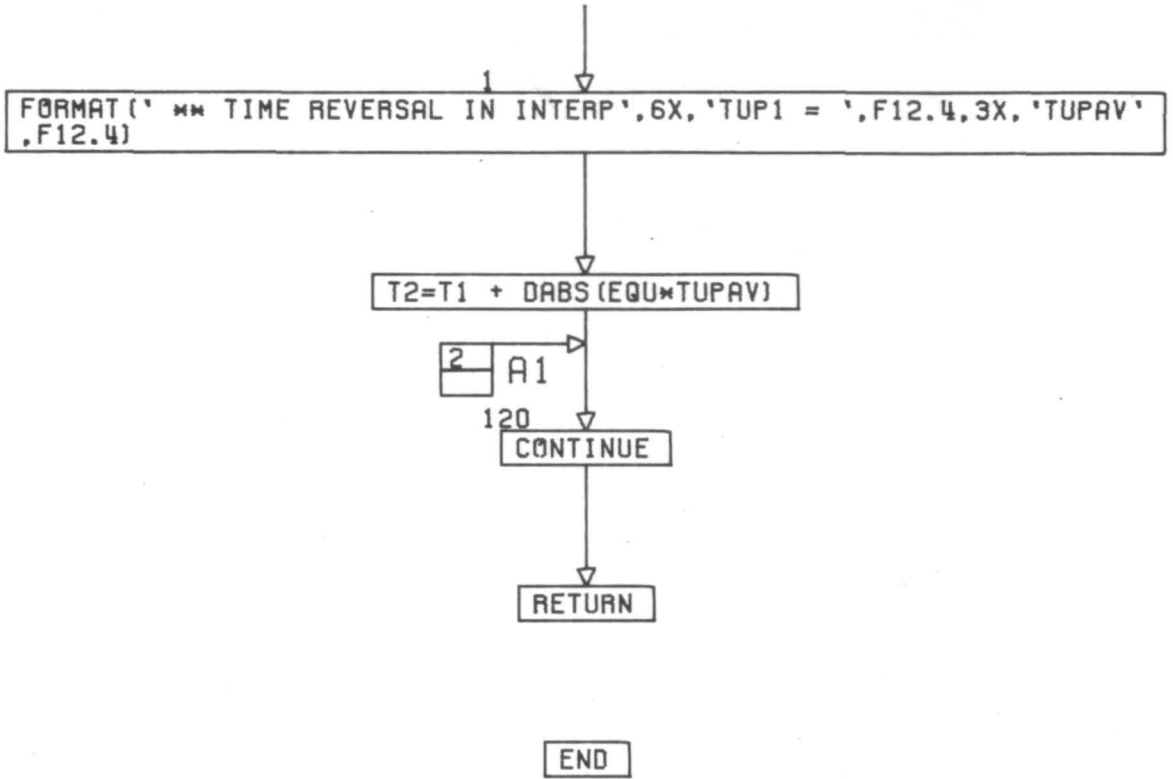
CALL PARAM (AKX,AKY,C,VX,VY,TUP1,XUP1,YUP1,AK1SQ)

CALL ARTLU (3,Z2,ZI,C,CI,VX,VXI,VY,VYI)

CALL PARAM (AKX,AKY,C,VX,VY,TUP2,XUP2,YUP2,AK2SQ)

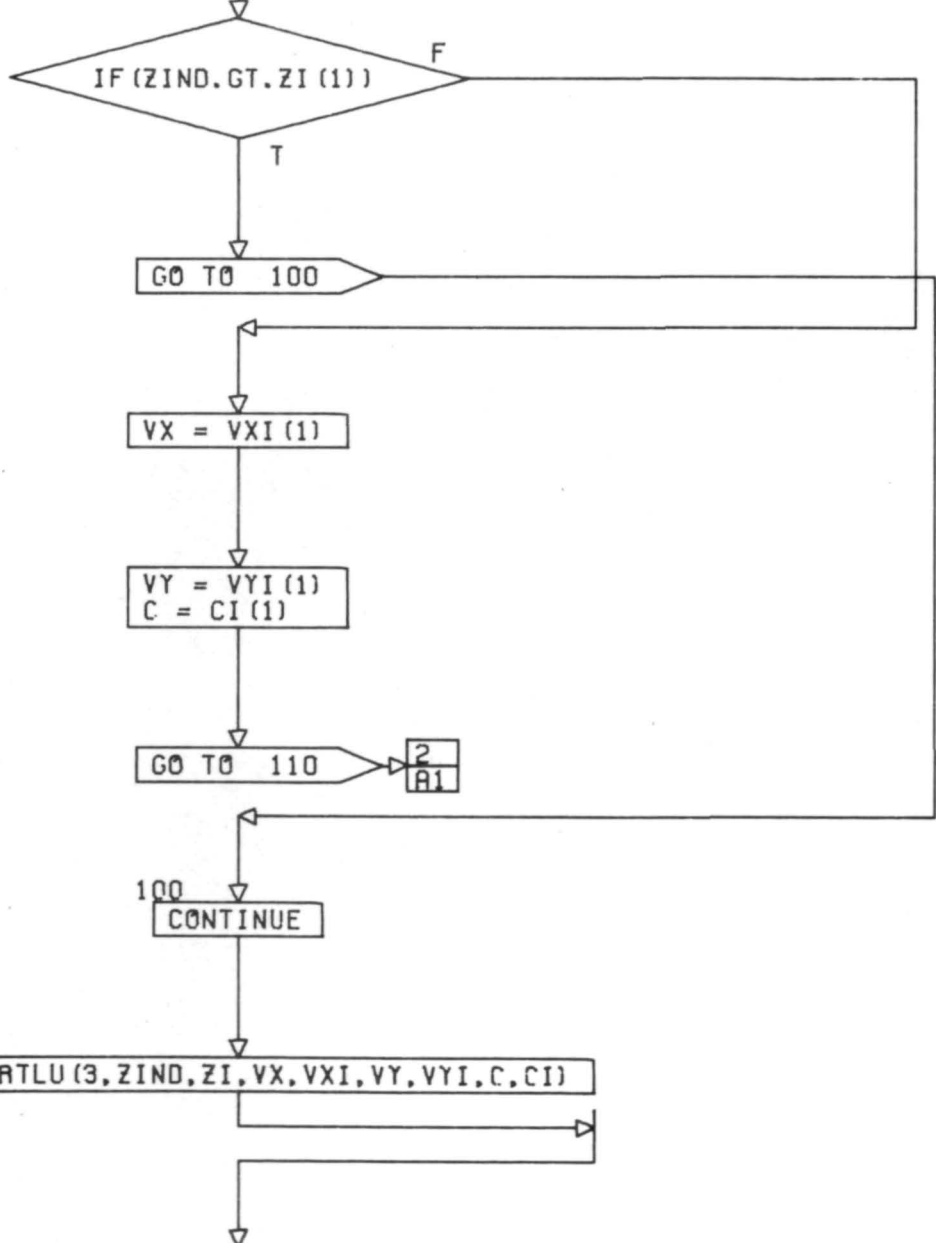
PLUS = -1.000
DSIG = TUP1*(Z2-Z1)

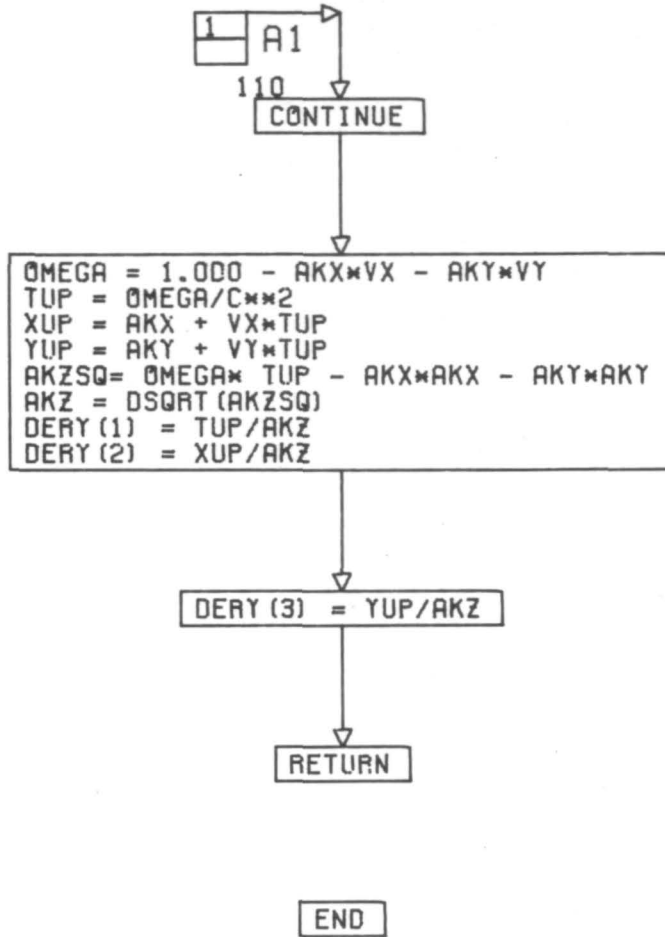





```
IMPLICIT REAL*8 (A-H,O-Z)
SUBROUTINE DEREQ (VALUE,ZIND,DERY,LOX)
DIMENSION VALUE (1),DERY (1)
COMMON/JULIA/AKX,AKY
```

```
COMMON/FAYE/CI (300),VXI (300),VYI (300),ZI (300),PLXT (600),PLYZ (600),
PLYX (600),PLY (600)
```





```
IMPLICIT REAL*8 (A-H,O-Z)
SUBROUTINE PARAM(AKX,AKY,C,VX,VY,DTUP,DXUP,DYUP,AKZSQ)
BOM=1.0-AKX*VX-AKY*VY
DTUP=BOM/C**2
DXUP=AKX+VX*DTUP
DYUP=AKY+VY*DTUP
AKZSQ=BOM*DTUP-AKX**2-AKY**2
```

RETURN

END